

**AN INVESTIGATION INTO THE COLD START
PERFORMANCE OF AUTOMOTIVE DIESEL ENGINES**

by

John Antony Burrows

Thesis submitted to the University of Nottingham
for the degree of Doctor of Philosophy, April 1998

Contents

ABSTRACT	i
ABBREVIATIONS	iii
NOMENCLATURE	iv
1. INTRODUCTION	1
1.1 Cold Start Performance	2
1.2 Diesel Cold Start: Previous Work	3
1.2.1 Factors Controlling Start Quality	3
1.2.2 Fuelling Strategies	5
1.2.3 Starting Aids	6
1.2.4 Design and Operational Variables	8
1.3 Objectives of this Thesis	10
1.4 Thesis Layout	11
1.5 Thesis Contribution to Diesel Engine Cold Starting	12
2. EXPERIMENTAL FACILITIES AND DATA ACQUISITION	14
2.1 Introduction	14
2.2 Cold Cell Facilities	14
2.3 Instrumentation	17
2.4 Test Procedures	19
2.5 Discussion	21
2.6 Conclusions	23
3. BASIC START CHARACTERISTICS, IDI ENGINE	25
3.1 Introduction	25
3.2 Basic Start Performance	25
3.2.1 Effect of Ambient Temperature	26
3.2.2 Effect of Cranking Speed	27
3.2.3 Effect of Oil Viscosity	28
3.2.4 Effect of Ancillary Loads	29
3.3 Conclusions	29
4. CONSTRAINTS ON START QUALITY, IDI ENGINE	31
4.1 Introduction	31
4.2 Starter Model Development	33
4.2.1 Battery and Lead Characteristics	33
4.2.2 Starter Motor Characteristics	35
4.2.3 Complete Starting System Model	35
4.2.4 Application to Engine Start Data	37

4.3	Basic Combustion Analysis	39
4.4	Friction Throughout Cold Starting	40
4.5	Constraints on Start Quality	41
4.6	Conclusions	42
5.	BLOWBY MEASUREMENT AND ANALYSIS	44
5.1	Introduction	44
5.2	Background	44
5.3	Experimental Study of Blowby	46
5.3.1	Correlation of Results	47
5.4	Blowby Model	49
5.5	Analysis and Discussion	52
5.5.1	Effect of Ambient Temperature	52
5.5.2	Effect of Engine Speed	54
5.5.3	Contribution of Individual Cylinders	55
5.5.4	Blowby Variation Between Test Engines	55
5.5.5	Effect of Firing	56
5.6	Conclusions	58
6.	COMBUSTION STUDIES	60
6.1	Introduction	60
6.2	Fuelling Strategy	60
6.2.1	Analysis Methods	61
6.2.2	Effect of Injection Quantity	63
6.2.3	Effect of Injection Timing	65
6.2.4	Effect of Injection Rate	66
6.3	Glowplug Operation	67
6.3.1	Temperature and Timing	67
6.3.2	Tip Protrusion	69
6.4	Conclusions	70
7.	MOTORING FRICTION STUDIES	73
7.1	Introduction	73
7.2	Measurement Method	74
7.2.1	Test Equipment	74
7.2.2	General Engine Testing Procedures	75
7.3	Steady-State Friction Results	79
7.3.1	Ford 1.8 litre IDI Engine	79
7.3.2	Ford 2.2 litre P-type Engine	83
7.3.3	Comparison with Competitor Engine: VW 1.9 TDi	85
7.4	Conclusions	86

8. INITIAL FRICTION TRANSIENT	88
8.1 Introduction	88
8.2 Magnitude of Start-up Friction	89
8.2.1 Experimental Measurement of Initial Friction	90
8.2.2 Full-Engine Results	92
8.2.3 Contribution by Component	93
8.3 Duration of Start-up Friction	95
8.4 Theoretical Consideration	97
8.4.1 Overview of Test Data	97
8.4.2 Model for Quasi-Steady Condition	99
8.4.3 Transient Model Development	103
8.5 Conclusions	105
9. SUMMARY AND CONCLUSIONS	107
9.1 Overview	107
9.2 Combustion Behaviour	109
9.2.1 Time Before First Fire	109
9.2.2 Firing-Assisted Cranking	110
9.2.3 Run-Up to Idle	112
9.3 Friction Characteristics	112
9.3.1 Quasi-Steady Operation	113
9.3.2 Initial Friction Transient	115
9.4 Conclusions	117
REFERENCES	
APPENDIX A	
FIGURES	

ACKNOWLEDGEMENTS

I would like to thank Ford Motor Company, and in particular Mr. Mike Murphy, for financial and technical support throughout this work, and Professor Paul Shayler, University of Nottingham, for his advice during the preparation of this thesis.

Thanks also to Mr. Brian Webster, for endless technical support during commissioning and testing, and Mr. Clive Tindle and Mr. Carlo Bianco for additional test data from the L-type and VW engines, and bearing temperature measurements.

ABSTRACT

An Investigation Into the Cold Start Performance of Automotive Diesel Engines

John Antony Burrows, 1998

The cold start performance of automotive diesel engines is currently poor when compared to similar gasoline units. This thesis describes an experimental and theoretical investigation into the factors limiting diesel cold start behaviour. Studies have been carried out on IDI and DI designs of engine. Start behaviour has been characterised in terms of times taken to complete various stages of start-up, engine speed variations and processes which affect these. Combustion and friction behaviour have been investigated in detail.

Engine friction losses are dependent on temperature. During start-up these losses are relatively high compared to those when the engine is fully-warm. The work output from combustion is low at low speeds, and prone to a further deterioration at lower temperatures. Consequently, combustion output during cold cranking is initially insufficient to overcome frictional losses. The start times are extended by the need to keep the starter motor engaged until heat generated in the engine causes frictional losses to fall. Eventually, when combustion output is able to overcome friction without the aid of starter motor work, idle speed is reached. Changes to fuel injection and glowplug parameters have been used to achieve a limited improvement in low-temperature starting.

Measurements of engine friction have been carried out to determine the influence of temperature and speed, and the relative contributions from each of the main component assemblies. At low temperatures, much of the friction originates in hydrodynamically lubricated components such as journal bearings, due to high oil viscosity at low temperature. Additionally, engine friction as rotation begins

has been shown to be far higher than measured by conventional "steady-state" motoring tests (over twice the quasi-steady state friction at -20°C). This initially high friction transient decays towards the quasi-steady values throughout the start.

For crankshaft bearings, a friction model has been developed for cold start-up through to fully warm engine conditions. The friction behaviour in the bearings is dependent on thermal conditions around the friction surfaces. Models for the starter system and blowby processes are also presented as part of a broader theoretical investigation to assess the impact of design changes on start quality.

ABBREVIATIONS

AirCon	Air Conditioning
ATDC	After Top Dead Centre
BMEP	Brake Mean Effective Pressure
BTDC	Before Top Dead Centre
CCS	Cold Cranking Simulator
DC	Direct Current
DI	Direct Injection
DOHC	Dual Overhead Camshaft
EGR	Exhaust Gas Recirculation
EMEP	Effective Brake Mean Effective Pressure
EPIC	Electronic Programmable Injection Controller (Lucas)
FIE	Fuel Injection Equipment
FMEP	Friction Mean Effective Pressure
FSD	Full Scale Deflection
IDI	Indirect Injection
IMEP	Indicated Mean Effective Pressure
MEP	Mean Effective Pressure
NA	Naturally Aspirated
OHC	Overhead Camshaft
PAS	Power Assisted Steering
PRT	Platinum Resistance Thermometer
SAE	Society of Automotive Engineers
SMEP	Starter Mean Effective Pressure
SOI	Start Of Injection
TCI	Turbocharged and Intercooled
TDi	Turbo Diesel Intercooled (VW engine designation)
TDC	Top Dead Centre

NOMENCLATURE

a, b	Constants in the Walther Equation [mixed units]
FR	Friction Ratio: subscript denotes at time t or initial value (' t ' or ' T ') [-]
K	Constant in Bishop's Equation [s/m]
n	Friction index (0.19-0.24 for gasoline, 0.24-0.39 for diesel) [-]
n	Step number [-]
P	Pressure [Pa]
r_c	Compression ratio [-]
S_p	Mean piston speed [m/s]
t	Time: subscript denotes to first fire, sustained fire or idle speed ('ff', 'sf' or 'idle') [s]
T	Absolute temperature [K]
V	Volume [m ³]
Δ_{FMEP}	Rise in FMEP due to gas pressure above the pistons [Pa]
ν	Kinematic viscosity [cSt, mm ² /s]
τ_{FR}	Time constant of friction ratio [s]

In the starter motor model:

I	Electrical Current: subscript denotes battery, glowplugs or starter ('B', 'G' or 'S') [A]
I_{ENG}	Engine inertia [kg.m ²]
P_{OUT}	Starter motor output power [W]
R	Electrical resistance: subscript denotes battery, leads, glowplugs or starter ('b', 'L', 'G' or 'S') [Ω]
V	Voltage: subscript denotes battery or starter ('b' or 'S') [V]
$W_{INERTIA}$	Work done on engine inertia [J]
η	Starter motor efficiency [-]
ω	Angular velocity: subscript denotes beginning or end of stroke ('B' or 'E') or starter velocity ('S') [rad/s]

In the blowby model:

A	Effective orifice area [m^2]
C_d	Discharge coefficient [-]
K_m, K_n	Constants: subscripts as defined in the text [mixed units]
m	Mass of gas: subscripts as defined in the text [kg]
n_{\min}	Minimum cyclic engine speed [rpm]
P	Gas pressure: subscripts as defined in the text [Pa]
R	Gas constant [J/kg.K]
γ	Ratio of specific heats for air [-]
ΔP	Pressure drop across orifice [Pa]
Δt	Time step [s]
ρ	Blowby gas density [kg/m^3]

In the fuel injection model:

A_{nozzle}	Injector nozzle area [m^2]
C_d	Discharge coefficient [-]
m_{fuel}	Mass of fuel [kg]
ΔP	Pressure drop across nozzle [Pa]
ρ_{fuel}	Fuel density [kg/m^3]

In the bearing friction model:

c	Bearing radial clearance [m]
c_m	Specific heat capacity of thermal inertia (mass) [J/kg.K]
D	Bearing diameter [m]
F	Frictional force [N]
L	Bearing length [m]
m_m	Mass of thermal inertia (mass) [kg]
P_{pump}	Oil pump gauge pressure [Pa]
\dot{q}	Oil mass flow rate: subscript denotes flow due to oil pump pressure, due to pumping action within the bearing, or total ('pressure', 'pumped' or 'total') [kg/s]

\dot{q}^*	Non-dimensional oil flow coefficient [-]
\dot{Q}	Heat flow: subscript denotes convection or conduction out of the oil ('conv' or 'cond'), or conduction from mass to block ('mb') [W]
R	Bearing radius [m]
R	Thermal resistance: subscript denotes oil to block, oil to mass, or mass to block ('ob', 'om' or 'mb') [K/W]
T	Temperature: subscript denotes oil feed or metal ('feed' or 'metal') [K]
\bar{T}_{oil}	Average oil film temperature [K]
U	Bearing surface speed [m/s]
ΔT	Temperature rise of thermal inertia (mass) above block [K]
ΔT_{oil}	Temperature rise in oil [K]
η	Dynamic viscosity [Pa.s]
ρ	Density of oil [kg/m ³]
σ	Specific heat of oil [J/kg.K]

Chapter 1

INTRODUCTION

This thesis is concerned with the cold-start behaviour of diesel engines, which factors control this behaviour, and how starting can be improved through design or calibration developments. The engine design must create a suitable air-fuel mixture in the cylinder and generate high enough pressure and, through compression heating, temperature for successful ignition to occur. Low fuel volatility, high losses, and reduced cranking speeds at sub-zero temperatures make starting particularly difficult to achieve. While the use of starting aids such as glowplugs can greatly extend the temperature range over which starting is possible, there is continuing pressure for improvements in consistency and start times at lower temperatures.

Until recently, most small capacity automotive diesel engines have been indirect-injection (IDI) engine designs with generally poor cold starting characteristics compared to gasoline spark-ignition engines. The contrast highlights the need for improvement in the diesel engine case. Parasitic load on the engine, increased by the trend towards "extra" ancillaries such as power-assisted steering and air-conditioning, can exacerbate the general problem of long starting times. Customer perception, and the possible durability implications of extended cranking times have also put pressure on start performance. The desire to build a single vehicle to operate in all climates (the so-called "world" car) means that special provision for cold-climate territories is now less acceptable; all vehicles will be expected to start well at low temperature.

Concerns over emissions could become a powerful driving force for further improvements. Research commissioned by Lucas [1.1] showed that the emissions benefits of diesel compared to gasoline became more pronounced as the journey

length is decreased (the trend in modern driving patterns [1.2]). The adoption of exhaust gas recirculation (EGR) and exhaust aftertreatment promises to reduce tailpipe emissions further. With the introduction of emissions test cycles including the start-up period [1.3], these potential benefits could be lost due to starting; long periods of cranking with excess fuel and many misfires could be disastrous.

The aim of the work described in this thesis has been to examine the mechanisms of cold starting, to understand and ultimately improve start performance. Investigations have been carried out using several Ford diesel engines and one competitor engine, all of a broadly similar configuration, but including both IDI and DI (Direct Injection) designs. Combustion studies were primarily undertaken on a Ford 1.8 litre IDI turbocharged engine fitted into a Sierra vehicle. Motoring studies have been performed using an intercooled variant of the above engine, and a 2.2 litre DI engine code named "P-type". Additional data has been obtained from a DI variant of the IDI engine, code named "L-type", and a Volkswagen 1.9 litre DI engine of similar specification. Key dimensions of all test engines can be found in Appendix A. Investigations of performance at temperatures below -25°C were possible, but most work was carried out at or above -20°C .

1.1 Cold Start Performance

An illustration of typical engine speed variation during starting at 0°C is given in Figure 1.1; the data were recorded from the Ford 1.8 litre IDI engine. The cold start can be divided into several stages: the time until combustion commences, the time until engine rotation continues without the starter motor, and the total time to idle speed. Here, these are referred to as time to first fire, time to sustained fire and time to idle (t_{ff} , t_{sf} and t_{idle}) respectively. These can be identified from speed traces: t_{ff} by the rapid speed rise in the expansion stroke, t_{sf} when the engine exceeds the maximum operating speed of the starter, and t_{idle} when the known idle speed is exceeded. Misfiring cycles may also be identified by a

deceleration over the stroke, allowing calculation of the misfire rate as a percentage of total cycles to idle speed. In the figure shown, the engine starts quickly, firing after about 0.3 seconds and reaching idle speed at 0.8 seconds.

Figure 1.2 illustrates a characteristic start at -20°C , showing how the cold start extends as the temperature falls (note the different time scale). In this case, the engine is reluctant to start, firing after 1.2 seconds and reaching idle speed at 36.0 seconds. The poor combustion during starting leads to the emission of significant pollutants; the 28 misfiring cycles alone could produce almost 1500 mg of unburned hydrocarbons. This rapid deterioration in start quality as the temperature drops is not acceptable, particularly in view of recent improvements made by some manufacturers which give start times of only a few seconds at -29°C .

1.2 Diesel Cold Start: Previous Work

1.2.1 Factors Controlling Start Quality

In early work, Austen and Lyn [1.4] reported that the start time of an automotive diesel engine under test rose sharply with falling temperature, even if cranking at constant speed. Any drop in cranking speed was shown to make the situation worse by lowering the compression pressure and temperature. This falling cranking speed at lower temperatures has been widely reported for all engine types over many years, for example by Brunner and Ruf in 1959 [1.5], Caracciolo and McMillan in 1979 [1.6] and Buck and Lohuis in 1994 [1.7]. This is related closely to the increase in viscosity of the engine oil at lower temperatures [1.5-1.12], especially if the viscosity is evaluated under proper shear conditions, such as using the Cold Cranking Simulator (CCS) viscosity test [1.13]. Additionally, battery performance suffers as the temperature drops, as reported by Brunner and Ruf [1.5], leading to a further reduction in cranking speed. They found that warming the battery could have a considerable impact on

cranking performance (verified by the work of Stewart [1.9] and Caracciolo and McMillan [1.6]), giving a corresponding improvement in start quality.

Reductions in cranking speed have a direct impact on the temperature and pressure achieved in the cylinder [1.4], due to increasing blowby of cylinder gasses past the pistons and heat transfer losses. Henein and co-workers [1.12] measured the in-cylinder conditions in a cranking DI engine. Reducing the ambient temperature from +20°C to -20°C caused the speed to drop sharply, reducing peak temperature and pressure considerably. The total energy loss (representing blowby and heat transfer) rose by over 40%. In earlier work using a different DI engine, Henein [1.14] found that blowby loss could account for over 10% of the charge at cranking speeds, leading to an estimated temperature reduction of about 100°C. Numerous proposals have been made to describe instantaneous spatially-averaged heat transfer from the cylinder [1.15], including widely used models by Annand [1.16] and Woschni [1.17, 1.18]. Although not generally developed for use in divided-chamber designs, similar correlations applied by Harigaya, Ohyagi and Tsuji [1.19] to IDI engines have given satisfactory results. All the models predict a rise in heat transfer losses as the time available increases (that is, with falling cranking speed) and with reducing metal temperatures. IDI designs suffer greater loss than DI, due to higher gas velocities and increased surface area.

In order to achieve satisfactory combustion, the injected fuel must be subjected to adequate temperature and pressure for a minimum period of time, called the ignition delay. This delay period extends as the temperature and pressure are reduced, up to a point where ignition fails completely. Lyn and Valdmanis [1.20] showed that this delay could not only be extended by the lower temperature and pressure during starting, but also by the need to evaporate the large quantities of fuel typically used in cold start strategies. Under starting conditions, which are adverse for ignition, mixture formation was found to become an important factor. Biddulph and Lyn [1.21] studied how the in-cylinder temperature required for

ignition varied at cranking speeds from 100 to 300 rpm, in engines without starting aids. For a DI engine, about 650 to 700K was required for ignition, while 620 to 700K was required in the IDI engine. These figures agree closely with the finding of Henein and others [1.22], that steady combustion in an unaided DI engine would only occur when the cylinder gas temperature exceeded 640K.

The situation is not helped by the poor performance of injection systems under cold starting conditions. According to Henein [1.14, 1.23], low speed and temperature leads to reduced injection pressure and hence inferior spray atomization. In conjunction with low compression temperatures and gas velocities, poor evaporation results. Added to the sometimes poor control of fuel quantity [1.22] and timing under these conditions, these factors contribute to increasingly unsteady combustion as the start temperature decreases.

1.2.2 Fuelling Strategies

The main fuelling strategy used to assist in starting diesels at low temperatures is the injection of excess fuel. Biddulph and Lyn [1.21] presented data for both DI and IDI engines, showing that increased fuelling led to reduced cold start times. Austen and Lyn [1.4] provided evidence that, during starting, the excess fuel not only increased the effective compression ratio, but also reduced blowby by helping to seal the piston rings. During unaided starting, accumulated fuel in the cylinder produced progressively higher temperatures and pressures on successive cycles until the onset of firing. They showed that the manual injection of fuel before cranking lead to higher compression pressure and immediate firing, although a considerable quantity of fuel was used (1.5 cm³ per cylinder). Additionally, other workers [1.14] have suggested that fuel could improve starting by lubricating the upper portion of the cylinder bore.

Studies into the impact of injection timing on start performance have produced conflicting recommendations. Lyn and Valdmanis [1.20] presented ignition delay

results for a number of engines and suggested using injection timing of $5-10^\circ$ before top dead centre (BTDC) during starting. This represents a retardation of about 5° compared to normal operation in the engines studied. Phatak and Nakamura [1.24], testing with a DI engine, found that retarding from 23° to 20° BTDC improved start quality. However, other work by Zahdeh and Henein [1.25] has shown that an advance may be required during starting to avoid erratic combustion with many misfires. Their tests on a DI engine performed best with injection 23° BTDC, with many misfires observed when the timing was retarded to 10° BTDC.

Injector design and placing can have a critical impact on cold start behaviour. Lyn and Valdmanis [1.20], in their study of ignition delay during unaided starting, found that injector design (hole-type, pintle and pintaux nozzles) had only a secondary effect in their IDI engine, operating without starting aids. Some effect was seen due to injection pressure, with increased pressure was found to slightly reduce ignition delay. Injector type was, however, found to affect work output after combustion commenced. The work of Biddulph and Lyn [1.21] showed a marked decrease in ignition delay when changing from pintle to pintaux nozzles in an IDI engine. Firing could be achieved with lower compression temperatures, and a considerable improvement in overall start quality was observed. In a study of injection parameters in a DI engine, Phatak and Nakamura [1.26] found that, for a number of injector and chamber designs, spray impingement on the chamber wall was detrimental to starting. In tests without cold starting aids, injector types promoting organised but non-uniform mixing gave the best performance.

1.2.3 Starting Aids

Starting aids may be broadly divided into three categories: those which attempt to ignite the mixture directly once it is in the combustion chamber, those which

heat the fuel or air charge (either as it enters the engine or in the cylinder), and those which heat part or all of the engine itself.

For small automotive diesel engines operating at low ambient temperature, the glowplug is currently the preferred starting aid. Falling into the first category, the plug protrudes into the combustion chamber (or prechamber in IDI engines) and helps to ignite the fuel/air mixture. French and Scott [1.27] found that optimum glowplug performance required a tip temperature of about 850°C, positioned to receive a fuel/air mixture at the fringe of the fuel spray. They found that the function of the plug was not to act as a heat source for the bulk gas, but rather as a "hot spot" in the chamber to initiate ignition. This confirms work by Austen and Lyn [1.4], who additionally showed that the relative placement of the glowplug and fuel injector had a strong influence on ignition delay. Phatak and Nakamura [1.26] also found that the plug should be positioned out of the direct fuel spray, but where it would receive a fuel/air mixture. Extended operation of the glowplugs was found to be beneficial, ensuring steady combustion both during and immediately after cold starting, and allowing operation down to at least -29°C. Other methods of igniting the mixture directly have been studied, such as spark or railplugs [1.28, 1.29], but so far with limited practical application.

Methods which heat the fuel or air charge aim to achieve higher temperatures at the time of fuel injection, to assist in forming a flammable mixture and achieving proper combustion. Heating of the fuel has been shown to be impractical [1.4] due to the very high heat transfer from the fuel both as it passes through the injector and within the combustion chamber. The compression temperature and pressure can be raised by introducing a greater air mass into the cylinder [1.26, 1.30], but commonly used systems rely on applying heat to the air charge as it passes into the engine. Heat may be supplied in several ways [1.31, 1.32], but the normal method is by placing heaters in the inlet system, either electrically powered or using small auxiliary burners. These

methods were investigated by Austen and Lyn [1.4] and found to give a significant reduction in start time.

Perhaps the most desirable starting aid would be to heat the entire engine, thereby raising the effective ambient temperature of the start. Here, in addition to improving the combustion characteristics, other factors which influence starting are also improved. Lubricating oil viscosity is lowered (and hence friction is lowered), fuel injection behaviour is enhanced and cylinder heat transfer losses are reduced. If the entire engine enclosure could be heated, ancillary friction would also be reduced, and a deterioration in battery performance avoided. Again, the heat source can be electrical, by combustion or by other methods such as latent heat storage devices (similar to those discussed by Tsantis and co-workers [1.32]). In practice, the energy can only be supplied in a limited number of ways, typically to the water jacket, fuel system or sump oil. Theoretical and experimental studies by Stecki and others [1.33] showed the benefits of heating the engine in this way, but also the limitations. Even when using quite high heating powers (over 4kW), a heating duration of up to 35 minutes was required to start the engine at temperatures below -23°C .

1.2.4 Design and Operational Variables

Several design parameters can be varied to improve starting, in addition to those mentioned above. For example, it is known that higher compression ratio is helpful, as demonstrated by Phatak and Nakamura [1.24]. They have also proposed that engines with rapid, uniform mixing will be more difficult to start [1.26]; this was suggested as a factor contributing to the poor behaviour of swirl chamber IDI designs, in addition to the increased heat losses. Other factors, such as the number of cylinders and the surface to volume ratio of the cylinders can also have a significant impact. However, most of these are chosen to optimise other performance considerations and cannot be altered simply to assist starting.

Many of the problems are related to the cranking speed reductions at low temperatures. According to Mina [1.34], following work by Poublon, Patterson and Boerma [1.35], it is important to prevent the engine from slowing down excessively as the piston approaches TDC. He recommended using a higher inertia flywheel or increasing the inertia of the starter motor. However, as pointed out by earlier workers [1.4], the ideal situation for starting would be to have very rapid compression (giving minimal losses) followed by a long dwell period near TDC (to allow for the ignition delay period). Biddulph and Lyn [1.21] showed that cranking their IDI engine at higher speed would lead to better starts, but that there was an optimum cranking speed for their DI engine. Cranking the DI engine too fast could cause a deterioration in start quality, as the high temperature and pressure needed for ignition was not held for long enough.

Reducing the high levels of friction under cold conditions would be useful, not only raising the cranking speed but reducing the combustion work required to accelerate the engine. Without changes to basic engine design, this could best be achieved by selecting engine oil of the lowest possible low temperature viscosity. In their review of the effect of engine oil on performance, Stewart and Selby [1.8] covered many factors relevant to the selection of oils which are still applicable today. It is known that losses begin to heat the oil at the friction surfaces as soon as the engine starts cranking and that this heat is eventually seen as a rise in general oil temperature (for example, as reported by Kytö for engine and gearbox operation [1.36, 1.37]). This temperature rise is opposed by conduction from the oil to the cold metal surfaces, and by the constant supply of cold oil from the sump. In a journal bearing under "normal" conditions, calculation shows [1.38] that a higher oil supply pressure lowers the oil film temperature and increases frictional losses. This gives the possibility that both the absolute frictional loss and its rate of decline after the start of cranking could be controlled by optimisation of the lubrication system.

1.3 Objectives of this Thesis

The ultimate aim of this work was to investigate the limits on cold start performance and how this can be improved for a series of engine design types. In practical terms, a start time of six seconds at -20°C represents a benchmark standard. The first objective was to gain an understanding of the mechanisms limiting start performance in the engines studied. However, a large investment is made in modern engine designs, which are highly optimised for "normal" (fully warm) performance. At the time of undertaking this work, it was very unlikely that any changes would be implemented which could have an impact on operation beyond cold starting. Further objectives were therefore weighted towards investigation of those factors influencing cold start only.

Combustion studies can attempt to improve start quality by changes to fuelling (such as timing, quantity and rate of fuel injection) and starting aid parameters (such as glowplug timing, temperature and dimensions). Similarly, friction studies seek to identify and reduce sources of friction either by changes to component design or lubrication (such as oil viscosity, lubrication circuit changes and delivery pressures). Finally, changes in blowby and heat transfer losses could affect starting by limiting ignition and reducing useful work output. The main objectives of this work were therefore identified as:

- To understand the factors limiting cold start performance in the engines studied.
- To examine the effect of changes to combustion during starting (with investigations primarily limited to fuelling parameters and starting aids).
- To investigate engine friction during starting, identifying the main sources and possible methods of reduction.

- To quantify the effect of blowby on in-cylinder conditions and identify the likely result of piston or ring changes on start quality.

1.4 Thesis Layout

Chapter 2 describes the equipment used during this work, including test facilities and data acquisition systems. In Chapters 3 and 4, the cold start behaviour of the Ford 1.8 litre IDI engine is investigated. Measurements are made to determine how important start characteristics change with falling temperature in the standard engine. A model is developed to allow the output of the starter motor to be estimated with reasonable accuracy, which is used along with recorded cylinder pressure and speed data to evaluate actual frictional losses throughout starting. Comparing these with measured combustion output, represented as indicated mean effective pressure (IMEP), important information about cold starting is revealed.

In Chapter 5, measurements of the levels of blowby loss under motoring conditions are presented. A simple correlation is developed for cycle-averaged blowby, which is demonstrated to be applicable throughout cold starting until idle speed is reached. An improved model is presented, based on a more realistic model of gas flow. This predicts instantaneous mass flow rates, and is suitable for use in cycle simulation and theoretical investigations of blowby effects.

Chapter 6 describes how minor changes in the combustion system alter cold start performance in the Ford 1.8 litre IDI engine. These include fuelling changes (timing, quantity, and rate of injection), and changes to the glowplugs (temperature, timing and protrusion into the prechamber). In Chapters 7 and 8, engine friction is examined. Chapter 7 describes steady motored friction, measured in a number of engines, and the relative contributions of each engine component assembly are identified. Changes with speed and temperature have been investigated, along with the differences between the friction characteristics

of the engines. Chapter 8 details investigations into actual friction levels encountered during starting, which may be considerably larger than the steady state measured values. By reference to lubrication theory a qualitative description of the processes is developed, which attempts to describe not only the magnitude of this friction "spike", but also its duration.

The final chapter includes a general summary and statement of the major conclusions of this work.

1.5 Thesis Contribution to Diesel Engine Cold Starting

This thesis furthers understanding of diesel cold starting in a number of areas:

- Development of a starter system model allows engine friction to be found throughout cold starting from engine speed and IMEP measurements (given a knowledge of engine, starter and battery parameters). This allows simple determination of engine friction during this critical phase with a minimum of equipment. Results from a series of free-start tests have been verified by direct measurement on a motored engine, and found to agree closely. This representation can also be used as a sub-model for more complete engine simulation programs.
- Measurement of low temperature engine friction and its breakdown under quasi-steady conditions has revealed a very different distribution throughout the engine at low temperatures to that measured when fully warm. Additional measurements revealed initially higher levels of friction when the engine begins turning at low temperature; the magnitude and duration of this phase has been characterised for the data available. A simple model, initially

covering journal bearings only, has been devised to explain the observed behaviour.

Combustion, friction and starter motor work have been examined to formulate a qualitative description of cold start processes. An understanding of the balance which occurs allows a number of strategies for improvement to be identified, and the likely effectiveness of each assessed.

Chapter 2

EXPERIMENTAL FACILITIES AND DATA ACQUISITION

2.1 Introduction

Cold start behaviour studies are generally carried out over a range of sub-zero temperatures. A test temperature of -29°C (corresponding to -20°F) is important as a benchmark used by several vehicle manufacturers for the lowest temperature at which engines should start without external aids. However, carrying out parametric studies at this limit is made difficult by the low rate at which tests can be performed. Most of the work reported in this thesis was carried out at a temperature of -25°C or higher, to allow testing to progress more rapidly. Up to six cold start tests were possible each day. Temperatures up to fully warm (over 100°C) were possible.

Investigations have been carried out on several Ford diesel engines, and one competitor engine. The engine data recorded were selected from an extensive array of possible instruments according to the requirements of the test sequence. These included measurement of turning torque, speed, cylinder pressures, fuel injection parameters and engine temperatures. Sampling according to crank angle or time was used, as required.

2.2 Cold Cell Facilities

Several facilities for low-temperature studies have been developed for use in this investigation. These have been based around the common philosophy of enclosing the engine or engine compartment in a sealed cold cell. In some cases, the engine was mounted inside the cell on a test bed, and coupled to a

motor/regenerator outside the cell. When the test engine was mounted in a vehicle, the cold cell enclosed the entire vehicle front end, forward of the windscreen. In all cases, cooling and operating arrangements were similar.

To lower the engine temperature to the target values, refrigerated coolant was circulated through the engine block and head coolant paths. A small refrigeration plant of typically 2.5 kW heat rejection rate at the minimum rated temperature of -30°C is used. This chiller cools a mixture of 50/50 percent tap water and BS6580 ethylene glycol antifreeze, which is then pumped through the test engine and enclosure. This internal (or forced) cooling of the engine structure has been found to be particularly effective in previous studies undertaken at Nottingham [2.1]; the soaking times needed with conventional external cooling arrangements can be substantially reduced. Low temperature test conditions (-20°C) can be achieved in typically three hours starting from ambient, and subsequent tests can be carried out at relatively short intervals (usually one hour apart). Figure 2.1 gives a schematic of the arrangement used.

When the engine is to be cooled, circuit valves are set to allow the coolant to circulate from the chiller plant through the radiator and engine block. The engine thermostat is either removed or fixed open to allow coolant flow. A fan on the radiator (permanently active during cold soaking) cools the air in the enclosure, promoting surface heat transfer. Since the engine oil is very slow to lose heat, finned heat exchanger piping is placed in the sump to provide extra cooling. Control of the temperature across the entire rig (including coolant, metal, oil and air temperatures) is better than $\pm 1^{\circ}\text{C}$. To reach the minimum test temperature of $-25^{\circ}\text{C} \pm 1^{\circ}\text{C}$ required just under five hours from laboratory ambient. Temperatures to -29°C were possible, but over eight hours were required for soaking down.

For "normal" operations including hot running, the cooling circuit is restored to its normal configuration, with a valve (C in the figure) used to control the

temperature, replacing the thermostat. Depending on test requirements, extra cooling may be provided for in the sump, augmenting the action of the normal engine oil cooler (not shown). This may be required since the usual air flow over the engine and radiator due to motion of the vehicle is not present in the test rig. Other modifications may be made depending on test requirements, described in the relevant sections.

Firing-engine studies were carried out with the engine mounted in a test vehicle. The engine intake, electrical and fuel systems were enclosed in a temperature-controlled cell. This is similar to installations previously used at Nottingham [2.1], and is shown in Figure 2.2. The basic enclosure is constructed of 60 mm thick "Styrofoam" insulating material, clad in aluminium sheet. Special attention is given to sealing around the vehicle, including possible paths behind body panels, through the ventilation system and around underbody features. Around the transmission and exhaust, where the irregular shape prevented accurate fitting of the enclosure, glass fibre insulation was used. This has good insulation properties, while being unaffected by the high temperatures of the exhaust system.

Since the seal around the vehicle cannot be perfect, problems can arise where damp air from the laboratory leaks into the enclosure, causing excessive frost to form on the radiator. This reduces its effectiveness to the point where the enclosure air temperature eventually begins to rise. To avoid this, a feed of dry air was used. Air from the laboratory compressor was dried using a desiccator, reducing the dew point to below -70°C . It was then passed through a pressure regulator and air cooler, allowing a feed temperature into the enclosure down to -27°C . This arrangement maintains a dry atmosphere within the enclosure, preventing frosting. In addition, it allows the engine to be run for extended periods with the enclosure sealed, if required.

The vehicle electrical system was modified to allow the use of an external battery to power the starter motor and glowplugs. A fully charged battery of the type normally in the vehicle was used for each test, soaked to test temperature. A fuel tank of approximately 4 litres capacity, also cooled to test temperature, was used to feed the engine with Gulf 40 reference fuel. The small size of this tank ensured that the fuel used was always fresh. Motorcraft SAE 10W/30 oil was used throughout unless otherwise noted. Most testing consisted of free starts, with the vehicle out of gear and the clutch disengaged. However, the drive wheels were placed on a chassis rolls dynamometer to allow operation under load when required. The dynamometer (absorbing only) was primarily used when running at high temperatures to condition the engine between series of tests. Exhaust gasses were taken from the tailpipe to an extractor and safely vented outside.

2.3 Instrumentation

Good data acquisition is particularly important when investigating low temperature behaviour since, often, each test represents a considerable investment of time and effort. It is vital that as much information as possible is recovered from each test sequence, and that any possible problems are identified easily. Therefore, the acquisition system was designed to allow a large amount of useful data to be collected from each test. Instrument calibrations were checked at intervals throughout the life of each sensor, and through the entire measuring chain wherever possible. Data were sampled from different sensors depending on test requirements, but the sections below give an outline of the instruments used.

Data acquisition was controlled by an IBM-PC compatible used with a commercial input/output card. Software was developed in-house to allow 16 input channels to be sampled at $\frac{1}{2}^\circ$ (crank angle) intervals at speeds to over 2000 rpm. Typically about 200 engine revolutions were captured, but the maximum limit depended only on free memory and the number of channels to

be sampled. The 12-bit digital data were recorded to hard disc in compressed form, along with calibration information to allow later analysis. Before each test the software checked the calibration of the system against two internal reference voltages, to identify any possible problems. This system was also able to record data at fixed time intervals if required, with sample rate (up to 25 kHz) specified in a small configuration file that also controlled parameters such as channels to sample and calibration information.

Crank position was derived from an optical shaft encoder on the crankshaft, having two outputs: 720 pulses per revolution (used to trigger data sampling) and one pulse per revolution (used to identify the TDC position). The TDC marker pulse was placed as accurately as possible using the mechanical timing marks on the engine, and then the methods of Douaud and Eyzat [2.2] used to identify the exact position of TDC in cylinder 1. This encoder was also used to provide engine speed data, using a specially developed circuit to process the 720 pulses into a DC voltage. The circuit was based on a phase-locked loop, giving an output representing speeds up to 2000 rpm with a frequency response of about 30 Hz, allowing relevant changes throughout starting to be accurately recorded. Calibration was performed using a signal generator and frequency meter to simulate input from the shaft encoder.

Cylinder pressures were measured using Kistler 6123 piezo-electric transducers (200 bar range), mounted flush with the top of the main combustion chamber, used with Kistler 5011 charge amplifiers. Pressure transducer/amplifier pairs were calibrated using a Budenberg deadweight tester. Due to durability problems, the protective coating recommended by previous investigators to reduce measuring errors (originally by Brown [2.3]) could not be used.

For fuel injection analysis, a Kistler type 4065A strain gauge pressure sensor was mounted in the high pressure fuel pipe, as close as possible to the cylinder 1 injector. Used with a Kistler type 4617 amplifier, this had a full scale output at

1000 bar. The measuring chain was calibrated using the deadweight tester, as above. Needle lift in the cylinder 1 was measured using a specially modified fuel injector, driven by a Lucas FM oscillator and amplifier designed for this purpose. This was calibrated by moving the needle by external means and measuring the displacement by a "Millivision" position sensor (resolution better than 0.005 mm).

Temperatures were measured at several points around the installation using K-type thermocouples, calibrated against a standard PRT probe in a calibration bath. Enclosure air, engine coolant, sump oil, metal temperatures and others were recorded as required. Sampling of temperatures could be either continuous (simultaneously with other engine data) or immediately before and after the test. Reference junction compensation was performed in software, using the facilities of the data acquisition board designed for this purpose.

2.4 Test Procedures

Most of the testing reported here can be divided into two types: free-starts, and motored engine studies for friction breakdown analysis. Free-starts (engine start-up in neutral, without external assistance) were used to analyse cold start behaviour in firing engines. These allowed the influence of temperature, oil viscosity, cranking speed, fuelling parameters and so on to be studied. Motored friction analysis was used to assess the friction behaviour of various engine assemblies at different speeds and temperatures. Motoring friction testing and other procedures, such as the measurement of blowby losses, are described in the relevant chapters. The description below is for free-start tests, but similar consideration were applied in all testing.

After ensuring that there was fuel in the tank, that the engine oil was clean and at the correct level, and that there were sufficient fully charged batteries in the test cell, the cooling phase began. This involved lowering the entire engine bay,

including fuel and batteries, to the selected test temperature over a period of several hours. Once at the target temperature, the engine was cranked (without fuel injection) to ensure that the lubrication system was fully primed. This is referred to here as pre-cranking, and its importance is discussed below. After this period of cranking the starter battery was replaced with one of the fully charged batteries in the test cell. A further hour was then allowed, holding at the selected test temperature, to ensure that all temperatures were steady across the entire rig. After this time, the first cold start attempt was made.

Each cold start was designed to simulate normal operation closely, although compromises were made to allow more rapid testing. The ignition switch was closed to allow operation of the glowplugs for a time determined by the standard electronic controller supplied with the vehicle. Then, with the gearbox in neutral and the clutch disengaged, cranking commenced. This continued until either the engine started (reaching idle speed) or the test failed (after about 350 revolutions); in the latter case an extra battery was added to achieve a start. In all cases, the engine was run for 20 to 30 seconds at moderate speed (about 2000 rpm) to expel any unburned fuel left over from the attempt. The forced cooling was maintained throughout the test to prevent undue temperature rise, thus allowing the next test to be performed quickly. After changing to the next fully charged battery and waiting a further hour for temperatures to stabilise, the next cold start attempt was made. At the end of each day the engine was conditioned by bringing it to normal operating temperature and running under load for about 30 minutes. This conditioning run was carried out to encourage any fuel or water to evaporate from the sump oil, and deposits in the combustion chamber to be removed. Care was taken throughout testing to ensure the cleanliness of the engine oil, with the oil and filter being changed regularly: typically every 25 tests (under three hours total running time).

Under this regime up to six starts could be made each day. Analysis of the data collected shows that there was no measurable change in engine performance

between the first and last tests. This is illustrated in Figure 2.3, showing the start time and variability for an "average" sequence of consecutive tests, performed as described above. The data here are derived from about fifty cold starts collected at -20°C using the same oil type and engine configuration, but using different injection timings. For this reason, the results are normalised by dividing by the average start time *for each injection timing*, thus removing this as an influencing variable. The figure shows that start time and variability are independent of test number, confirming that later tests are not influenced by earlier ones.

If the engine is not pre-cranked, the first test is clearly quite different, as shown in Figure 2.4. This graph is based on a reduced number of tests, but clearly shows that starts are considerably shorter for the first test in each sequence, with increased variability. It has been found that this effect is caused by differences in the state of the lubrication circuit at the start of each test series, following a period of conditioning and a lengthy standing time. Although this may be closer to conditions in actual service, only one test per day could be achieved if this test method were employed. Additionally, the increased variability shows that conditions are not accurately repeated for this first test. For these reasons (extremely low test throughput and poor repeatability), pre-cranking was employed before testing, as described above.

2.5 Discussion

While care was taken with the installation and calibration of the equipment, there are naturally limits on the accuracy of any data collected. These arise due to uncertainties in calibration of the measuring chain and limits in equipment performance. Careful calibration reduces these errors to a low level in most cases: for example, temperature, speed, and fuel line pressure measurements are estimated to be within 1% FSD. However, some operations present special difficulties; in particular, a number of measurements require accurate pressure-volume data to be obtained. Brown [2.3] calculated that, for diesel combustion

studies, the error in pressure-volume phasing should be less than 0.1° to keep IMEP errors below 1%. Ball and others state that this phase error translates to a possible 4% error in FMEP [2.4]. Other authors [2.5, 2.6] suggest that a less onerous limit may be acceptable: 0.2° to 0.3° , depending on the rates of pressure rise. In the work described here, the methods of Douaud and Eyzat [2.2] were applied to achieve the best possible accuracy, estimated at between 0.1° and 0.2° (crank angle). The sample interval used here (0.5° crank angle) was adequate for even the most sensitive analysis [2.6].

The difficulties faced when measuring cylinder pressure are widely reported [2.3, 2.5, 2.6], particularly the problems associated with short term drift in the pressure sensors [2.7]. Due to installation and operational difficulties, this work used non-cooled transducers showing moderate short term drift [2.8] without any protective coating [2.3]. The resulting drift (caused by thermal "shock" to the sensor during compression and combustion) may reduce the measured IMEP by 0.2 to 0.4 bar, depending on operating conditions. This also makes meaningful analysis of the gas exchange process impossible, so this part of the cycle was neglected (pressures set to atmospheric). This simplification was tolerable since, at the low speeds studied here, very little pumping work was required. To obtain a reference point for the recorded pressures, atmospheric pressure was selected at TDC in the open part of the cycle. At this point the piston is stationary, with both inlet and exhaust valves open, while the low engine speeds mean that the turbocharger is inactive and the pressure drops across the inlet and exhaust systems are minimal. Selection of this reference point has no impact on IMEP or friction calculations. Note that only one pressure transducer was used in each cylinder, placed in the main combustion chamber. This allowed accurate calculation of IMEP, but any combustion calculations will be subject to errors due to the (unmeasured) pressure drop through the prechamber throat.

To achieve a higher rate of testing, compromises were made during the free start testing programme, which may lead to differences compared to "normal" cold

climate operation in the field. The rapid rate of cooling employed before the first test may cause the engine oil to behave differently to the more traditional cold soaking schedule, as shown by Henderson [2.9] and May and Smith [2.10]. The forced cooling was maintained throughout testing, preventing any rise in water jacket temperature through the start. This has been found to reduce variability and slightly lengthen starts. With the tests carried out at one hour intervals and a period of pre-cranking before the first test, it was found that the lubrication system remained primed between tests, especially at lower temperatures. Thus the effect of leaving the vehicle to stand overnight is not simulated, where the engine oil would drain to some extent from the engine, oil pump and filter. In addition, modifications to allow a separate battery for each test (for glowplug and starter power) may alter start performance. Longer battery leads are generally required, but different cable types and the slight reduction in battery load (since the cranking battery does not power other vehicle systems) makes the overall effect unclear. However, the limitations described above are offset by the ability to achieve relatively rapid testing with good repeatability. These tests allow direct comparison when any one variable is altered.

2.6 Conclusions

The experimental arrangement developed at Nottingham has proved capable of supporting a test schedule of typically six tests at -20°C each working day. An absolute minimum temperature of -29°C could be achieved, but only one test cycle per day was possible in this case. The minimum test temperature was limited by the capacity of the cooling plant used.

Several possible difficulties have been identified, resulting either from measuring problems or limitations in the experimental methods. These have been minimised wherever possible (consistent with the required rate of testing) to allow collection of the best possible data. While it is accepted that the results obtained may not be exactly representative of actual conditions in service, it is felt that they give

a good approximation and are suitable for the research purposes described in this thesis.

Chapter 3

BASIC START CHARACTERISTICS, IDI ENGINE

3.1 Introduction

The following contains details of cold start data collected from the Ford 1.8 litre IDI diesel engine in standard production form. This engine variant was used for most of the starting and combustion studies described in this thesis, and is representative of IDI designs in current production. Detailed analysis of the starting process covering combustion calculations, friction measurements, and energy balance evaluations is given in later chapters. Here, the aim has been to identify the general changes in start characteristics which occur with falling temperature, and to provide a reference set of data against which the effect of engine modifications may be evaluated. Characterisation of start behaviour is made in terms of the times to complete each of the three main phases identified within the start: the period up to the start of combustion, the period throughout which input is required from the starter motor, and the total period up to idle speed. These initial investigations cover the effects of cranking speed, oil viscosity and ancillary loads as start temperature is lowered.

3.2 Basic Start Performance

The Ford 1.8 litre IDI diesel engine was used in its production form, as fitted into a 1994 model "Sierra" vehicle, with the standard mechanical fuel injection system used throughout [3.1]. The turbocharged engine variant was used, as detailed in Appendix A. Motorcraft engine oil was used, with SAE 10W/30 grade used down to -20°C and 5W/30 below this point, unless otherwise noted.

As described in Chapter 1, a typical cold start can be divided into several stages. Here, the duration the phases are called the time to first fire, time to sustained fire and time to idle (t_{ff} , t_{sf} and t_{idle}). Also recorded for each start are the misfire rate, glowplug pre-heat times (the period before cranking when the glowplugs are active) and the minimum, average and maximum cranking speeds.

3.2.1 Effect of Ambient Temperature

As test temperature is lowered, the time to achieve first fire rises slowly at first, and then relatively rapidly below -10°C , as shown in Figure 3.1. The time to idle speed rises in a similar manner, but the changes are much more pronounced: above 0°C , idle is reached in under one second, rising sharply below -10°C to an average of about 34 seconds at -20°C . This rapid rise below a critical temperature suggests that, below this point, either: useful combustion cannot be achieved, or combustion output is unable to overcome rising friction and other losses.

Cranking speed falls progressively with falling temperature due to the increase in frictional losses associated with rising oil viscosity [3.2, 3.3] and a simultaneous fall in battery output [3.4, 3.5]. This is illustrated in Figure 3.2, showing data collected using SAE 10W/30 viscosity oil down to -20°C , the minimum temperature for which this oil is recommended. The reduction in cranking speed makes starting progressively more difficult as blowby (the flow of cylinder gasses past the pistons into the crankcase) and heat transfer losses increase, leading to difficulty achieving ignition and a loss of useful output during combustion. Indeed, the manufacturer of this engine specifies the less viscous SAE 5W/30 grade oil below -20°C partly in order to maintain an adequate cranking speed for starting.

Instantaneous engine speed traces show that, for temperatures above -10°C , firing commences in four to six strokes. The difference in times to first fire is due to changes in engine cranking speed, which alter the time to the first and subsequent

fuel injections. For the data collected below -10°C , combustion may commence much later, with up to twelve strokes required before firing is observed. This not only contributes to the longer average time to first fire, but to the increased variability observed. After firing is achieved, combustion is fairly consistent: misfires occur in only 10-15% of cycles up to idle, and are largely unaffected by changing temperature.

Changes in time to first fire make up only a small part of the observed change in time to idle speed. Therefore the problem is not in obtaining firing cycles but in achieving enough useful combustion work to overcome friction and other losses. Once enough combustion output is available (that is, after achieving sustained fire at t_{sf}) idle speed is quickly reached, but tests show that below a critical temperature, there is an extensive period of firing-assisted cranking. Speeds during this phase are well above those achieved by unaided cranking, but combustion does not provide quite enough power to complete the speed run-up to idle. This phase makes up an increasing proportion of the start time as temperature decreases, as Figure 3.3 shows.

3.2.2 Effect of Cranking Speed

In order to separate the effects of temperature and cranking speed, tests were performed where the power to the starter motor was deliberately reduced by introducing extra resistance into the starter circuit. This had the effect of lowering cranking speed at any given temperature. The speeds achieved are presented in Figure 3.4; temperatures below -10°C were not included due to the extremely low minimum speeds obtained.

Reducing cranking speed causes start quality to deteriorate considerably, especially at lower temperatures, as shown in Figure 3.5. The increased time to first fire is partly due to the longer time to the first and subsequent injections, but also because firing does not commence for several strokes. At normal cranking

speeds, firing typically commences after five fuel injections at -10°C and three at -1°C . Lower speeds require double the number of injections to achieve first fire under the same conditions. In the limiting case, cranking too slowly leads to complete failure of combustion, making starting impossible. The figure shows that time to idle speed is lengthened considerably over this temperature range. In this case, this is mostly as a result of changing time to first fire, although there could be an effect on firing assisted cranking that is not apparent at these temperatures.

3.2.3 Effect of Oil Viscosity

In order to reach idle speed, the useful work produced by combustion must exceed all the losses in the engine and associated equipment. This suggests that start performance will be improved when using a lower viscosity engine oil to reduce friction [3.2, 3.3]. To examine this possibility, start tests were repeated using a less viscous SAE 5W/30 graded engine oil. The kinematic viscosity of this oil is similar to the SAE 10W/30 at higher temperatures, but considerably reduced at lower temperatures, as shown in Figure 3.6 [3.6].

At higher temperatures, oil viscosity is relatively low and the absolute difference between SAE 5W/30 and 10W30 oils has a negligible effect on cranking speeds. At sub-zero temperature the effect is more marked, with a 13% rise in cranking speed observed at -25°C , as illustrated in Figure 3.7. Start quality is also improved slightly by changing to the lower viscosity oil. The data given in Figure 3.8 reveal that this improvement is due to shortening of the firing-assisted cranking phase rather than the time to achieve first fire. Note that in exploratory tests at -25°C with the SAE 10W/30 oil, no starts could be achieved within 350 engine revolutions.

3.2.4 Effect of Ancillary Loads

High frictional losses in engine ancillaries and their associated drive arrangements may be expected to lengthen starting times, both by reducing cranking speeds and by absorbing some of the combustion energy which would otherwise be available to accelerate the engine. Conversely, any reduction in this parasitic loss would be expected to improve start quality, in a similar way to reduced oil viscosity. This has been investigated by carrying out tests where the non-essential ancillaries were removed from the test engine. By removing the relevant drive belts, losses due to the power steering pump, coolant pump, alternator, two poly-vee drive belts and idlers were eliminated. Comparative tests were performed using the less viscous SAE 5W/30 graded engine oil, to make the effect of changing ancillary loads more easily measurable. Figure 3.9 shows the impact of removing the ancillary loads on time to idle speed. Changes to cranking speed and first fire were minimal. It can be seen that the impact at higher temperatures (over -10°C) is negligible, but that the effect becomes significant by -20°C where a reduction of over six seconds (about 25%) in start time results.

3.3 Conclusions

Reducing ambient temperature causes a progressive fall in cranking speed, due to reduced starter output (primarily due to reducing battery performance) coupled with increasing friction (due to rising oil viscosity). Lower cranking speeds correspond to a greater delay before firing commences. This longer delay is due to increased heat transfer and blowby losses which lower temperature and pressure in the cylinder at the time of fuel injection. If the cranking speed drops too far firing cycles may either fail to occur or become so infrequent that starting fails.

Starting at temperatures above -10°C is rapid. Firing commences almost immediately and the engine reaches idle speed in typically under one second. As the temperature drops below this range, a period of firing-assisted cranking begins to become dominant. During this phase many firing cycles occur, but not enough output is generated to accelerate the engine up to idle speed. A plateau speed is reached at which the starter motor remains engaged and assists in maintaining engine rotation. Typically this is in the range from 200 to 400 rpm. After a period of this firing-assisted cranking, which may account for up to 95% of the total start duration, the engine will accelerate to idle speed without further need of the starter motor (sustained fire is reached). The periods up to first fire and after sustained fire are relatively insensitive to start temperature. As described in later chapters, combustion and starter motor output are balanced against frictional losses during the firing-assisted cranking phase. The engine cannot be accelerated further because the power output of the starter motor falls rapidly towards zero at engine speeds above about 500 rpm.

Measures taken to reduce total engine friction, such as removing ancillaries and using less viscous oils, shorten start times by reducing the firing-assisted cranking phase. These do not significantly alter other stages of the start-up. At higher temperatures rapid starts are possible because the friction losses are relatively low compared to the work output produced by combustion. In this case, the firing-assisted cranking phase of the start-up is effectively eliminated.

Chapter 4

CONSTRAINTS ON START QUALITY, IDI ENGINE

4.1 Introduction

The data presented in Chapter 3 shows that, at lower temperatures, a long period of firing-assisted cranking makes up much of the total start time of the Ford 1.8 litre IDI diesel engine. During this period, a balance is maintained between frictional losses and the work available from the starter and combustion. A more detailed understanding of this constraint is developed in the following, based on further experimental studies and construction of a model which allows the relevant effects to be studied more systematically.

Understanding conditions controlling speed variations during low temperature starting has been approached by investigating the balance of work done on the crankshaft. The terms taken into account are: the work done on the piston by cylinder gasses, the work done on the engine by the starter, the total frictional losses in the engine and ancillaries (but not including gas pumping work), and the effective brake output available at the crankshaft. In each case, these are expressed as mean effective pressure values (IMEP, SMEP, FMEP and EMEP respectively), obtained by dividing the work per cycle by the cylinder volume displaced:

$$\text{MEP [bar]} = \frac{\text{Work per cycle [J]}}{\text{Swept Volume [m}^3\text{]} \times 10^5 \text{ [Pa/bar]}} \quad (4.1)$$

From equilibrium of work input and output at the crankshaft, the relationship between these four pressures is given by:

$$\text{IMEP} + \text{SMEP} = \text{EMEP} + \text{FMEP} \quad (4.2)$$

In order to eliminate the effect of reciprocating masses, the energy balance is evaluated for each complete stroke.

IMEP is evaluated in the conventional way from pressure-volume data recorded in all four cylinders of the engine, over a range of speeds and temperatures. In the ideal case, IMEP would be evaluated based on the integral of cylinder pressure with cylinder volume over the complete cycle. This would give the net IMEP acting on the piston and includes any contribution during the gas exchange phase. However, as described in Chapter 2, thermal shock in the cylinder pressure sensor prevented analysis of the open part of the cycle. IMEP was therefore evaluated only over the closed part (compression and expansion strokes), ignoring the gas exchange phase; this is referred to as the gross IMEP. The difference between gross and net values is associated with undesirable flow losses through the inlet, exhaust and valves, and possible action of the turbocharger at higher speeds. However, since the cycles of interest here occur at low engine speeds, the work done on the gasses during the neglected strokes is insignificant. In this analysis, gross IMEP values are used throughout, but are almost identical to net figures.

EMEP represents the effective brake output. Brake output at the flywheel, BMEP, would normally be evaluated by analysis of output torque, measured at steady speed by a dynamometer. In the free start testing reported here BMEP is zero, as the engine is started in neutral with no output taken from the flywheel. Instead EMEP is used, representing the energy which goes into accelerating the engine. It was evaluated by considering the change in engine speed over the

stroke, coupled with the known inertia. This allows the work done, W_{INERTIA} , to be evaluated from:

$$W_{\text{INERTIA}} = \frac{1}{2} I_{\text{ENG}} \times (\omega_E^2 - \omega_B^2) \quad (4.3)$$

where ω_B and ω_E are the engine angular velocity at the beginning and end of the stroke respectively, and I_{ENG} is the engine inertia. Inertia for the total engine is approximated by that for the flywheel and pressure plate assembly, crankshaft and big ends (Appendix A). W_{INERTIA} is then used to derive EMEP, using equation (4.1). This leaves the starter and friction work, SMEP and FMEP, unknown in equation (4.2). Although the friction contribution is not measured directly, starter input was calculated using a suitable model, described below, when the FMEP can then be inferred.

4.2 Starter Model Development

To calculate starter motor input, models for the entire electrical system involved in starter operation are required: the battery, connecting leads, starter motor and gearing, and any other relevant electrical loads. The model has been developed from a set of assumptions and component experiments. It allows the starter input to be calculated over a more general range of speeds and temperatures without further specific measurements being made.

4.2.1 Battery and Lead Characteristics

The lead-acid batteries used in this work (specified in Appendix A) are described in the model by the equivalent circuit of Figure 4.1, with the lower graph showing values used at different temperatures. These values were determined by measurements made on a set of five fully charged batteries, soaked to the test temperature for several hours.

Open circuit voltage, V_b , was measured directly at the battery terminals with no current flowing. Since this value drops as the battery becomes discharged, it was measured both before and after a cold start. The mean of these two figures was then used, in an effort to obtain a value close to the "average" condition during starting. The five-battery average figures are shown, rising from 12.0 V at -29°C to 12.8 V at $+10^{\circ}\text{C}$.

Internal resistance, R_b , is a measure of the drop in voltage at the battery terminals when current is drawn, and cannot be measured directly. Instead, a high power resistor was used to draw up to 250 A, with the battery terminal voltage and current recorded throughout. Simple application of Ohm's Law then allows calculation of R_b . Again, the five-battery averages are shown, falling from 7.5 m Ω at -29°C to 5.9 m Ω at $+10^{\circ}\text{C}$.

Lead resistance, R_L , could not be measured accurately by direct methods, due to its very low value. Instead, it was calculated by measuring the voltage drop across the lead with a known current flowing (again, up to about 250 A). As before, Ohm's Law allowed the resistance to be calculated: for the installation here, a total lead resistance of 1.09 m Ω was measured. This included not only the leads themselves, but all associated crimped and bolted connections.

The combined effects of the changes in R_b and V_b result in a considerable fall in battery output with changing temperature. For example, if 400 A (not an unreasonable starting current) is drawn at $+10^{\circ}\text{C}$, about 4.2 kW will be delivered to the load; at -29°C this drops to about 3.6 kW. An additional 170 W must be subtracted from these figures if the resistance of the leads is included. These effects add to the difficulty in starting the engine at low temperatures both by reducing cranking speeds (making it more difficult to achieve firing cycles), and by reducing the energy input by the starter during the phase of firing-assisted cranking.

4.2.2 Starter Motor Characteristics

The manufacturer of the motor supplied data in the form of graphs showing starter voltage, speed, and torque against starter current, measured at various temperatures from -29°C to +10°C [4.1, 4.2]. This information enables the calculation of the effective electrical "resistance" of the motor at each temperature and speed, as well as the input and output power at each condition to allow determination of the efficiency. The effective resistance and efficiency were found to vary only slightly with changing temperature over the range for which data were supplied, and subsequently these variations have been neglected. However, both parameters are strongly dependent on starter speed, ω_s , as Figure 4.2 shows. They are represented in the model as functions of starter speed: $R_s(\omega_s)$ and $\eta_s(\omega_s)$ for effective resistance and efficiency respectively. Thus, if the starter motor speed and terminal voltage, V_s , are known, the output power, P_{OUT} , can be calculated from:

$$P_{OUT} = \frac{V_s^2}{R_s(\omega_s)} \times \eta_s(\omega_s) \quad (4.4)$$

A model in this form can be used to estimate starter output at any given speed, over the temperature range -29°C to +10°C. There is no reason to believe that the model could not be extended to cover a greater range of temperatures provided that data were available to verify that single curves for starter effective resistance and efficiency were still valid.

4.2.3 Complete Starting System Model

The complete starting system was modelled by combining the component elements described above; the equivalent circuit is shown in Figure 4.3. During test work, the starting system was powered using a separate battery to that

supplying other vehicle systems. In this case, the only electrical loads to be considered are those associated with the glowplugs and the motor itself.

Equation (4.4) can be used to calculate starter output power, if the voltage across the motor, V_s , is known. If the glowplugs and associated cables are represented by a resistance R_G , then the total battery current, I_B , must be evaluated. This is equal to the sum of starter and glowplug currents ($I_B = I_s + I_G$). It was found that the glowplug current (controlled by the resistance R_G) required a complex model to give a good representation, due to a basic dependence temperature coupled to rapid changes in current with time. However, the contribution to I_B is typically less than 10% at cranking speeds and can be neglected under these conditions. At the higher speeds reached during firing-assisted cranking, the starter current is lower and I_G becomes more significant. Under these conditions, however, the contribution of the starter is relatively small compared to combustion work, so the accuracy of the starter model is correspondingly less important. This allows the simplifying assumption to be made that the glowplug resistance is infinite and hence the current is zero ($R_G = \infty$, $I_G = 0$). Therefore, since $I_B = I_s$, the voltage across the starter motor is given by:

$$V_s = V_b \times \frac{R_s(\omega_s)}{R_s(\omega_s) + R_L + R_b} \quad (4.5)$$

Combining equations (4.4) and (4.5) gives an equation for output power, P_{OUT} :

$$P_{OUT} = \frac{V_b^2 \cdot R_s(\omega_s)}{[R_s(\omega_s) + R_L + R_b]^2} \times \eta_s(\omega_s) \quad (4.6)$$

Figure 4.4 shows how modelled output power and torque change with speed. Solutions at -29°C and $+10^{\circ}\text{C}$ are shown, demonstrating the considerable change in output with changing temperature.

4.2.4 Application to Engine Start Data

The model described by equation (4.6) allows the starter output power to be calculated at any speed, based on simple functions (or tables of values) describing changes in battery and starter motor performance with speed and temperature. The model allows the input from the starter motor to be calculated for real cold start tests, and hence values for engine friction can be inferred. The method used involves calculation of instantaneous starter speed to give starter input evaluated over each complete stroke.

Instantaneous speed has been calculated in 360 steps per stroke, corresponding to the samples obtained during data acquisition. At the start of the first stroke, the starter speed was set to zero; subsequent strokes used an initial value based on the end of the previous stroke. Initially assuming the starter to be disengaged, speed at the next step was calculated using the known inertia of the starter and the value of P_{OUT} from equation (4.6). This was then compared with measured engine speed data; if it was higher (after accounting for the gearing), then the motor must be engaged with the flywheel and true starter speed was set from measured data. However, if the calculated value was lower, the starter was disengaged (on its overrun clutch) and the calculated speed was used as the initial condition for the next step.

Figure 4.5 shows measured engine speed and calculated starter speed (referred to the crankshaft) for cranking at $+19^{\circ}\text{C}$. Note that, for demonstration purposes, the starter power was limited during this test by increasing the lead resistance ($R_L \approx 20 \text{ m}\Omega$). This separates the two speed traces in the figure for clarity. Under these conditions the starter motor is free-running from about 180° to 270° (that

is, during the expansion stroke). When the starter motor re-engages with the flywheel, it causes a series of "spikes" in the measured engine speed trace, drives the engine through the compression stroke, and disengages again at about 360°. Although exaggerated by the lowered starter power in this case, this cycle of free-running and driving is typical of starter operation over a wide range of temperatures.

During calculation, the work done by the starter, both on the engine and on its own inertia, was evaluated by integration of P_{OUT} with respect to time. At the end of each stroke, a simple energy balance is applied to evaluate the work done by the starter on the engine. The total work done, $\int P_{OUT} dt$, was known, as were the initial and final speeds of the starter motor. The useful work transferred to the engine was simply the total minus any change in rotational kinetic energy of the starter motor (ignoring friction in the starter).

There are a number of factors which may affect the accuracy of model predictions. Potentially the most serious is that generic specifications are used to describe that starter and battery. The specification of starter characteristics is derived from typical values supplied by the manufacturer, and the parameters are for an "average" battery. In practice there are differences in battery performance and potentially large differences between starter motors. The actual variance of each specific component from these averages is unknown; calibration of each would be required for improved accuracy. Similarly, neglecting the effects of glowplug current, slight changes in starter characteristic with temperature, ohmic heating of the starter system, and changes due to battery discharge throughout starting. The impact of omitting these considerations is small but difficult to quantify.

This model for SMEP was used in equation (4.2), leaving FMEP as the only unknown. Figure 4.6 shows how the separate terms make up the calculation of FMEP for a period of firing-assisted cranking at -20°C. EMEP was very small

over the interval shown, due the small speed changes throughout each revolution; it is not shown in the figure. The shape of the FMEP line gives a good indication that the SMEP calculation is quite accurate: the friction does not vary despite large fluctuations in measured IMEP. Over the 40 revolutions shown in the figure, FMEP falls smoothly from 9.5 bar to 7.6 bar. Data collected from a motored engine under similar conditions allowed direct measurement of FMEP; the initial value of 10.0 bar agrees well with the calculated value here.

4.3 Basic Combustion Analysis

The useful combustion output is represented by the indicated mean effective pressure, IMEP, described above. This gives a measure of the work done by the cylinder gasses on the piston. Examination of the way in which IMEP changes with speed and ambient temperature can give important insight into the mechanisms controlling cold starting, and areas requiring attention in order to improve performance may be identified.

To achieve rapid cold starting, the combustion of fuel in the cylinder should commence within a few injections, and enough useful work should be transferred to the crankshaft in each stroke to accelerate the engine against friction and other losses. As described earlier, at lower temperatures combustion does not release enough usable energy to accelerate the engine without continued aid from the starter motor. At higher temperatures (above about -10°C) the situation is better, with combustion output quickly accelerating the engine to idle speed, either because IMEP is higher or FMEP is lower. Looking at the variation of IMEP with engine speed at two temperatures (Figure 4.7), indicates that changes in IMEP are not the prime effect. In the non-firing cycles under cranking conditions, blowby and heat transfer losses contribute about -2 bar to IMEP at both -20°C and $+10^{\circ}\text{C}$. In firing cycles, the IMEP at both temperatures appears to be similar up to about 450 rpm: starting from -2 bar at cranking speed, it rises

sharply to 4 bar at 250 rpm and thereafter more slowly to 5 bar at 350 rpm and almost 6 bar at 450 rpm.

The speeds up to 450 rpm are critical during starting, since this covers the range of firing-assisted cranking which dominates start times at lower temperatures. Since, over this range, the IMEP is unaffected by temperature, it seems that changes in combustion are not the primary cause of reduced start quality at low temperatures. At higher speeds, as idle conditions are established, the characteristics appear to separate. The IMEP at -20°C is higher than at $+10^{\circ}\text{C}$. This may be explained by the action of the fuel pump idle governor, coupled with different friction levels in each case. At steady idle speed with no load on the engine, all the useful combustion output goes to overcoming friction, with the injection pump cutting down the fuel (therefore controlling IMEP) to balance the two. In this case we may surmise from the figure that the friction at idle speed is about 4 bar at $+10^{\circ}\text{C}$, rising to about 7 bar at -20°C .

4.4 Friction Throughout Cold Starting

Application of equation (4.2), in conjunction with the starter model of equation (4.6), allows engine friction throughout starting to be calculated from free start data. The results show that the initial level of friction is very dependent on start temperature, as Figure 4.8 shows. Comparing this with Figure 4.7, a fundamental difficulty with starting this engine is revealed: below -10°C , the maximum IMEP of about 7 bar is less than the initial FMEP values. However, FMEP falls steadily with time after the start of engine cranking, eventually allowing the speed run-up to idle to be completed. At -20°C , about 100 revolutions were required before the friction drops to the point where IMEP exceeds FMEP and idle speed was reached. Start quality at these lower temperatures can therefore only be improved by either raising IMEP or reducing friction considerably.

Changing to the less viscous SAE 5W/30 oil gave slightly reduced friction levels (Figure 4.9), which would explain the previously reported improvements in start time noted in Chapter 3. With this oil, a reduced number of turns was required for the friction to reach the critical level (about 75 revolutions to reach 7 bar at -20°C). As an approximate measure, this equates to an improvement of 4-8 seconds at typical firing-assisted cranking speeds of 200-400 rpm. This compares favourably with the improvement of about 8 seconds observed in start tests. The change in friction when the non-essential ancillaries were removed is less marked, as illustrated in Figure 4.10. The change was not easily measurable at higher temperatures, but the time to 7 bar reduced from 75 to about 60 revolutions at -20°C. Making an estimate as before, this corresponds to about 2-4½ seconds at typical firing assisted cranking speeds, compared with the measured change of about 6 seconds.

4.5 Constraints on Start Quality

The work described in previous sections allows the main constraints on start quality to be identified. At higher temperatures (Figure 4.11), firing commences almost immediately (on the second stroke), with the IMEP exceeding the FMEP (5½ bar against just over 4 bar). The engine quickly accelerates to idle speed, where the injection pump reduces fuelling until the combustion work matches the friction losses. This happens in only a few engine revolutions, with the start time being controlled by the rate of acceleration in the run-up phase. This is controlled by the effective brake MEP available, EMEP (equal to IMEP + SMEP - FMEP) and the inertia of the engine.

At lower temperatures (Figure 4.12), about four strokes are required to achieve strong firing cycles, but this period is insignificant when compared with the total start duration of over 100 revolutions. The IMEP achieved after first fire is similar to the higher temperature case (about 5½ bar), but this is far short of the frictional loss of almost 10 bar, and an extended phase of firing-assisted cranking

is entered. The friction gradually falls, with the engine rotating at about 300 rpm under the influence of steady firing and the starter motor. As the FMEP falls further, the speed begins to climb. This has the effect of raising the IMEP because of the dependence of IMEP on speed (refer to Figure 4.7), which causes the speed to rise further. However, the engine still does not start, since the output from the starter (still required to maintain rotation) falls off sharply as speed rises. Finally, after some 115 revolutions, the friction drops to such an extent that the IMEP is greater than FMEP, and the engine can run without the support of the starter motor. At this point, the engine runs quickly up to idle speed, and the start is complete.

4.6 Conclusions

The output available from combustion in the Ford 1.8 litre IDI engine is insensitive to temperature, but extremely sensitive to engine speed. IMEP values of about 7 bar can be generated at engine speeds above about 500 rpm, but are considerably reduced at lower speeds. As geared, the starter motor work input to the crankshaft falls more rapidly than combustion work rises with engine speed. At low temperatures, the sum of SMEP and IMEP balances initial frictional losses at less than idle speed, and rapid starting is not achieved.

A model for starter motor input has been developed. This, along with a simple energy balance equation, allows total engine friction to be evaluated throughout cold starting. The friction has been shown to rise sharply with falling temperature, reaching an initial value of about 10 bar with the SAE 10W/30 grade oil at its minimum operational temperature of -20°C . However, this frictional loss is observed to fall steadily with time, allowing the engine start to be completed eventually even at the lowest temperature examined. Changes in start time due to viscosity reductions and the removal of non-essential ancillaries have been investigated. The experimental results have been explained by examination of the

resulting friction changes, showing that a given reduction produces a predictable improvement in start quality.

Above a critical temperature, (about -12°C for 10W/30 and -15°C for 5W/30), the firing IMEP exceeds FMEP at the start of the test, and the engine will start quickly. Below this temperature, IMEP is insufficient to overcome initial friction and the start begins to extend. In this case, there is a period of firing-assisted cranking while the friction falls to meet the available IMEP. Engine will not start until IMEP exceeds FMEP; up to this point, the speed cannot exceed 450-500 rpm, because input is needed from the starter motor.

Decreasing either the time to first fire or the run-up time after sustained fire would give only a relatively small improvement, and would only be useful after other areas have been addressed. To achieve a more useful improvement in start times, two main strategies can be formulated from interpretation of the results obtained. These are based on either increasing IMEP by changes to the combustion system, or decreasing the absolute level of friction. The former may be achieved by changes to blowby or heat transfer factors, fuelling strategies, combustion chamber design, or glowplug parameters. Measures which might be taken to reduce friction are more difficult to define and relevant further investigations are described in later chapters. However, it has been shown here that reducing FMEP improves start time as expected, although only limited changes were possible. Changes to the lubrication system, ancillaries or bearing surfaces may give further improvements. Similar changes may also increase the rate at which friction falls during firing-assisted cranking.

Chapter 5

BLOWBY MEASUREMENT AND ANALYSIS

5.1 Introduction

Blowby is the leakage flow of cylinder gasses past the pistons and into the crankcase. This flow occurs because of the imperfect sealing of the piston rings and the pressure differential between the cylinder and crankcase. The mass loss due to blowby, typically a few percent of the charge trapped at inlet valve closing, reduces the temperature and pressure of the charge, affecting the probability of successful compression ignition when fuel is injected. The effects of blowby on cold starting are potentially serious. Because cylinder pressure and temperature are changed, heat transfer losses are also altered. Without independent knowledge of either blowby or heat transfer, the influence of these cannot be separated.

The study reported in this chapter has been carried out to assess the importance of blowby to cold start performance. The experimental work provides quantitative data on blowby rates. Initially, blowby was correlated using a simple function, developed from incompressible flow formulae. This correlation provides a conveniently simple rationalisation of net blowby per cycle. Subsequently, to examine conditions within the cycle, a model has been developed from a more fundamental description of the blowby process.

5.2 Background

Brunner and Ruf [5.1] reported that lower cranking speeds were encountered at low temperature, due to increased engine friction and reduced battery

performance. A reduction in cranking speed with falling temperature has been observed by many other investigators [5.2, 5.3, 5.4]. Henein and others [5.5, 5.6] have observed that blowby increases sharply as engine speed falls, reaching about 10% of the trapped mass at 200 rpm. It was suggested that this level of blowby could result in reduction of some 100°C in peak cylinder temperature in the direct injection diesel engines studied. Therefore, this rapid rise in blowby is likely to have an important influence on cold starting.

Henein reported no significant change in blowby with changing temperature at constant speed (from below -40°C to +20°C). Neveu [5.7] reported that, in two fully warm test engines at 1500 to 2500 rpm, blowby was reduced by using monograde engine oils of higher viscosity. It has been shown by Austen and Lyn [5.8] that fuel injected into a diesel engine under cranking conditions can reduce blowby by assisting ring sealing. Wentworth [5.9] reported that blowby flow was dominated by the area of the smallest piston ring gap, although Munro [5.10] points out that the ring gap "effective area" is altered by numerous factors including temperature effects (changing clearance, bore distortion), supporting lands (clearance, chamfers), groove, bore and ring condition (deposits, progressive wear) and motion effects (ring twist, piston slap). Measurements made by Furuham and other workers [5.11] showed that the "effective area" through which blowby occurred could be up to at least six times that due to the ring gap.

Many mathematical models describing blowby have been developed, of varying complexity. The simplest models assume a single piston ring, with compressible gas flow through the ring gap, such as that proposed by Rao, Gardiner and Bardon [5.12]. In this model, the ring gap was assumed to be fixed, with no movement of the ring from the bottom face of its groove, and with the gas flow being cooled to metal temperature by the large surface area. To obtain good agreement with experimental results, the leakage area had to be raised as a reciprocal function of speed below 1000 rpm. When used with suitable heat

transfer models, reasonable predictions of cylinder temperature and pressure in a small diesel engine were made. The model predicted that blowby (together with heat transfer) caused a significant reduction in peak cylinder temperature and pressure, especially at lower speeds, leading to possible starting difficulties.

A more complex model considers the path from combustion chamber to crankcase as a series of connected volumes separated by the compression rings, such as that described by Munro [5.10]. In this work, similar assumptions to the above are employed. Additionally, it was assumed that the pressure was uniform within each volume, pressure above the top ring was equal to cylinder pressure, and that there was no pressure drop across the oil control ring. Munro reported that, for a variety of engines, the deduced leakage areas were 1½ to 6 times those predicted by measurement of the ring gap; this agreed well with other workers [5.11]. No data were presented to allow correlation between this model and instantaneous measured results to be judged.

The most complex model reviewed here is represented by the work of Namazian and Heywood [5.13]. This is based on the connected volume model described above, with additional allowance for piston ring motion, as suggested by Furuhashi and other workers [5.11]. Experimental results were reported which verified that the gas flowing through the crevice regions could be assumed to be at metal temperature. Using similar assumptions to the works above, this model was able to make predictions that agreed closely with observed data.

5.3 Experimental Study of Blowby

An initial study was carried out using the Ford 1.8 litre IDI engine (turbocharged variant) under cranking conditions. Using this engine, the effects of ambient temperature and cranking speed were examined, along with measurement of the individual contribution of each cylinder to total blowby. This study was then extended to include the basic blowby characteristics of various other test engines

under unfuelled cranking (or motoring) conditions. Additionally, the impact of fuelling and firing cycles on blowby was examined.

Figure 5.1 is a schematic of the system used to measure blowby to the crankcase. Blowby gas from the crankcase was exhausted to atmosphere through a (wet type) positive displacement gas meter, with measurement of gas temperature and pressure to allow the cumulative mass to be calculated. All possible leakage paths from the crankcase were sealed to ensure that all blowby was measured; pressure in the crankcase was not measurably changed by these alterations. The gas meter was initially calibrated by passing air through it and collecting the output over water in a large glass column, showing the meter to be accurate within 1% if set up carefully.

When tests at higher speeds caused excessive back pressure in the crankcase, or where firing operation caused the blowby gas temperature and pressure to fluctuate significantly, this method of directly coupling the gas meter to the engine could not be used. In these cases, the blowby gas was collected in a specially constructed bag, having a maximum volume of about 1.5 m³. To measure the mass of gas collected, it was allowed to cool to a steady temperature and then evacuated through the gas meter at constant pressure.

5.3.1 Correlation of Results

Initially, a simple correlation was developed with the aim of synthesising results with the minimum of calculation effort. This is based on the Bernoulli equation for incompressible flow through an orifice:

$$\dot{m}_{bb} = C_d \cdot A \sqrt{2 \cdot \Delta P \cdot \rho} \quad (5.1)$$

Here \dot{m}_{bb} is the mass flow rate of blowby gas, with C_d and A the orifice discharge coefficient and area respectively. The pressure drop across the orifice, ΔP , was calculated as the difference between the logged cylinder pressure and the known crankcase pressure. ρ is the gas density, evaluated at liner temperature and cylinder pressure, as in reference [5.13]. A calibration for the "effective blowby area" ($C_d \cdot A$) is obtained by matching the integral of equation (5.1) over the cycle to measured values of blowby. This integration is done using measured cylinder pressure variations throughout the cycle.

Calculations showed that, whilst correlation was very good at higher speeds (over the range 100 to 1000 rpm), equation (5.1) underestimates blowby rates at lower speeds by up to 5%. The discrepancy is similar to that found by Rao, Gardiner and Bardon [5.12]. Using data from the Ford 1.8 litre IDI engine (the only engine for which very low speed data are available), a modifying factor was derived to bring the predictions in line with measured values. This gave a correlation for blowby, described by:

$$\dot{m}_{bb} = (1 + K_m \cdot e^{-K_n \cdot n_{min}}) \cdot C_d \cdot A \sqrt{2 \cdot \Delta P \cdot \rho} \quad (5.2)$$

Where K_m [-] and K_n [rpm⁻¹] are constants and n_{min} is the minimum engine speed during the cycle. For the engine used here, $K_m = 0.78$ and $K_n = 0.048$ rpm⁻¹ was found to give the best fit to the experimental data. The effective blowby area was found to be about twice the calculated area of the smallest ring gap (Wentworth [5.9] states that blowby correlates with the smallest gap). Furuham et al [5.11] observed factors of up to six in their investigations under normal conditions.

Figure 5.2 shows output crank angle resolved results predicted using the correlation for a typical cycle. The results show close agreement between predicted and measured values of blowby over the cycle. Overall, when using

experimental data from the Ford 1.8 litre IDI engine, this correlation gave an average error of 0.3%. The standard deviation was 4.6% over all test results, which is comparable to the spread of experimental data. These data cover ambient temperatures from -26°C to $+20^{\circ}\text{C}$, at average speeds from about 70 rpm to 250 rpm, and are illustrated in Figure 5.3. Similar analysis of data from other test engines at higher speeds show that this accuracy is maintained up to at least 1000 rpm.

5.4 Blowby Model

The simple correlation developed above allows the total (per cycle) blowby throughout cold starting to be calculated over a range of speeds and temperatures. This allows the analysis of factors which may be measured in terms of blowby fraction; for example the effects of speed, temperature, fuelling, piston and ring changes and others. However, to accurately determine the trapped mass at any point in the cycle (for example, as required for heat release calculations), a more complex model is needed.

The model developed here is similar to that of Munro [5.10] and others. The blowby flow path is treated as a number of volumes connected by narrow passages. Within each volume the temperature and pressure of the gas is assumed to be constant, and the connecting orifices are assumed to be of fixed size. The piston rings are assumed to be against the bottom of the groove throughout the cycle; previous experimental studies by other workers [5.11] have shown that this is true throughout almost the entire compression and expansion strokes during normal operation. Figure 5.4 shows the system as modelled here, based on two compression rings. The oil control ring assumed to present a negligible resistance to blowby flow. Region (1) is above the top ring, region (2) is between the rings and region (3) is below the second ring, effectively in the crankcase. All regions are assumed to be at metal temperature, with region (1) assumed at cylinder pressure and region (3) at crankcase pressure. The initial mass in region (2) is set

by assuming it to be at the mean of cylinder and crankcase pressures. The pressures in the cylinder and crankcase are known, so we must solve for region (2) for each step Δt from time (n) to (n+1). Assuming no changes in gas temperature, we have:

$$P_{2(n+1)} = P_{2(n)} \cdot \frac{m_{2(n)} + (\dot{m}_{12} - \dot{m}_{23}) \cdot \Delta t}{m_{2(n)}} \quad (5.3)$$

Where:

$P_{2(n+1)}$ = pressure in region (2) at step (n+1) [Pa]

$P_{2(n)}$ = pressure in region (2) at step (n) [Pa]

$m_{2(n)}$ = mass of gas in region (2) at step (n) [kg]

\dot{m}_{12} = mass flow rate across plane (A) during the step [kg/s]

\dot{m}_{23} = mass flow rate across plane (B) during the step [kg/s]

Δt = time interval between step (n) and step (n+1) [s]

The mass flow rates between regions (\dot{m}_{12} across plane A and \dot{m}_{23} across plane B) are modelled by the following equations for compressible gas flow through a restriction [5.13]:

$$\dot{m} = \frac{C_d \cdot A \cdot P_o}{\sqrt{RT}} \left(\frac{P}{P_o} \right)^{\frac{1}{\gamma}} \sqrt{\frac{2\gamma}{\gamma-1} \left[1 - \left(\frac{P}{P_o} \right)^{\frac{\gamma-1}{\gamma}} \right]} \quad \text{for } \frac{P}{P_o} > \left(\frac{2}{\gamma+1} \right)^{\frac{\gamma}{\gamma-1}} \quad (5.4)$$

$$\dot{m} = \frac{C_d \cdot A \cdot P_o}{\sqrt{RT}} \sqrt{\gamma} \left(\frac{2}{\gamma+1} \right)^{\frac{\gamma+1}{2(\gamma-1)}} \quad \text{for } \frac{P}{P_o} \leq \left(\frac{2}{\gamma+1} \right)^{\frac{\gamma}{\gamma-1}}$$

Where:

\dot{m} = mass flow rate [kg/s]

C_d = orifice discharge coefficient [-]

- A = orifice area [m^2]
- P_o = upstream pressure [Pa]
- P = downstream pressure [Pa]
- R = gas constant for air [J/kg.K]
- T = gas temperature (taken as metal temperature) [K]
- γ = ratio of specific heats for air [-]

The values used for P_o and P depend on the direction of flow: the higher pressure is always used as P_o . The known levels of cycle-averaged blowby under different operating conditions allow solution for the effective blowby area (the product $C_d.A$), although here there are two orifices to be determined.

This model was applied to the Ford 2.2 litre DI engine, code named P-type, for which full details of the pistons and ring pack were readily available. The critical parameters required were the inter-ring volume and the effective blowby areas, taken to be related to the first and second ring gaps. The inter-ring volume, including the space above and behind the second compression ring, was calculated from the manufacturers specifications. Similarly the ring gap areas, bounded by the ends of the ring, the piston and the cylinder bore, were calculated from specifications of average dimensions. When "calibrating" the model to fit experimental results, the effective areas for blowby through planes A and B (Figure 5.4) were modified together, keeping them in proportion to the two ring gap areas. This gave effective blowby areas of approximately twice the ring gap area. No correction needed for changing engine speeds.

Accuracy was found to be similar to the simple correlation of equation (5.2), with similar predictions for blowby over the complete cycle. However, predictions within the cycle are quite different. Typical output from the model is shown in Figure 5.5, for operation at 200 rpm. Rising pressure in the cylinder (P_1) during the compression stroke forces gas from the combustion chamber into the inter-ring gap, raising the pressure in region two (P_2). This in turn leads to blowby

into the crankcase. During the expansion stroke, this situation continues until cylinder pressure falls to equal the inter-ring pressure, after which they are approximately equal. Blowby continues into the crankcase, but there is minimal change in the mass trapped in the combustion chamber. The apparent fall in cumulative blowby from 450° onwards is due to over-expansion of the charge (due to high levels of blowby and heat transfer) leading to a cylinder pressure slightly below ambient. Figure 5.6 shows similar calculations made at an engine speed of 1000 rpm. In this case the situation is similar, but the more rapid fall in cylinder pressure (with time) means that there is considerable flow from the inter-ring gap and back into the cylinder, as well as out into the crankcase, as previously reported by Namazian and Heywood [5.13].

5.5 Analysis and Discussion

The interpretation of blowby effects requires some means of relating these to the level of leakage. Basing this on volume flow rate for a given brake output power as suggested by Munro [5.10], cannot be used under cranking conditions. Measurements based on blowby volume (or mass) per revolution are more useful, but make no allowance for different engine sizes or operating conditions. The measure adopted here is blowby fraction, defined as the mass of gas lost to blowby as a fraction of the trapped mass; similar measures have been used by other workers previously [5.5]. This form of normalisation takes account of differences in engine capacity and volumetric efficiency which would otherwise obscure comparisons of blowby across a range of engines.

5.5.1 Effect of Ambient Temperature

Henein [5.6] reported little change in blowby rates over a wide range of temperatures when measured in a direct injection diesel engine. Similar tests have been carried out by the author on the Ford 1.8 litre IDI engine, to record blowby fraction under unfuelled cranking conditions over a range of temperatures and

speeds. Engine speed was controlled by introducing resistive loss into the starter motor circuit to reduce starter power, with test durations being between 5 and 30 revolutions, at temperatures from -26°C to $+20^{\circ}\text{C}$. Figure 5.7 shows typical results when using SAE 10W/30 grade oil; results with SAE 5W/30 oil were similar. In the upper graph, lines of constant average speed are plotted against ambient temperature, with the data suggesting a rise in blowby fraction with rising temperature of about 3% from -20°C to $+20^{\circ}\text{C}$.

The reference speed commonly used to characterise conditions is the average over the engine cycle. This has been widely used by other investigators. However, the critical factors controlling blowby (apart from the leakage areas) are the pressure difference between cylinder and crankcase, and the time available for leakage. Examination of typical cylinder pressure and crankshaft speed traces shows that peak pressure and minimum engine speed both occur just before TDC in the compression stroke. It would therefore be expected that the conditions at this moment would correlate more closely with blowby fraction than the average condition over the cycle. Average engine speed should only be used if there is a clearly defined relationship between average and minimum cranking speeds.

An apparent dependence of blowby fraction on temperature is observed when characterising cycles by average speed. However, this is directly attributable to fluctuations in cranking speed caused by the limited output power of the starter motor. The fluctuation changes both with temperature (due to changes in friction and battery performance) and with the method used to control average cranking speed (the addition of extra resistive losses). For example, at -20°C the starter circuit is used unmodified, giving an average speed of 155 rpm and a minimum speed of about 103 rpm. At $+20^{\circ}\text{C}$ extra resistance is required in the starter circuit to achieve an average speed of 155 rpm, which gives a minimum speed of only about 82 rpm. Thus the use of resistive loss to control starter motor power upsets the relationship that would normally occur between average and

minimum cranking speeds. If minimum cranking speed is used to characterise test conditions, blowby rate becomes independent of ambient temperature over the range studied, as illustrated in the lower graph of Figure 5.7. This result supports Henein's conclusion that there is no measurable effect on blowby as the temperature is changed (here, from -20°C to $+20^{\circ}\text{C}$). Any possible effects due to changing oil viscosity, component clearances, or other factors described in the literature were not observed here, possibly due to the relatively small changes in temperature that occur when the engine is not firing.

5.5.2 Effect of Engine Speed

Other workers [5.5, 5.6] have shown that the blowby fraction rises sharply at low engine speeds, particularly below about 1000 rpm. Using a vehicle starter motor, only a relatively narrow range of average cranking speeds could be investigated: typically up to 250 rpm at $+20^{\circ}\text{C}$ and up to 155 rpm at -20°C , with the minimum limited to about 75 rpm at all temperatures. However, as shown in Figure 5.8, a considerable effect due to engine speed may be observed, even over this limited range. The figure presents data from the unfuelled Ford IDI engine using SAE 10W/30 oil, as in the previous section. A range of temperatures are represented (-26°C to $+20^{\circ}\text{C}$), but this has been demonstrated to have only a very small effect on blowby rates.

Of particular interest is the very large change in blowby that can occur over the range of cranking speeds: under 12% of the charge is lost at an average speed of 250 rpm, while over 30% is lost at 80 rpm. This underlines the need for a high cranking speed to avoid excessive charge loss and the possibility of cylinder temperature being too low for ignition. As described above, blowby fraction would be expected to depend on minimum engine speeds, as these relate to points of maximum cylinder pressure. Figure 5.8 also shows the blowby fraction plotted against this parameter, clearly showing an improved correlation over the use of average speed.

5.5.3 Contribution of Individual Cylinders

To determine the likely variation in blowby between engines of the same design, the contribution from individual cylinders in the Ford 1.8 litre IDI was measured. This was done under unfuelled cranking conditions, with all cylinders decompressed except the one under test. The cylinders were decompressed by removing the injectors and glowplugs. Analysis of instantaneous pressure in these decompressed cylinders showed that their blowby contribution is typically 200 times less than the compressed cylinder at cranking speeds. Repeating the process for each cylinder in turn allowed the distribution of blowby losses across the engine to be examined. The total blowby previously measured for the unmodified engine was compared with the sum of individual cylinders as a check on the validity of results. The sum of the individual cylinders was found to vary from the expected total by less than 1%; this slight difference is thought to be due to the small contribution from the decompressed cylinders.

Measurements were made over a range of temperatures and cranking speeds, with Figure 5.9 showing typical results, normalised against average blowby fraction. Examination of the figure shows that the variation between cylinders is quite large: Cylinder 1 losses are 29% greater than the average, with cylinder 4 losses 15% lower. This small sample size does not allow statistical analysis, but the variability of total blowby fraction between nominally similar engines could clearly be considerable.

5.5.4 Blowby Variation Between Test Engines

"Whole engine" blowby fraction has been measured on four engines under unfuelled cranking (or motoring) conditions. When correlated with minimum engine speed, blowby fraction has been found to be unaffected by test temperature over the range -20°C to $+20^{\circ}\text{C}$, as described above. Blowby fraction is plotted against engine speed in Figure 5.10 for typical tests carried out at an

ambient temperature of +20°C. The general shape of the curves is similar in all cases, closely matching that found by Henein [5.5] in his investigations. Blowby levels are about 2% at higher speed, rising rapidly below about 1000 rpm to 10% at 200 rpm (average speeds). Data from the Ford 1.8 litre IDI and 1.9 litre Volkswagen engines extend below this speed range, and show that blowby rises prohibitively as the speed drops further.

The data presented in the figure show that blowby fraction varies significantly between engines, even those of very similar design. For example, the P-type and L-type engines are of approximately equal size (2.2 and 1.8 litres respectively), both having similar piston and ring design and compression ratios; however, the P-type has only about 60% the blowby of the L-type. From the limited data available, the 1.9 litre Volkswagen engine seems to have lower blowby again. These results must, however, be viewed in the light of the known variability that may occur between individual cylinders in an engine, and therefore between engines of identical design.

5.5.5 Effect of Firing

If blowby predictions are to be useful in the analysis of cold starting, blowby behaviour during firing cycles must be modelled correctly. To examine firing cycles, the Ford IDI engine was started and allowed to reach a steady idling condition at 1000 rpm. The blowby gas was then collected over a fixed interval (using the collecting bag described above) and the total blowby mass measured. Pressure-volume data were captured from a number of cycles during the collection period. Predictions of blowby were made using the correlation of equation (5.2), since this is simpler to apply than the more detailed model and there is good agreement between these for the blowby total per cycle, as has been noted earlier.

Comparing with predicted blowby masses showed that the measured values were about 27% lower than expected. To determine the cause of this discrepancy, blowby volume flow rate was examined. It was assumed that the blowby correlation was correct for conditions during the starting phase and that, as idle speed is reached, conditions in the engine are the same as during this initial phase. If these assumptions hold, it should be possible to observe a fall in blowby of about 27% from reaching idle speed until steady conditions are achieved. The general arrangement of Figure 5.1 was used, but with the gas meter replaced by a rotameter covering a suitable range. Absolute calibration of this instrument was not required, as its known linearity allowed relative changes in flow rate to be identified. Figure 5.11 shows the changes in blowby, measured in arbitrary flow units. It was not possible to read the flow rate at zero time, so this was estimated by extrapolation back from data collected in the first few seconds, as shown by the fine line in the figure. In these tests the blowby flow rate fell, on average, from 16.8 to 12.4 (again, measured in arbitrary units). This represents a reduction of 26% and suggests that the correlation of (5.2) is valid, including for firing cycles, up to the point of achieving idle speed.

Once sustained running has been achieved, changes within the engine cause the effective blowby area to change significantly. A number of mechanisms will contribute to producing this change. Component tolerance changes due to heating of the cylinder, piston and rings will alter the effective blowby area. Higher gas pressures may lead to a change in the sealing of the piston rings in their grooves. Other changes in the engine, for example changes in the thickness of oil films around the pistons and rings, may also be involved. In addition, the blowby correlation depends on estimation of the gas temperature as it passes around the piston. This becomes difficult after a significant number of firing cycles, when temperatures rise considerably. The higher gas temperatures and velocities may also cause the assumption that the flow is isothermal with the crevice walls to become less appropriate.

5.6 Conclusions

Blowby loss is dominated by the effect of engine speed. For any given design, a fall in minimum engine speed (which occurs close to the point of peak cylinder pressure) causes a rise in blowby. This rise becomes prohibitive below average speeds of typically 100 to 200 rpm, which are often reached during cranking at low temperatures.

Variation between different engines is considerable, with differences of over 100% observed for test engines of similar size and specification. Measurements made in individual cylinders of one engine suggest that variation between nominally identical engines can be in the region of 30%, which is sufficient to cause differences between cylinder behaviour during starting. Changes in blowby characteristics due to ambient temperature, engine oil viscosity or firing cycles have not been detected in these tests. However, once steady idling conditions are reached, blowby has been shown to fall by almost 30% in one engine over a period of about five minutes.

A simple correlation has been developed, treating blowby loss as incompressible flow through a single orifice. This requires a minimum of calculation and can predict total blowby per cycle throughout cold starting over a range of conditions. Based on measured values of cylinder pressure and metal temperature, the correlation can be used to examine factors affecting blowby on a cycle-averaged basis. These include the effects of speed, fuel injected during cranking and changing oil viscosity. Although suitable for analysis of average blowby throughout the cycle, this correlation cannot predict instantaneous rates. Also, as well as the calibration for orifice area, an additional factor is required at low speeds due to the simple treatment used.

A more complex model predicts blowby based on consideration of compressible flow past two compression rings. It predicts similar blowby per cycle, but quite

different instantaneous mass flow rates. Since it more closely represents the physical processes involved, no correction at lower speed is required. Predictions using this model suggest that blowby losses before TDC may be higher than shown by the simple correlation, leading to significantly lower temperature and pressure. Some of this lost gas flows back into the cylinder from the inter-ring crevices during the expansion stroke, thus preventing it from being measured as blowby out of the crankcase vent. This model may be used wherever knowledge of the instantaneous blowby is required, for example during heat release calculations. Also, since both the rings and the volume between them are represented, it allows the effect of limited changes to piston and ring design to be assessed with respect to blowby performance. Indeed, predictions using this work have recently allowed a useful reduction in blowby of the L-type engine to be achieved. By reducing the area of the second ring gap, blowby in the L-type engine at low speed was reduced by 18-25%, in line with model predictions [5.14].

Chapter 6

COMBUSTION STUDIES

6.1 Introduction

This chapter describes investigations of how fuel injection parameters and glowplug design affect the cold start behaviour of the Ford 1.8 litre IDI engine. This power unit has been in production for several years and the degree to which cold start performance had been optimised was uncertain. Modifications that could affect aspects of performance other than starting have not been considered. Reported here is the effect of fuel injection quantity, timing and rate, and the glowplug dimensions, on-time and temperature. All results are based on free start tests, with the engine started as if in normal service. A fixed start-up temperature of -20°C was used throughout, to allow a reasonable testing rate while still operating at conditions adverse to good start quality. Methods have been developed to allow comparison of combustion during cold starting on a more sophisticated basis than "time to idle speed" and similar. Analysis of cylinder pressure data allows the changes in start quality to be related to combustion, and the preferred fuelling and glowplug arrangements to be identified. The fuelling strategy currently implemented on production vehicles was found to be close to optimum, although improvements to glowplug design and operation were identified for the test engine used here.

6.2 Fuelling Strategy

The fuel injection pump fitted to the standard engine had no facilities to enable the fuelling strategy to be varied for testing purposes [6.1]. This was replaced with the IDI variant of the Lucas EPIC (Electronically Programmed Injection

Control) pump [6.2], which allowed the timing and fuelling to be set independently over a wide range. Figure 6.1 shows that start times using EPIC are similar to those for the standard fuel pump at -20°C , when using nominally similar fuelling parameters. Using the EPIC pump gave a slight reduction in start times, along with a large reduction in variability. Examination of engine speed data shows that time to first fire was slightly increased, as EPIC requires one full engine revolution to achieve synchronisation before fuel injection; the standard pump injects in the first stroke. However, this disadvantage is more than offset by the improved control system of the EPIC pump, allowing timing control to be achieved within a few revolutions. At low temperature and speed the standard fuel pump may require most of the start (up to 100 revolutions) to achieve proper control. The EPIC pump was used throughout the work reported in this chapter.

6.2.1 Analysis Methods

Since the data here were collected from free starts, conditions in the engine were changing rapidly throughout each test. Combustion analysis is more difficult under these circumstances than when operating conditions are stable. The approach adopted here was to first analyse each cycle to obtain the required information and then to group together cycles having the same temperature, speed and timing. These groupings allowed engine performance to be analysed in terms of the behaviour of a "typical" cycle under each set of conditions; figures for typical IMEP, the probability of misfire, and so on, can be calculated. By pooling together data from several repeated cold starts, it was possible to ensure that each grouping contained enough cycles for analysis. Clearly, large numbers would give improved results, but the number of tests was constrained by time and resources, so groups of five or more cycles were used in this work. By comparing the "typical" figures from different groupings it becomes possible to see, for example, how IMEP varies with changing injection timing or engine speed.

In addition, some knowledge of the actual mass of fuel injected was required. Although the EPIC pump is designed to allow control of fuelling levels electronically, the unit cannot be reliably calibrated at the very low speeds considered here. To measure the injection mass, an instrumented injector was used in cylinder 1, measuring needle lift and fuel line pressure. Fuel injection was then calculated from the equation for incompressible flow through an orifice [6.3, 6.4]:

$$\dot{m}_{\text{fuel}} = C_d \cdot A_{\text{nozzle}} \sqrt{2 \cdot \Delta P \cdot \rho_{\text{fuel}}} \quad (6.1)$$

Where \dot{m}_{fuel} is the mass flow rate of fuel, C_d and A_{nozzle} the nozzle discharge coefficient and area, ΔP the pressure drop across the nozzle, and ρ_{fuel} is the fuel density. A calibration was performed through tests on a bench rig, to account for the approximations involved when applying this equation to the throttling-pintle type injector used here [6.5, 6.6]. The bench rig results relate effective discharge coefficient, C_d , as a function of needle lift under steady flow conditions. The resulting model was checked against actual operating conditions by starting and running the engine on three cylinders, collecting the fuel from the instrumented fourth injector for measurement. The final calibrated model was found to predict injected mass to within 5% for speeds up to 1000 rpm.

An indication of the fuel burned in each cycle was derived from a simple heat release model developed at Nottingham by Tindle [6.7]. It was assumed that heat transfer losses could be represented using the Woschni correlation [6.8] and that the detailed blowby model of Chapter 5 was applicable. The combustion chamber gasses were assumed to be homogenous in composition, temperature and pressure [6.9, 6.10]. The calorific value of the fuel was estimated to be 42.5 MJ/kg. The output parameters were the mass of fuel burned and the ignition delay, taken as the interval between start of injection and the earliest time heat release from burning fuel is detected.

6.2.2 Effect of Injection Quantity

Previous studies have shown that increasing the mass of fuel injected can lead to improved cold starting in both DI and IDI engines [6.11, 6.12]. This was confirmed by the tests reported here, as illustrated in Figure 6.2. These data were recorded at -20°C with timing fixed at 4°BTDC , changing fuelling from about 20 to 50 mg per injection. This improvement is due to two distinct changes as fuelling was increased: a reduction in the time to first fire, and subsequently a more rapid acceleration to idle speed.

With increasing fuelling, the time to first fire fell from about 2.0 to 1.2 seconds (from the ninth to the fifth injection). Investigation of cylinder pressures during fuelled cranking showed that the cyclic peak pressure rose steadily as cranking progressed until firing commenced. Figure 6.3 shows the peak cylinder pressure with and without fuelling, with firing inhibited by disabling the glowplugs at a test temperature of -10°C . Since test conditions were similar, the pressure rise cannot be due to temperature or engine speed changes. However, this rise can be explained by a reduction in clearance volume equivalent to about 50 mm^3 in each cycle; this is the volume of fuel injection used in these tests. Thus it appears that injecting more fuel shortens the time to first fire by increasing the effective compression ratio of the engine as fuel accumulated in the cylinders. It should be noted, however, that the improvement here is small compared to the total duration of the start.

It has been suggested that fuel injected during cold starting may reduce blowby by helping to seal the piston rings [6.11], although the work concerned referred primarily to direct injection engines. To investigate this, the Ford 1.8 litre IDI engine was used to measure blowby after a period of cranking with fuel injection. Tests were carried out at -10°C with the glowplugs (normally used as a cold starting aid) disabled to prevent firing cycles from occurring. The engine was cranked for a number of cycles with injection enabled, to introduce a quantity of

fuel into the engine. A total injected volume of up to 1.4 ml per cylinder was used. The blowby correlation of Chapter 5 was then used to examine blowby loss during further (unfuelled) cranking. Using this correlation, changes due to the injected fuel would be detected by their impact on the effective blowby area. Calculation showed that no detectable change in blowby occurred, with the effective area being unchanged for tests with and without fuelling. Thus fuel injection cannot be shown to have a significant effect on blowby under normal cold starting conditions.

After firing was achieved, the engine accelerated to idle speed more quickly at the higher fuelling levels. This change accounted for the greatest proportion of the improvement in start quality, falling from 77 to 22 seconds as the fuelling increased. Analysis of cylinder pressure data throughout starting showed that the IMEP at any given speed was higher when more fuel was injected. The results of heat release calculations presented in Figure 6.4 show that more fuel was burned. Referring to Figure 6.2, start times were very sensitive to fuelling below 30 mg, with only a small sensitivity to changes above 40 mg. This agrees with the changes in IMEP and fuel burned, which showed a decreasing sensitivity as fuelling increased.

Further studies were performed using the maximum fuel delivery settings for the injection pump. This provided 50 mg per injection and gave the shortest start times. The standard mechanical fuel pump has a peak cold start fuelling of about 45 mg per injection. In these tests, fuelling had not reached the point where starting was actually impaired [6.13], but the diminishing returns of higher fuelling levels must be balanced against the increased emissions of unburned hydrocarbons. Examination of cumulative fuel injected throughout starting showed that, under the conditions here, fuelling of 30-40 mg per injection allowed the engine to start with the lowest total fuel supplied. Below this range, although most of the fuel was burned (75% with 20 mg injection), the increased start duration meant that more fuel was required overall. Above this range, less

cycles were required to start but the fuel was used less efficiently (45% burned with 50 mg injection). Although 30-40 mg gave the best use of fuel, start times were 40-30 seconds over this range, compared with 25 seconds at 50 mg injection.

6.2.3 Effect of Injection Timing

Retarding the start of injection (SOI) timing can help cold starting in some cases [6.13, 6.14], although too much retardation can lead to erratic combustion with many misfires [6.3]. Figure 6.5 shows how start time changed as timing was swept from 10°BTDC (advanced) to 1°ATDC (retarded). Minimum start times were achieved with SOI at about $3\frac{1}{2}^{\circ}\text{BTDC}$, which corresponds to the timing used in the standard mechanically controlled fuel pump.

Examination of individual cycles showed that injection timing must be selected according to conflicting requirements, giving maximum IMEP with minimum misfires. If the IMEP *for firing cycles only* is considered (indicated by the light lines in Figure 6.6), it is clear that retarding injection gives higher work done on the crankshaft. This can be explained by considering combustion phasing. At low speeds and temperatures, blowby and heat transfer losses are extremely high and cause a rapid decay of the pressure generated by the burning fuel. If combustion occurs too close to TDC, the pressure decays before the piston begins to move significantly and the useful output (calculated from $\int P.dV$) is low. If combustion occurs later, the high pressures coincide with a greater rate of volume change, allowing more work to be transferred to the crankshaft. However, if injection is too late, the falling cylinder temperature and pressure after TDC do not allow proper ignition, and combustion fails.

Analysis of individual cycles, both at Nottingham and elsewhere [6.15], has failed to show convincingly why some cycles fire properly while other apparently similar cycles misfire. The work at Nottingham included investigation of

injection timing and profile, in-cylinder pressure and temperature, and the time available for ignition, but no conclusion could be reached. When the IMEP from these misfiring cycles was included to calculate an "average" (indicated by the heavy lines in Figure 6.6), the onset of misfiring with SOI timing later than about 5°BTDC lead to lower cycle-averaged IMEP overall. The shape of this "average" explains observed changes in start time. The best start times shown in Figure 6.5 coincide with the highest values of average IMEP, which were achieved with a SOI timing of about $3\frac{1}{2}^{\circ}\text{BTDC}$.

6.2.4 Effect of Injection Rate

Injection is significant as it affects fuel spray behaviour and the mixing of fuel and air. In this work, the rate of fuel injection was adjusted by changing the characteristics of the injection pump to examine the effect on start performance. Three injection pumps were used to cover a range of rates suitable for the test engine. These pumps, designated EPIC-10, EPIC-12 and EPIC-14, had injection rates in the ratio 1.0:1.2:1.4 respectively (a 40% variation from lowest to highest rate). Figure 6.7 shows how injection behaviour changed with these three pumps. The upper graph shows the rate of pressure rise in the fuel line prior to injection; at this point there is no fuel delivery. The pressure rise was approximately in proportion to the base injection rate of the pumps, with about 45% variation from the lowest to highest rate. Once injection begins, complex interactions occur between the injector, fuel pump and connecting pipes. When the average injection rate was calculated (fuel mass injected divided by injection duration), about a 20% difference between the lowest and highest rates was observed, as shown in the lower graph. This was lower than the pump specifications suggested.

Figure 6.8 shows start quality with the low and high rate pumps, measured as time to idle speed. Tests results obtained with the intermediate rate EPIC-12 pump (not shown on the graph) generally lie on these lines. It is clear that the

changes in start times were not significant compared to the start-to-start variability. The fairly small change in rate was not enough to cause any significant effect on start performance. Analysis of IMEP with varying timing (similar to that shown in Figure 6.6) showed no measurable change in combustion output with changing rate.

6.3 Glowplug Operation

In the sections above, the impact of fuelling changes on start quality have been explored. The second route for improving the performance of this engine was to alter parameters of the glowplugs used as a starting aid. The placement of the plug in the swirl prechamber was fixed by production and operational considerations, but alterations to tip temperature, on-time and plug geometry were possible.

6.3.1 Temperature and Timing

Previously, French and Scott [6.16] examined the impact of the glowplug starting aid when used in a Ricardo Comet combustion chamber which is similar to that employed in the Ford IDI engine. They concluded that the glowplug acts as an ignition source, contributing little to heating the charge. This agrees with earlier work by Austen and Lyn [6.11], who showed that ignition fails if the surface temperature of the plug is lowered while maintaining the same total heat input. French and Scott found that ignition delay could be reduced to an almost constant value, relatively unaffected by in-cylinder conditions, if the glowplug tip exceeded about 850°C. Temperatures above this gave little further improvement. Lower temperatures caused a rapid rise in ignition delay. Longer delay translates into an increased likelihood of misfire under cold cranking conditions, where ignition must occur close to TDC before the temperature and pressure fall too far to support combustion.

Investigations of glowplug temperature effects were carried out on the Ford IDI engine using a specially modified glowplug with a thermocouple embedded in the tip. Controlling the tip temperature by switching the plug supply current, the effect of glowplug temperature on individual cycles during starting was examined. Tip temperatures from 400°C to 1000°C were investigated. Figure 6.9 summarises results from a number of cold start tests at -20°C, using the EPIC fuel pump at maximum fuelling. All cycles up to engine speeds of 550 rpm are included. Injection timing was advanced (about 8°BTDC) to extend the start and allow enough data for interpretation to be collected, although the trends shown here are repeated at more normal timings. Variability of ignition delay is described here *for firing cycles only* by the coefficient of variation, COV, defined as the standard deviation divided by the mean (in milliseconds) and expressed as a percentage. The results show that a tip temperature of at least 850°C is desirable. Rising glowplug temperature reduced misfires, from 80% of cycles at 400°C to under 5% at 900°C. Temperatures above 850-900°C gave no further reduction. There was also a reduction in the variability of ignition delay, with COV falling steadily from over 200% to about 50%. At low tip temperatures the delay period was very variable, with times up to 35 ms and many misfires, but above 850°C a fairly steady value of 8-10 ms was reached.

A second possible change could be to consider the impact of pre-heat times on starting. It seems possible that a longer pre-heat could elevate the temperature of the swirl chamber walls, reducing gas heat transfer losses and enhancing fuel evaporation. In practice, related work by Tindle [6.17] showed that there was no benefit to increased times, and the data showed that less than 10 seconds pre-heat was actually required at -20°C (compared to about 20 seconds used on the standard test engine). Measurements in the swirl chamber showed only slightly higher temperatures after 60 seconds pre-heat than after 18 seconds, with most of the energy from the glowplug being conducted away to the coolant. Calculation and experiment also showed that the glowplug had only a minor effect on cylinder charge temperature during cranking.

6.3.2 Tip Protrusion

In earlier work, researchers have found that the glowplug should be placed so that the hot tip is in the path of a fuel and air mixture for best start behaviour. Specifically, French and Scott [6.16] presented photographic evidence showing that, at starting speeds, the fuel and air mixture is close to the chamber wall in the Ricardo Comet type system. This suggests that the hot tip of the glowplug should be positioned with minimal protrusion into the swirl chamber. This low protrusion also minimises the obstruction presented to swirl flow [6.16, 6.18], and may help with mixing.

The standard glowplug fitted to the IDI test engine was 21 mm long, giving a protrusion into the swirl chamber of 6 mm (here, designated STANDARD plugs). This was a slim plug with 3½ mm tip diameter, designed to minimise the disturbance of air flow [6.1]. To investigate the effect of using less protrusion, tests were also carried out with plugs giving a protrusion of 1½ mm into the swirl chamber (here, designated RETRACTED plugs). The tip diameter was increased to about 5.3 mm to maintain the plug volume and hence the compression ratio. Figure 6.10 shows that the start times were significantly reduced from a minimum of 24.5 seconds to 20.3 seconds when using retracted plugs, although more advance was required for optimum performance. In Figure 6.11 we see that, at "best start" injection timing, the IMEP generated with the retracted plugs was slightly higher (typically about 0.5 bar), explaining the improved start quality.

To distinguish between changes due to the location of the hot glowplug tip and the physical obstruction presented by the plug body, further tests were performed. Using each plug design in turn, the engine was cooled to +5°C and started without energising the glowplugs. Under these conditions starts were just possible with the standard plugs, with an average time to idle speed of 27 seconds. Figure 6.12 shows how the start times reduced to an average of 13 seconds when retracted plugs were used. Since the plugs were not energised

in these tests, the reduction must be due to the physical shape of the plug protruding into the swirl chamber, rather than the location of the hot tip. Tests undertaken by Ford support this finding, showing an improvement of some 5% in engine output at fully warm conditions. Although this test demonstrates that the obstruction presented by the standard glowplug is detrimental, practical difficulties meant that no tests were performed to identify the optimum position of the ignition "hot-spot".

6.4 Conclusions

Changes that can be made to a mature engine design to improved cold starting by increasing combustion output are necessarily limited. Here, the scope to optimise cold start fuelling strategies and starting aid parameters has been investigated for the Ford 1.8 litre IDI engine.

Increasing fuel injection quantity improved start times both by reducing the time to first fire and increasing firing IMEP. This is attributable to an increase in the effective compression ratio due to the increased volume of fuel injected, and an increase in the quantity of fuel burned in firing cycles. Tests showed that accumulated fuel in the cylinder as cranking progresses raises the compression ratio until firing commences, and that increased injection mass shortens this time. Although start times are reduced with rising injection mass, much of the extra fuel is not burned and, by inference, emission of hydrocarbons increases. Under the test conditions here the fuel is best used with injection masses of 30-40 mg, and the shortest starts with the maximum possible mass of just over 50 mg. This "maximum possible fuel" strategy was already implemented in the standard test engine.

Retarded injection timing, defined by start of injection (SOI), gives increased IMEP on firing cycles, but also gives rise to an increase in misfires. Later injection causes the highest pressures to coincide with a greater rate of cylinder

volume change, raising the amount of useful work done on the crankshaft. However, this is offset by the rising number of misfiring cycles that occur, due to the rapid fall in cylinder temperature and pressure from TDC onwards. The combination of these two effects gives the highest IMEP (and the quickest starts) with SOI set at about $3\frac{1}{2}^{\circ}\text{BTDC}$; this is close to the timing already used in the standard test engine.

Changes to injection rate may well affect start quality, but operational limitations on durability, emissions and performance mean that only a relatively narrow range of rates are feasible. Within this range, effects on start quality are small.

The effect of glowplug tip temperature on the time to reach idle speed and combustion parameters in individual cycles has been measured. A tip temperature of 850°C reduces misfires to a minimum; higher temperatures give no further improvement. Start tests and temperature measurements in the swirl chamber showed that, providing enough time is allowed for the glowplug to reach 850°C , extended pre-heat times offer very little benefit. At -20°C , a tip temperature of 850°C and a pre-heat of under 10 seconds are required.

Reducing the glowplug tip protrusion from 6 mm to $1\frac{1}{2}$ mm gave an improvement in start times by raising IMEP in firing cycles. This appears to be due, at least in part, to the removal of the physical obstruction from the swirl chamber to allow higher swirl rates and improved mixing. IMEP may also be improved by moving the hot tip of the plug to a more favourable position close to the chamber wall, but this has not been demonstrated directly.

The investigations here have shown that the existing fuel injection arrangements on the standard engine are close to optimum, within the limits of the injection equipment. However, beneficial changes to start performance due to changes in glowplug parameters have been identified: reduced protrusion into the swirl chamber, a specific target tip temperature and reduced pre-heat times. These

changes have been implemented on more recent engine designs, giving improvements in start quality.

Chapter 7

MOTORING FRICTION STUDIES

7.1 Introduction

The relative magnitude of indicated work produced by combustion and frictional dissipation during low-temperature starting have a strong influence on start-up behaviour, as has been described in Chapter 4. Investigations of combustion and the changes that may be made to improve IMEP were described in Chapter 6. Here, the focus is on work done to measure the level of mechanical friction in engines at low temperature. Additionally, by measuring the contribution of engine sub-assemblies to the total frictional load, further investigations may be targeted at the areas offering the largest potential benefits. Data are presented for the Ford 1.8 litre IDI and the 2.2 litre P-type, with reference to limited data from the 1.9 litre TDi Volkswagen (VW) engine and the Ford 1.8 litre DI L-type engine.

When an engine begins rotating, low-temperature friction changes particularly rapidly during the first few seconds before stabilising to relatively steady levels. This initial "transient" friction is described in a later chapter. In the quasi-steady state, the friction values can be related to measured oil temperature at a given time, independent of test history. The quasi-steady friction after start-up scales with earlier friction levels and also has an impact on idle quality, driveability, and emissions immediately after starting. Quasi-steady friction levels rise sharply with falling temperature, under the influence of rising oil viscosity. Typically, friction mean effective pressure at fully warm idle speed is about 1.0 bar, rising to between 4.3 and 5.0 bar at -20°C . These values are representative for all engines tested. However, the relative contribution of component parts to the total

is engine specific and temperature dependent, as will be described in the following sections.

7.2 Measurement Method

Friction for the whole engine under firing conditions has been calculated from data collected during free starts in the 1.8 litre IDI engine (described in Chapter 4). However, this method is difficult to apply during low speed and low temperature conditions. In addition, no breakdown of the friction due to each engine assembly can be obtained without using extra equipment [7.1]. In the work described here, friction was measured instead by the progressive breakdown of a motored engine. Differences between motoring and firing conditions have been reported by previous authors [7.2, 7.3, 7.4], but these are relatively small and motored engine results are generally accepted as salient to firing conditions.

7.2.1 Test Equipment

For motoring operation, the engine installation arrangement is similar to that used for the firing engine tests, as illustrated in Figure 7.1. Here, the engine was turned by a variable speed 24 kW DC motor, giving a turning torque of up to 200 Nm and speeds up to 1000 rpm. Cooling arrangements were very similar to the firing rig, with the engine being force cooled via the block, radiator and sump. Sealing of the enclosure was very good, so the dry air feed was found to be unnecessary to avoid ice formation. To achieve higher temperatures, two electrical heaters totalling 5 kW were used to heat the oil, water and (using the radiator in the enclosure) cell air. As in the firing engine, Gulf 40 reference fuel and Motorcraft SAE 10W/30 engine oil were used unless otherwise noted. To prevent firing in the engine, the fuel injection pump was connected to a set of injectors fitted into a manifold, returning fuel back to the tank. Through this arrangement, the load due to the fuel injection pump was maintained during

motored operation. The normal injectors in the head were left in place to maintain compression.

Data acquisition was controlled by an IBM-PC compatible with a suitable analogue input card, allowing data to be sampled five times per second. Engine speed was derived from a tachometer circuit driven from the input shaft, calibrated at steady speeds against a commercial electronic (optical) tachometer. Temperatures around the engine and enclosure were measured using K-type thermocouples, calibrated against a PRT in a calibration bath. Here, the reference junction compensation was done electronically, using a standard integrated circuit. Turning torque was measured with an in-line torque transducer and electronic indicator unit, calibrated using a set of standard weights on a calibration arm. As with the firing test rig, errors were estimated to be better than 1% FSD.

When cylinder pressure-volume data were required, the acquisition system from the firing rig was temporarily employed. This provides the facility to acquire data at the necessary high rate. The pressure in cylinder 1 was measured using a Kistler 6123 pressure transducer fitted into a modified fuel injector, with crank angle data from a magnetic pickup placed on the teeth of the flywheel. The number of pulses per revolution depended on the engine, but 135 was a typical figure. By sampling using a suitable time interval, the data could later be post-processed to give data every $\frac{1}{2}^\circ$ crank angle. TDC was identified by one oversized tooth on the flywheel, with the exact position identified using the methods of Douaud and Eyzat [7.5].

7.2.2 General Engine Testing Procedures

Preparation for testing was similar to the methods used for free start testing described earlier, taking care to ensure a steady temperature across the apparatus and suitable oil cleanliness. To obtain a large database in a reasonable time, the

method of "speed sweeps" was developed. In this methodology the engine was cooled to about -25°C and held at this temperature for one hour. The chiller plant was then shut down and the engine rotated. Frictional heating caused the temperature to rise gradually, with the additional electrical heating being used above about 40°C. Due to the action of the oil cooler and vehicle radiator, temperatures across the rig generally remained uniform to within a few degrees. Here, no data were collected until the first target temperature of -20°C (5°C above the initial soak temperature) by which time stable running conditions were established and the results were repeatable. At each selected temperature, data were collected at each speed from 1000 rpm to zero and back, in steps of 100 rpm. In the worst case, due to the continuous rise in temperature, each speed sweep had to be finished in under two minutes. This ensured that engine temperature was within $\pm\frac{1}{2}^{\circ}\text{C}$ of the target value, and avoided difficulties when interpreting the data.

Initially, friction in the complete engine was measured with all components driven and the engine compressed as normal. Total turning torque was used to find the mechanical friction loads by subtracting the known cylinder pumping losses, calculated using pressure-volume data collected under the same motoring conditions. The remainder was then attributable to the rubbing friction in the engine and ancillaries. Friction results from firing and motored engine tests at 1000 rpm are shown in Figure 7.2; the firing data is reproduced from Chapter 4. The two sets of data were obtained from different 1.8 litre IDI engines, but the two engines differ only in minor features such as the ancillary drive arrangement. The agreement between firing and motored results is very good, especially considering the known differences between firing and motoring operation, and that friction in nominally identical engines can differ by 10% [7.4].

Due to limitations of the experimental equipment, fully-warm temperatures could not always be achieved in the motored engines. This meant that the results could not be directly compared with those from other sources, where testing was

typically carried out at normal operating temperature (typically 80-90°C). To overcome this problem, a method of predicting engine friction was developed based on earlier work carried out at Nottingham by Darnton and others [7.6]. They showed that, in their studies, friction during warm-up could be related to fully warm friction by using the viscosity such that:

$$\text{FMEP} = \text{FMEP}_{\text{ref}} \left(\frac{\nu}{\nu_{\text{ref}}} \right)^n \quad (7.1)$$

Where "ref" denotes values measured at the fully-warm reference condition. The index n was found to be between 0.19 and 0.24 for the petrol engines tested in this previous work. Measured in a number of diesel engines, typical values of 0.25 to 0.32 were found for n in this investigation. Viscosity was calculated based on oil temperature measured at the inlet to the block and using the Walther equation [7.7]:

$$\ln \ln (\nu + 0.6) = a + b \ln T \quad (7.2)$$

Here, T is absolute temperature, and a and b are constants determined from oil viscosity data supplied by the manufacturer. It follows from equation (7.1) that the friction (FMEP) plotted against viscosity should be a straight line if log scales are used on each axis. Figure 7.3 presents the data for the full IDI engine as above, plotted in this way. Using graphs of this type, the friction at fully warm conditions may be estimated, based on data collected at lower temperatures. For example, the fully-warm ($\approx 85^\circ\text{C}$) viscosity of the SAE 10W/30 oil used here is 14.7 cSt, while at 60°C (the highest temperature shown for the motored tests) it is 30.3 cSt. The fully warm FMEP may be estimated by linearly projecting the line down to 14.7 cSt with only a small uncertainty in value, comparable with the scatter between tests. Fully warm friction was measured directly where possible,

but this method was used to make an estimate when running temperatures could not be reached.

To identify the contribution of each engine assembly, a progressive engine breakdown was performed. Starting with a complete engine, the remaining mechanical friction was measured after each engine assembly was sequentially removed. Thus the contribution of each sub-assembly could be identified, and the influence of speed and temperature investigated. At points in the investigation where oil pump load needed to be isolated, the drive from the crankshaft was replaced by small motor. This allowed the oil pump to be driven independently at engine speed, maintaining system oil pressures while still allowing the oil pump load to be identified. Finally, the main drive was disconnected from the engine entirely leaving one remaining bearing on the input shaft, but still measured by the torque transducer. Measuring the loss in this bearing allowed accurate determination of friction in the last engine assembly (the crankshaft).

The effect of gas pressure on the pistons in a motored engine may increase the frictional loss by altering the load on the pistons, rings and bearings [7.2, 7.8]. This can give misleading results if compression is removed during a breakdown study, typically when removing the head or pistons. To avoid this, the engine was decompressed before removing other components by using spacers between the cylinder head and block, opening the cylinders to atmosphere. The spacers allowed normal conditions to be maintained: bolt tightening torques were unaltered, and the oil and water galleries were carried through to the head. Lengthened drives (belt or chain) were used to allow normal operation of the camshafts, valves and so on. The resulting cylinder pressures, measured at speeds up to 1000 rpm, were negligible. By measuring the total friction before and after this decompression, the effect of gas pressure was measured independently of any other assemblies. In this work, gas loading is assumed to act only on piston and ring friction, and is usually considered together with these elements.

7.3 Steady-State Friction Results

7.3.1 Ford 1.8 litre IDI Engine

Friction loads in the TCI (turbocharged and intercooled) variant of this engine (Appendix A) has been investigated. This is not identical to the engine used in the firing studies, as the TCI engine has slightly different ancillary drive arrangements and water pump capacity. However, the differences are small, and judged not to have a significant influence on the results described in the following. The total friction was broken down into the following components, determined by operational considerations:

- Crankshaft: the five main bearings, thrust bearings, and two oil seals.
- Oil pump: the oil pump ONLY, not including its drive shaft (see "Valvetrain Assembly" below).
- Piston Assemblies: the pistons and rings, and connecting rods (containing big and small end bearings).
- Gas loading: the extra friction associated with the effect of compression pressure on the pistons, rings, and bearings. This predominantly affects piston and ring friction.
- Valvetrain assembly: the camshaft, followers and valves, and toothed drive belt with tensioner. Also included was the water pump, a layshaft used to drive the oil pump (although NOT the oil pump itself), and a small vacuum pump.
- Fuel Injection Equipment (FIE): the injection pump and toothed drive belt, including the tensioner.
- Ancillaries: the non-essential ancillaries comprising alternator, air-conditioning pump (AirCon) and power assisted steering pump (PAS). This included the poly-vee drive belts and tensioners, with the alternator not charging and the normal steering circuit in place. Although measured, this component is not included in the analysis.

Values between 0.53 bar and 0.12 bar were recorded (highest to lowest).

Friction measurements were taken over a range of speed and temperature. Data for engine speeds less than 1000 rpm were obtained with the engine decompressed, because of limitations associated with large torque fluctuations in the compressed engine. Consequently, the effect of gas loading on piston and ring friction could only be directly measured at 1000 rpm or above. Figure 7.4 shows how the gas loading increased friction at this fixed speed, with the solid line showing the linear relation used in this work. To estimate the influence of gas loading at lower speeds, the empirical relation due to Bishop was used [7.8]. Neglecting any throttling in the inlet, this can be expressed in the form:

$$\Delta_{FMEP} = 411 \times \frac{\text{stroke}}{\text{bore}^2} \times \left[0.088 r_c + 0.182 r_c^{(1.33 - K.S_p)} \right] \quad (7.3)$$

Where Δ_{FMEP} is the rise in friction due to gas loading of the pistons, rings and bearings, characterised by mean piston speed (S_p in m/s) and compression ratio (r_c). The constant in the original equation and the factors required to give this result in Pascals (when inputs are in S.I. units) are combined to give the factor of 411, having units of N/m. The constant K was 2.38×10^{-2} s/m [7.8]. The equation gives a result slightly higher than the measured value (0.53 bar against 0.33 bar measured). Equation (7.3) was applied to scale the measured data for speeds below 1000 rpm. As the speed drops from 1000 rpm to zero, Bishop's equation suggests only a small rise in the gas loading effect of about 15%; this compares with about a 35% change measured over the temperature range. Although the actual friction breakdown was performed with the engine decompressed throughout, the extra component due to gas loading must be considered with the piston and ring friction for analysis purposes.

A friction breakdown at 1000 rpm is given in Figure 7.5. This shows how the various component contributions make up the total friction over a range of temperatures. Data provided by Ford [7.9] for a similar engine under firing conditions allow comparison at the fully warm temperature of 82°C. These data were less detailed and the contributions from several assemblies have been necessarily added together for comparison. The total mechanical friction without the ancillaries (alternator, AirCon and PAS) of 1.02 bar compares favourably with the figure of 0.94 bar measured in the current work, and the fraction attributed to each assembly also agrees well.

Total engine friction rises sharply as temperature falls, from under one bar at fully-warm to about 4½ bar at -20°C. The proportion of the total friction due to each component changes markedly as the temperature is reduced, with the speed held at 1000 rpm. Under normal operating conditions the piston and ring friction (including the increase due to gas loading [7.2, 7.8]), makes up about 65% of the total, with the cam assembly contributing 21%. The remaining 14% is split between the oil pump, crankshaft, and fuel injection system. Reducing the temperature to -20°C, the pistons and rings (with gas loading) still form most of the friction (47%). The valvetrain becomes less important (reduced to 14%), with the oil pump and FIE relatively unchanged. However, the crankshaft assembly, which contributed under 4% at 82°C is now responsible for 22% of the total.

Examination of the data shows that the main rise in friction with falling temperature is due to the crankshaft and piston assemblies (excluding the gas loading effect): these two alone cause a rise of 2.4 bar at 1000 rpm. Both have a large component due to viscous friction losses in the main and big-end journal bearings [7.10], which would be expected to increase sharply with rising oil viscosity. Other components show a lower sensitivity to temperature. In the tests reported here the effect of gas loading on friction was not strongly influenced by temperature, and Bishop [7.8] reported no speed dependence, suggesting that it is a non-viscous friction effect. Similarly the friction contribution of the

valvetrain, which has flat followers on an overhead camshaft and operates in predominantly mixed and boundary lubrication regimes [7.10], showed a relatively low dependence on temperature.

The variation of friction with speed, both fully warm and at -20°C , is illustrated in Figure 7.6. At high temperature, friction MEP is just under one bar and almost independent of speed over the range measured. There is a small increase at very low speeds, due to an upturn in valvetrain friction. This is consistent with a gradual increase in mixed and boundary lubrication, as reported by previous workers [7.10, 7.11]. Piston assembly friction (including the effect of gas loading) dominates engine friction at all speeds. At low temperature, total friction rises from under $2\frac{1}{2}$ bar at 100 rpm to $4\frac{1}{2}$ bar at 1000 rpm. Crankshaft and piston assembly friction show a considerable dependence on engine speed, consistent with a hydrodynamic lubrication regime [7.10]. The effect of gas loading on the pistons and rings is derived from (7.3), and shows a minimal speed effect. The valvetrain friction showed a slight speed dependence, and no upturn in friction was measured at speeds down to 100 rpm. This may be explained if the higher oil viscosity allows an increased proportion of hydrodynamic lubrication to occur at low temperatures. However, the limited effect of speed shows that mixed and boundary lubrication regimes are still prevalent.

Tests have also been carried out at Nottingham on a direct injection variant of this engine (the L-type prototype engine [7.12]) for comparison. This early model had almost all major friction components in common with the IDI engine described here except for piston design. This engine was found to have similar characteristics to the IDI: a similar effect due to gas loading, and the same total and proportional breakdown of engine friction.

7.3.2 Ford 2.2 litre P-type Engine

The second design for which friction characteristics have been determined is the Ford P-type engine. This is a 2.2 litre DI unit, having four valves per cylinder operated by twin overhead camshafts with roller followers (Appendix A). The valvetrain was driven using a duplex chain from the crankshaft, which also operated the fuel injection pump. Two balancer shafts were fitted, driven by a simplex chain. As before, the friction was broken down into components determined by operational considerations. These assemblies were the same as in the IDI case, with the following exceptions:

- Oil pump: including a component of the simplex chain associated with the oil pump drive.
- Valvetrain assembly: the camshafts, followers and valves, and duplex chain drive with tensioner. Also included were small vacuum and fuel lift pumps.
- Water pump: including its poly-vee belt drive and tensioner. To allow comparison with the IDI data, the water pump was added to the valvetrain friction in the analysis here.
- Balancer shafts: including the remainder of the simplex chain drive and tensioner (not included in "oil pump" above).
- No external ancillaries were fitted to this engine.

Bishop's equation (7.3) predicts a reduced gas loading effect of 0.47 bar for the P-type engine, due to the lower compression ratio. However, the measured value was found to be only about 0.1 bar. The reason for this difference is unknown at present, but improvements in design since the formulation of equation (7.3) in 1964 may be responsible. Additionally, it is known that the IDI engine has low tangential ring loads, relying on gas pressure to provide a seal. This would tend to make it more sensitive to gas pressure than designs with higher static ring

loading. As before, the equation was used to scale the measured value from 1000 rpm tests to provide an estimate at lower speeds.

Figure 7.7 shows the friction breakdown at 1000 rpm, similar to that presented above for the IDI engine. Data from a similar P-type engine under firing conditions is presented for comparison at fully warm conditions [7.13]. The sets of test data for firing and motored operation are in good agreement, both in total friction and the relative contributions. The higher crankshaft friction recorded at Nottingham may be due to damage discovered in one of the main bearings, but the reasonable agreement with Ford data suggests that this did not have a major influence. Comparing the P-type results with those from the IDI engine (Figure 7.5), the similarities are clear. At normal operating temperatures the P-type has slightly lower friction, despite the use of twin camshafts and four valves per cylinder. At low temperature the friction is higher (5.07 against 4.52 bar), but this extra is due to the balancer shafts, a feature not implemented on the IDI engine. The friction behaviour of the balancer shafts is similar to the crankshaft, suggesting predominantly hydrodynamic lubrication, giving a strong dependence on oil viscosity.

The relative importance of friction contributions is also broadly similar to the IDI engine. At fully warm conditions, piston assembly friction (including gas loading) dominates, as before. This contributes 42% of the total, with valvetrain friction adding 26%. Both crankshaft and oil pump add about 12% each, with the remaining 8% from the balancers and fuel injection system. Reducing the temperature to -20°C, piston assemblies (with gas loading) still contribute 36%, with the valvetrain, oil pump and FIE remaining relatively unchanged. As in the IDI, the crankshaft assembly becomes more significant (rising to 19%), along with the balancer shafts which rise to 12% of the total. As in the IDI engine, the largest increase in friction as the engine cools is contributed by components having a large proportion of hydrodynamic lubrication (predominantly from journal bearings): the balancer shafts, crankshaft, pistons and connecting rods.

The valvetrain friction once again shows only a relatively small change with temperature, although slightly greater than in the IDI engine.

As above, changes with speed are illustrated in Figure 7.8 at fully warm and -20°C . As in the IDI engine, the valvetrain is fairly insensitive to speed with the same rise in low-speed friction at higher temperatures, suggesting a large proportion of mixed and boundary lubrication. At low temperatures, this upturn is not observed. Piston assemblies and balancer shafts show a strong sensitivity to speed at -20°C , although the effect on the crankshaft is unclear: this may be due to damage to a main bearing noted above. In general, however, the friction behaviour of engine assemblies with changing speed and temperature is similar for P-type and IDI engines.

7.3.3 Comparison with Competitor Engine: VW 1.9 TDi

Friction breakdown results from the two Ford engines above were compared with data collected from a direct injection VW unit [7.14]. This engine was of comparable rating and mechanical design to the IDI and L-type engines, suitable for installation in the same classes of vehicle (Appendix A).

The friction breakdown for all three engines is shown in Figure 7.9, at normal operating temperatures and 1000 rpm. Note that the VW tests did not separate the crankshaft and oil pump friction, so these are shown together for all engines. The Fuel Injection Equipment (FIE) figure for the VW is also an estimate. Although piston assembly friction is shown added to the gas loading effect, the two were measured separately. The gas loading effect was found to be between that of the IDI and P-type engines: 0.23 bar at 1000 rpm and $+20^{\circ}\text{C}$. As before, Bishop's equation (7.3) was used to scale the VW result for speeds other than 1000 rpm.

At this fully warm condition, the VW engine has significantly lower friction than the Ford engines, primarily due to the very low losses in the valvetrain assembly;

other contributions are comparable between engines. In all cases piston assemblies contribute the most friction, although the P-type engine suffers from higher valvetrain friction (twin camshafts) and the extra loss associated with the balancer shafts. At low temperature (Figure 7.10) the VW and IDI engines have similar friction mean effective pressures of about $4\frac{1}{2}$ bar. The P-type engine produces a slightly higher value of about 5 bar. The P-type engine has low piston friction, but very high valvetrain friction, in conjunction with a considerable contribution from the balancer shafts. Piston friction is highest in the VW engine, although that may be expected due to the higher piston speeds associated with its longer stroke, but this disadvantage is offset by the lower crankshaft and valvetrain friction.

7.4 Conclusions

Motoring friction breakdown provides data on the relative contribution of each engine assembly to the total friction. Despite the known differences in local conditions within the engine, the motored breakdown agrees closely with results obtained from firing tests, both in terms of total friction and the proportion attributed to each sub-assembly.

Variations in quasi-steady friction (that is, excluding the initial period where friction changes very rapidly) can be adequately represented by the simple equation (7.1), based on oil viscosity. This viscosity is calculated using the oil temperature measured at a representative point in the lubrication circuit: here, the inlet to the main gallery in the block. It allows the total engine friction to be predicted; based on measurements taken below $+60^{\circ}\text{C}$, predictions of friction at up to $+90^{\circ}\text{C}$ have proved to be reliable. However, this range ($+60^{\circ}\text{C}$ to $+90^{\circ}\text{C}$) represents only a relatively small viscosity change, with projections to lower temperatures (below -20°C) more difficult.

Measurement of low temperature friction in several engines has shown that the proportions attributable to each engine assembly may be quite different to those measured under normal operating conditions. Although friction from the piston group was the highest single element at all temperatures, other components become more significant as temperature is lowered. In particular, the low levels of friction normally seen from journal bearings rises very rapidly, giving unexpectedly high friction from the crankshaft of all three engines (and the balancer shafts of the P-type unit). Friction from the valvetrain appears to be less of a problem at lower temperatures because it is less sensitive to oil viscosity than the engine as a whole.

A VW competitor engine was found to have similar or lower friction than Ford units at all conditions, despite having higher piston friction. The latter may be due to the high piston speed, since the VW had the longest stroke of the set of engines. However, this was more than offset by low crankshaft and particularly low valvetrain friction.

In order to reduce cold friction, this work suggests that attention should clearly be paid to the piston group (piston and rings, small end and big end bearings). This makes the largest single contribution to total friction. The low piston friction in the P-type engine, both as a percentage and in absolute terms, shows that improvement of the IDI design is possible. An unexpected finding is that the crankshaft, and balancer shafts on the P-type engine, also merit investigation. The crankshaft friction can rise sharply with falling temperature, contributing typically 20% of the total at -20°C. The P-type balancer shafts, which are also basically a single shaft supported in journal bearings, show a similar characteristic, rising sharply to over 10% of the total at -20°C. Although these two components contribute less than 10% of the total under fully warm conditions, they clearly have a greater impact under cold starting conditions.

Chapter 8

INITIAL FRICTION TRANSIENT

8.1 Introduction

The results described in the previous chapter were acquired during periods of engine motoring when quasi-steady conditions apply. In this case, friction can be related to the feed temperature of the lubricating oil. During the first seconds of engine running friction losses are higher (typically by a factor of two at -20°C) and initially change more rapidly than would be predicted by the quasi-steady dependence on oil feed temperature. Generally, an engine cold start is completed before these steady conditions can be established and hence this initial transient phase is particularly important. The investigation of friction during the transient phase is described in the following sections.

The ratio of initial to corresponding steady state friction has been used to characterise initial friction values. This will be shown to be independent of oil viscosity, but dependent on test temperature. Test data from several Ford engines (both firing and motored) and the 1.9 litre TDi VW engine have been analysed to show that the duration of the transient is similar in the Ford engines tested, but considerably shorter in the competitor engine. In all cases, however, it exceeds the length of a typical cold start and, at lower temperatures, it is the characteristics of this initial friction transient that control the cold start duration in the Ford engines.

Using friction data from breakdown tests on the engine, the relative contribution of each engine assembly to the initial transient level of friction has been examined. The largest contribution will be shown to come from components

having the highest proportion of hydrodynamic lubrication, especially journal bearings. Investigations of journal bearings suggest that the high initial friction levels are associated with differences between the oil temperature measured at the inlet to the block and that at the friction surfaces. A simple model of the crankshaft main bearings is developed, representing operation under quasi-steady conditions. This model is then extended to include the initial transient period, and is able to correctly predict the magnitude and duration of the friction transient with changes to temperature and speed.

8.2 Magnitude of Start-up Friction

Previously it has been shown that under quasi-steady conditions, engine friction can be related to oil feed temperature by an empirical equation based on oil viscosity [8.1] such that:

$$\text{FMEP} = \text{FMEP}_{\text{ref}} \left(\frac{\nu}{\nu_{\text{ref}}} \right)^n \quad (8.1)$$

Equation (8.1) implies that the viscosity of the oil at the friction surfaces maintains a fixed relationship to the viscosity based on the measured oil temperature (at the inlet to the block). Under steady-state conditions this assumption holds because local heat generation is largely balanced by steady conduction to the surrounding engine structure. However, when the engine first begins turning, friction depends not only on engine temperature but also the time from the start of the test. Initially the entire system is at the cold-soak temperature, including the oil at the friction surfaces. At these points, frictional heating causes a rapid rise in oil and metal temperature until equilibrium is reached, causing the initially high level of friction to decay to a steady state value. Because the temperature changes are localised, general data such as feed oil, water or block temperature do not measure this phenomenon.

Paradoxically, the relative magnitude of the initial friction transient depends largely on the conditions at steady-state. Although the design of each bearing contact influences its cold friction, initial conditions are always the same: the entire engine structure and all lubricant and coolant at the cold starting temperature. Thus absolute value of friction is fixed by the basic engine design (dimensions, clearances and so on), and can theoretically be determined by consideration of each sliding contact throughout the engine, using these known initial conditions. Such analysis in the steady-state, however, additionally requires evaluation of local heat generation and how this is transported away from the contact surface. Under these conditions the materials and physical design of the entire structure can influence the results: coolant passages, supporting castings, lubrication circuit and so on. The duration of the initial transient is similarly influenced by these secondary design features, inasmuch as they alter the time taken to reach steady conduction conditions.

8.2.1 Experimental Measurement of Initial Friction

Test methods were similar to those used to collect the "speed sweep" data previously described. To examine friction during the early seconds of motoring, data acquisition was started before the engine was rapidly accelerated and held at a steady test speed. As before, frictional heating (with additional electrical heating above +40°C) was used to provide the range of temperatures required for each test. Starting at different temperatures and running at different speeds allowed a matrix of test data to be built up. Typical data are shown in Figure 8.1, with test results starting from -10°C to over +40°C for SAE 20W/50 oil. The figure shows how the initially high friction (here, up to 8 bar at -10°C) falls after the start of each test until it reaches a base level which then depends on temperature and falls from about 3½ bar at +5°C to 1½ bar at +60°C. Although not shown when presented in this form, the time taken for the initial friction to decay to the base level is typically 100 seconds for the data here. The base level

corresponds to the value measured in the "steady-state" testing previously described.

Since the quasi-steady friction variations follow the form of (8.1), plotting the data against oil viscosity (evaluated at the oil feed temperature using the Walther equation as before) on log scales makes the effect of the initial transient clearer, as shown in Figure 8.2. In this figure, the "base" level of friction appears as an approximately straight line, falling from about 3½ bar at 2500 cSt to 1½ bar at 75 cSt. Individual cold starts at different temperatures start with high friction and high viscosity (top right) and, along with falling viscosity, the friction falls until the steady-state value is reached; all tests fall on this single base line after the initial period. This initial friction transient has been defined here by using the ratio of the instantaneous to steady-state friction, such that:

$$FR_t = \frac{FMEP_t}{FMEP_\infty} \quad (8.2)$$

Where FR_t (friction ratio) describes the friction transient at time t , $FMEP_t$ is the absolute friction measurement, and $FMEP_\infty$ is the steady-state friction at the corresponding temperature (conceptually at infinite time).

Although motoring torque could be measured from the instant rotation started, a finite time is required to accelerate the engine up to test speed. During this time, the instantaneous evaluation of friction FMEP using inertia estimates with speed and torque data proved unreliable. Although the most rapid acceleration possible was employed, the time to reach test speed increased at higher target speeds and lower temperatures because of the limited motoring torque available. Attempts to project back to zero time proved unsuccessful, due to differences in the acceleration rate up to the desired speed. Instead, the initial friction ratio (FR_t) was evaluated at a fixed time after the start of rotation. Across the range of

tests performed here, the target speed could be reached in typically five seconds in the worst case, so this time was selected. (Exceptionally, it was necessary to project back linearly to obtain a figure at this time). It was assumed that the value of FR_I evaluated at five seconds was approximately equal to that at zero time due to the relatively short period involved and the lower rotation speed during acceleration. This method has some weakness since, for example, FR_I is evaluated after a fixed time but a variable number of engine revolutions. However, it is a clearly defined methodology which yields repeatable and self-consistent results. The steady-state friction, $FMEP_{\infty}$, was taken from friction breakdown data.

8.2.2 Full-Engine Results

Due to excessive torque fluctuations, motoring data could not be collected from engines running at less than about 1000 rpm unless the engine was decompressed by raising the head. This speed was therefore selected for tests to examine the behaviour of FR_I in normal full-engine configurations, corresponding to the situation at idle speed just after cold starting. Motoring data were collected from the 1.8 litre IDI and the 2.2 litre P-type (series O) DI engines. Additionally, the analysis has been extended to include data from motored tests on a 1.8 litre L-type (series O) DI engine [8.2], and two gasoline spark ignition engines under firing conditions. The latter are Ford 1.1 litre "Valencia" [8.3] and 2.0 litre DOHC [8.1] engines. A single competitor engine, the 1.9 litre VW TDi (a DI engine), was also included. Where possible, the engines were tested without non-essential ancillaries such as alternator, air conditioning or power steering equipment. Data from the gasoline engines were collected with all normal ancillaries in place.

The magnitude of the initial friction transient (FR_I) at 1000 rpm, defined in equation (8.2), correlates reasonably well with oil viscosity, but better using the oil feed temperature directly. In the latter case, FR_I becomes virtually

independent of engine type and oil viscosity grade, and dependent only on test temperature at a given speed, as shown in Figure 8.3. This characteristic can be represented by a straight line, demonstrated in Figure 8.4. The "best fit" line cannot pass below unity, as this would imply initial friction lower than the steady-state; this has not been observed.

To investigate the effect of engine speed on FR_I , the P-type engine was decompressed to allow steady running at speeds below 1000 rpm. A comparison of compressed and decompressed results at 1000 rpm shows that decompression has little effect on FR_I at temperatures around -20°C , but caused a slight reduction above this, as shown in Figure 8.5. The reduction is relatively small, giving an average decrease in initial friction of about 7%. The cause is unclear, but has to be accepted since decompression of the engine was required to allow tests at lower speeds.

Testing at speeds of 250, 500 and 700 rpm over a range of temperatures was completed. These results, along with comparable tests at 1000 rpm, are shown in Figure 8.6. Tests at lower speeds proved to be particularly demanding, with the reduced levels of steady-state friction amplifying the effect of measurement errors on FR_I , increasing scatter. Considering data at or above 500 rpm, no significant change with speed is observed. However, despite small number of test results and the relatively high scatter, the data at 250 rpm are significantly lower, reduced by about 12%. Reference to Chapter 7 (Figure 7.8) shows that this behaviour is in line with total measured steady-state friction: rising from zero to about 500 rpm and then beginning to level out above this.

8.2.3 Contribution by Component

During the friction breakdown testing described in Chapter 7, data were collected to allow the contribution of each engine assembly to the total initial friction to be identified. This was carried out at -20°C and 1000 rpm to ensure that the

transient was large enough to be measured with reasonable accuracy as more engine assemblies were removed. These tests were carried out with the engine decompressed throughout. To measure the component of FR_I associated with each assembly, equation (8.2) was used as before. In this case $FMEP_I$ was the initial friction due ONLY to the engine component under consideration, measured as the difference between two builds starting under the same conditions: -20°C and 1000 rpm. As before, FR_I is referred to a time five seconds after the start of engine rotation. $FMEP_{\infty}$ was the steady-state friction for the relevant engine assembly ONLY, taken from the friction breakdown data previously described. Thus the values of FR_I calculated here refer to each engine assembly in isolation, as if it was tested alone. This normalisation for each assembly allows the sensitivity to initial conditions to be compared directly. To calculate the absolute contribution, the product of FR_I and the steady-state friction can obviously be used.

Data were collected from the 1.8 litre IDI and 2.2 litre P-type DI engines. Motored breakdown data were also available for the 1.8 litre L-type DI engine [8.2]. FR_I is plotted in Figure 8.7, comparing each major assembly in these engines. For all engines, the crankshaft and pistons show the largest transients, with initial friction being between 1.9 and 2.4 times the steady-state value for these components. The values for the piston assemblies includes both connecting rod bearings but excludes the effect of gas loading. The balancer shafts in the P-type engine have an initial friction transient of a slightly lower value, about 1.7. The value of FR_I for the valvetrain is lowest, varying between 1.5 and 1.0 (in which case no transient effect is observed).

The oil pumps fall into two groups with FR_I at 1.0 for the P-type and about 2.2 for the IDI and L-type. This variation is attributed to differences in oil pump design. The IDI and L-type both use an internal gear pump of common design, driven by a layshaft running in two small journal bearings. The P-type pump is of similar basic design, but having a smaller diameter rotor and without the

layshaft, being driven directly by a chain and sprocket. The combined result of these changes is to give the P-type oil pump a lower dependence on oil viscosity than the other design, as can be seen from the steady-state breakdown data of Chapter 7. At the test condition examined, it appears that the IDI/L-type design operates in the hydrodynamic lubrication regime to a greater extent than the P-type pump. The component of FMEP due to the actual pressure work done pumping the oil is very low. For example, the IDI/L-type pump produces a pressure rise of up to 3½ bar and a flow of under 8 litres per minute at 1000 rpm. This adds only about 0.03 bar to FMEP, almost independent of temperature because of the action of the pressure relief valve in the pump outlet.

All of these results suggest that the highest sensitivity to initial conditions, and the highest values of FR_I , are associated with components which operate predominantly in the hydrodynamic lubrication regime. These include the piston assemblies (with the connecting rod bearings but excluding gas loading effects), crankshaft and, in the P-type unit, balancer shafts [8.4]. In all these cases friction is dominated by hydrodynamic operation, mostly in journal bearings. The valvetrain has a low sensitivity to oil viscosity due to the boundary and mixed lubrication regimes in which exist in its operation [8.4, 8.5]. Consequently, initial friction levels are only marginally higher than the projected steady-state values. The effect of this initial transient is very significant for the piston assemblies, crankshaft and (for P-type) balancer shafts, due to the size of FR_I coupled with the large low-temperature friction.

8.3 Duration of Start-up Friction

The work above allows friction to be estimated as the engine starts turning, based on measured steady-state values and a simple function depending on engine temperature, FR_I . However, friction immediately begins to decay towards the steady-state level and the rate of decay has an equally important influence on

cold start performance at low temperatures. The decay can be described using an exponential function of the form:

$$FR_t = 1 + (FR_I - 1) e^{-t/\tau_{FR}} \quad (8.3)$$

A fit to the experimental results is illustrated in Figure 8.8. The time constant τ_{FR} depends on test conditions. From tests on a P-type engine carried out using SAE 10W/30 grade oil, Figure 8.9 shows the dependence on temperature (at 1000 rpm) and speed (at a temperature of -20°C). Friction decays more slowly at lower temperatures, with time constants rising from about 7 seconds at +40°C to 36 seconds at -20°C. The lower graph shows how reducing speed (here, at -20°C) lengthens the decay time still further. Although P-type cold start times are not presented, they are similar to the 1.8 litre IDI engine; the initial friction transient therefore lasts for considerably longer than the start under all conditions.

Data were also available from the 1.8 litre IDI engine and the VW competitor unit. Adding these to the results from the P-type (Figure 8.10) indicates that the two Ford engines behave in a similar manner: τ_{FR} falls as speed and temperature rise. The VW engine reaches its steady-state friction value far more quickly under all conditions. The transient at 1000 rpm takes approximately half the time of the Ford engines, and this difference becomes more marked as the speed decreases. A similar reduction of τ_{FR} in the Ford engines would have a very significant effect on low temperature starting, where a long period of firing-assisted cranking is required until the friction falls below a critical level. If the friction decay characteristics of the IDI engine matched those of the VW, cold start times at -20°C would reduce from about 30 seconds to under 15 seconds.

As described above, changes to the oil viscosity grade were found to have no effect on FR_b , since the change in initial friction was matched by a corresponding change in steady state friction with changing oil. However, as shown in

Figure 8.11, using the more viscous SAE 20W/50 oil increases τ_{FR} from about 30 seconds (with SAE 10W/30) to over 70 seconds at -10°C . The dependence of oil viscosity on temperature does not account for this effect, as plotting the time constant against kinematic viscosity of the oil at the inlet to the block shows that the two are not directly related. The explanation for this is uncertain; it is possible that a different additive blend is used for the higher viscosity oil, giving it a different dependence on shear rate.

8.4 Theoretical Consideration

To gain further insight into the conditions giving rise to the friction characteristics during the early period of engine running, a special test rig was constructed. An isolated crankshaft running in main bearings was instrumented to record relevant data about torque, oil flow rates and local bearing temperature. The crankshaft, together with a separately driven oil pump to maintain normal oil flow, was motored in the block of a 1.8 litre Ford IDI engine. The assembly was installed in a refrigerated enclosure allowing temperatures from ambient to below -20°C . The development of this facility was carried out in collaboration with a co-worker, who undertook the test work. The results obtained are described in greater detail elsewhere [8.6]. Here, the results are used in conjunction with basic theoretical considerations to develop a model for bearing friction in the crankshaft.

8.4.1 Overview of Test Data

The crankshaft assembly was installed in a small refrigerated enclosure providing soak temperatures from ambient to below -20°C . A small DC motor turns both the oil pump and, through a torque measuring device, the crankshaft at speeds up to 1000 rpm. Temperature measurements included that of the oil after the oil pump, at the inlet to the block, as previously used to characterise oil temperature. Importantly, thermocouples were placed to measure the temperature in the main

bearing oil film. This was done by drilling through the bearing cap and shell, perpendicular to the bearing surface, and inserting a 0.5 mm diameter thermocouple. The thermocouple tip was located flush with the bearing surface, but not in contact with the walls of the drilling. In this way, the thermocouple was protected from damage by the rotating journal, but the temperature recorded closely approximated the actual oil temperature in the film.

During a motored test at fixed speed starting at -20°C , the temperature measured in the bearing oil film was found to be quite different from the oil feed temperature, as shown in Figure 8.12. The small initial drop in oil feed temperature is due to an initial difference between block and oil temperatures. When the cold oil was picked up from the sump, the block was initially cooled slightly. Disregarding this fall, the oil feed temperature rises slowly but steadily after a short initial delay. However, at the low temperature shown here, the temperature in the bearing oil film rises very sharply as rotation begins, being about 4°C warmer than the feed when the first sample is taken after one second. This corresponds to a drop in oil viscosity of about 33% (from 3790 cSt to 2540 cSt), which takes place before any data can be collected. By 50 seconds, viscosity has dropped a further 55% to 1120 cSt, accompanied by a significant fall in friction.

The rapid change in oil film temperature is not characterised by oil feed or bulk structure temperatures, and provides a likely explanation for the initial transient friction. If the friction is plotted against viscosity on log scales (Figure 8.13), it can be seen that the initial friction transients (upper graph) are not observed if the temperature in the bearing is used to calculate viscosity (lower graph). That is, crankshaft frictional losses are linearly related to viscosity evaluated at the measured oil temperature in the journal bearing. To predict the film temperature, however, requires a description of thermal conditions around the rubbing surfaces. At the time of writing, work is ongoing at Nottingham to develop models for engine friction which take account of variations in local oil film

temperatures. Here, an interim model is developed to examine sensitivity of friction to various design variables. In this model, only the behaviour of the crankshaft journal bearings is considered, and use is made of experimental data to provide values for block and oil feed temperatures.

8.4.2 Model for Quasi-Steady Condition

The model is based on the Cameron's assumption [8.7] that energy dissipated due to friction is balanced by convective heat transport at fully warm, high speed conditions. For cold start conditions, this is modified to allow for conduction to the engine structure, originally neglected by Cameron. The effect of shear on the viscosity of multigrade oil is also modelled; at low temperatures, this is significant at even moderate speeds. Assuming that the bearing is fully flooded with oil and has low eccentricity, friction can be modelled by Petroff's equation [8.7]:

$$F = \frac{2\pi \eta U R L}{c} \quad (8.4)$$

Where F is the frictional force, η is the dynamic viscosity, and U is the bearing surface speed. R , L and c are the bearing radius, length and radial clearance respectively. Petroff's equation is suitable for use during cold starting, which has conditions of high lubricant viscosity and low load engine operation [8.8]. Frictional heat input is simply $F \times U$, and this is equated to heat transfer from the bearing by convection and conduction. Considering convection first: if the oil temperature rises linearly by ΔT_{oil} between entering the centre groove and leaking out at the bearing edge, and \dot{q}_{total} is the volume oil flow rate, then:

$$\dot{Q}_{conv} = \dot{q}_{total} \rho \sigma \Delta T_{oil} \quad (8.5)$$

Where \dot{Q}_{conv} is the power convected from the bearing, ρ and σ are the density and specific heat of the oil. The total oil flow consists of a component due to the pumping action of the hydrodynamic wedge in the rotating bearing (pumped flow, \dot{q}_{pumped}) and a component due to the feed pressure (pressure flow, $\dot{q}_{\text{pressure}}$). From Cameron, using short bearing theory, the pumped flow through the bearing is given by:

$$\dot{q}_{\text{pumped}} = \dot{q}^* \frac{U c L}{2} \quad (8.6)$$

with \dot{q}^* , the non-dimensional flow coefficient, put equal to $0.6 \times (2 - L/D)$ with D the bearing diameter. Again from Cameron, assuming that the oil feed is through a central groove along 180° of the circumference and with P_{pump} equal to the gauge oil feed pressure, gives:

$$\dot{q}_{\text{pressure}} = \frac{c^3 \pi D P_{\text{pump}}}{6 \eta L} \quad (8.7)$$

Experimental results collected by Bianco [8.6] show that these equations adequately predict oil flow for the range of conditions studied here.

Considering conduction: assuming that all the metal in the engine is all at block temperature, and the oil is at this temperature as it enters the bearing and rises linearly by ΔT_{oil} before leaking out at the bearing edge. The average oil temperature, \bar{T}_{oil} , is given by:

$$\bar{T}_{\text{oil}} = T_{\text{feed}} + \frac{1}{2} \Delta T_{\text{oil}} \quad (8.8)$$

and, since the oil feed is at the metal temperature, ($T_{\text{feed}} = T_{\text{metal}}$), the temperature difference between oil film and metal is:

$$\bar{T}_{\text{oil}} - T_{\text{metal}} = \frac{1}{2} \Delta T_{\text{oil}} \quad (8.9)$$

Using this temperature difference to characterise conduction, consideration of basic heat transfer gives an equation for heat flow from oil to block, \dot{Q}_{cond} :

$$\dot{Q}_{\text{cond}} = \frac{\frac{1}{2} \Delta T_{\text{oil}}}{R_{\text{ob}}} \quad (8.10)$$

Here, R_{ob} represents the thermal resistance between the oil film and the bulk of the block. The value of R_{ob} will depend on a number of factors, including:

- The surface area over which heat transfer can occur, both into the journal and the bearing shell ($2\pi DL$).
- The thermal conductivities of the materials involved (oil, journal, shell and block).
- The thermal coupling between these materials (oil to surrounding metal, bearing shells to the block).
- The characteristic lengths involved (oil film thickness, bearing shell thickness).

In practice, the oil temperature would be expected to vary throughout its thickness, and the bearing surfaces would experience local heating. These factors are not explicitly modelled here, but are represented by a change in the effective thermal resistance to the block. This is a simplified description which requires the value of R_{ob} to be derived from matching with experimental results.

In the steady-state, the heat generated must be balanced by heat removal, so $FU = \dot{Q}_{\text{conv}} + \dot{Q}_{\text{cond}}$. The equations above can be solved iteratively for ΔT_{oil} , provided the correct viscosity can be evaluated. According to Cameron, the effective temperature in the bearing can be calculated as the feed temperature (here, block temperature) plus about 0.8 times the temperature rise. The viscosity of multigrade oils is dependent on both temperature and the rate of shear; the effects of pressure are neglected here. Although normally associated with high bearing speeds, Bartz and Reynolds [8.9] showed that, at low temperatures, this loss can become significant at relatively low speeds. At cold start temperatures it cannot be neglected. The oil manufacturer and suppliers were unable or unwilling to provide the relevant information about the test oils used in this work, so a simple method was developed to characterise the shear effect. By measuring the turning torque on the crankshaft test rig over a range of speeds and temperatures, Petroff's equation (8.4) was solved to estimate the actual dynamic viscosity. Using the measured temperature in the oil film, the expected viscosity was compared with the actual to evaluate the percentage reduction. This did not yield enough data to justify the use of the more complex equations for viscosity shear loss [8.8, 8.10], but Cameron presented data showing that the viscosity reduction depends on shear stress (the product of shear rate and dynamic viscosity). The test results plotted in Figure 8.14 conform with this dependence: no viscosity loss occurs at shear stresses below about 7500 Pa, and above this threshold value the viscosity loss is linearly dependent on the log of shear stress. In the main bearings considered here no reduction would occur below about 4000 rpm when fully warm, but some viscosity loss would be seen at 330 rpm at +20°C and at 15 rpm at -20°C.

Using the shear/viscosity relation shown in Figure 8.14 allows the equations set above to be closed, subject to setting values for the thermal resistance R_{ob} . Using $R_{\text{ob}} \approx 0.07 \text{ K/W}$ gives good agreement between measured and predicted quasi-steady friction levels, as illustrated in Figure 8.15. Comparison with data

supplied by the engine manufacturer [8.11] shows that the model is still within 20% of measured values at 6000 rpm and 85°C.

Cameron [8.7] stated that most of the heat is removed by convection to the oil, and Dowson, Ruddy, Sharp and Taylor [8.12] calculated that the bearing friction could be significantly altered by the oil supply arrangement. Results from the model developed here show that, at low temperatures and speeds, convection has only a secondary effect and removes less than 10% of the generated heat. This means that, providing enough oil is supplied to maintain a lubricant film, the effect of oil flow rate on friction will only be small under cold starting conditions. This simple model cannot, however, predict friction during the initial transient period at the start of each test; this requires the way in which temperature changes with time to be modelled.

8.4.3 Transient Model Development

To represent the conditions affecting the crankshaft during transient operation, the model has been extended to include the influence of nearby thermal masses. Metal in close contact with the crankshaft bearings is represented by a thermal inertia, connected by thermal resistances, as shown diagrammatically in Figure 8.16. Heat generated in the oil film is conducted out to the metal around the bearing and then into the bulk of the block. In this simple treatment the block temperature is set from experimental results, above which each of the other temperatures are evaluated. The following physical significance can be attached to the various parts of the model:

- The thermal resistance from the oil to the thermal inertia, R_{om} , controls conduction between the oil and the metal of the bearing. It governs the magnitude of initial friction.
- The thermal resistance from the thermal inertia to the block, R_{mb} , controls conduction away from the metal of the bearing to the bulk

of the block. In conjunction with R_{om} it regulates the steady-state friction.

- The thermal inertia represents that body of metal in close contact with the journal bearing whose temperature controls heat transfer from the oil. Along with the thermal resistances, it sets the rate of decay of initial friction.

The thermal inertia does not necessarily represent a specific component such as the bearing journal or cap, and must be calibrated against experimental data. Similarly, the thermal resistances must be calibrated, but should sum up to the value of R_{ob} used above, to maintain the good steady-state match.

The modified model was solved iteratively, as before, with the additional requirement to calculate changes to the nearby metal temperature with time. Denoting the temperature of the thermal inertia above the block as ΔT , the temperature rise at step $n+1$, a small time Δt after step n , was calculated as:

$$\Delta T_{n+1} = \Delta T_n + \frac{\Delta t (\dot{Q}_{cond} - \dot{Q}_{mb})}{m_m \cdot c_m} \quad (8.11)$$

\dot{Q}_{conv} flows into the mass and \dot{Q}_{mb} flows out of the mass to the block (both evaluated at step n), and the thermal inertia, $m_m \cdot c_m$, is the product of mass and specific heat.

The modified model gives predictions of friction which are in good agreement with experimental results. A comparison of experimental and predicted results for start temperatures from -20°C to $+20^\circ\text{C}$ and speeds up to 1000 rpm is given in Figure 8.17. Future extensions to this model would include prediction of block temperature (currently underway at Nottingham) and modification for other engine components such as connecting rods, balancer shafts, and camshafts.

Similar methods could also be applied to other engine assemblies such as the pistons. However, in the form presented here, the sensitivity of cold friction to theoretical design changes can be examined easily.

8.5 Conclusions

Friction levels during cold starts can be much higher than values measured during steady motored tests. The oil films at the friction surfaces take some time to reach quasi-steady conditions, when the oil feed and film temperatures are related. Until equilibrium is reached, the local oil viscosity (and therefore friction) is far higher than under quasi-steady operation. This can lead to the full-engine friction at -20°C being about twice the steady state value, measured with the same indicated conditions.

Journal bearings, which have already been shown to contribute heavily to low temperature friction under steady-state conditions, are a particular problem. Operating almost entirely in the hydrodynamic regime, they are especially sensitive to changes in oil viscosity. Elements such as camshafts, which operate with a significant proportion of boundary lubrication, are less prone to a large start-up spike.

All measured engines show a similar relationship between steady state and initial friction, defined by the ratio FR_i . This ratio is controlled by the two conditions involved: initial friction depends on the initial oil temperature and the bearing dimensions; steady state friction depends on the balance between frictional heating and conduction (and convection) away from the rubbing surfaces. At -20°C the initial friction is about twice the steady-state value, with the size of the initial transient dropping as temperature rises, being negligible above $+40^{\circ}\text{C}$. Although fairly insensitive to speed (up to 1000 rpm), the transient is smaller at very low speeds.

The duration of the initial transient increases at low speeds and temperatures, making cold starting more difficult (low temperatures and low cranking / firing assisted cranking speeds). Although the Ford engines appear similar, a competitor engine of nominally similar design shows a far more rapid decay in this initial friction; the reason for this is unclear. The viscosity grade of the oil used also has a large impact on decay time, with a more viscous oil approximately doubling the duration in one engine. The reason for this change with viscosity grade remains an open issue at present.

For multigrade oils, the sensitivity to shear stress acts to significantly reduce friction; at low temperatures (around -20°C) a reduction in viscosity occurs at very low speeds. This change is helpful during cold starting, when oil temperatures are lowest, giving highest shear stress (the product of shear rate and dynamic viscosity), conditions which promote viscosity reductions and lower friction.

A model for crankshaft journal bearings based on lubrication theory and a simple heat transfer model has been shown to correctly predict friction over a wide range of cold starting speeds and temperatures. This may be used to examine the likely effect of design changes on cold start friction, and may be used as the basis of a more complete treatment of the entire engine.

Chapter 9

SUMMARY AND CONCLUSIONS

9.1 Overview

The work presented in this thesis identifies a number of factors which significantly influence the cold start behaviour of diesel engines at low temperatures. Tests on an IDI engine in current production, along with development of a model for starter motor performance, have revealed that the relative magnitude of combustion work output and frictional losses is particularly important. As temperature reduces, increasing losses reduce the net work available to accelerate the engine to idle speed. Input is required from the starter motor until friction throughout the engine (FMEP) drops below the useful combustion output (IMEP). Low temperature starting is a balance between these two, with any shortfall in IMEP made up by the starter motor.

Since the starter provides significant power output only at relatively low engine speeds, a successful start requires IMEP to exceed FMEP. At higher temperatures (typically above -10°C for the IDI engine studied here) this occurs immediately, and a start is quickly achieved. After a few strokes, firing commences and the engine is rapidly accelerated to idle speed by combustion work. At lower temperatures, however, raised frictional losses are initially greater than the available combustion work, and start times are extended. Once firing is achieved, IMEP acts against friction to turn the engine, but input is still required from the starter. This leads to a period of firing-assisted cranking, where speeds are considerably above those during normal cranking, but the engine stalls if the starter is switched off. As cranking progresses, local heating within the engine lowers friction by reducing oil viscosity at critical bearing surfaces. This causes

an increase in engine speed, giving an improvement in IMEP (due to reduced blowby and heat transfer losses, and improved fuel utilisation). However, the rising speed also causes a sharp reduction in starter output, restoring the temporary equilibrium. Eventually, friction reduces and speed rises enough for IMEP to exceed FMEP and the starter is no longer required. A start is therefore achieved, providing enough energy is available from the battery to maintain cranking for long enough.

Any mechanism that changes this balance will have an effect on cold starting:

- Heat transfer and gas leakage losses have an adverse effect and reducing these is advantageous. They reduce the probability of ignition during cranking and lower work output once firing is achieved, especially at low speeds.
- Poor combustion characteristics leading to misfire, poor fuel utilisation, or badly phased combustion have a similar effect to the above. Poor IMEP at low speeds is largely due to very low fuel utilisation. Improved combustion phasing can increase IMEP by increasing the useful output from a given amount of fuel burned.
- High frictional losses reduce cranking speed, making initial firing less likely. These also increase the work input required to turn the engine and accelerate to idle speed. Reducing friction improves starting, particularly at lower temperatures where the firing-assisted cranking phase accounts for a greater part of the start-up. If the friction fell more quickly during starting, this would shorten lower-temperature starts further.
- Starter motor and battery performance can have a significant impact, since adequate speed must be achieved for firing to be initiated. At lower temperatures input from the starter may also be required for some time, during the firing-assisted cranking phase. Here, higher

starter power (and therefore higher engine speed and IMEP) leads to a more rapid fall in friction and hence quicker starting.

9.2 Combustion Behaviour

There are three distinct phases of an engine start: from key on to first-fire, the phase of firing-assisted cranking, and finally the phase from this through the run-up to idle speed. During the first phase, the starter motor is required to turn the engine at a speed at which firing cycles can occur. In the second, the firing-assisted cranking phase, work from combustion accelerates the engine above normal cranking speed but idle cannot be reached. This phase does not occur at higher start temperatures, where IMEP immediately exceeds FMEP. The third phase is usually very short; input from the starter no longer required and the engine quickly accelerates to idle speed. Throughout all three phases, maximising combustion output and avoiding misfires is important. Requirements in these three phases are discussed below, using findings from the Ford 1.8 litre IDI engine.

9.2.1 Time Before First Fire

Glowplugs are typically powered on a short time before cranking commences and maintained at temperature until several seconds at idle running have elapsed. Here, it was found that a minimum tip temperature of 850°C is required for best performance [9.1]. This can be reached in under ten seconds at -20°C. Longer pre-heat times give no improvement in start quality. After the longer time, measurements by a co-worker showed that temperatures in the combustion chamber were only slightly higher [9.2]. Most of the extra energy was conducted away to the coolant, with the remainder being lost during the gas exchange part of the first cycle. These measurements showed that the glowplug did not act to raise the temperature of the metal or bulk cylinder gasses; rather the hot tip acts as an ignition source (as shown by previous studies [9.2, 9.3]). In the IDI engine

studied here, reducing the tip protrusion led to firing in earlier cycles. This is attributed to reducing the adverse effect on swirl in the prechamber [9.4] and possibly due to moving the location of the hot tip.

At low temperatures, poor battery performance and high frictional losses lower cranking speeds and make ignition less likely. This is attributed to the detrimental changes in blowby, heat transfer and fuel injection/preparation. If cranking speed falls too low, ignition never occurs. Modelling and experiments show that blowby loss is strongly dependent on minimum cranking speed, which occurs simultaneously with peak cylinder pressure. Raising minimum speed, even if average cranking speed is reduced, should therefore result in reduced blowby. This may be achieved by either raising engine inertia, raising starter motor inertia [9.5] or changing the starter torque/speed relationship [9.6]. Reduced blowby or heat transfer would benefit this phase, since the resulting higher temperature and pressure around TDC would increase the probability of successful firing.

Injection of excess fuel is helpful during this cranking phase. Fuel accumulated on successive cycles gradually increases the effective compression ratio, making ignition more likely. No fall in friction or blowby as a result of fuelling has been detected in the IDI engine, although in a DI, fuel may get to the piston rings more easily. Injection timing is not critical, as much of the fuel in the cylinder is carried over from previous cycles.

9.2.2 Firing-Assisted Cranking

In this phase, combustion is more likely than during unaided cranking, due to the higher speeds achieved (about 200-400 rpm at -20°C). However, the IMEP produced by firing cycles is very low at these speeds due to poor mixture preparation and high losses due to blowby and heat transfer. The glowplugs are still required to aid ignition and limit misfiring. Retracted glowplugs, which

move the hot tip close to the chamber wall and increase swirl in the prechamber, increase IMEP slightly in firing cycles and help to reduce start times.

Reducing heat transfer and blowby losses may limit misfires and increase IMEP during firing-assisted cranking. The higher gas temperature and pressure during the ignition delay would reduce misfires and (through increased spray breakup and fuel evaporation) means more fuel may be burned. After ignition, reduced blowby would mean more air available for combustion; this is advantageous because the engine runs very rich during starting. Additionally, reducing these losses would clearly allow more of the energy from combustion to be available as IMEP.

Injecting excess fuel is still beneficial in this phase, as it raises IMEP by allowing more fuel to be used. In the engine studied here, up to 50 mg of fuel was injected per cylinder per cycle. Although not more than 20-25 mg is burned the excess is still required for best starts, as lower quantities reduce the amount burned. Here, fuelling could not be increased enough to cause a deterioration in start quality, but calculations show that a maximum of 32 mg could be burned if all the air charge was used. In practice, 100% air utilisation seems impossible, primarily due to poor mixture preparation and the presence of crevice volumes where burning cannot occur. The 20-25 mg of fuel burned with 50 mg injected represents about 70-80% air utilisation. Injection of fuel further in excess of 50 mg would be expected to increase emissions of unburned hydrocarbons for very little starting benefit.

Fuel injection timing is important during firing-assisted cranking. Late injection raises IMEP in firing cycles at the expense of increased misfires. If injection is too early, blowby and heat transfer cause an adverse decay in cylinder pressure generated by combustion while the piston is still close to TDC. Because the piston motion is small in this region, little useful work is done on the crankshaft (calculated as the integral of cylinder pressure with volume, $\int P \cdot dV$). If injection

is too late, ignition cannot occur in the time available close to TDC before the downward motion of the piston causes temperature and pressure to fall rapidly, and a misfire occurs.

9.2.3 Run-Up to Idle

This phase begins when the indicated work done on the piston exceeds all other losses, and the engine can accelerate away from the starter and up to idle speed. As the speed rises, blowby and heat transfer fall, more fuel is burned and IMEP increases dramatically. The glowplugs are still required to control misfires, with the retracted plugs showing similar benefits to earlier phases. Injection timing and fuelling levels become much less critical: providing enough fuel is injected and the timing is approximately correct, the start is very unlikely to fail (falling back to one of the earlier phases) at this point.

After idle speed is reached, glowplugs are required for a short period to control misfires. However, heat transfer and blowby losses drop quickly with rising metal temperatures, and combustion becomes stable and well controlled. After a short time, glowplugs are no longer required. As the engine oil warms and friction falls, the fuel delivery system can gradually reduce the volume injected to maintain a steady idle speed.

9.3 Friction Characteristics

Friction losses at fully-warm operation conditions scale up dramatically at low temperatures. At normal operating temperatures (80-90°C) the oil viscosity is relatively insensitive to temperature and temporary viscosity loss (due to shearing the oil) only occurs at fairly high speeds. Local frictional heating of the bearing and oil does occur, but temperature differences are limited and the sensitivity of viscosity to these changes low.

At low temperatures, oil viscosity depends strongly on shear rate. Large temperature differences are generated between the oil film and the surrounding metal, with oil viscosity being very sensitive to these variations. High friction power leads to considerable conduction to the metal around the friction surfaces. Conditions are unsteady during starting, with the thermal properties of engine components having a considerable effect on friction behaviour. These factors mean that low temperature friction characteristics differ greatly from "normal" measured values. In addition, friction as the engine begins turning is different to the quasi-steady conditions usually measured by motoring or firing tests.

9.3.1 Quasi-Steady Operation

This situation arises after typically 50 to 100 seconds of engine operation. After this time engine friction depends only on the current operating conditions and the viscosity of the engine oil. Oil viscosity is evaluated at the inlet temperature to the main gallery, using the Walther equation. This dependence has been characterised by:

$$\text{FMEP} = \text{FMEP}_{\text{ref}} \left(\frac{v}{v_{\text{ref}}} \right)^n \quad (9.1)$$

This equation agrees well with measured results in a wide variety of engines over limited temperature ranges. Although typically in the range 0.19 to 0.24 for gasoline and 0.25 to 0.32 for diesel engines, the value of the index n depends on engine build and speed, and oil type. Additionally, if the temperature range is extended sufficiently, changes in index n are seen.

The temperature used does NOT represent that of the oil at the rubbing surfaces, but is related to it. Local heating raises the oil film temperature to higher values than the feed temperature by typically 5 to 20°C. Using Petroff's model, the value of n would be unity for hydrodynamically lubricated friction with no significant

change in viscosity due to local heating or temporary viscosity loss due to shearing. In reality, n is reduced because not all surfaces are hydrodynamically lubricated, viscosity is reduced when shear stress is applied to the oil, and local heating reduces viscosity from that calculated using the feed temperature.

The relative contribution of each engine component changes with falling temperature. The large increase in oil viscosity with falling temperature causes friction components which are most sensitive to viscosity to increase most significantly. Engine assemblies operating primarily in the hydrodynamic lubrication regime (such as crankshaft main and big-end bearings) generally make a small contribution to friction under fully-warm conditions; with falling temperature these components become increasingly important. Assemblies having considerable mixed or boundary lubrication (for example, the valvetrain and piston rings) may often contribute considerably to fully-warm friction. However, they become less significant as temperature drops due to their relatively low sensitivity to oil viscosity.

Although equation (9.1) characterises experimental data well over a substantial temperature range, it is purely empirical. As a first step towards developing a full model for low-temperature friction, a simple model based on the crankshaft has been implemented. This used Petroff's Equation to calculate frictional loss based on fully developed hydrodynamic lubrication in a journal bearing, with additional consideration for local heating effects and the impact of shear stress on oil viscosity. Although secondary effects are neglected (such as the crankshaft oil seals and thrust bearings), the model accurately predicts crankshaft friction for temperatures from -20°C to fully warm and speeds up to 1000 rpm. Beyond this range, the prediction was found to be within 20% of the fully-warm friction measured at 6000 rpm.

According to calculations used in this model (verified by measurements), oil flow rate is very small at low speed and temperature, limiting the amount of heat

which can be removed by convection. Therefore oil flow rate has no significant effect on friction, providing the bearing is not starved. The model predicts that, at least in journal bearings, low temperature friction is dominated by the oil characteristics and the effects of conduction. The viscosity/temperature relationship of the oil, along with the dependence on shear stress, has a major impact on friction, since (according to Petroff's Equation) friction is proportional to local oil viscosity. Under quasi-steady conditions, local heat generated by friction is balanced by conduction out of the bearing to the block. This limits how far the oil temperature can rise, thus preventing a further fall in local oil viscosity. It is this balance between heat generation and removal, along with the oil characteristics and bearing geometry, which determines the steady-state friction.

9.3.2 Initial Friction Transient

The local heating of oil films and bearing surfaces which occurs throughout the engine, and a drop in viscosity due to shear stress in the oil, limit the rise in steady-state friction as temperature falls. However, some time is required for this heating to occur and initial friction values are higher than steady-state results imply. Measurements made in a crankshaft journal bearing show that, after an initial very rapid rise, temperatures in the oil film are controlled by conduction to the surrounding metal (see above). Thus the system experiences unsteady heat flow from the oil (where the frictional heating occurs) to both the journal and bearing shells. From here, it passes through to the block and the ambient air. Similar arguments would hold for the entire engine, with the dynamic behaviour of this system controlling the magnitude and duration of the initial friction.

The transient period of friction change has been characterised using the ratio of measured initial friction to the quasi-steady friction under the same conditions (engine build, speed, oil feed temperature and so on). The value of this ratio at a known time after the start of engine rotation has been defined as FR_t , the

friction ratio at time t . Further, the initial magnitude and duration have been defined as FR_I and τ_{FR} . The time constant τ_{FR} was evaluated by assuming an exponential decay for the friction ratio, with the magnitude FR_I evaluated as FR_t close to time zero. True measurement at zero time proved impossible due to experimental limitations, but FR_I (here, evaluated at five seconds) was assumed to be approximately equal to FR_0 in this work. As cranking progresses, FR_t drops from the value FR_0 towards unity at FR_∞ : that is, measured friction equals quasi-steady friction after enough time has elapsed.

Before beginning this work, it was expected that the initial magnitude would be strongly related to oil viscosity, evaluated at the test temperature. Although viscosity gave a reasonable correlation, testing revealed that the strongest relationship was with actual test temperature. For tests at 1000 rpm, a single line relating FR_I to oil feed temperature could be used for different oil viscosity grades and for a number of different engines (including several gasoline and a competitor engine). At -20°C , initial friction was about twice the steady value; at $+40^\circ\text{C}$ this initial increase was not measurable. After accounting for this temperature dependence, no further correlation with engine or oil type was detected. However, values were seen to fall by about 10% when the speed was reduced from 1000 rpm to 250 rpm. The size of the transient is controlled by the difference in local oil temperature when rotation first starts (the cold start temperature) and that when steady state is reached (that is, local heat generation balanced by quasi-steady conduction to the structure of the engine). These results suggest that the factors controlling this relationship are common to a wide range of engine designs.

Lower test temperatures (and hence higher oil viscosities) gave an increase in the initial friction ratio, as expected. However, increasing the oil viscosity by changing oil specification at the same temperature caused no definite change in FR_I . This result is unexpected and the mechanism is unclear. It appears most likely that the metal temperatures in the engine play a dominant role in

determining the actual viscosity of the oil at the bearing surfaces. As viscosity rises at fixed temperature, initial friction rises but the steady state friction rises roughly in proportion, keeping FR_i approximately constant. As start temperature falls, however, the difference between initial and steady oil temperature increases. Coupled with the increased sensitivity of viscosity to temperature, this gives a greater difference between initial and steady friction, and hence higher values of initial friction ratio.

The duration of the transient, defined by τ_{FR} , increases with reducing temperature and engine speed. This has an adverse effect on cold start characteristics. At low temperatures and cranking speeds, when starting is most difficult, the initial friction transient takes the longest time to decay. In addition, limited data show that changing the oil in one engine for a higher viscosity grade resulted in a considerable increase in τ_{FR} .

Not surprisingly, it was found that the engine assemblies having the largest rise in friction from high to low temperature also showed the largest initial friction transients. Components having a large proportion of hydrodynamic lubrication (crankshaft, balancer shafts) and therefore a strong dependence on oil viscosity, have high values of FR_i . Components with mainly mixed or boundary lubrication (camshaft assemblies) and thus a weak dependence on oil viscosity, showed minimal friction transients at start-up.

9.4 Conclusions

GENERAL

- Forced cooling of a test engine allows a rapid rate of cold start testing, subject to minor limitations. Five tests per day are possible, instead of one using more conventional cold soaking. Test methods have been developed to allow the sensitivity to various combustion

parameters to be identified. Similar methods have been applied to motoring friction tests, allowing the contribution of each engine assembly to be identified at different speeds and temperatures.

- With falling temperature, rising engine friction and reduced battery performance lowers cranking speed significantly. This increases blowby and heat transfer losses, which in turn adversely affects combustion characteristics. After firing is achieved, the engine can require a considerable further period of starter motor assistance until total engine friction falls below the available combustion output. This extended phase of firing-assisted cranking is typical of the longest part of engine starting at low temperatures.

MODELLING

- Blowby processes have been adequately described using a compressible flow model treating the leakage paths as a number of volumes connected by orifices. After calibration, this model is able to predict blowby changes with changing speed, temperature and engine design.
- A model describing the starting system (battery, leads and starter motor) has been developed, and applied to cold starting data. This allows the input from the starter to be determined, enabling the calculation of engine friction on a stroke by stroke basis. Results agree closely with data from motored engine tests.
- A simple model has been developed and applied to data collected from a crankshaft at various speeds and temperatures. Petroff's journal bearing theory has been used with simple models for oil flow and heat transfer, and an empirical model for viscosity lost at high

shear stress. This allows the temperature and viscosity of the oil films, and therefore the friction in the bearings, to be predicted.

GLOWPLUGS

- The glowplugs, used as a starting aid, do not raise bulk gas temperature or heat the combustion chamber walls significantly. They provide a hot spot in the chamber to initiate combustion of the air-fuel mixture.
- Raising the temperature of the glowplug tip reduces misfires and variability in ignition quality (defined by ignition delay). Temperatures above about 850°C provide only a marginal improvement, but misfires increase sharply if the temperature is reduced below this.
- In one engine, reducing the protrusion of the glowplug improves start performance, due to improved fuel utilisation. Although possibly affected by moving the position of the hot tip closer to the wall, this effect has been shown to be largely due to removing the physical obstruction from the swirl chamber.

COMBUSTION

- During cranking, fuel remains in the cylinder between successive cycles. Accumulated fuel gradually raises the effective compression ratio, making combustion more likely. Increased fuel injection makes this process more rapid.

- Increased fuel injection quantity gives an increase in the amount burned in firing cycles, raising IMEP. However, much of the fuel injected during cold starting has been found to remain unburned.
- Due to the high losses experienced during starting, retarded fuel injection has been shown to improve IMEP in firing cycles. This is due to the combustion energy being utilised more efficiently at a later crank angle. However, this is offset by an increasing likelihood of misfiring. In one test engine, optimum timing for start of injection has been found to be about $3\frac{1}{2}^{\circ}$ BTDC.
- Changing the rate of injection has not been shown to significantly alter start performance, although only a narrow range of injection rates could be achieved in the test engine.

FRICITION

- The variation of engine friction measured during warm-up under quasi-steady conditions can be characterised using the oil feed temperature to the main gallery. Using this temperature, whole-engine friction has been approximated by a simple equation relating friction to a measured reference value. Oil viscosity is the controlling parameter. Friction scales in proportion to viscosityⁿ, where n was about 0.19 to 0.24 for gasoline and slightly higher (0.25 to 0.32) for diesel engines.
- Local heating of oil films and bearing surfaces throughout the engine significantly reduces friction in the steady-state case. This is especially relevant at low temperatures, where temporary viscosity loss under high shear stress causes a further reduction.

- Initial friction at low temperature, as the engine first begins turning, is far higher than values measured at steady-state. This is because some time is required for local heating to raise oil and metal temperatures. At -20°C , initial friction is about twice the steady value; by $+40^{\circ}\text{C}$ this initial increase is not measurable. The duration of this high friction level depends strongly on engine design and oil type, but rises with falling temperature and speed. In all cases, the duration is longer than the cold start time.

RECOMMENDATIONS FOR FURTHER WORK

- Further investigation of combustion parameters with the aim of raising IMEP at low speeds. This could include changes to fuel injector design or fuelling schedule, or changes to the combustion chamber design.
- Closer examination of the factors controlling the decay in initial friction, to understand the differences between engine designs. This may include changes in bearing geometry or oil feed arrangement, or changes in the thermal coupling of components around the bearing surfaces.

REFERENCES

Chapter 1

- 1.1 Merriks Publishing Limited, "Electronic FUTURE", pp 104-106, Diesel Car Magazine, September 1993
- 1.2 André M, "In Actual Use Car Testing: 70,000 Kilometres and 10,000 Trips by 55 French Cars under Real Conditions", SAE paper number 910039
- 1.3 Greening P, "The Future of European Emission Regulations", European Commission, Conference 'Engine and Environment', 1997
- 1.4 Austen A E W and Lyn W-T, "Some Investigations on Cold Starting Phenomena in Diesel Engines", Proc. IMechE, Number 5, 1959-60
- 1.5 Brunner M and Ruf H, "Contribution to the Problem of Starting and Operating Diesel Vehicles at Low Temperatures", Proc. IMechE, Number 5, 1959-60
- 1.6 Caracciolo F and McMillan M L, "Effect of Engine Oil Viscosity on Low-Temperature Cranking, Starting, and Fuel Economy", SAE paper number 790728
- 1.7 Buck W H and Lohuis J R, "Lubricant Effects on Low-Temperature Diesel Engine Cold Starting", SAE paper number 940097
- 1.8 Stewart R M and Selby T W, "The Relationship Between Oil Viscosity and Engine Performance - A Literature Search", SAE paper number 770372

- 1.9 Stewart R M, "Engine Pumpability and Crankability Tests on Commercially 'W' Graded Engine Oils Compared to Bench Test Results", SAE paper number 780369
- 1.10 von Petery C, Kruse H and Bartz W J, "Influence of the Viscosity of Polymer Containing Engine Oils on the Startability of Engines", SAE paper number 780370
- 1.11 Alexander A G, May C J and Smith C R, "Factors Affecting Pumpability and Cold Cranking in Heavy Duty Diesel Truck Engines at Low Ambient Temperatures - Part II", SAE paper number 920023
- 1.12 Zahdeh A, Henein N and Bryzik W, "Diesel Cold Starting: Actual Cycle Analysis Under Border-Line Conditions", SAE paper number 900441
- 1.13 Cold Cranking Simulator (CCS) test using ASTM test procedure D5293, specified within the SAE J300 viscosity classification, 1991
- 1.14 Henein N, "Starting of Diesel Engines: Uncontrolled Fuel Injection Problems", SAE paper number 860253
- 1.15 Heywood J B, "Internal Combustion Engine Fundamentals", Chapter 12, McGraw-Hill Book Company, ISBN 0-07-100499-8, 1988
- 1.16 Annand W J D, "Heat Transfer in the Cylinders of Reciprocating Internal Combustion Engines", Proc. IMechE, Volume 177 Number 36, 1963
- 1.17 Woschni G, "A Universally Applicable Equation for the Heat Transfer Coefficient in the Internal Combustion Engine", SAE paper number 670931

- 1.18 Huber K, Woschni G and Zeilinger K, "Investigations on Heat Transfer in Internal Combustion Engines under Low Load and Motoring Conditions", SAE paper number 905018

- 1.19 Harigaya Y, Ohyagi S and Tsuji H, "An Experimental Study on Heat Transfer in a Pre-Chamber Type Diesel Engine", SAE paper number 905019

- 1.20 Lyn W-T and Valdmanis E, "The Effects of Physical Factors on Ignition Delay", Proc. IMechE, Volume 181 Part 2A Number 1, 1966-67

- 1.21 Biddulph T W and Lyn W-T, "Unaided Starting of Diesel Engines", Proc. IMechE, Volume 181 Part 2A Number 1, 1966-67

- 1.22 Henein N, Zahdeh A R, Yassine M K and Bryzik W, "Diesel Engine Cold Starting: Combustion Instability", SAE paper number 920005

- 1.23 Henein N A and Lee C-S, "Autoignition and Combustion of Fuels in Diesel Engines Under Low Ambient Temperatures", SAE paper number 861230

- 1.24 Phatak R and Nakamura T, "Cold Startability of Open-Chamber Direct-Injection Diesel Engines - Part I: Measurement Technique and Effects of Compression Ratio", SAE paper number 831335

- 1.25 Zahdeh A R and Henein N, "Diesel Engine Cold Starting: White Smoke", SAE paper number 920032

- 1.26 Phatak R and Nakamura T, "Cold Startability of Open-Chamber Direct-Injection Diesel Engines - Part II: Combustion Chamber Design and

Fuel Spray Geometry and Additional Air and Glow Plug as a Starting Aid", SAE paper number 831396

- 1.27 French G R and Scott W M, "Giving the IDI Diesel a Fresh Start", SAE paper number 850452
- 1.28 Mohr H and Urlaub A, "Improvement of the Cold Start Qualities of Diesel Engines with Swirl Chambers", SAE paper number 940075
- 1.29 Shen K, Matthews R D, Chui J P, Darden M H, Faidley R W, Nichols S P and Weldon W F, "Initial Study of Railplugs as an Aid for Cold Starting of Diesels", SAE paper number 940108
- 1.30 Gustavsson G and Cederberg H-O, "Unique Cold Start Method Used on Volvo's New 12L Unit Injector Diesel Engine", SAE paper number 940109
- 1.31 Sun R, Sweet J, Zurlo J R and Pfefferle W C, "Diesel Engine Cold Starting with Catalytically Ignited Recirculated Exhaust Gas", SAE paper number 940086
- 1.32 Tsantis A P, Brown J S, Hutter R J, Lyon P M and Singh T, "Improvements in Heater, Defroster and Emissions Performance Using a Latent Heat Storage Device", SAE paper number 940089
- 1.33 Stecki J S, Cichocki W, Garbacik A and Szewczyk K, "Heating Systems for Cold Starting of IC Engines", SAE paper number 920002
- 1.34 Mina T I, "A detailed study of the start and run-up behaviour of a multi-cylinder direct injection diesel engine", IMechE paper number C372/011, 1989

- 1.35 Poublon M, Patterson D J and Boerma M, "Instantaneous Crank Speed Variations as Related to Engine Starting", SAE paper number 850482
- 1.36 Kytö M, "Study of Automotive Gear Lubrication at Low Temperatures", SAE paper number 920021
- 1.37 Kytö M, "Engine Lubrication in Cold Start-Up", SAE paper number 890033
- 1.38 Cameron A, "Basic Lubrication Theory", Third Edition, Ellis Horwood Limited, 1981

Chapter 2

- 2.1 Teo Y C, "Mixture Ratio Control of a Spark Ignition Engine during Transient Operations", PhD Thesis, University of Nottingham, 1994
- 2.2 Douaud A and Eyzat P, "DIGITAP - An On-Line Acquisition and Processing System for Instantaneous Engine Data Applications", SAE paper number 770218
- 2.3 Brown W L, "Methods for Evaluating Requirements and Errors in Cylinder Pressure Measurement", SAE paper number 670008
- 2.4 Ball W F, Jackson N S, Pilley A D and Porter B C, "The Friction of a 1.6 Litre Automotive Engine - Gasoline and Diesel", SAE paper number 860418
- 2.5 Lancaster D R, Krieger R B and Lienesch J H, "Measurements and Analysis of Engine Pressure Data", SAE paper number 750026

- 2.6 Kuratle R H and Märki B, "Influencing Parameters and Error Sources During Indication on Internal Combustion Engines", SAE paper number 920233
- 2.7 Stein R A, Mencik D Z and Warren C, "Effect of Thermal Strain on Measurement of Cylinder Pressure", SAE paper number 870455
- 2.8 Kuratle R, "Combustion Engine Measurement Technology", Kistler Instruments Limited, February 1990
- 2.9 Henderson K O, "Low Temperature Performance of Commercial SAE 5W-30 Oils in Engines and Their Correlation with Bench Tests", SAE paper number 920650
- 2.10 May C J and Smith C R, "The Importance of Lubricant Low Temperature Performance to Vehicle Operation or 'Will it Still Go When its 30 Below?'" , SAE paper number 920024

Chapter 3

- 3.1 Lawrence R J and Evans R W, "The Ford 1.8L Four Cylinder Turbocharged Diesel Engine for Passenger Car Applications", SAE paper number 901716
- 3.2 May C J and Smith C R, "The Importance of Lubricant Low Temperature Performance to Vehicle Operation or 'Will it Still Go When its 30 Below?'" , SAE paper number 920024
- 3.3 Stewart R M and Selby T W, "The Relationship Between Oil Viscosity and Engine Performance - A Literature Search", SAE paper number 770372

- 3.4 Brunner M and Ruf H, "Contribution to the Problem of Starting and Operating Diesel Vehicles at Low Temperature", Proc. IMechE No. 5, pp 124-136, 1959-60
- 3.5 Stewart R M, "Engine Pumpability and Crankability Tests on Commercial 'W' Graded Engine Oils Compared to Bench Test Results", SAE paper number 780369
- 3.6 Personal communication from Ford Motor Company, "Oil Viscosity Test Results for Cold Room Test Oils AL3683 and AL3714", Electronic mail, 1993

Chapter 4

- 4.1 Robert Bosch GmbH, "Technical data: Starter EV 12V 2.2 kW", 18 August 1994
- 4.2 Caracciolo F and McMillan M L, "Effect of Engine Oil Viscosity on Low-Temperature Cranking, Starting, and Fuel Economy" , SAE paper number 790728

Chapter 5

- 5.1 Brunner M and Ruf H, "Contribution to the Problem of Starting and Operating Diesel Vehicles at Low Temperatures", Proc. IMechE No. 5, pp 124-136, 1959-60
- 5.2 Caracciolo F and McMillan M L, "Effect of Engine Oil Viscosity on Low-Temperature Cranking, Starting, and Fuel Economy", SAE paper number 790728

- 5.3 Zahdeh A, Henein N A and Bryzik W, "Diesel Cold Starting: Actual Cycle Analysis under Border-Line Conditions", SAE paper number 900441
- 5.4 May C J and Smith C R, "The Importance of Lubricant Low Temperature Performance to Vehicle Operation or 'Will it Still Go When its 30 Below?'" , SAE paper number 920024
- 5.5 Henein N A "Starting of Diesel Engines: Uncontrolled Fuel Injection Problems", SAE paper number 860253
- 5.6 Henein N A and Lee C-S, "Autoignition and Combustion of Fuels in Diesel Engines Under Low Ambient Temperatures", SAE paper number 861230
- 5.7 Neveu C, "A Study of the Significance of Lubricant Viscosity in Blow-By Control", SAE paper number 770375
- 5.8 Austen A E W and Lyn W-T, "Some Investigations on Cold-Starting Phenomena in Diesel Engines", Proc. IMechE No. 5, pp 111-123, 1959-60
- 5.9 Wentworth J T, "Piston and Ring Variables Affect Exhaust Hydrocarbon Emissions", SAE paper number 680109
- 5.10 Munro R, "Blow-By in Relation to Piston and Ring Features", SAE paper number 810932
- 5.11 Furuhashi S, Hiruma M and Tsuzita M, "Piston Ring Motion and Its Influence on Engine Tribology", SAE paper number 790860

- 5.12 Rao V K, Gardiner D P and Bardon M F, "Effects of Gas Leakage and Crevices on Cold Starting of Engines", SAE paper number 940078
- 5.13 Namazian M and Heywood J B, "Flow in the Piston-Cylinder-Ring Crevices of a Spark-Ignition Engine: Effect on Hydrocarbon Emissions, Efficiency and Power", SAE paper number 820088
- 5.14 Personal communication from Clive Tindle, "L-type piston effects on blowby losses", University of Nottingham, 1997

Chapter 6

- 6.1 Lawrence R J and Evans R W, "The Ford 1.8L Four Cylinder Turbocharged Diesel Engine for Passenger Car Application", SAE paper number 901716
- 6.2 Merriks Publishing Limited, "Electronic FUTURE", pp 104-106, Diesel Car Magazine, September 1993
- 6.3 Zahdeh A R and Henein N, "Diesel Engine Cold Starting: White Smoke", SAE paper number 920032
- 6.4 Heywood J B, "Internal Combustion Engine Fundamentals", Section 10.5, McGraw-Hill Book Company, ISBN 0-07-100499-8, 1988
- 6.5 Knight B E, "Fuel-Injection System Calculations", Proc. IMechE, Number 1, 1960-61
- 6.6 Kim C, Tseregonounis S I and Scruggs B E, "Deposit Formation on a Metal Surface in Oxidized Gasolines", SAE paper number 872112

- 6.7 Personal communication from Clive Tindle, "Heat Release analysis in the Ford 1.8 L IDI engine", University of Nottingham, 1996
- 6.8 Woschni G, "A Universally Applicable Equation for the Heat Transfer Coefficient in the Internal Combustion Engine", SAE paper number 670931
- 6.9 Hayes T K, Savage L D and Sorenson S C, "Cylinder Pressure Data Acquisition and Heat Release Analysis on a Personal Computer", SAE paper number 860029
- 6.10 Grimm B M and Johnson R T, "Review of Simple Heat Release Computations", SAE paper number 900445
- 6.11 Austen A E W and Lyn W-T, "Some Investigations on Cold Starting Phenomena in Diesel Engines", Proc. IMechE, Number 5, 1959-60
- 6.12 Biddulph T W and Lyn W-T, "Unaided Starting of Diesel Engines", Proc. IMechE, Volume 181 Part 2A Number 1, 1966-67
- 6.13 Lyn W-T and Valdmanis E, "The Effects of Physical Factors on Ignition Delay", Proc. IMechE, Volume 181 Part 2A Number 1, 1966-67
- 6.14 Phatak R and Nakamura T, "Cold Startability of Open-Chamber Direct-Injection Diesel Engines - Part I: Measurement Technique and Effects of Compression Ratio", SAE paper number 831335
- 6.15 Zahdeh A, Henein N and Bryzik W, "Diesel Cold Starting: Actual Cycle Analysis Under Border-Line Conditions", SAE paper number 900441

- 6.16 French G R and Scott W M, "Giving the IDI Diesel a Fresh Start", SAE paper number 850452
- 6.17 Personal communication from Clive Tindle, "Ford 1.8 L IDI glowplug studies", University of Nottingham, 1996
- 6.18 Tawfig M E, Charlton S J and Prest P H, "An investigation of air motion and gas temperature in a motored indirect-injection diesel engine", IMechE paper number C433/002, 1991

Chapter 7

- 7.1 Ball W F, Jackson N S, Pilley A D and Porter B C, "The Friction of a 1.6 Litre Automotive Engine - Gasoline and Diesel", SAE paper number 860418
- 7.2 Millington B W and Hartles E R, "Frictional Losses in Diesel Engines", SAE paper number 680590
- 7.3 Ciulli E, "A review of internal combustion engine losses Part 2: studies for global evaluations", Proc. IMechE Volume 107, p229, 1993
- 7.4 Monaghan M L, "Engine friction - a change in emphasis", Proc. IMechE Volume 202 Number D4, p215, 1988
- 7.5 Douaud A and Eyzat P, "DIGITAP - An On-Line Acquisition and Processing System for Instantaneous Engine Data Applications", SAE paper number 770218
- 7.6 Darnton N J, "Fuel Consumption and Pollution Emissions of Spark Ignited Engines During Cold-Started Drive Cycles", PhD thesis. University of Nottingham, 1997

- 7.7 Schilling A, "Motor Oils and Engine Lubrication", Second Edition, Scientific Publications (G.B.) Limited, 1968
- 7.8 Bishop I N, "Effect of Design Variables on Friction and Economy", SAE paper number 812A, January 1964
- 7.9 Owen N J, "Firing Friction Breakdown of a Ford 1.8L IDI Diesel Engine", Ricardo Report Number DP89/1098, August 1989 (Ford Motor Company internal report)
- 7.10 Patton K J, Nitschke R G and Heywood J B, "Development and Evaluation of a Friction Model for Spark-Ignition Engines", SAE paper number 890836
- 7.11 Staron J T and Willermet P A, "An Analysis of Valve Train Friction in Terms of Lubrication Principles", SAE paper number 830165
- 7.12 Personal communication from C R Tindle, "Friction breakdown of the Ford L-type engine, series O", University of Nottingham, 1997
- 7.13 Marcroft A, "Frictional Benchmarking of P-type Series O", from Ricardo Report, February 1996 (Ford Motor Company internal report)
- 7.14 Personal communication from C R Tindle, "Friction breakdown of the VW 1.9 TDi engine" University of Nottingham, 1997

Chapter 8

- 8.1 Darnton N J, "Fuel Consumption and Pollution Emissions of Spark Ignited Engines During Cold-Started Drive Cycles", PhD thesis, University of Nottingham, 1997

- 8.2 Personal communication from Clive Tindle, "L-type start-up friction data", University of Nottingham, 1997
- 8.3 Christian S J, "A Spark Ignition Engine Model for Heat Flow and Friction Characteristics", PhD thesis, University of Nottingham, 1992
- 8.4 Patton K J, Nitschke R G and Heywood J B, "Development and Evaluation of a Friction Model for Spark-Ignition Engines", SAE paper number 890836
- 8.5 Staron J T and Willermet P A, "An Analysis of Valve Train Friction in Terms of Lubrication Principles", SAE paper number 830165
- 8.6 Personal communication from Carlo Bianco, "Crankshaft test rig results", University of Nottingham, 1997
- 8.7 Cameron A, "Basic Lubrication Theory", Third Edition, Ellis Horwood Limited, 1981
- 8.8 Taylor R I, "Engine Friction: the influence of lubricant rheology", Proc. IMechE, Volume 211 Part J, 1997
- 8.9 Bartz W J and Reynolds T, "Influence of the Effective Viscosity on Bearing Performance", SAE paper number 810799
- 8.10 Sorab J, Holdeman H A and Chui G K, "Viscosity Prediction for Multigrade Oils", SAE paper number 932833
- 8.11 Owen N J, "Firing Friction Breakdown of a Ford 1.8L IDI Diesel Engine", Ricardo Report Number DP89/1098, August 1989 (Ford Motor Company internal report)

- 8.12 Dowson D, Ruddy A V, Sharp R S and Taylor C M, "An analysis of the circumferentially grooved journal bearing with consideration of lubricant film reformation", Proc. IMechE, Volume 199 Number C1, 1985

Chapter 9

- 9.1 French G R and Scott W M, "Giving the IDI Diesel a Fresh Start", SAE paper number 850452
- 9.2 Personal communication from Clive Tindle, "Ford 1.8 L IDI glowplug studies", University of Nottingham, 1996
- 9.3 Austen A E W and Lyn W-T, "Some Investigations on Cold Starting Phenomena in Diesel Engines", Proc. IMechE, Number 5, 1959-60
- 9.4 Tawfig M E, Charlton S J and Prest P H, "An investigation of air motion and gas temperature in a motored indirect-injection diesel engine", IMechE paper number C433/002, 1991
- 9.5 Mina T I, "A detailed study of the start and run-up behaviour of a multi-cylinder direct injection diesel engine", IMechE paper number C372/011, 1989
- 9.6 Poublon M, Patterson D J and Boerma M, "Instantaneous Crank Speed Variations as Related to Engine Starting", SAE paper number 850482

APPENDIX A

Test Engine Specifications

	Ford 1.8L IDI	Ford 2.2L P-type	Ford 1.8L L-type	VW 1.9L TDi
Type	In-line 4-cyl 8 valves Indirect Injection Single OHC Flat followers	In-line 4-cyl 16 valves Direct Injection DOHC Roller Followers (Hydraulic)	In-line 4-cyl 8 valves Direct Injection Single OHC Flat followers	In-line 4-cyl 8 valves Direct Injection Single OHC Flat followers (Hydraulic)
Inlet	Turbocharged Air-to-air intercooler (TCI only)	Turbocharged Water-to-air intercooler	Turbocharged Air-to-air intercooler	Turbocharged Air-to-air intercooler
Volume	1753 cc	2198 cc	1753 cc	1896 cc
Bore	82.5 mm	86.0 mm	82.5 mm	79.5 mm
Stroke	82.0 mm	94.6 mm	82.0 mm	95.5 mm
Compression Ratio	21.5 nominal	19.0 nominal	19.4 nominal	19.5 nominal

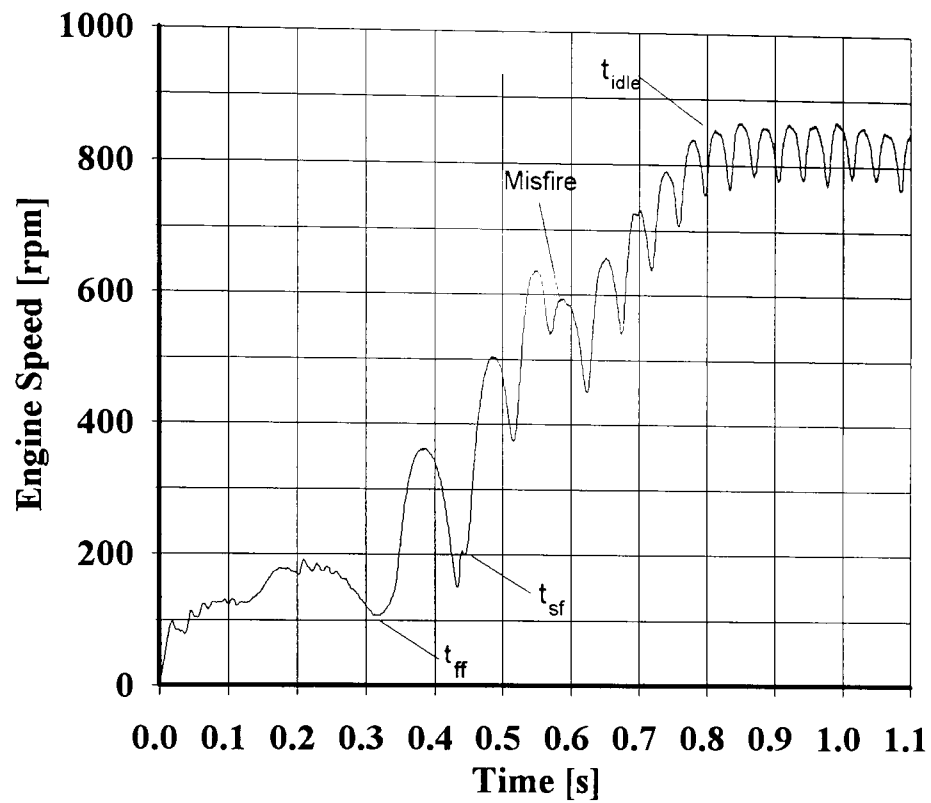
Note: Series O engines are prototype level.

Battery (all engines): Motorcraft 12 V, 650 A, 130 RC
Lead acid, approximately 90 Ampere-Hours

Ford 1.8L IDI (used in firing tests):

Starter: Bosch EV 12V 2.2 kW
Starter Inertia = 0.00292 kg.m²
Gearing to engine = 13.5:1

Engine inertias: Crankshaft = 0.017 kg.m²
Big-ends = 0.003 kg.m²
Flywheel = 0.179 kg.m²
Pressure-plate assembly = 0.038 kg.m²



In this example:

First Fire = 0.32 s

Sustained Fire = 0.43 s

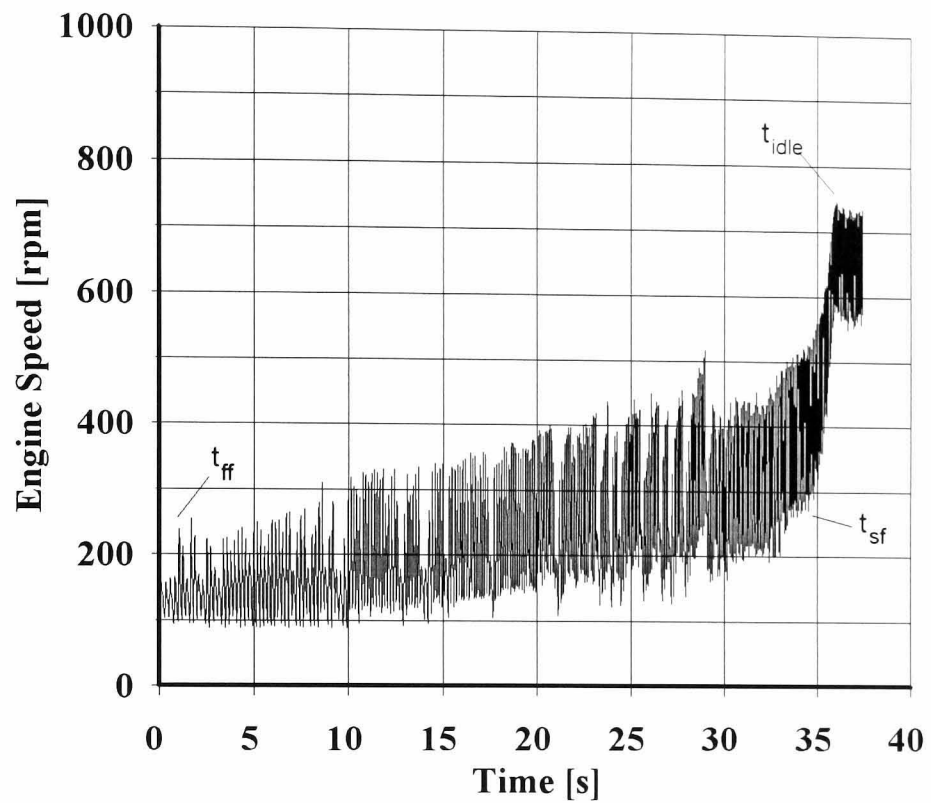
Time to Idle = 0.80 s

Misfire rate = 1/8 (13%)

Figure 1.1

Typical start at -1°C

(Ford 1.8L IDI TC, Standard Sierra Installation)



In this example:

First Fire = 1.2 s

Sustained Fire = 34.8 s

Time to Idle = 36.0 s

Misfire rate = 28/288 (10%)

Figure 1.2

Typical start at -20°C

(Ford 1.8L IDI TC, Standard Sierra Installation)

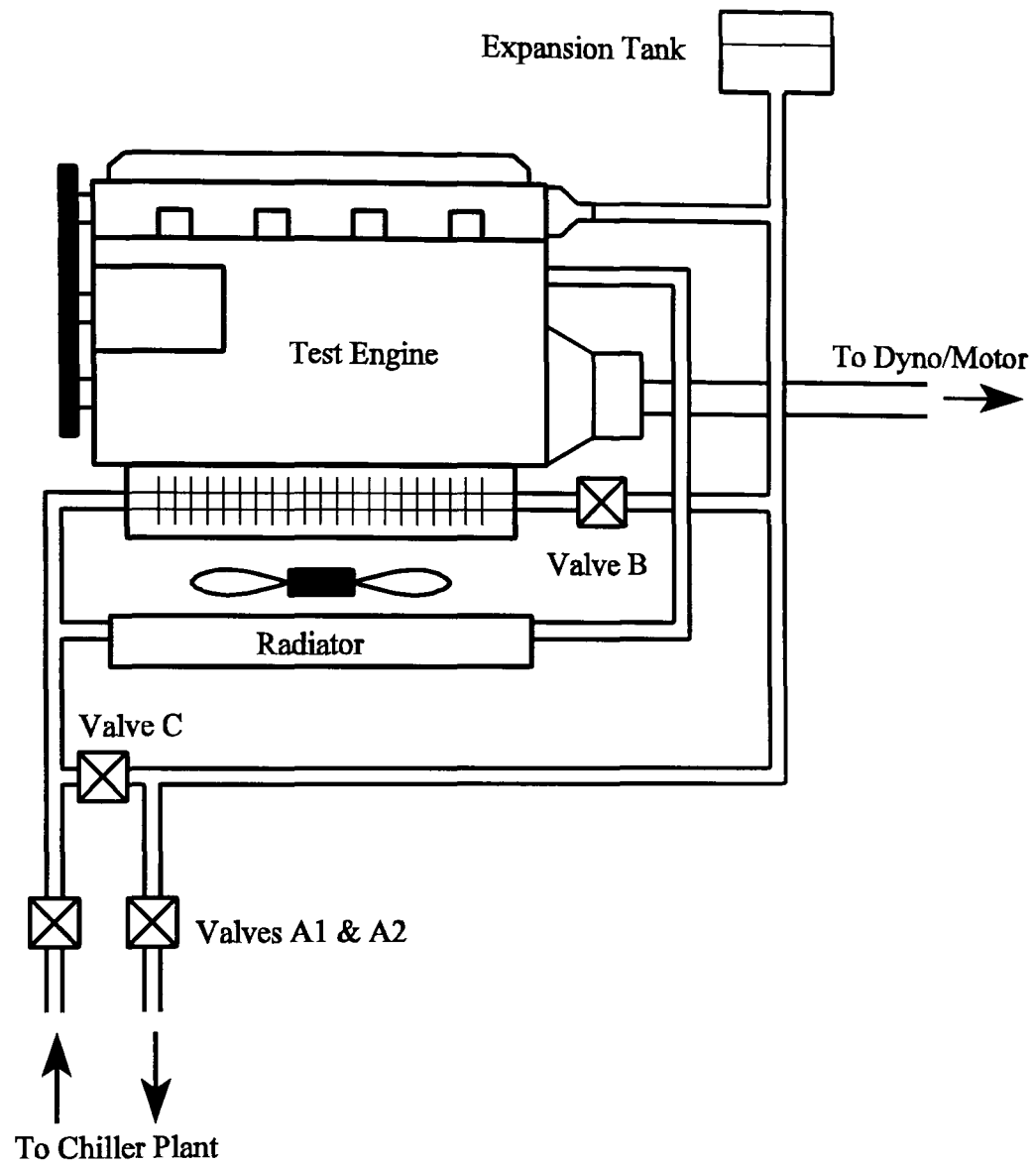


Figure 2.1 :
Schematic of Engine Cooling Facilities

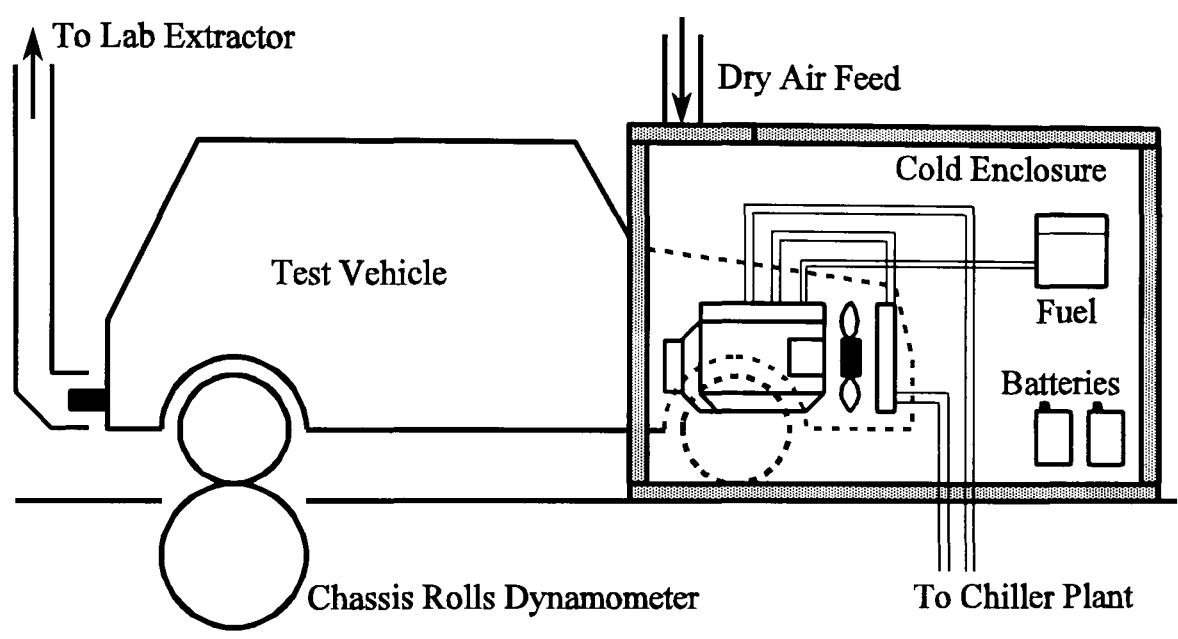


Figure 2.2 :
Test Rig Layout Schematic:
Firing Engines

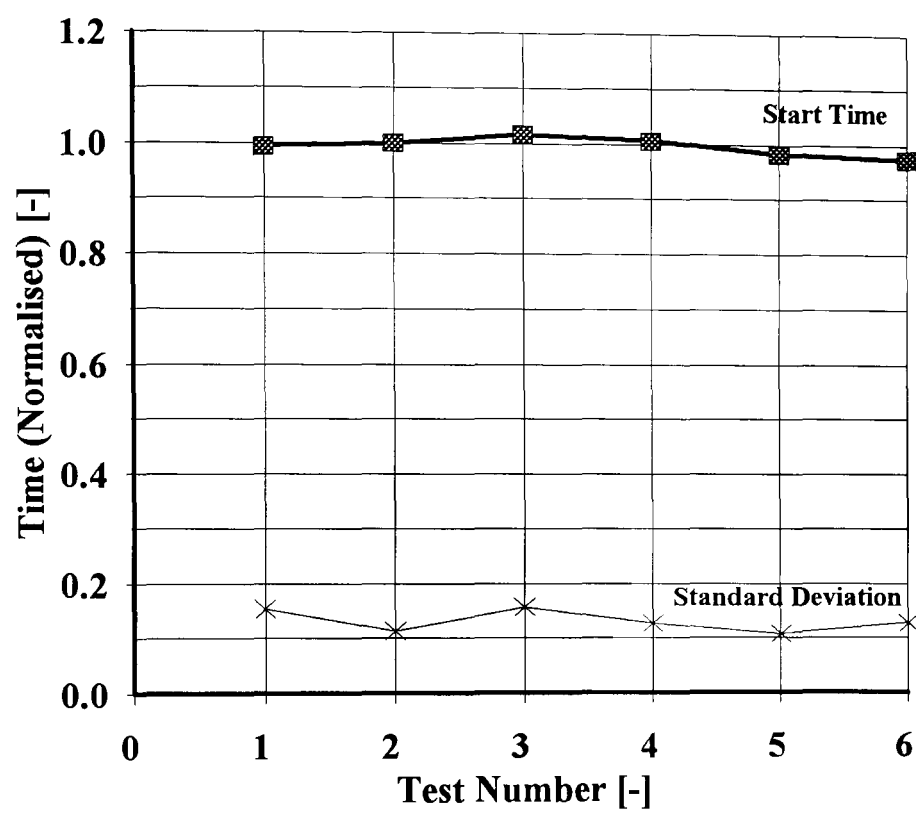


Figure 2.3
Variation in Start Quality For Repeated Tests
(Engine pre-cranked)
Normalised Start Time and its Standard Deviation

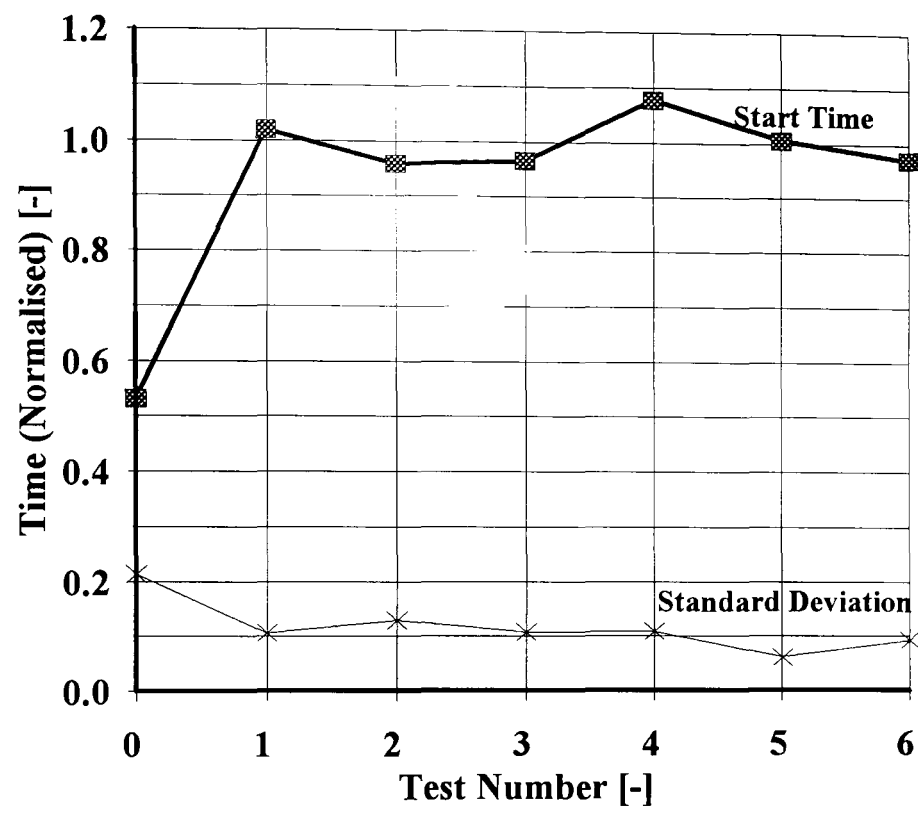


Figure 2.4
Variation in Start Quality For Repeated Tests
(Engine NOT pre-cranked)
Normalised Start Time and its Standard Deviation

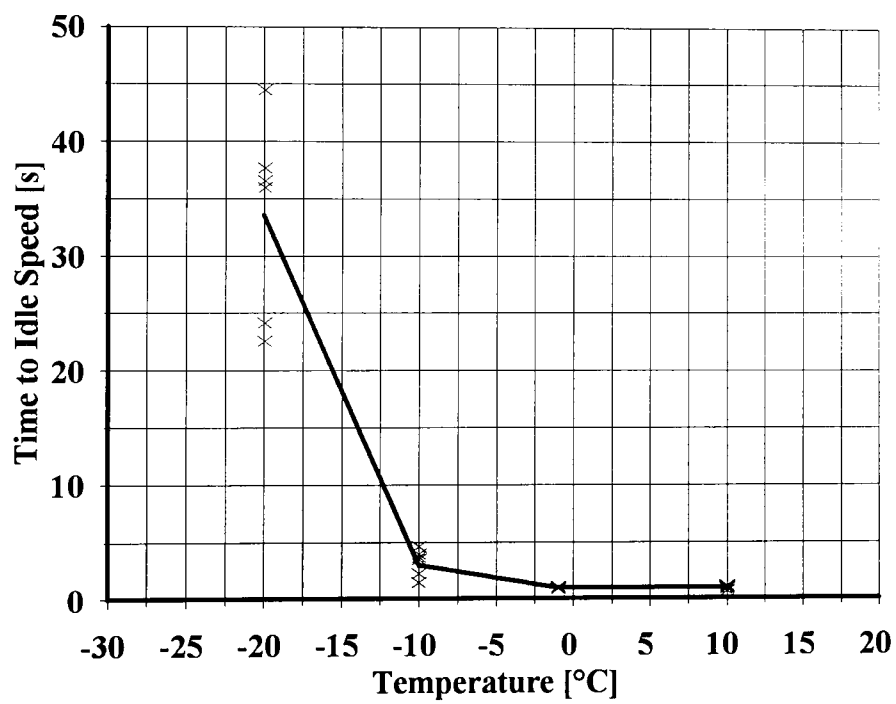
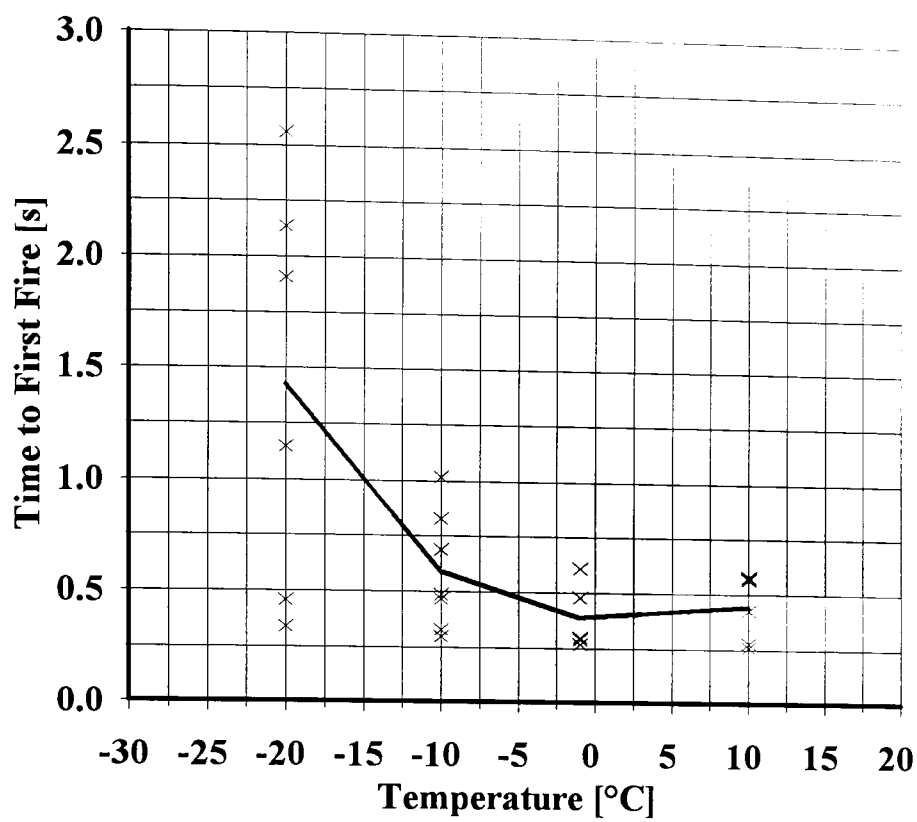


Figure 3.1

The Effect of Temperature on Start Quality

(Ford 1.8L IDI Engine, SAE 10W/30 oil)

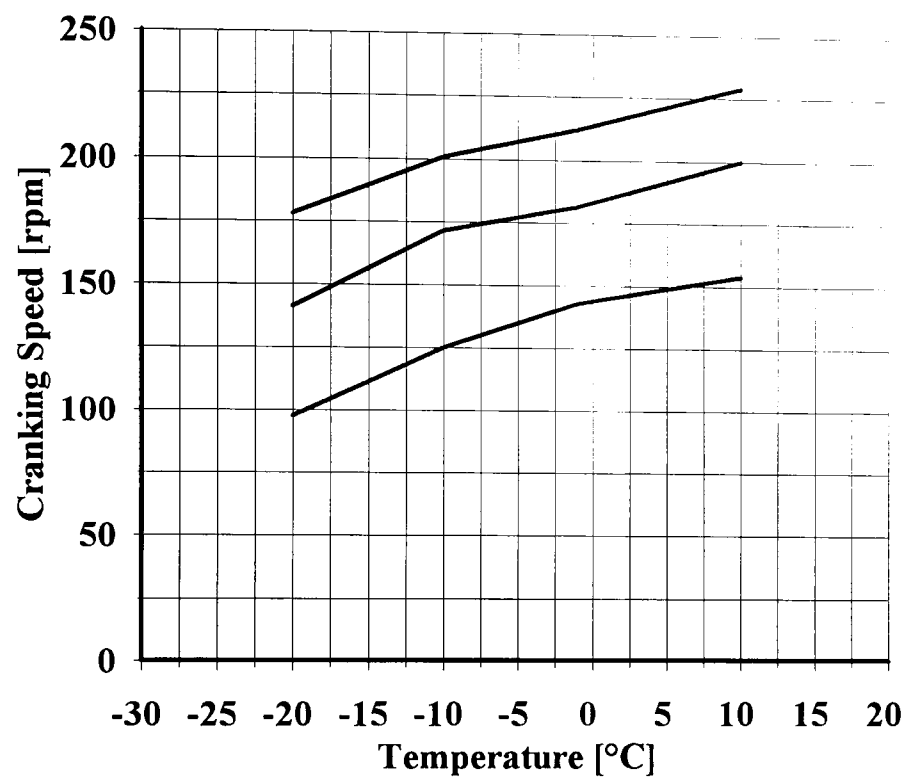
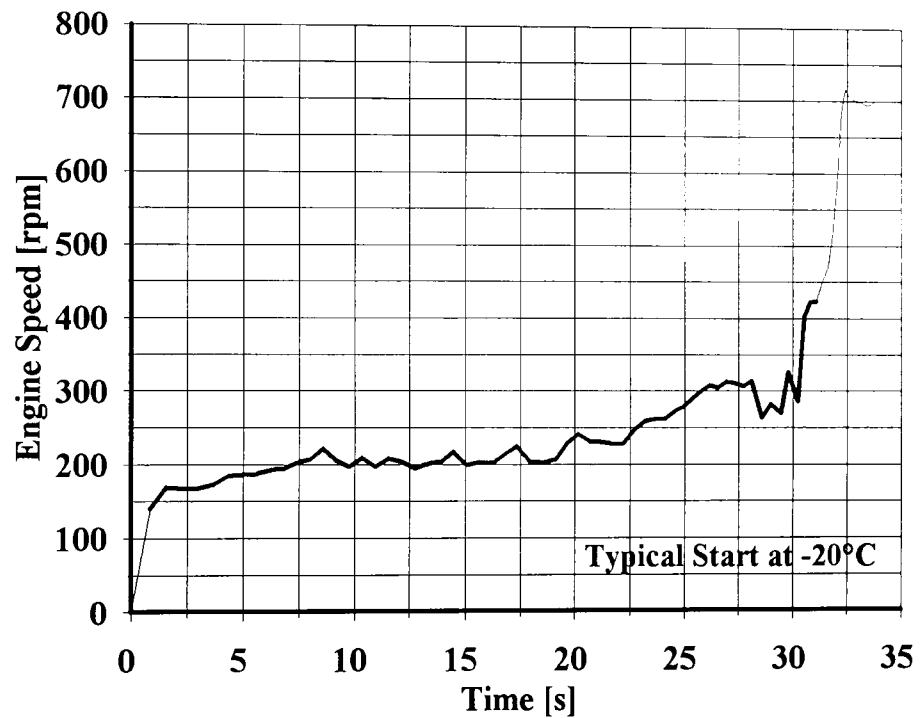
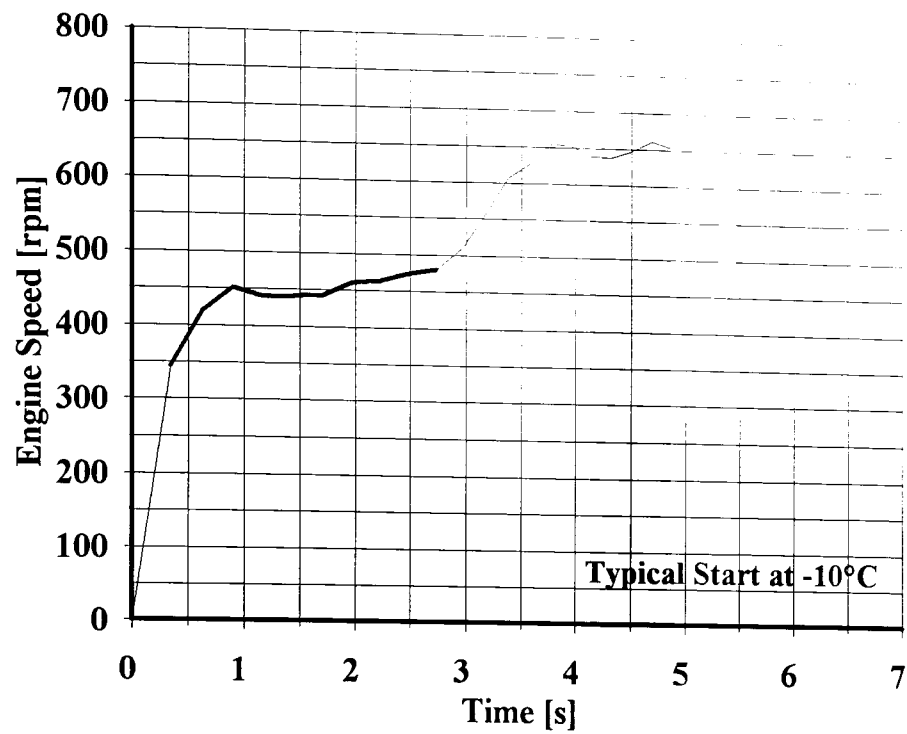


Figure 3.2

The Effect of Temperature on Cranking Speeds

(Minimum, Average and Maximum Speeds shown)

(Ford 1.8L IDI Engine, SAE 10W/30 oil)



— Firing-Assisted Cranking Phase

Figure 3.3 :

Period of Firing-Assisted Cranking During Cold Starting
(Ford 1.8L IDI Engine, SAE 10W/30 oil)

NOTE : time axes have differing scales

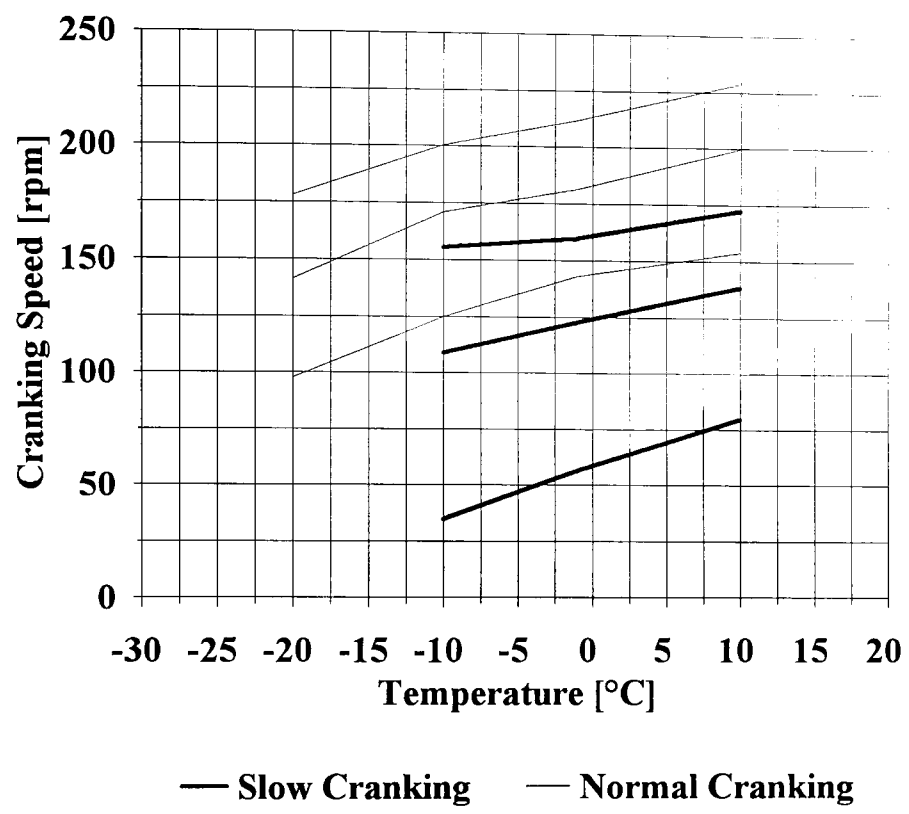
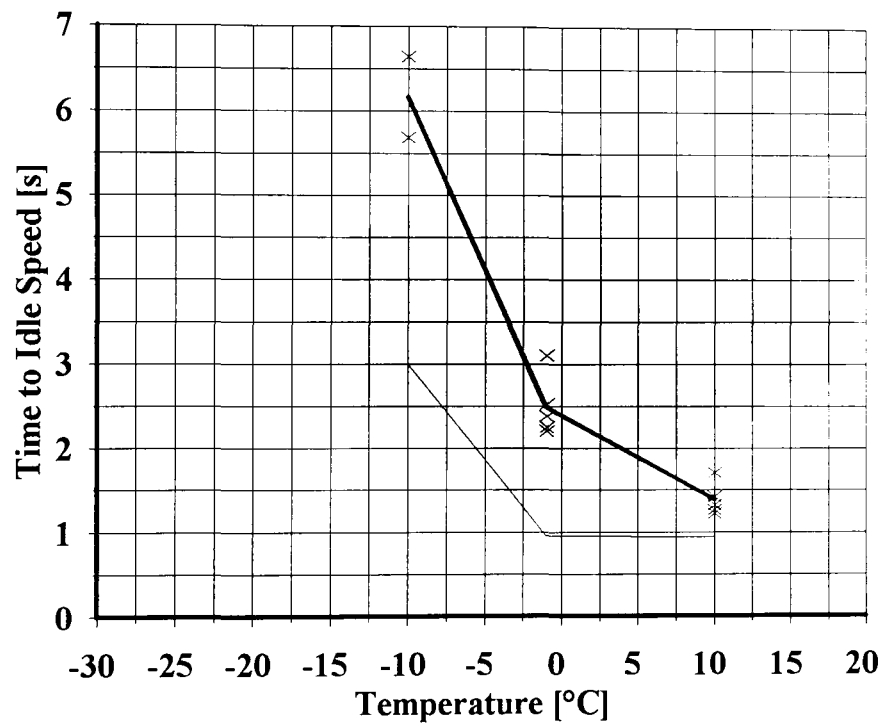
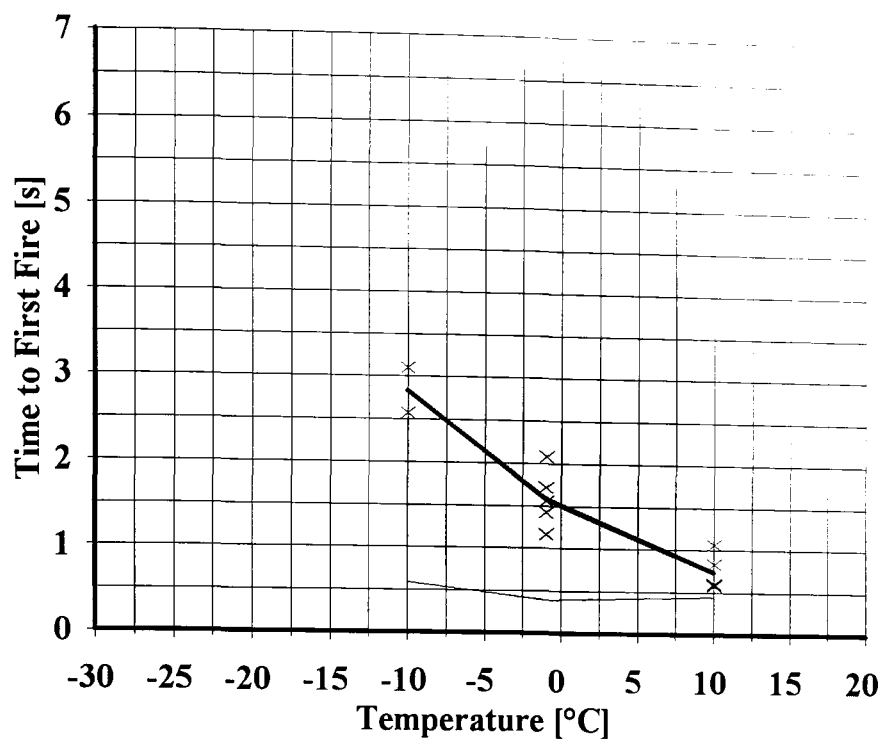


Figure 3.4
Reduced Minimum, Average and Maximum Cranking Speeds
(Ford 1.8L IDI Engine, SAE 10W/30 oil)



— Slow Cranking — Normal Cranking

Figure 3.5

The Effect of Cranking Speed on Start Quality
(Ford 1.8L IDI Engine, SAE 10W/30 oil)

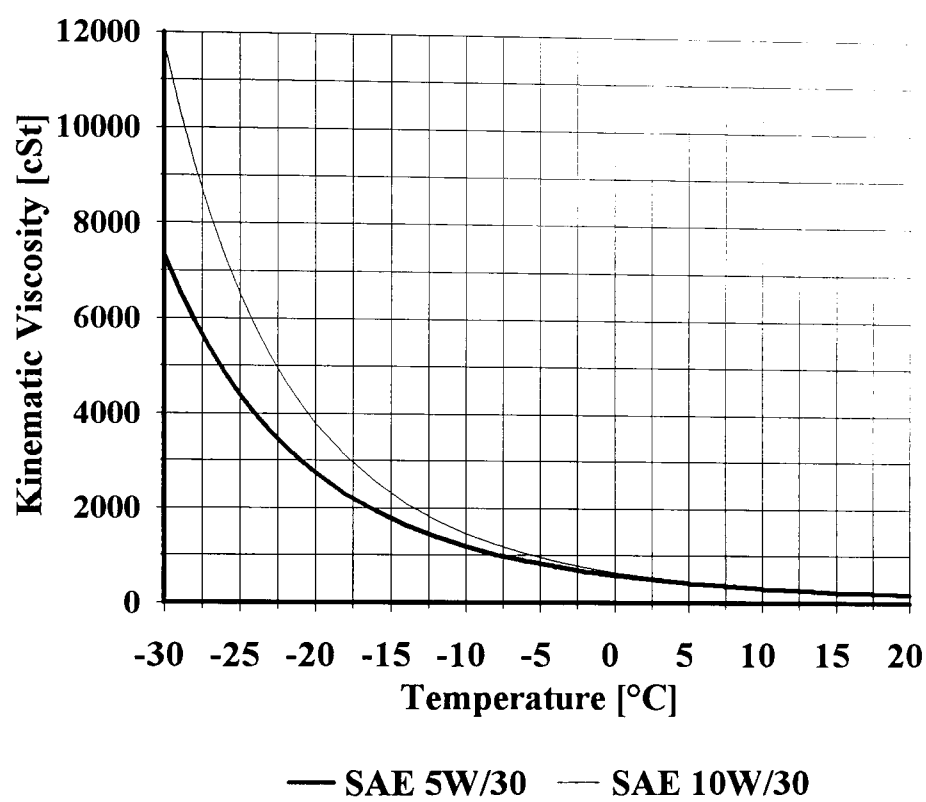


Figure 3.6 :

Kinematic Viscosities of the Test Oils Used

[1 cSt = 1 mm²/s = 1e-6 m²/s]

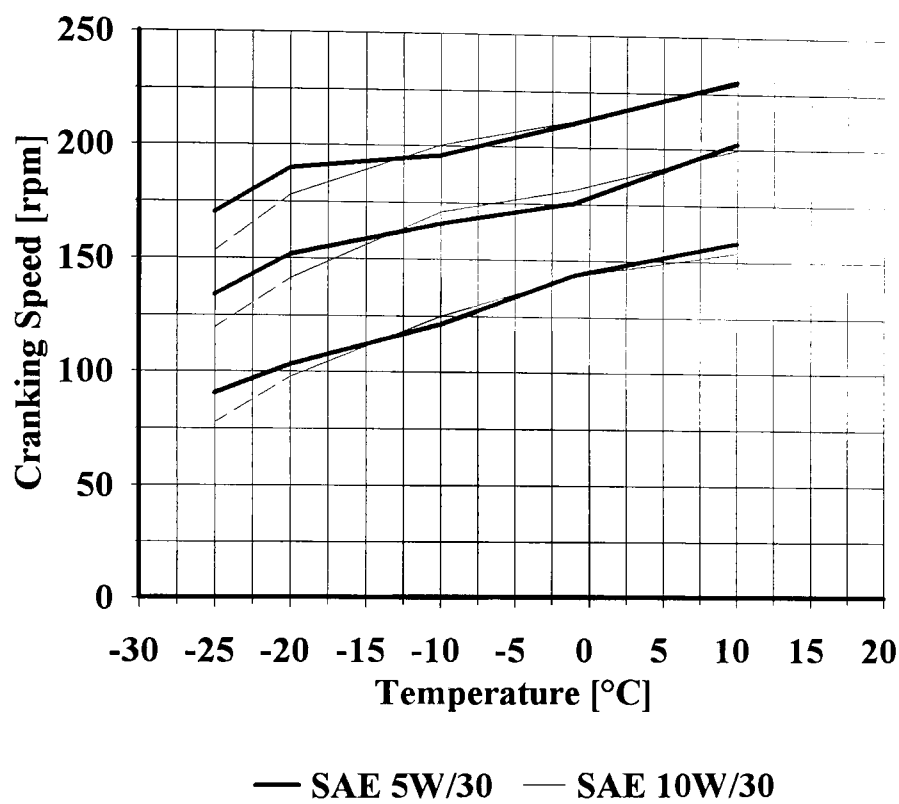
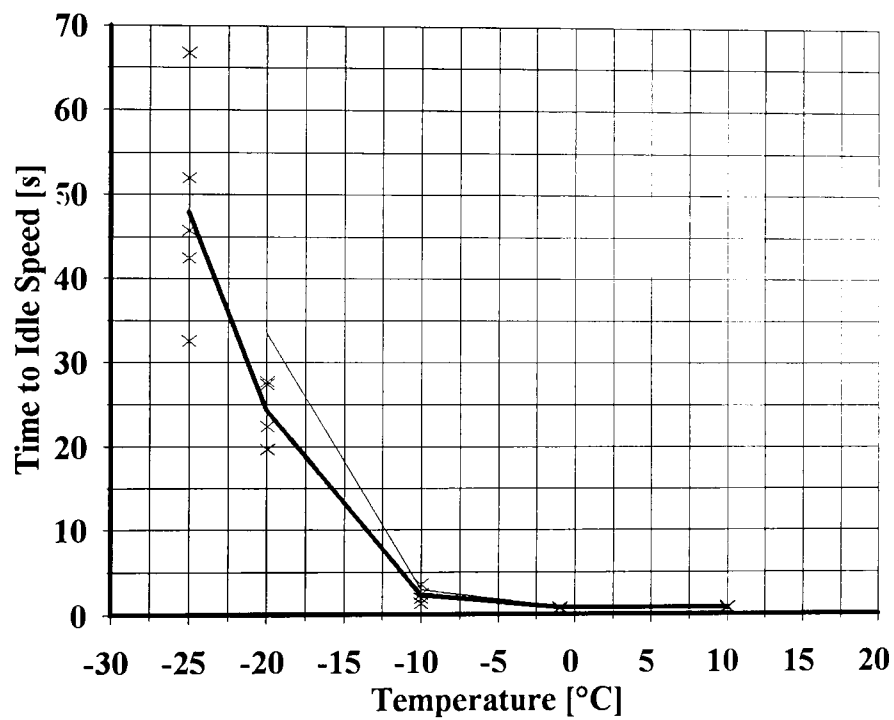
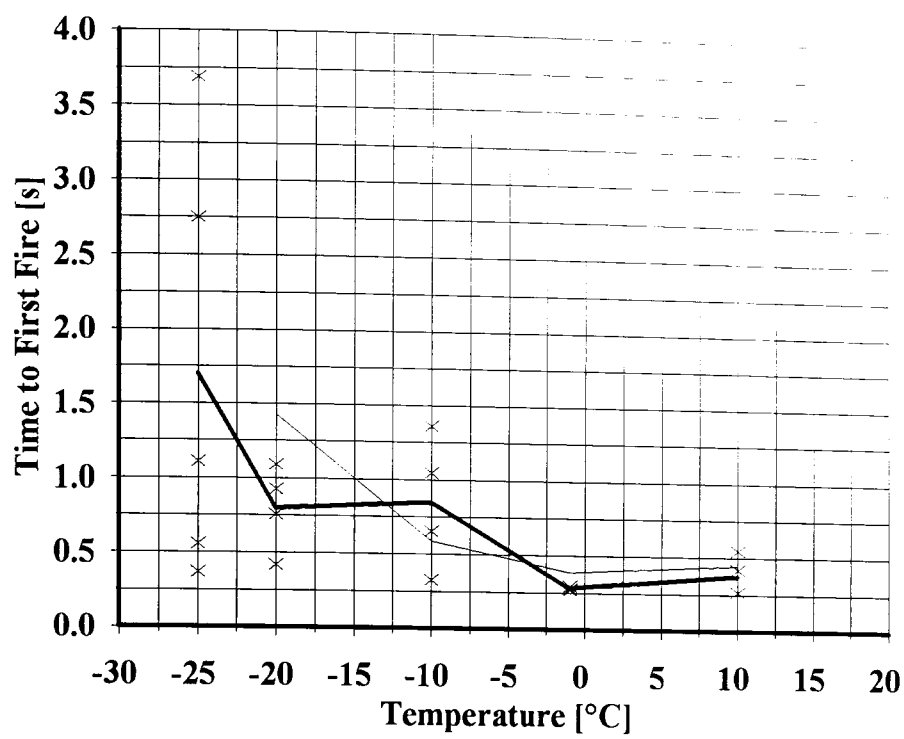


Figure 3.7

Cranking Speeds With Reduced Oil Viscosity

(Minimum, Average and Maximum Speeds shown)

(Ford 1.8L IDI Engine)



— SAE 5W/30 — SAE 10W/30

Figure 3.8
The Effect of Oil Viscosity on Start Quality
(Ford 1.8L IDI Engine)

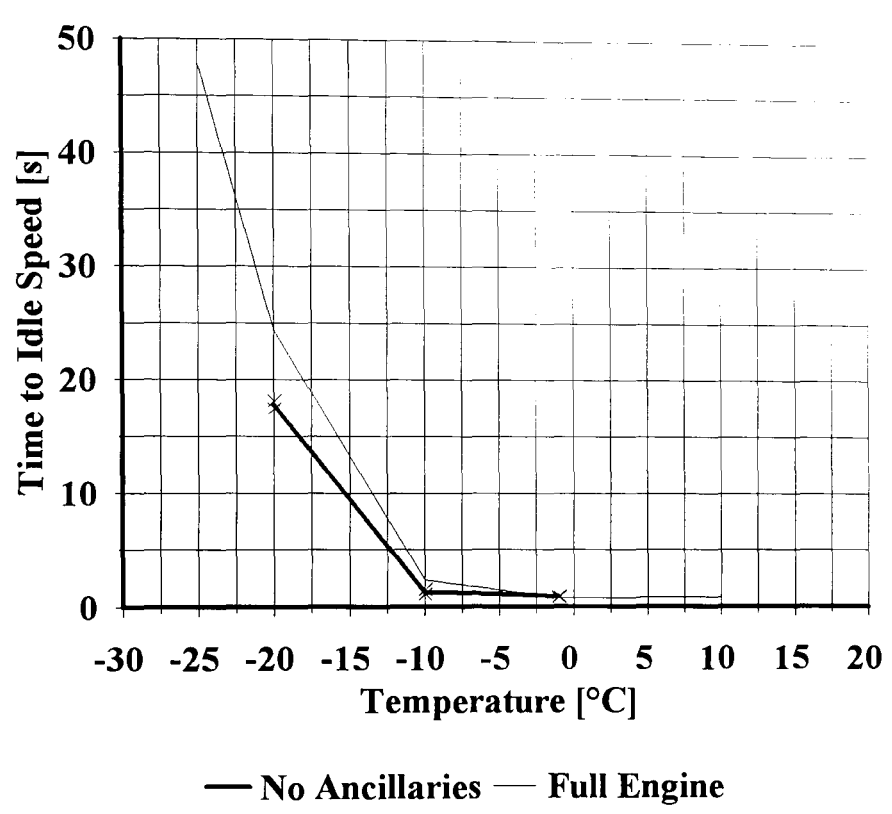


Figure 3.9
The Effect of Non-essential Ancillaries on Time to Idle Speed
(Ford 1.8L IDI Engine, SAE 5W/30 oil)

Lead Acid Battery Equivalent Circuit

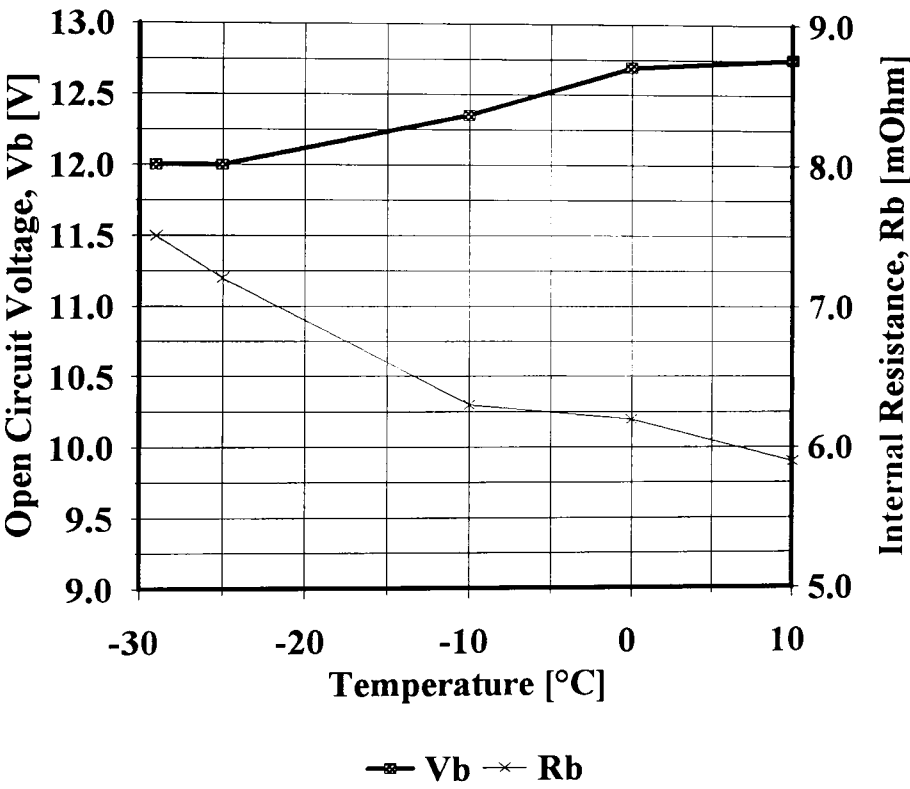
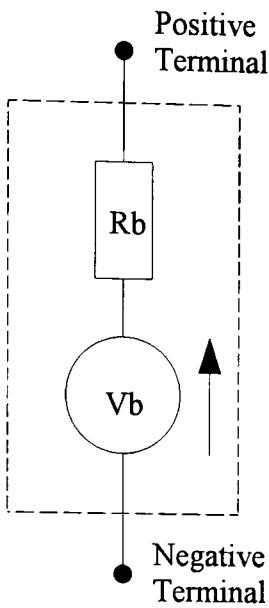


Figure 4.1
Model Representation of Lead-Acid Battery
(Motorcraft 650A 130RC)

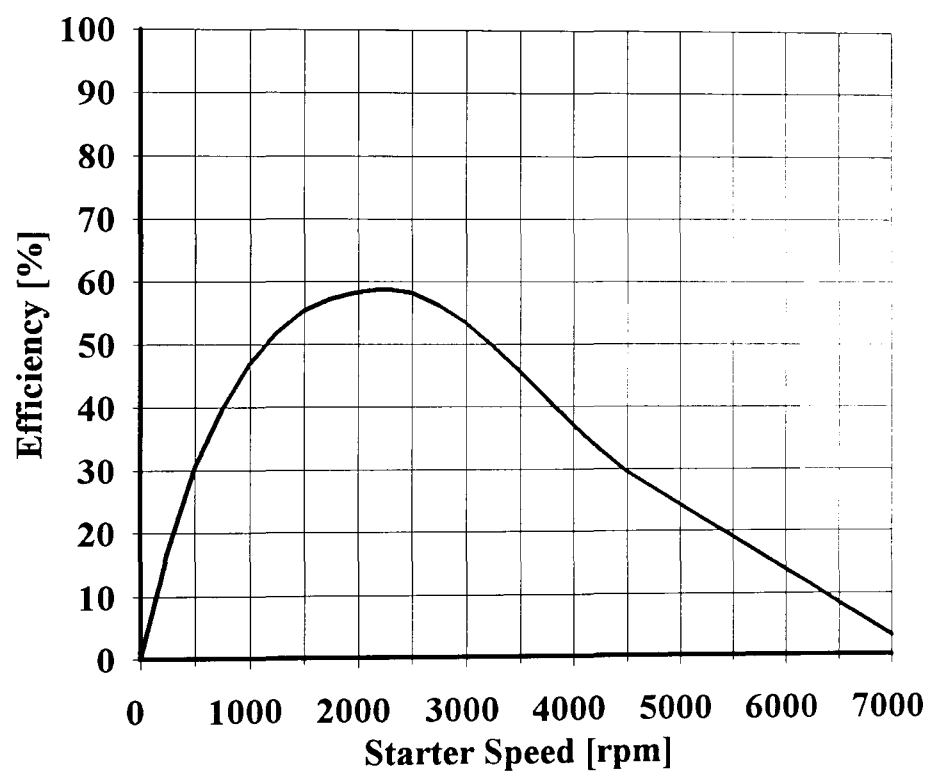
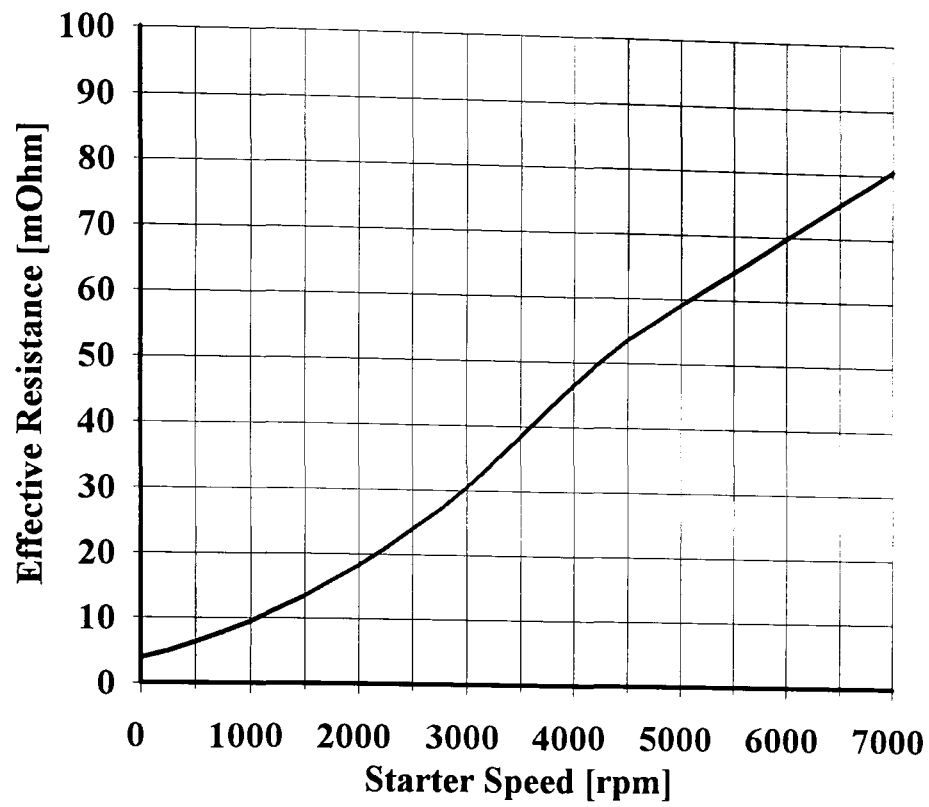


Figure 4.2

Parameters for Starter Motor Model

Effective Resistance and Starter Efficiency

(Bosch EV 12V 2.2 kW, -29°C to +10°C)

(Calculated from reference [4.1])

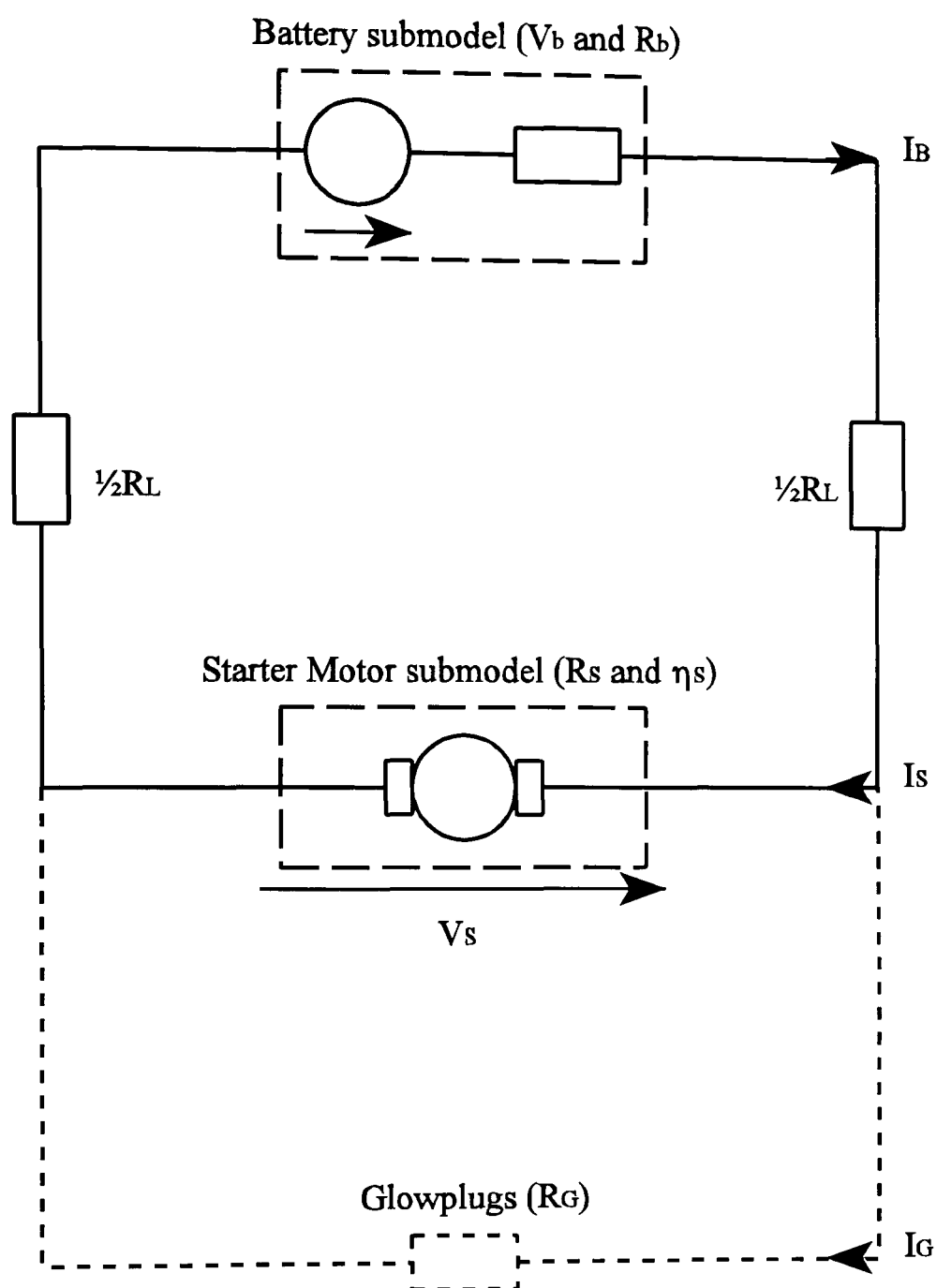
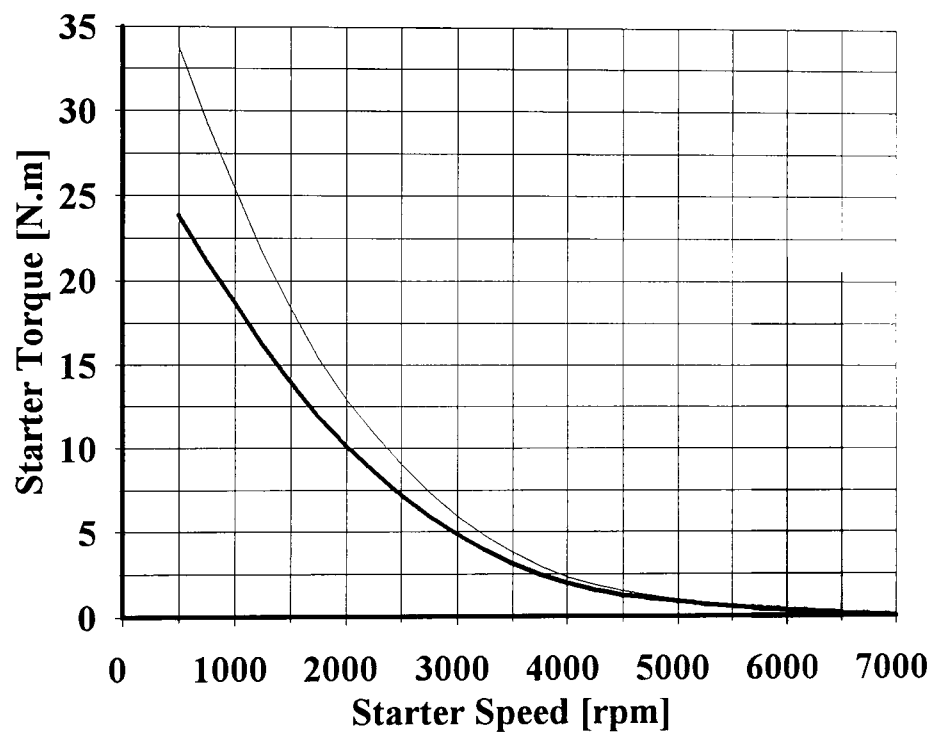
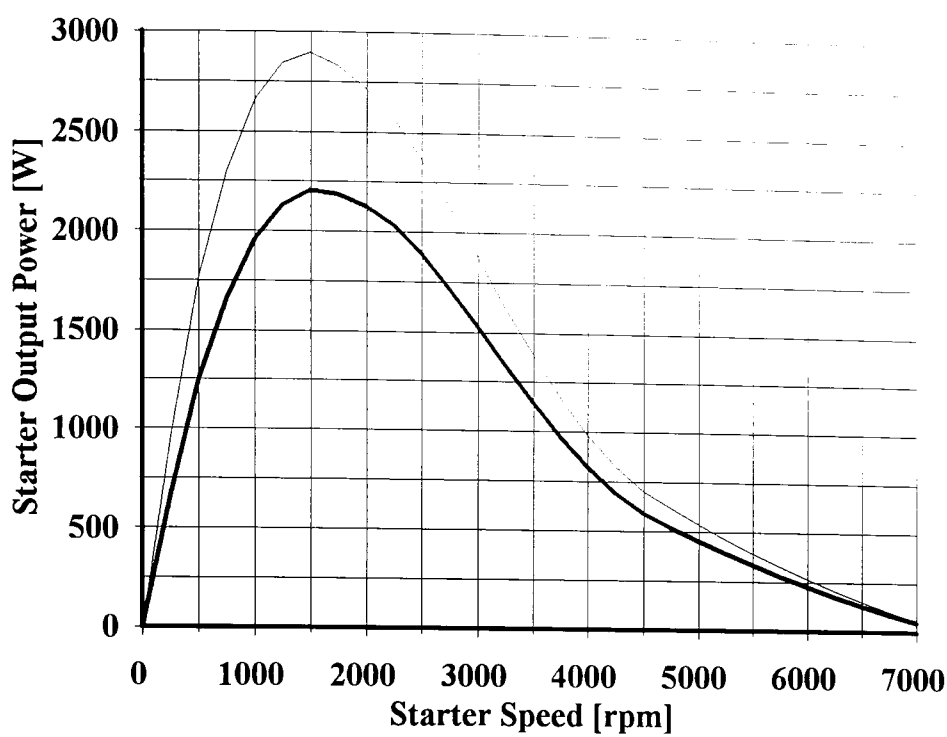


Figure 4.3 :
Starter System Equivalent Circuit



— -29°C — +10°C

Figure 4.4

Predicted Starter Motor Output

(Motorcraft 650A 130RC battery, Bosch EV12V 2.2kW starter)

(-29°C and +10°C)

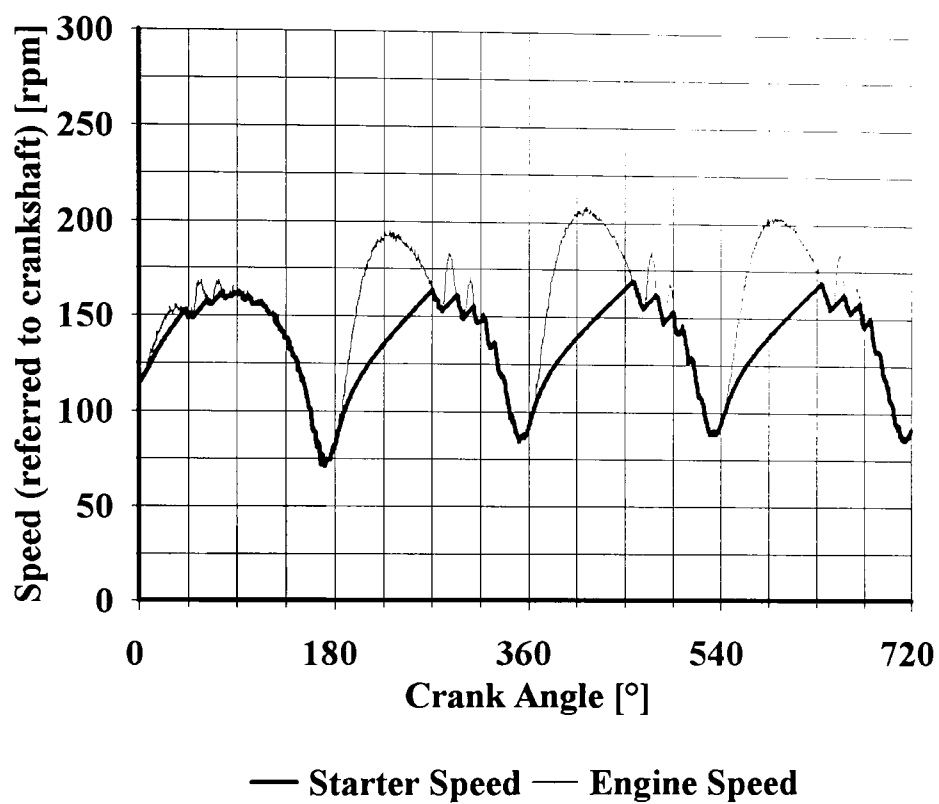


Figure 4.5

Predicted Starter Motor Speed (Slow Cranking)

(Motorcraft 650A 130RC battery, Bosch EV12V 2.2kW starter)

(Ford 1.8L IDI Engine, SAE 10W/30 oil @ +19°C)

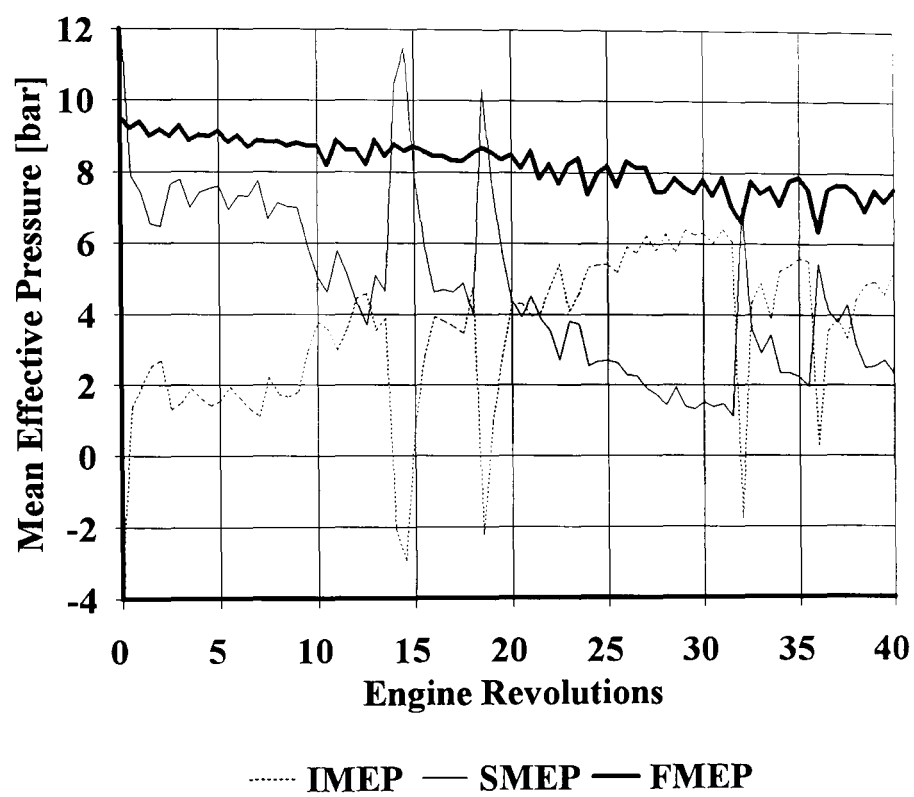


Figure 4.6

FMEP Calculated From Energy Balance at Crankshaft

(Ford 1.8L IDI Engine, SAE 10W/30 oil, -20°C)

(Motorcraft 650A 130RC battery, Bosch EV12V 2.2kW starter)

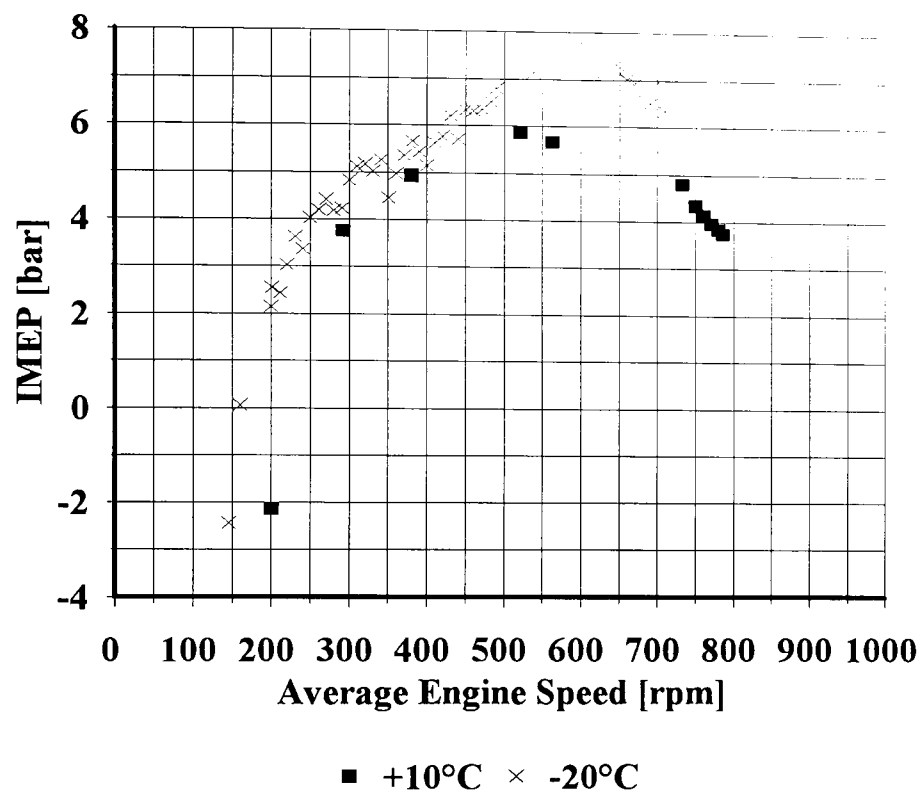


Figure 4.7

IMEP with Engine Speed, Showing the Effect of Temperature
(Ford 1.8L IDI Engine, SAE 10W/30 oil)

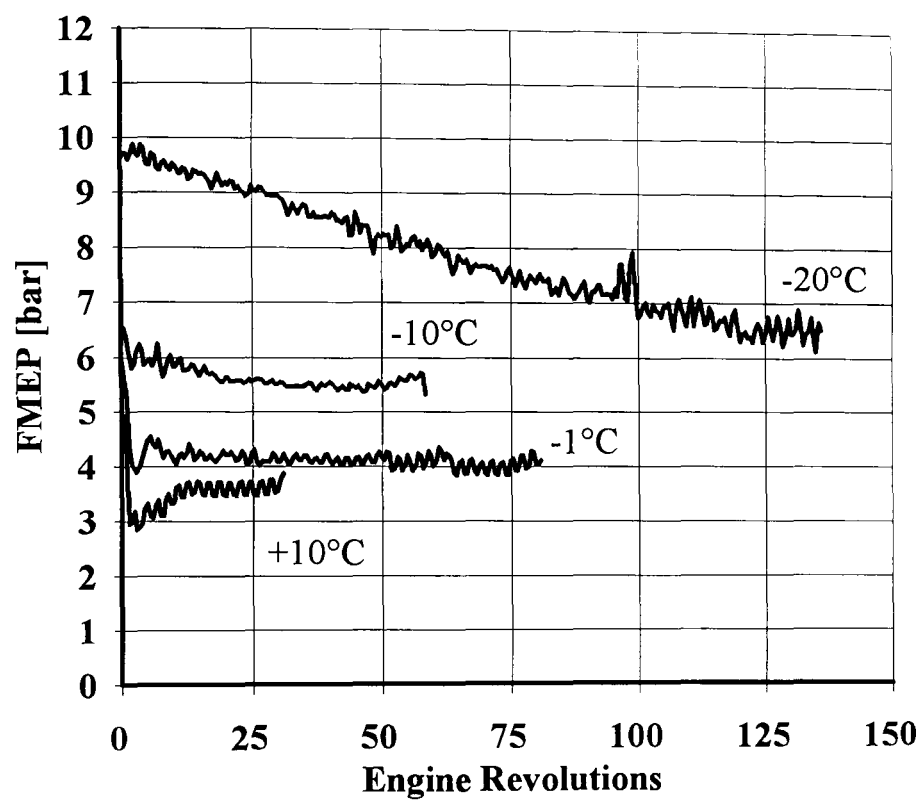


Figure 4.8

Changing FMEP With Temperature

(Ford 1.8L IDI Engine, SAE 10W/30 oil)

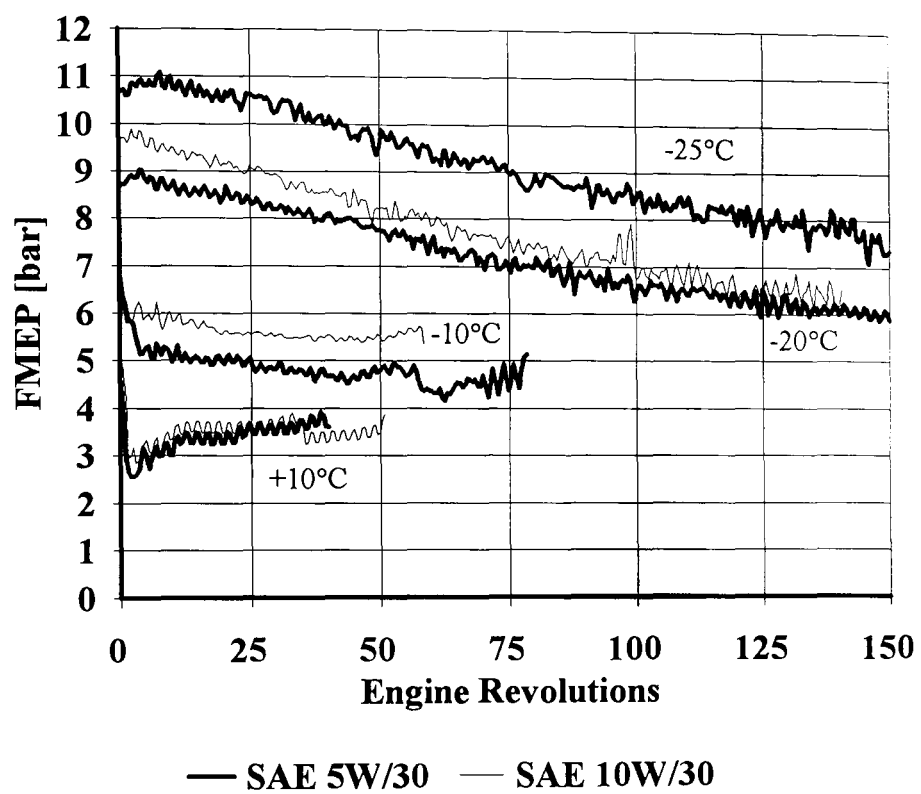


Figure 4.9
Changing FMEP With Reduced Oil Viscosity
(Ford 1.8L IDI Engine)

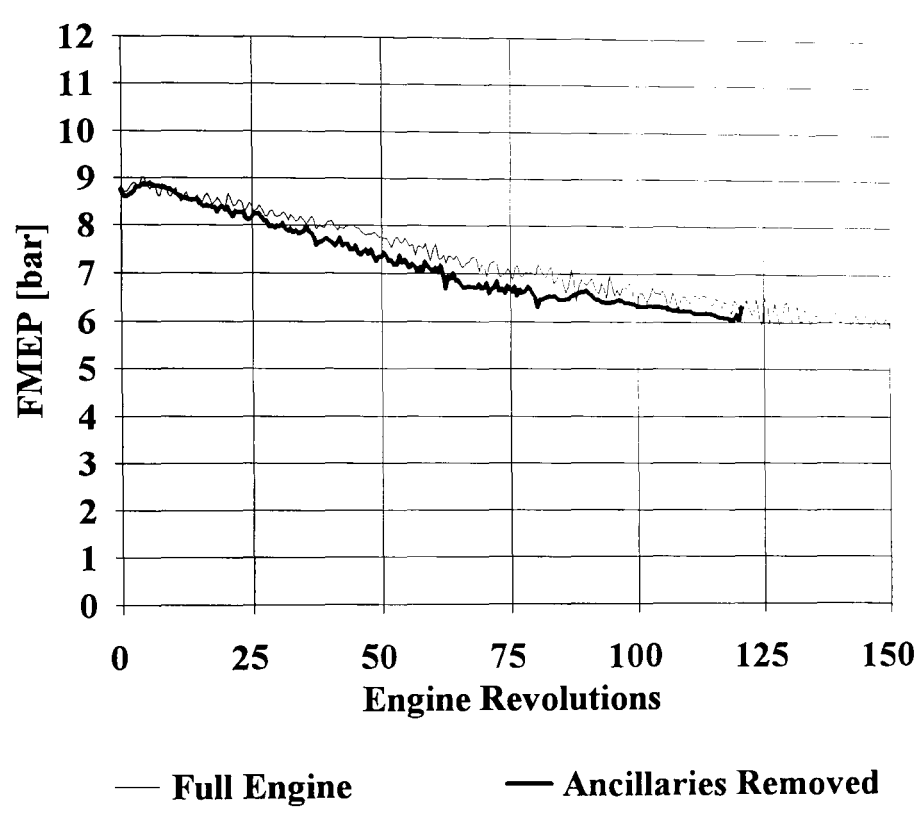


Figure 4.10
Impact of Non-essential Ancillaries on FMEP at -20°C
(Ford 1.8L IDI Engine, SAE 5W/30 oil)

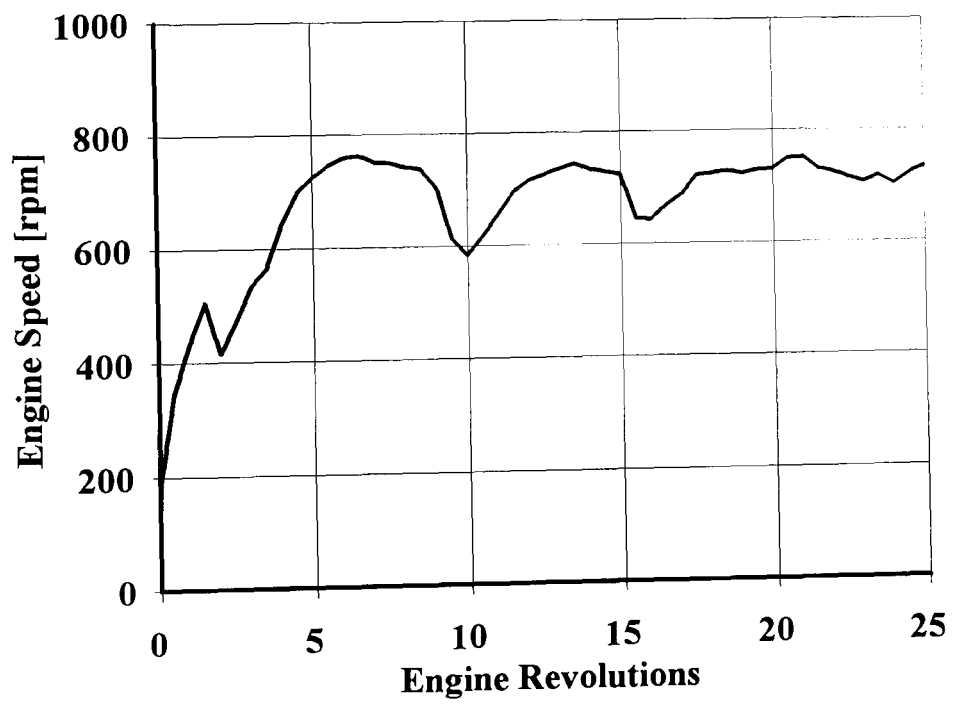
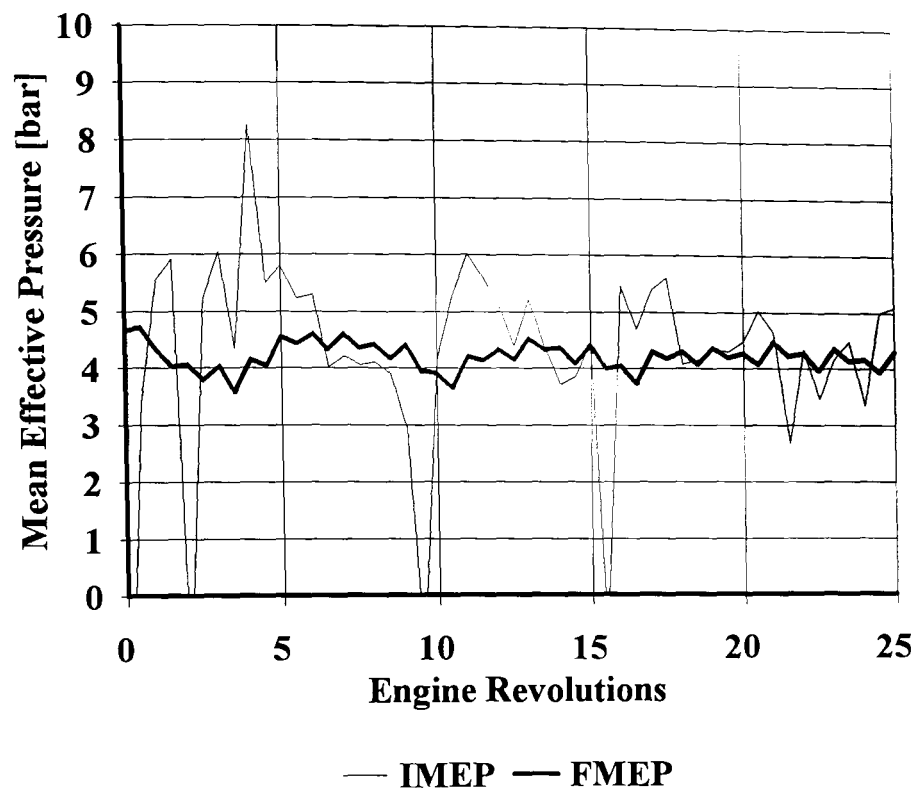


Figure 4.11

Rapid Starting at -1°C

Initial IMEP exceeds FMEP

(Ford 1.8L IDI Engine, SAE 10W/30 oil)

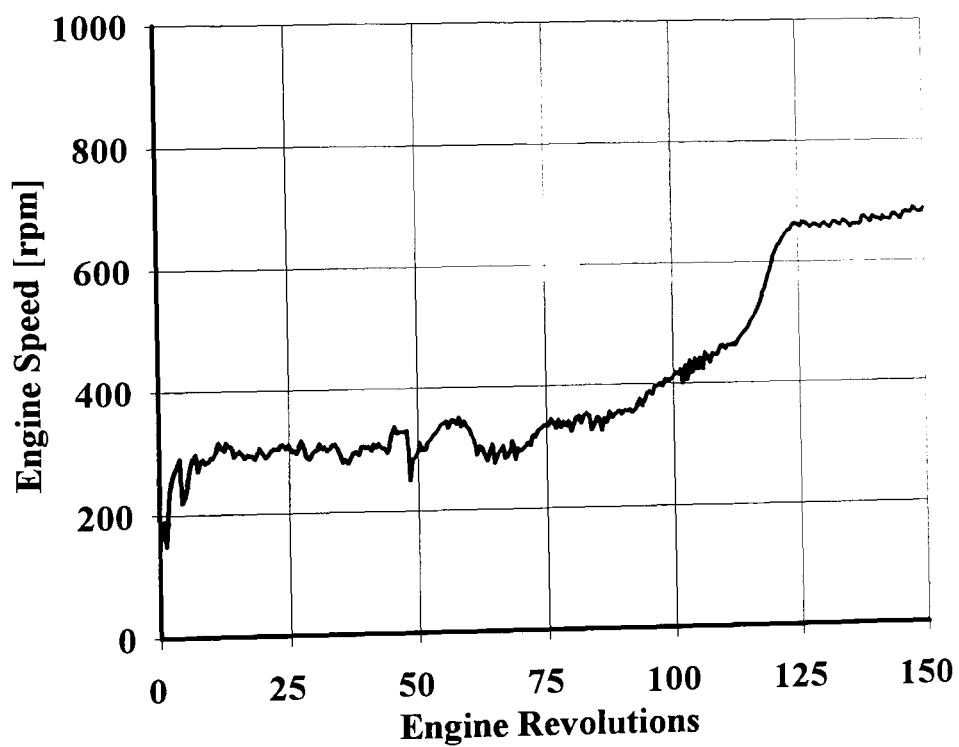
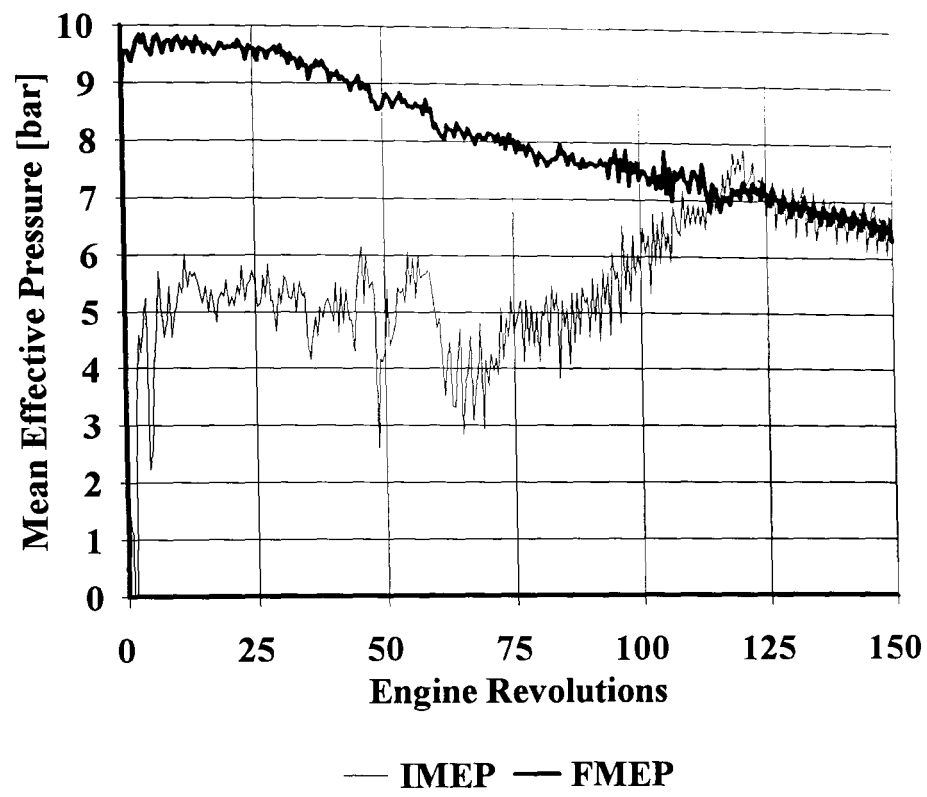


Figure 4.12

Poor Starting at -20°C

Initial IMEP Less Than FMEP

(Ford 1.8L IDI Engine, SAE 10W/30 oil)

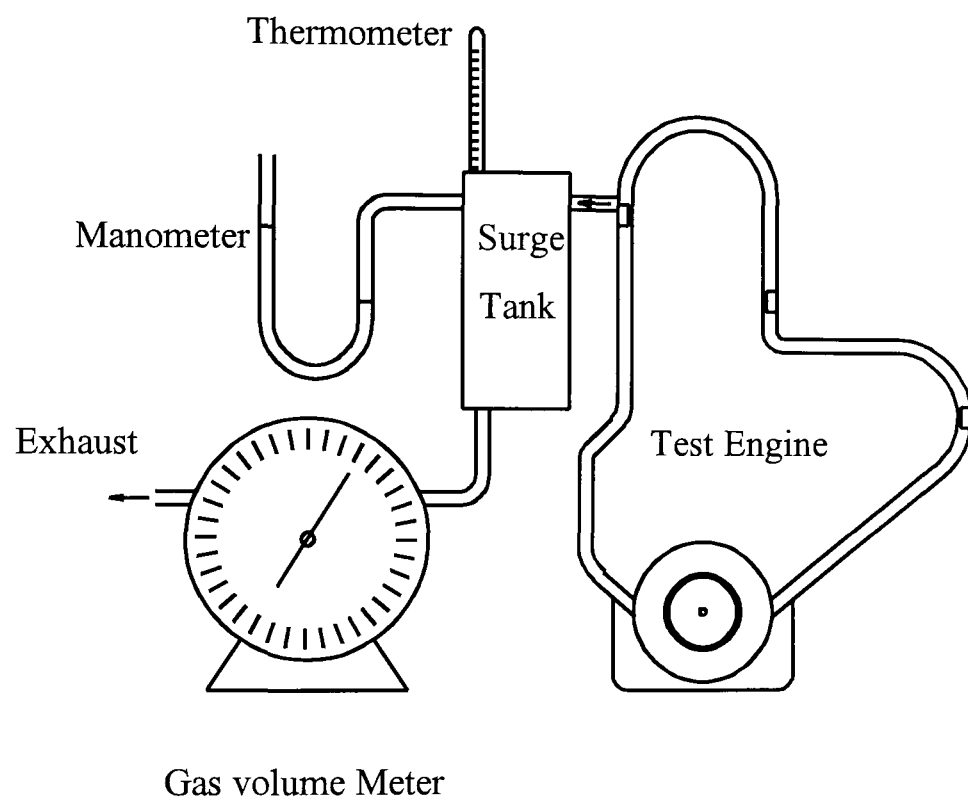


Figure 5.1 :
General scheme for measurement of blowby loss.

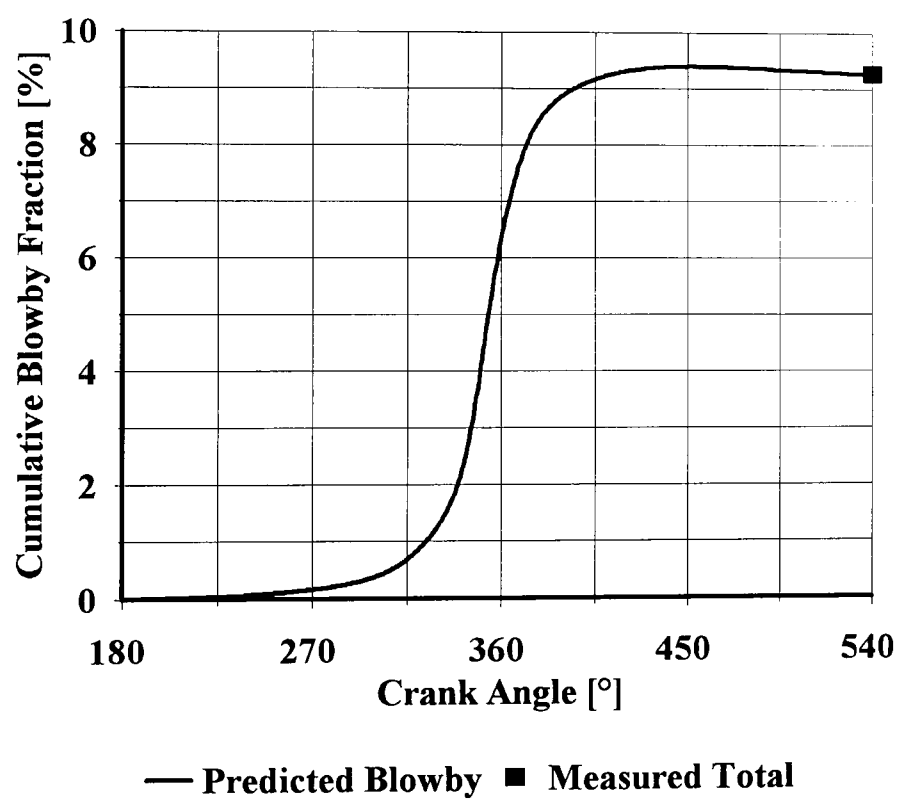
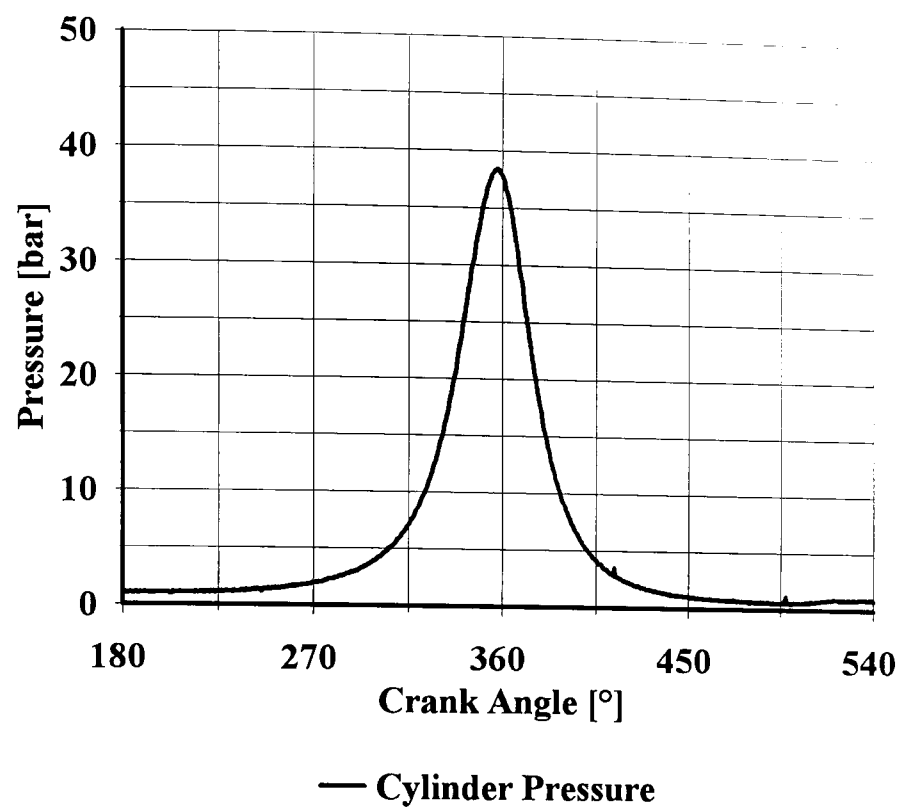


Figure 5.2
Blowby Correlation, 200 rpm Average Speed
(Ford P-type engine, SAE 10W/30, Motoring @ +30°C)

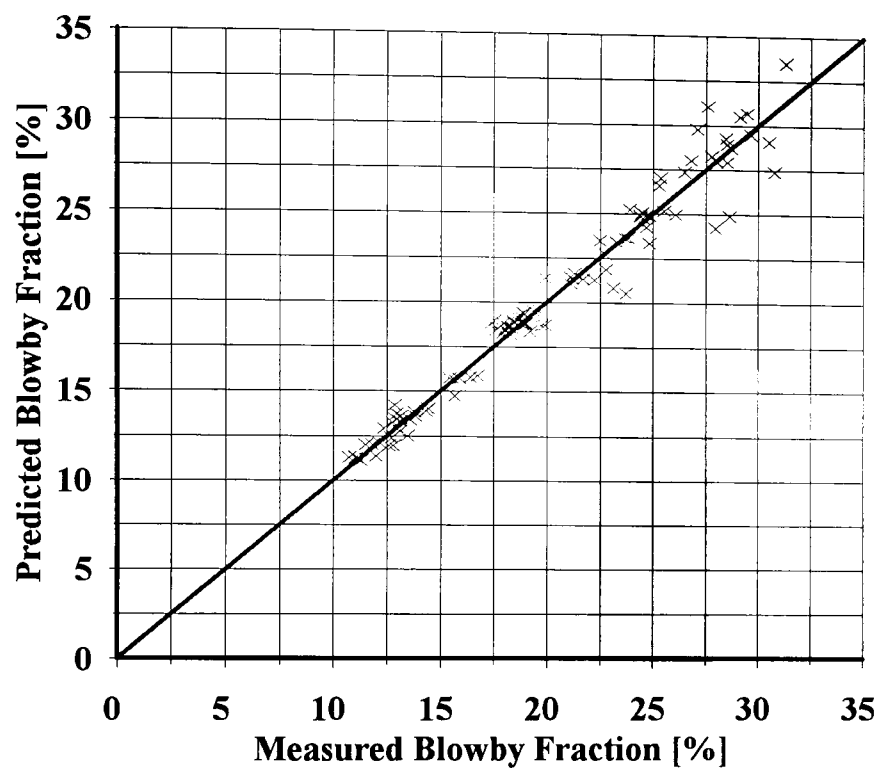


Figure 5.3
Blowby Correlation Accuracy
(Ford 1.8L IDI Engine, Cranking)
Temperatures -26°C to +20°C
Speeds up to 250 rpm

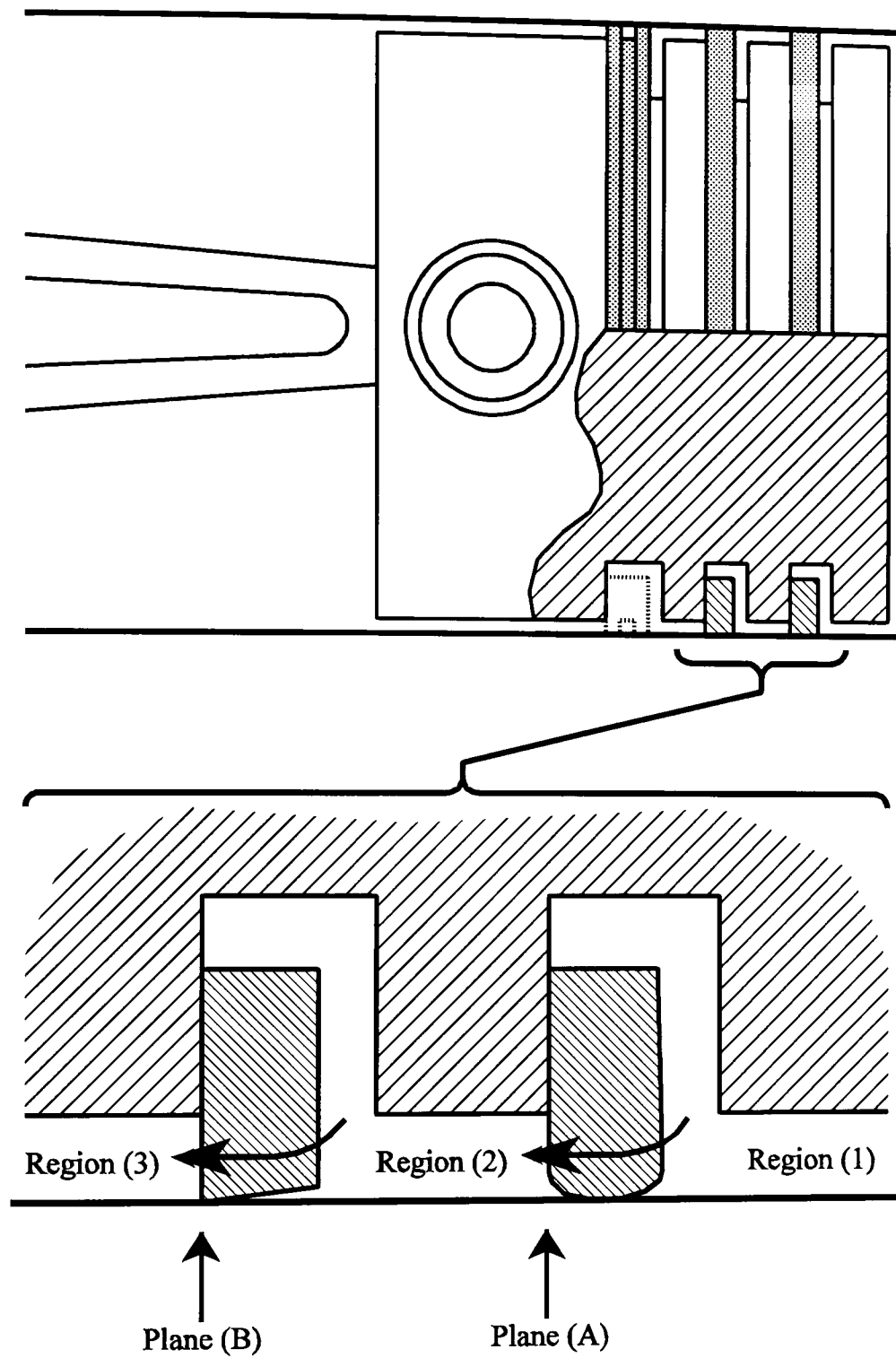


Figure 5.4 :

Schematic for Blowby Model.

Enlargement shows piston and rings against cylinder wall.

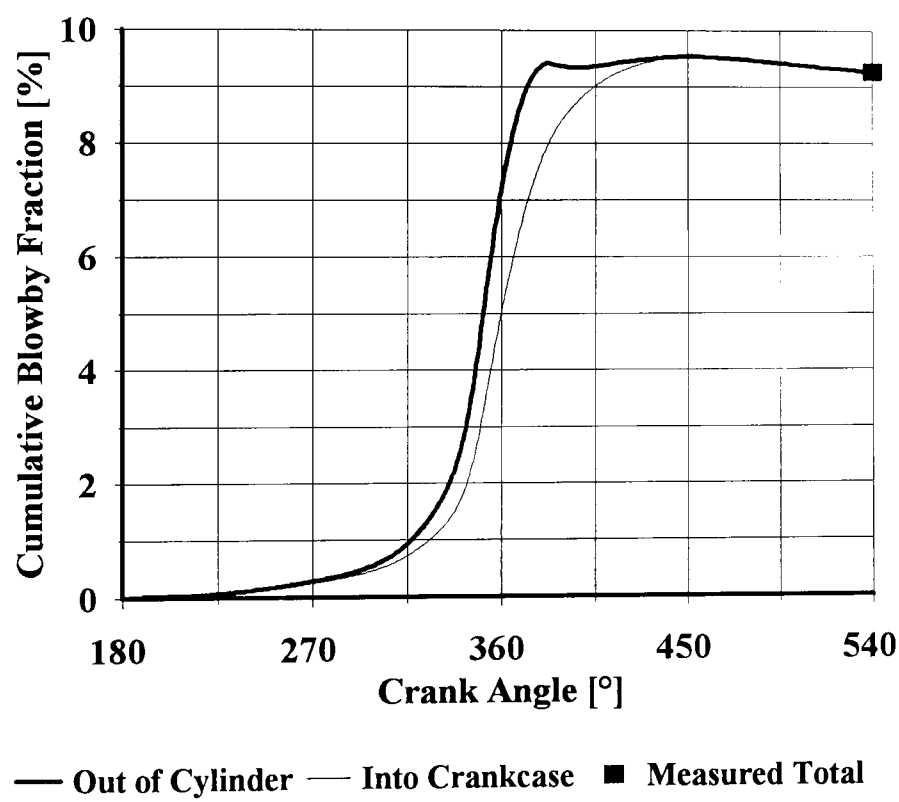
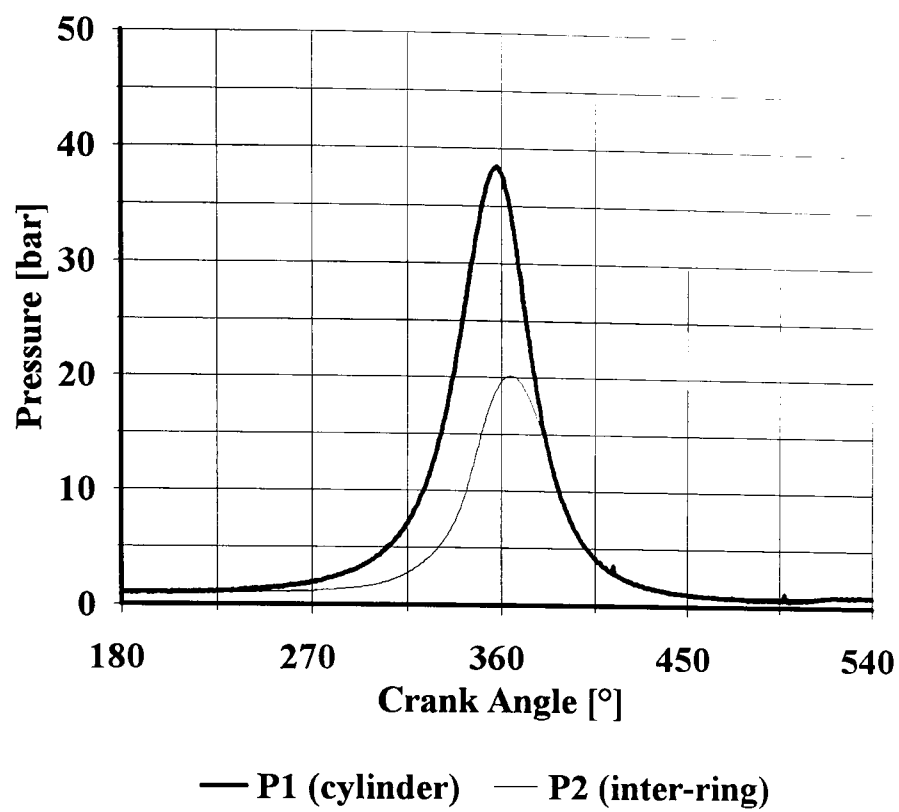


Figure 5.5
Improved Blowby Predictions, 200 rpm Average Speed
(Ford P-type engine, SAE 10W/30, Motoring @ +30°C)

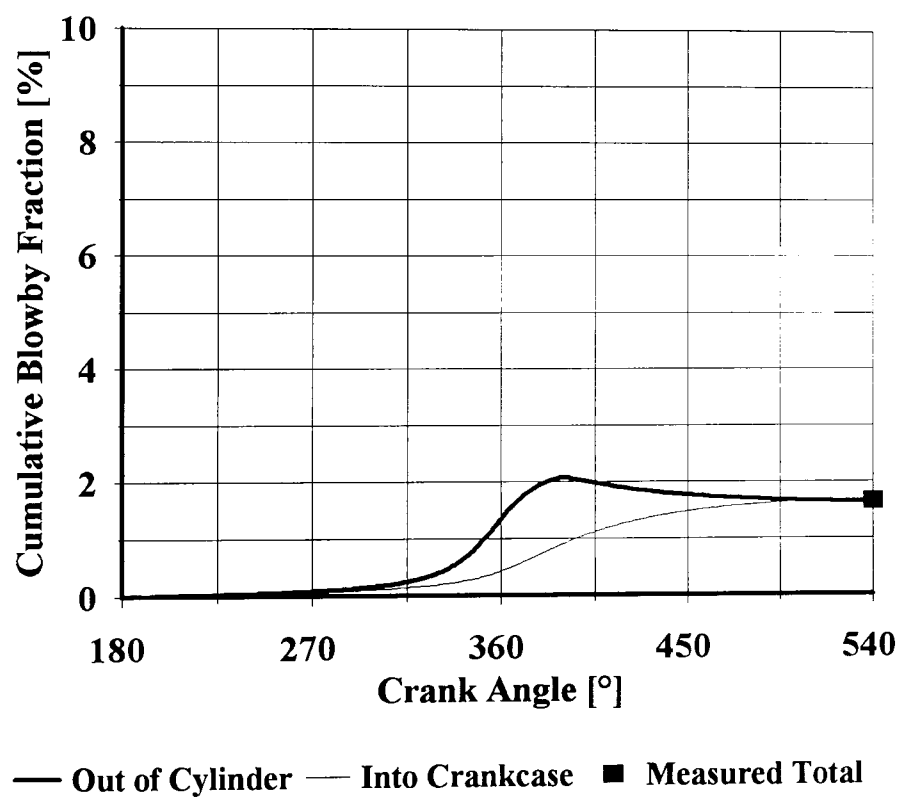
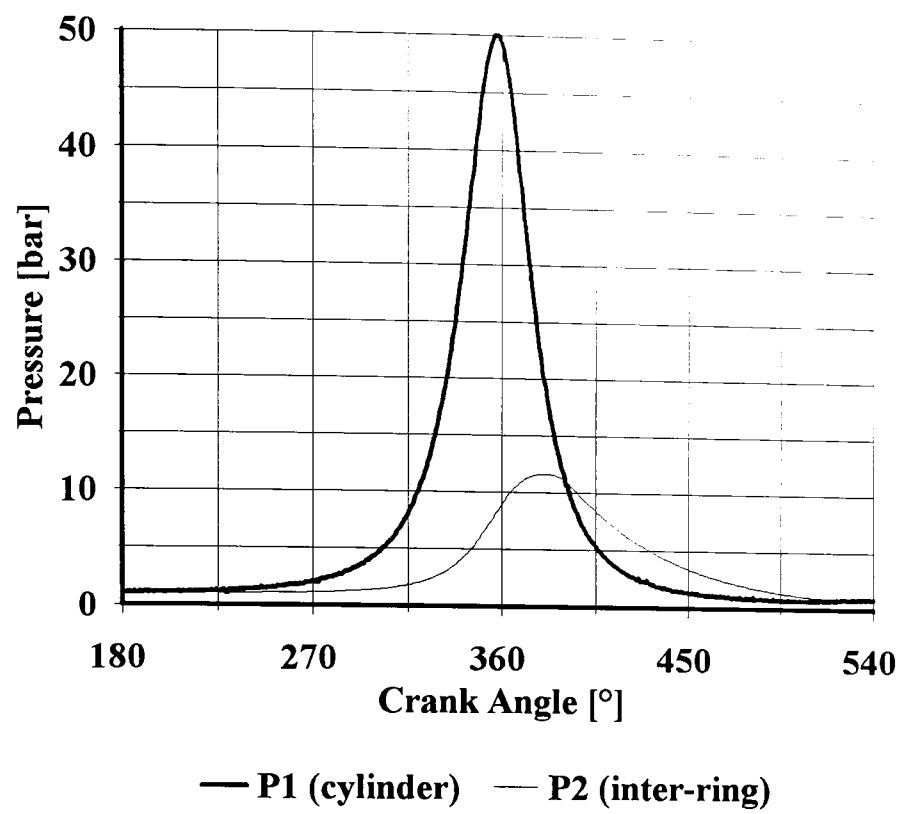
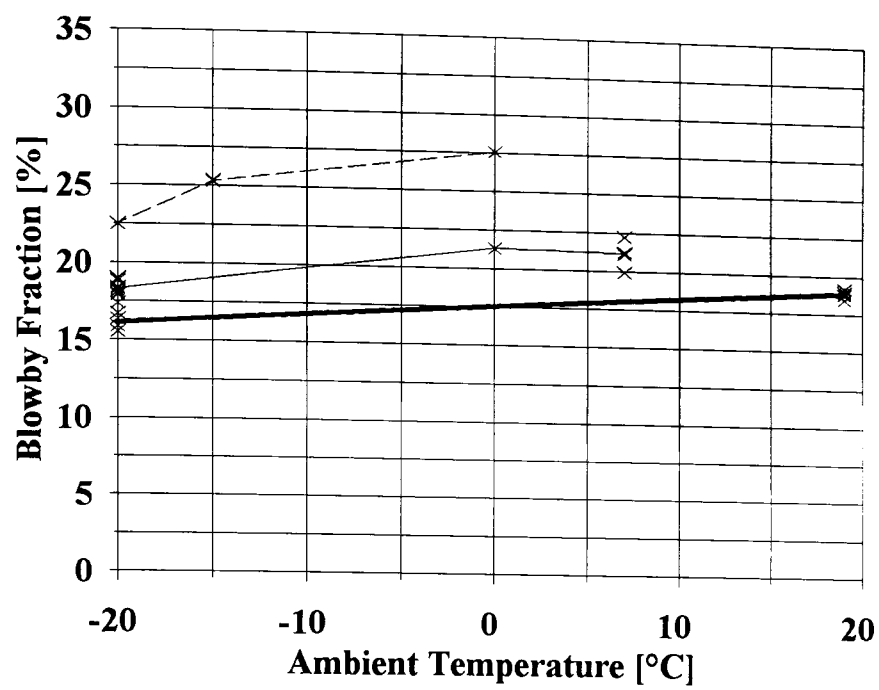
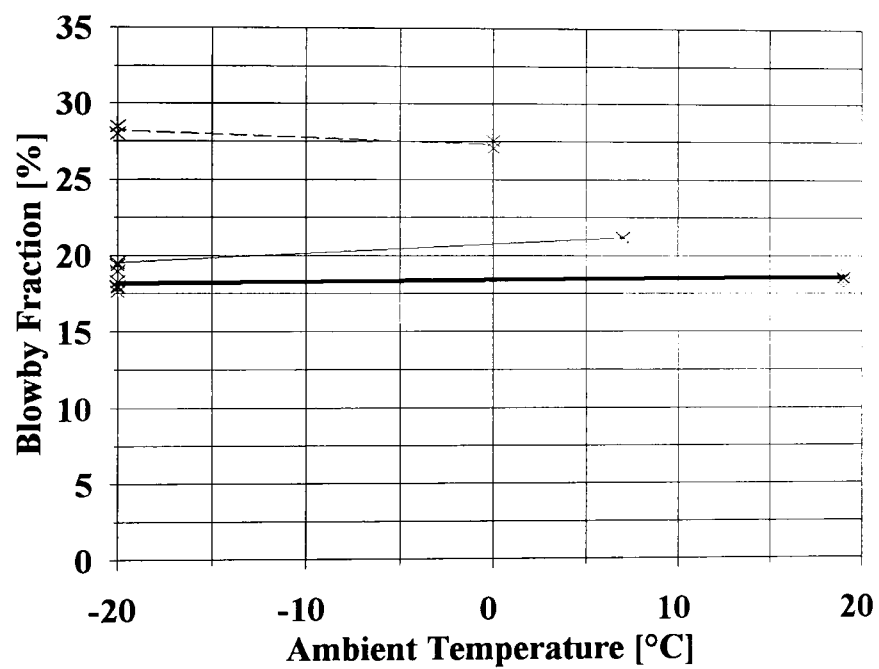


Figure 5.6
Improved Blowby Predictions, 1000 rpm Average Speed
(Ford P-type engine, SAE 10W/30, Motoring @ +30°C)



--- 110 rpm (ave) — 136 rpm (ave) — 154 rpm (ave)



--- 33 rpm (min) — 66 rpm (min) — 80 rpm (min)

Figure 5.7

Influence of Ambient Temperature on Blowby Losses

(Ford 1.8L IDI Engine, SAE 10W/30 oil, Cranking)

Blowby Measured at Various Cranking Speeds

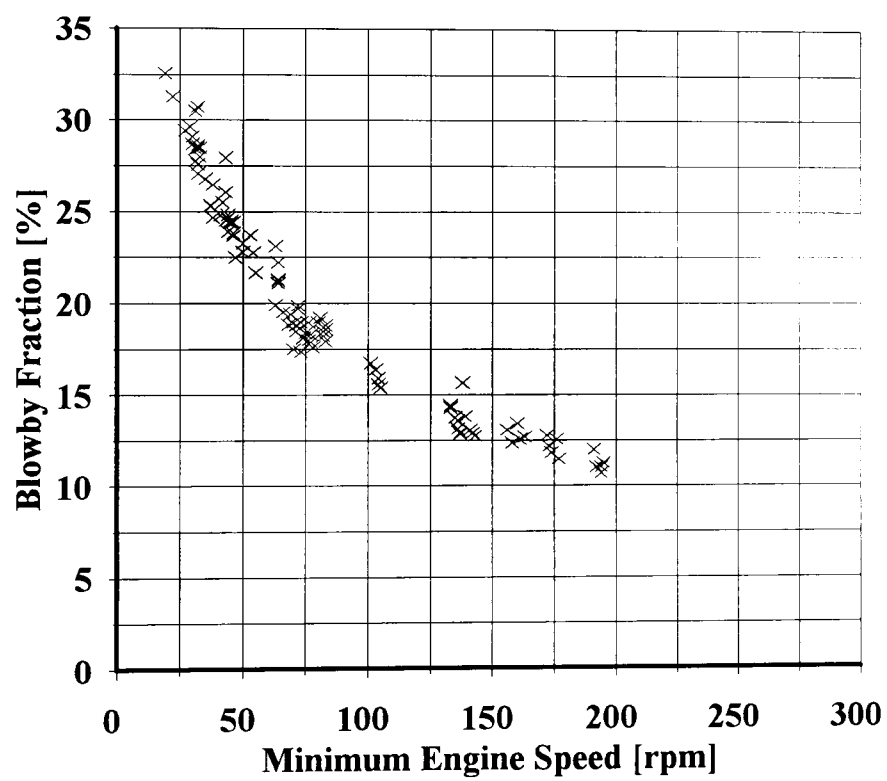
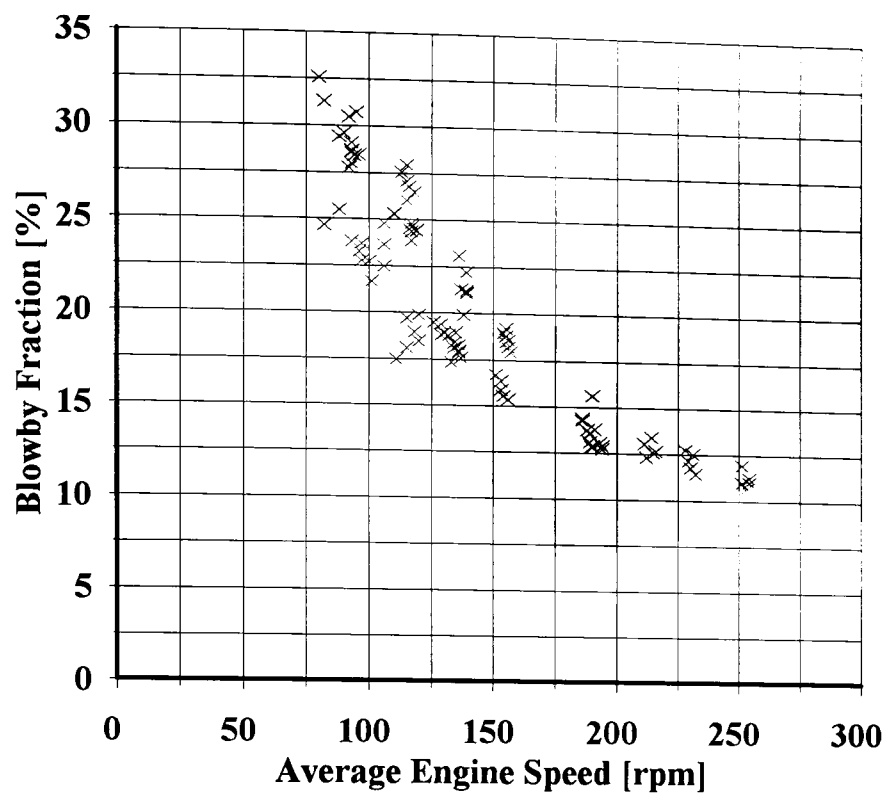


Figure 5.8

Influence of Engine Speed on Blowby Losses

(Ford 1.8L IDI Engine, SAE 10W/30 oil, Cranking)

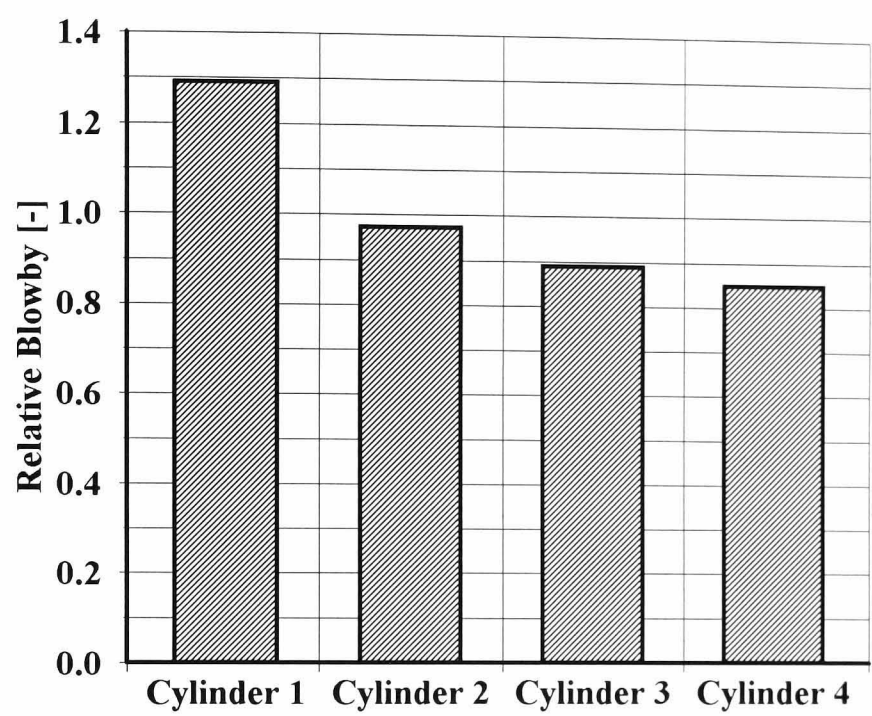
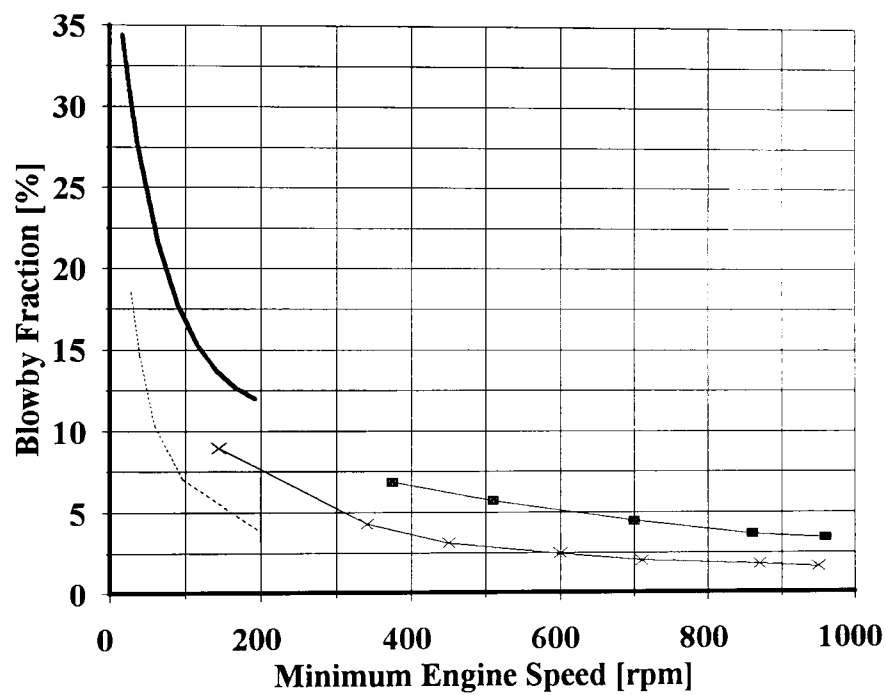
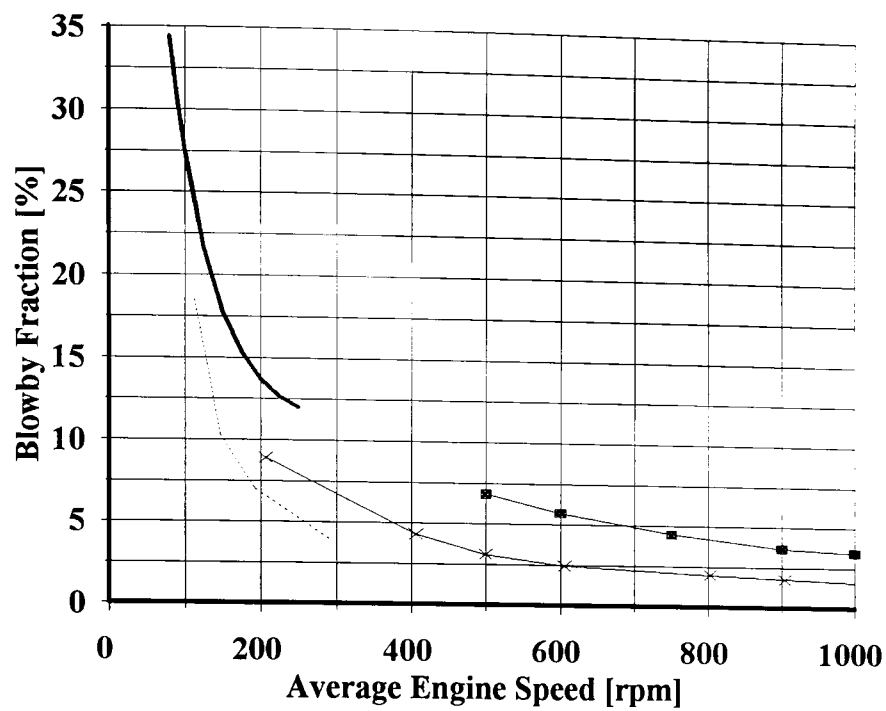


Figure 5.9 :
Relative Blowby Losses - Variation Between Cylinders
(Ford 1.8L IDI Engine, SAE 10W/30 oil, Cranking)



— 1.8L IDI × 2.2L P-type ■ 1.8L L-type 1.9L VW

Figure 5.10 :
 Blowby Losses with Speed - Variation Between Engines
 (All Engines : SAE 10W/30 oil, Cranking/Motoring @ +20°C)

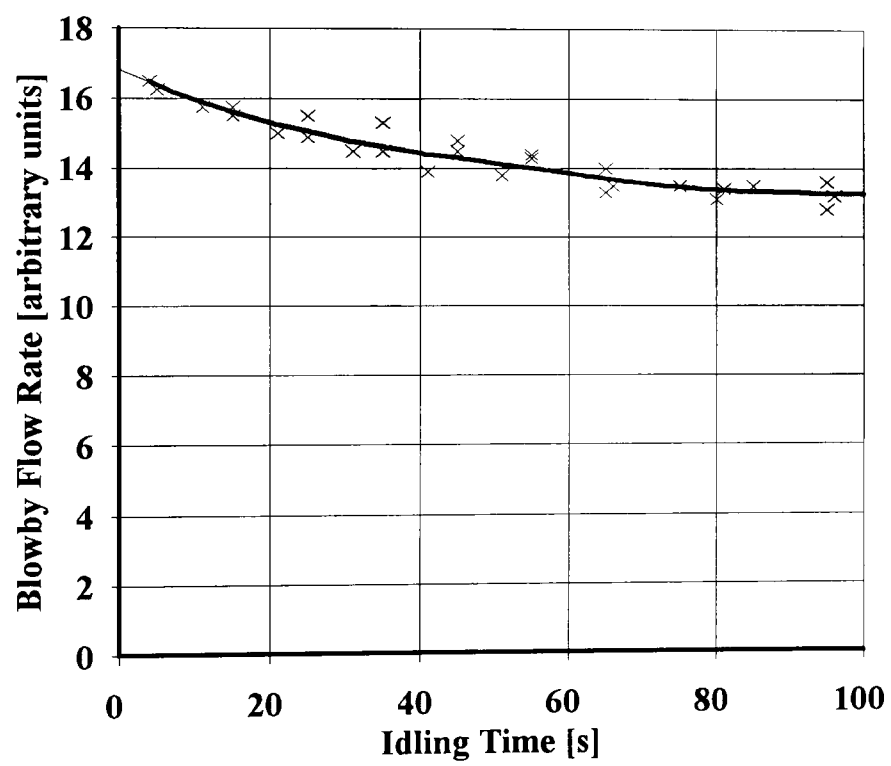
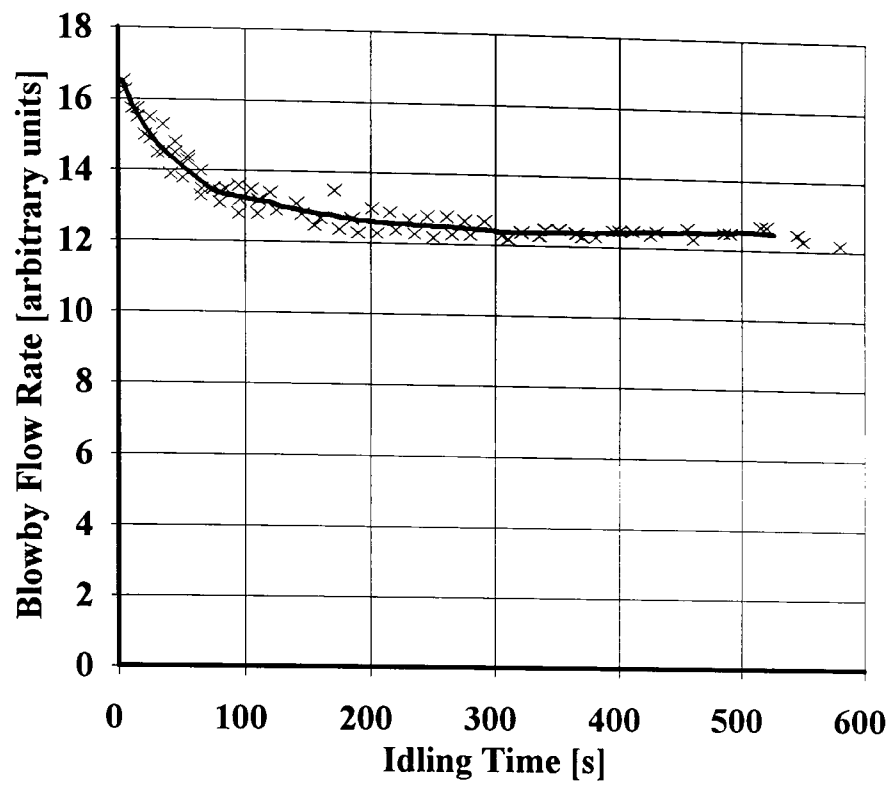


Figure 5.11 :
Changing Blowby Losses at Idle
(Ford 1.8L IDI, SAE 10W/30 oil, Idling @ 1000 rpm, +20°C)
Showing Projection to Zero Time

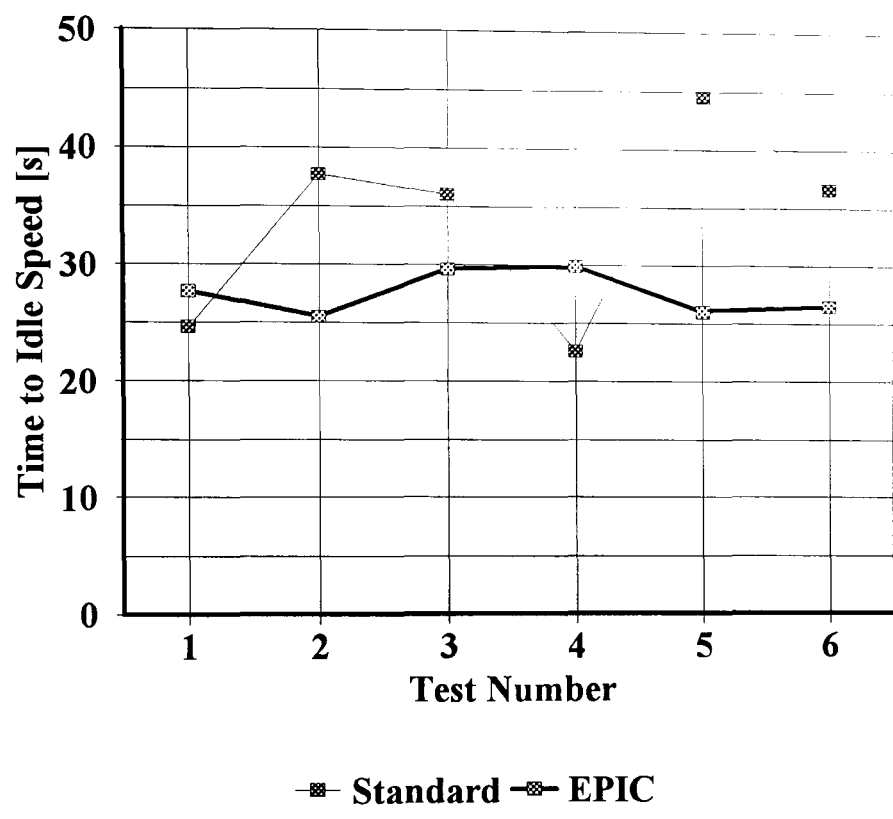


Figure 6.1
Standard and EPIC Fuel Pump Performance at -20°C
(Ford 1.8L IDI TC, Standard Sierra Installation)

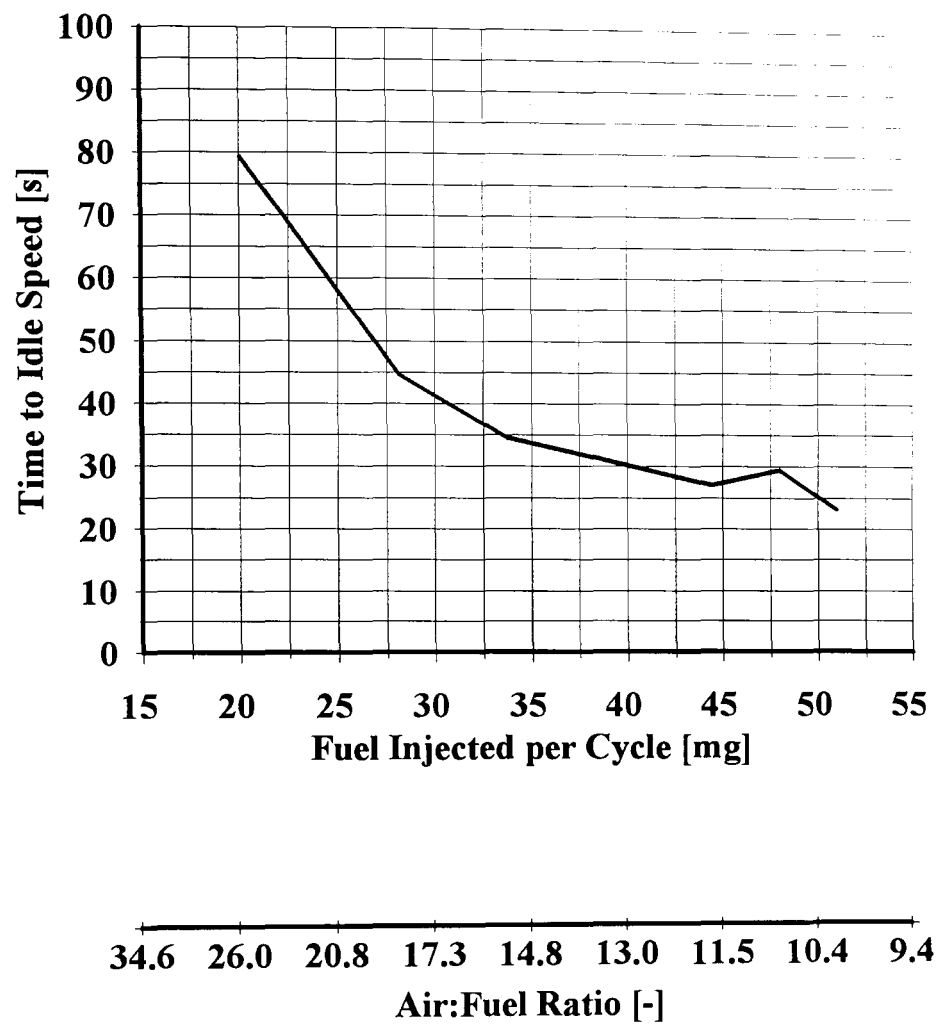


Figure 6.2

Reduced Start Time (Time to Idle) with Increased Fuelling
(Ford 1.8L IDI TC, EPIC Fuel Pump, SOI $4\pm\frac{1}{2}^{\circ}$ BTDC)
(SAE 10W/30 Oil, -20°C)

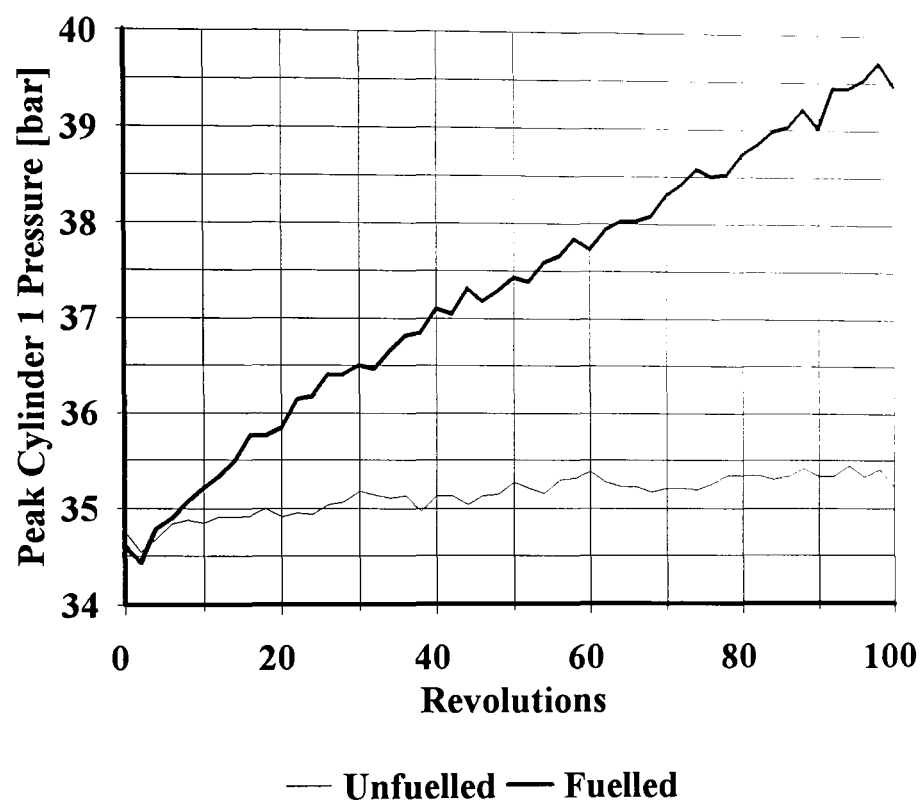


Figure 6.3

Rise in Peak Pressure with Fuelled Cranking

(Ford 1.8L IDI TC, EPIC Fuel Pump, 50mg injection)

(SAE 10W/30 Oil, -10°C, glowplugs disabled)

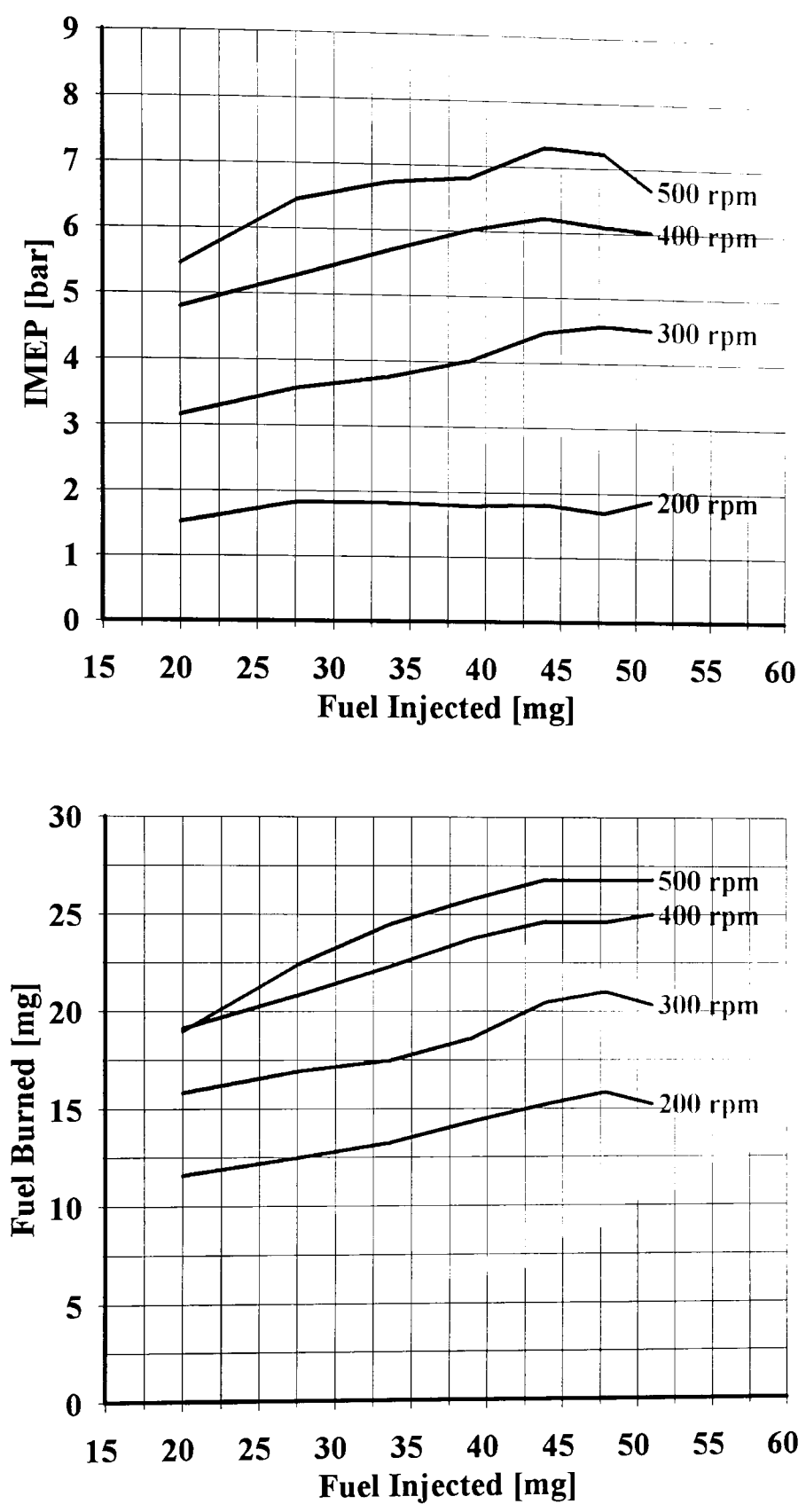


Figure 6.4
IMEP and Fuel Burned (Firing Cycles ONLY)
(Ford 1.8L IDI TC, EPIC Fuel Pump, SOI $4\pm\frac{1}{2}^{\circ}$ BTDC)
(SAE 10W/30 Oil, -20°C)

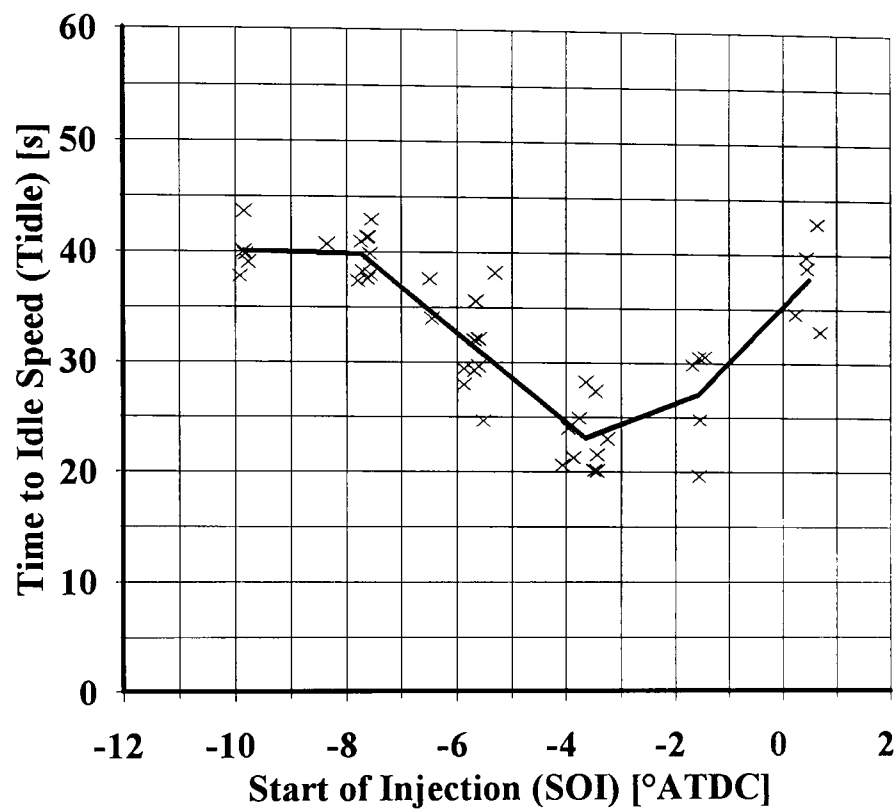


Figure 6.5

Start Time with Varying Injection Timing

(Ford 1.8L IDI TC, EPIC Fuel Pump, 50mg injection)

(SAE 10W/30 Oil, -20°C)

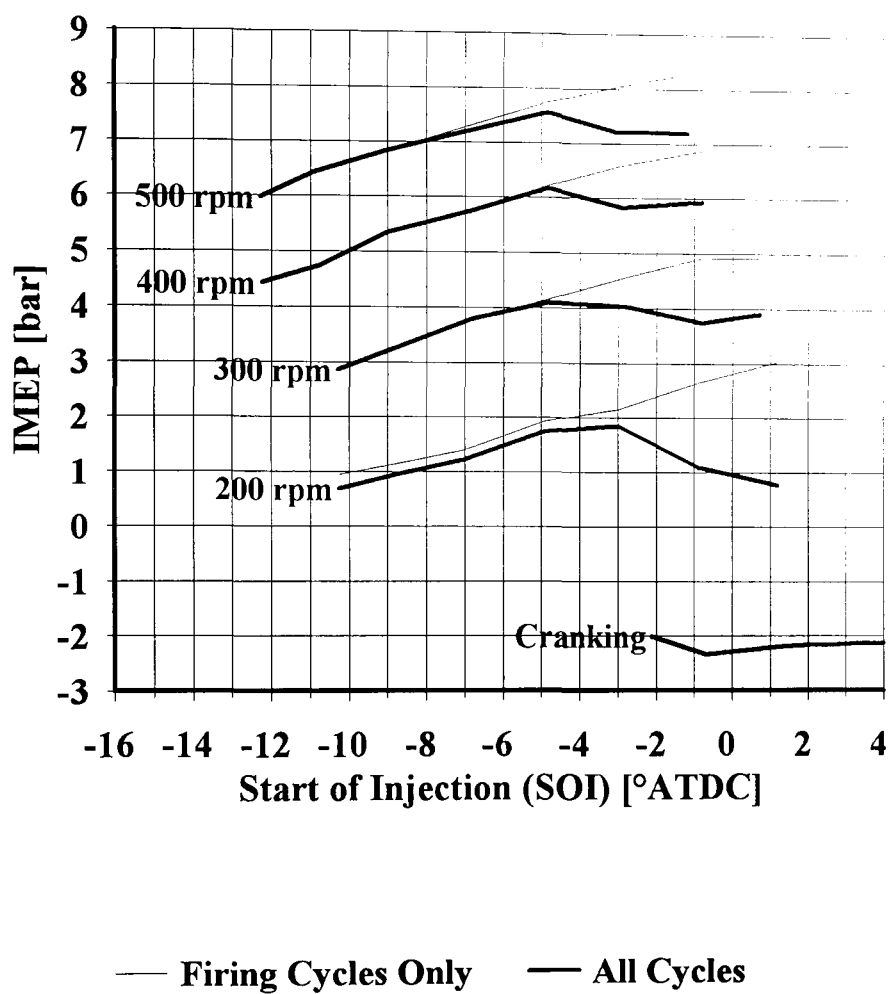


Figure 6.6

IMEP with Varying Injection Timing

(Ford 1.8L IDI TC, EPIC Fuel Pump, 50mg injection)

(SAE 10W/30 Oil, -20°C)

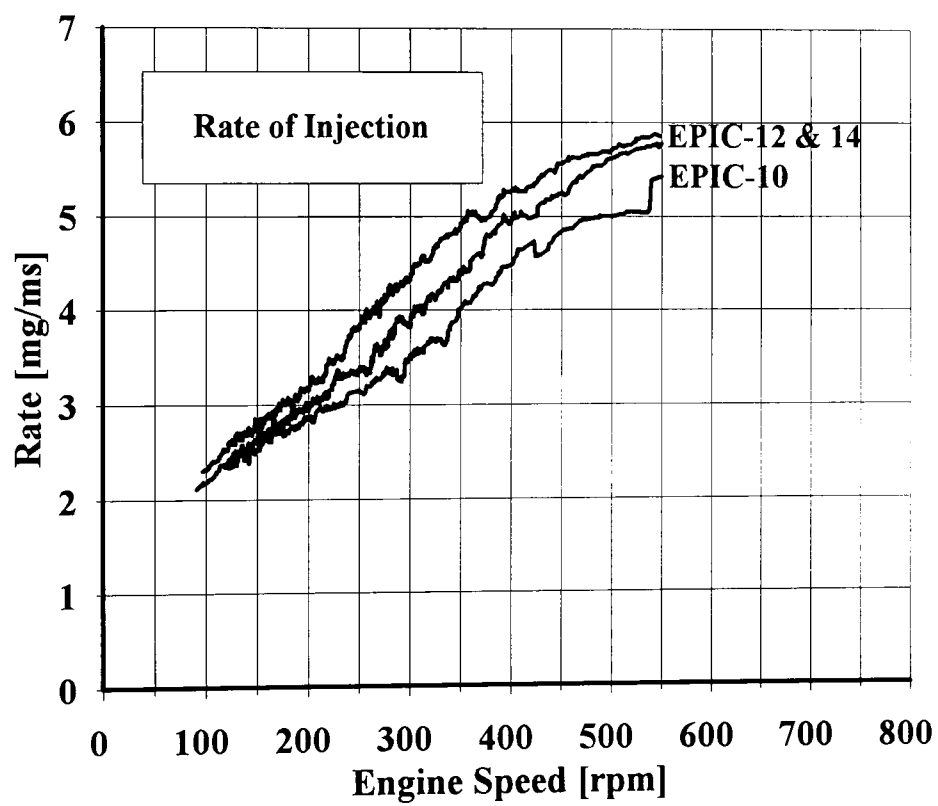
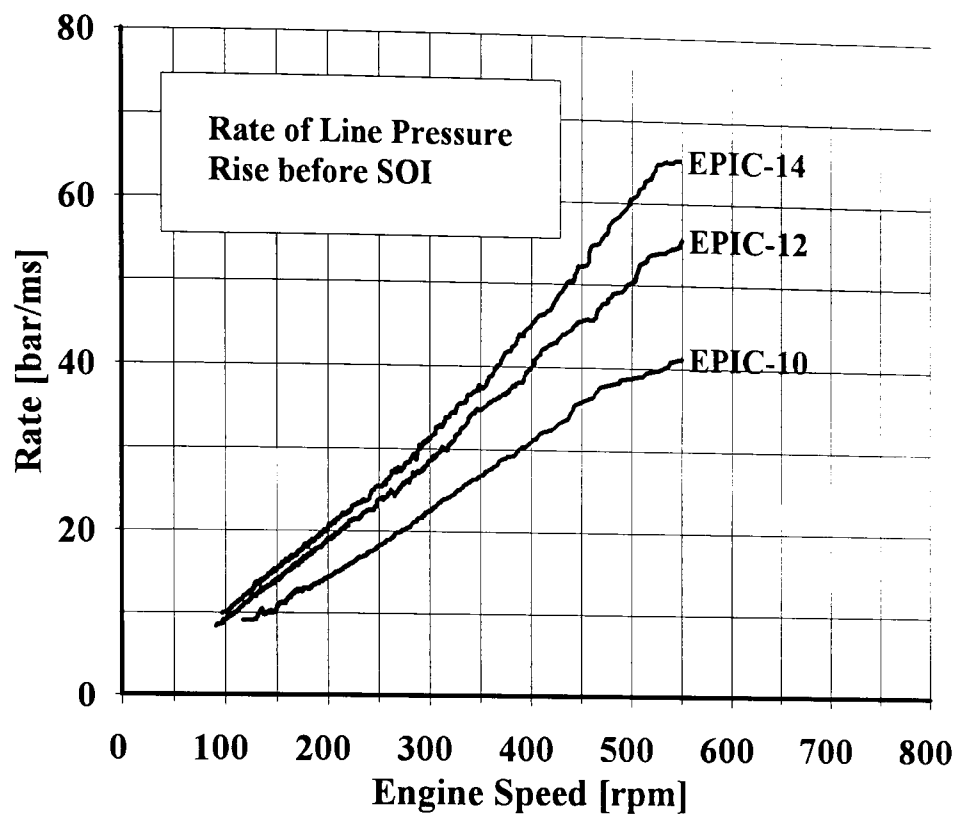


Figure 6.7
Variation of Fuel Injection Rates
(Ford 1.8L IDI TC, -20°C)
(EPIC Fuel Pumps, 50mg injection)

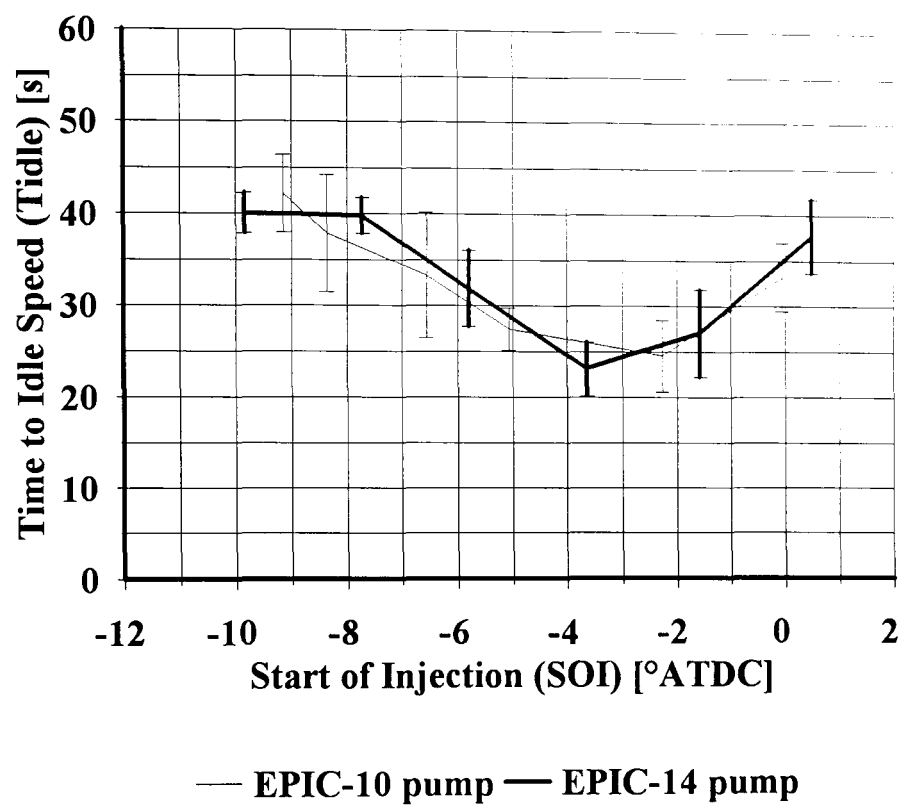


Figure 6.8

Effect of Injection Rate on Start Time

(Ford 1.8L IDI TC, EPIC Fuel Pump, 50mg injection)

(SAE 10W/30 Oil, -20°C)

NOTE : Verticals show \pm one standard deviation

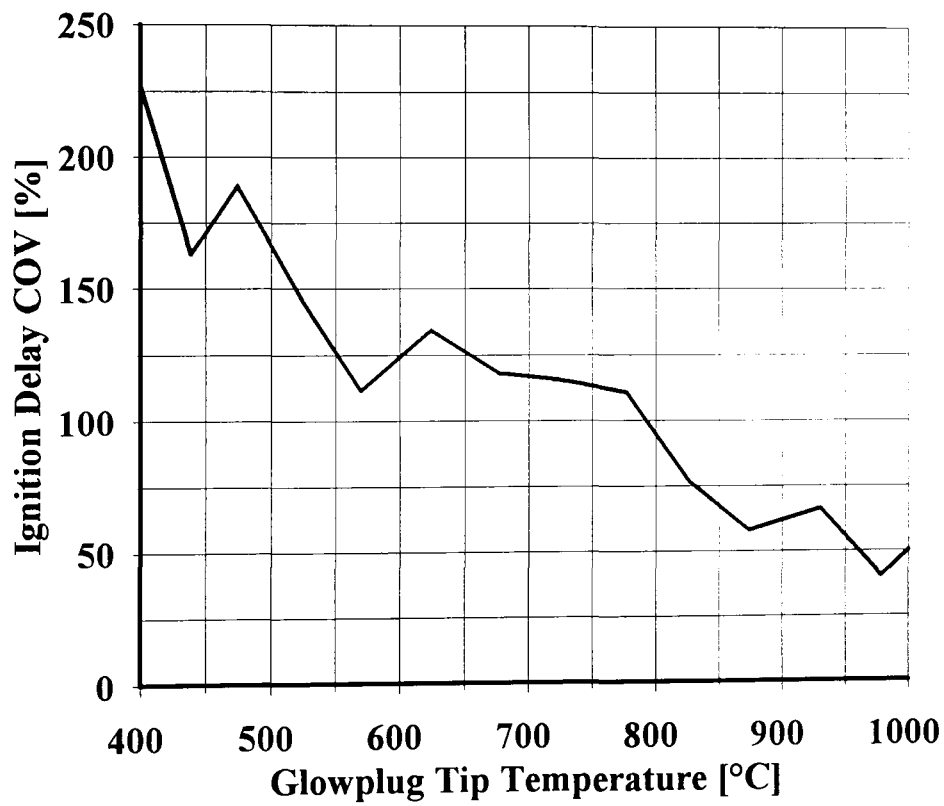
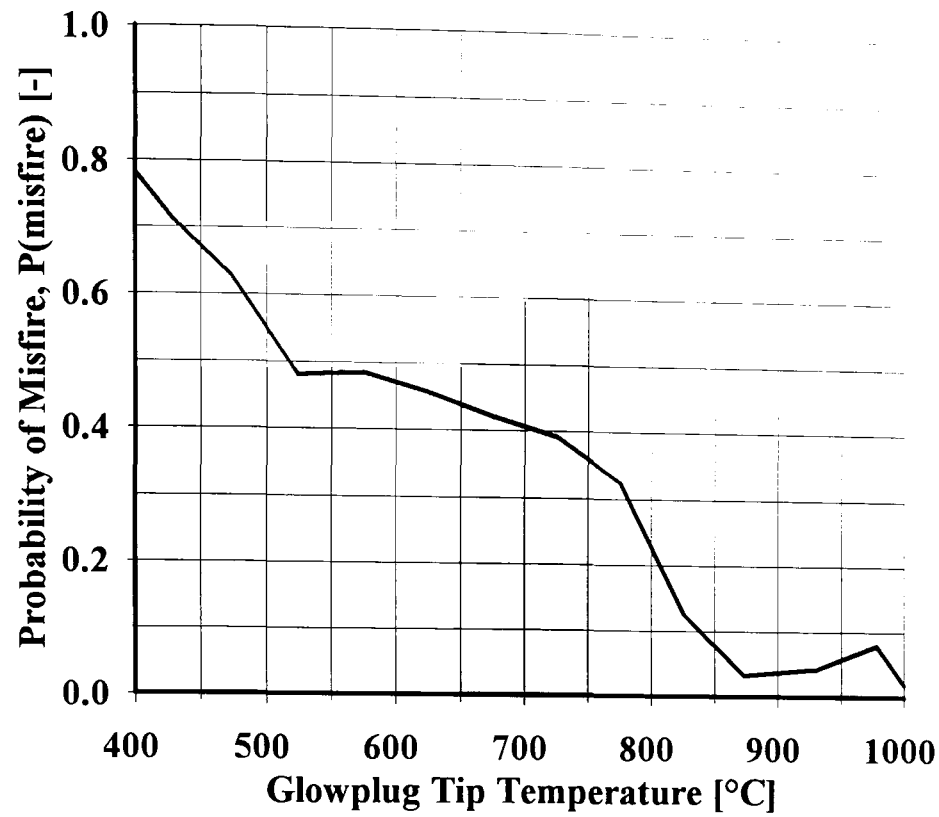


Figure 6.9
Effect of Glowplug Tip Temperature on Ignition Quality
(Standard Glowplug, Standard Controller Settings)
(Ford 1.8L IDI TC, -20°C, EPIC Fuel Pump, 50mg injection)

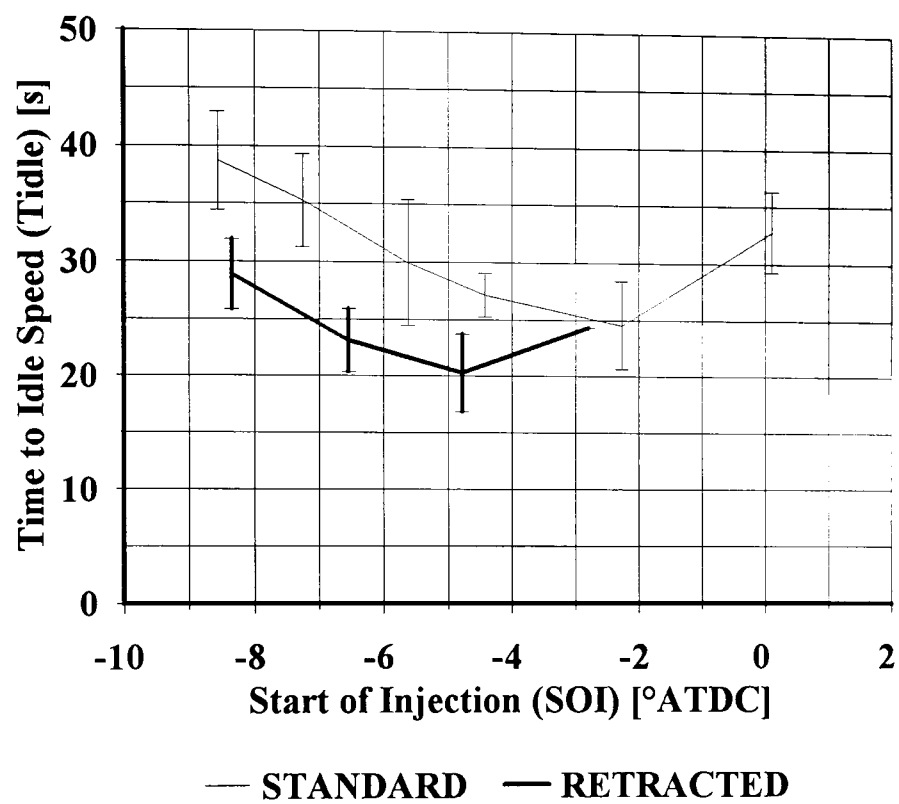


Figure 6.10

Start Time with STANDARD and RETRACTED Glowplugs
(Ford 1.8L IDI TC, EPIC Fuel Pump, 50mg injection)
(SAE 10W/30 Oil, -20°C)

NOTE: verticals show \pm one standard deviation

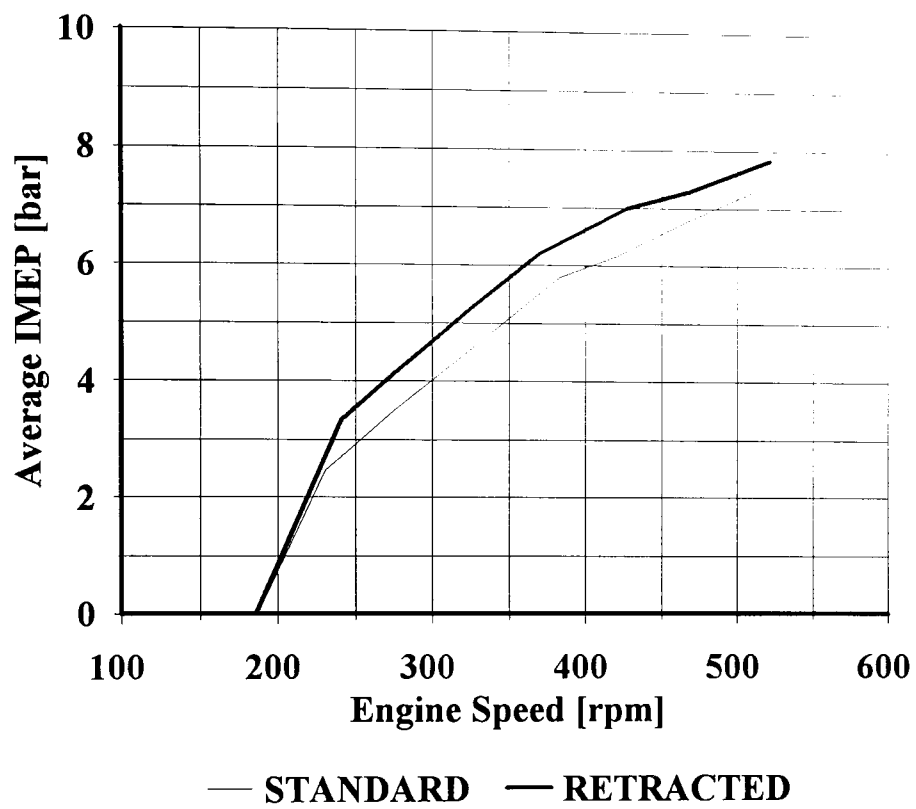


Figure 6.11

Average IMEP with STANDARD and RETRACTED Glowplug
(Ford 1.8L IDI TC, EPIC Fuel Pump, 50mg injection)
(SAE 10W/30 Oil, -20°C)

NOTE: average includes misfiring cycles

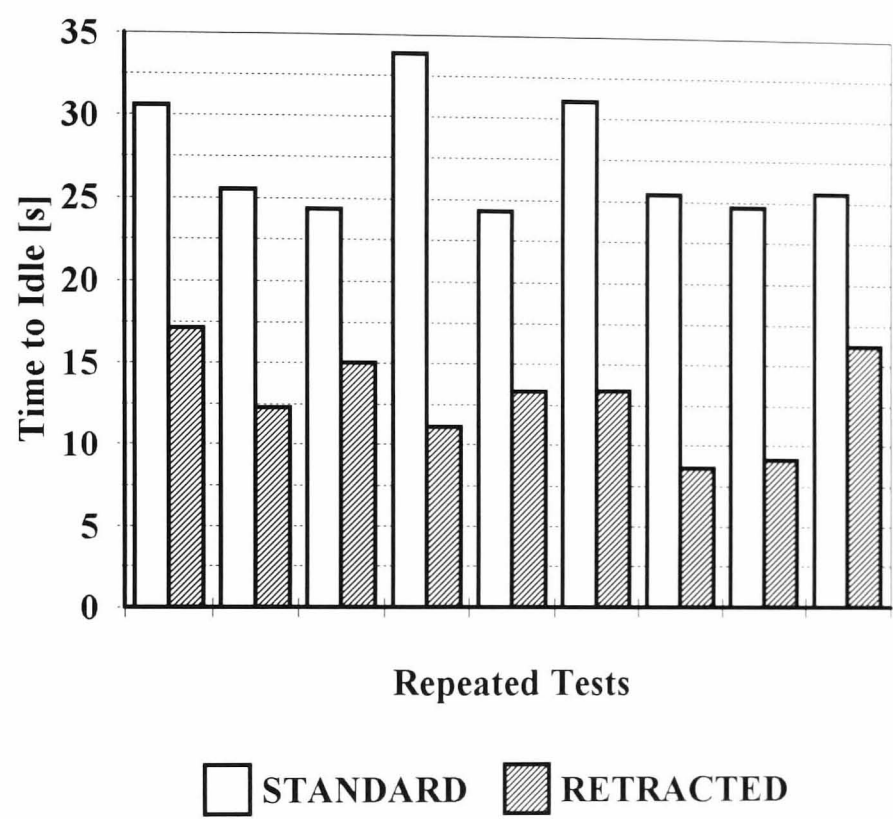


Figure 6.12
Improved Starts With Retracted Glowplugs (NOT Energised)
(Ford 1.8L IDI TC, EPIC Fuel Pump, 50mg injection)
(SAE 10W/30 Oil, +5°C)

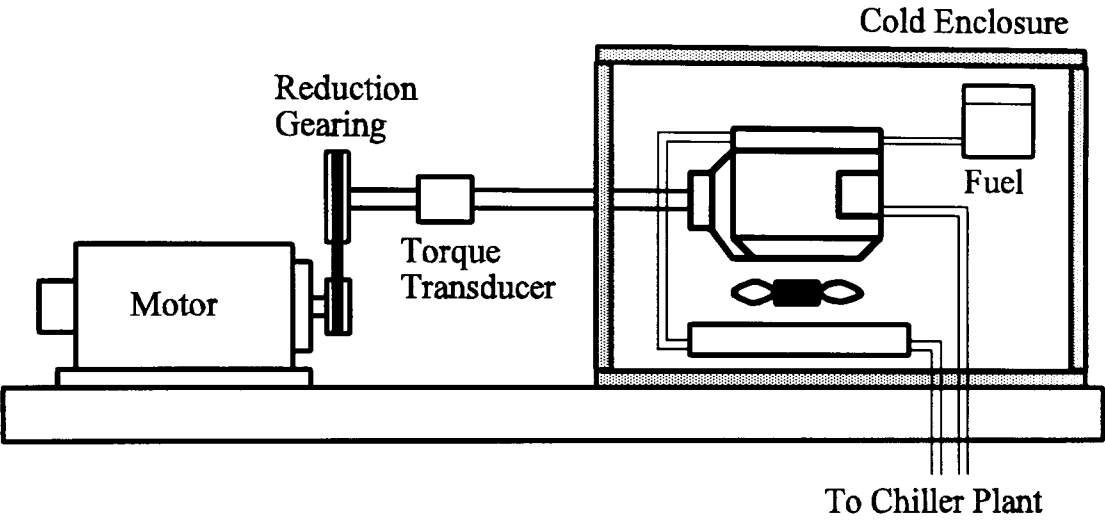


Figure 7.1 :
Test Rig Layout Schematic:
Motoring Engines

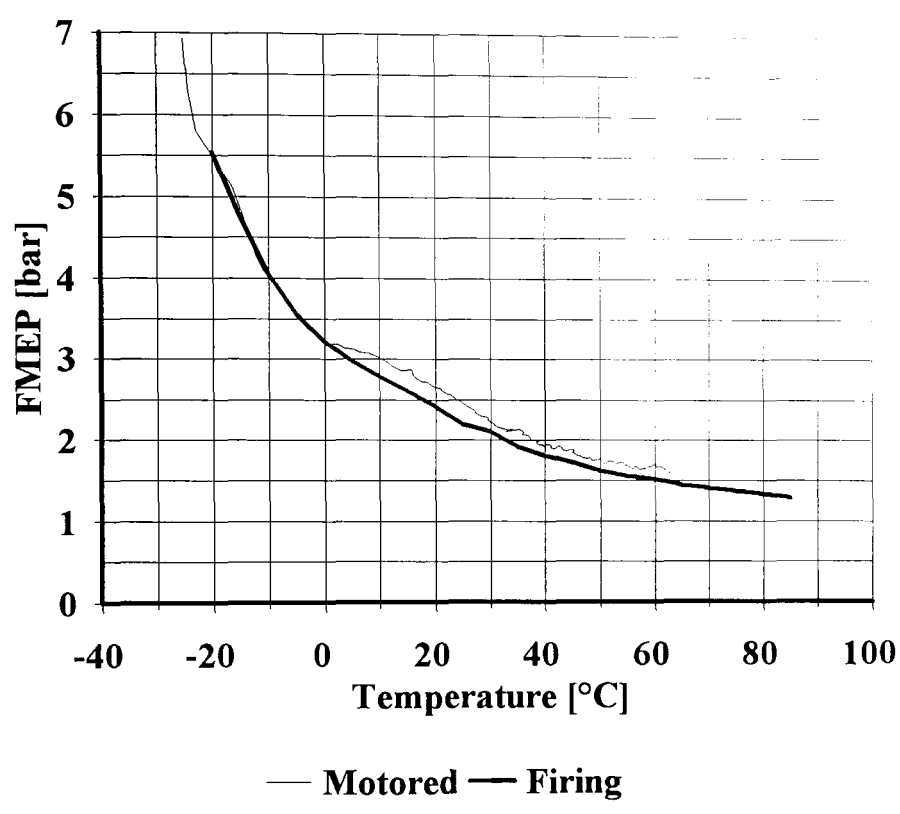


Figure 7.2
FMEP, Firing and Motored
(Ford 1.8L IDI Engine, SAE 10W/30 oil)

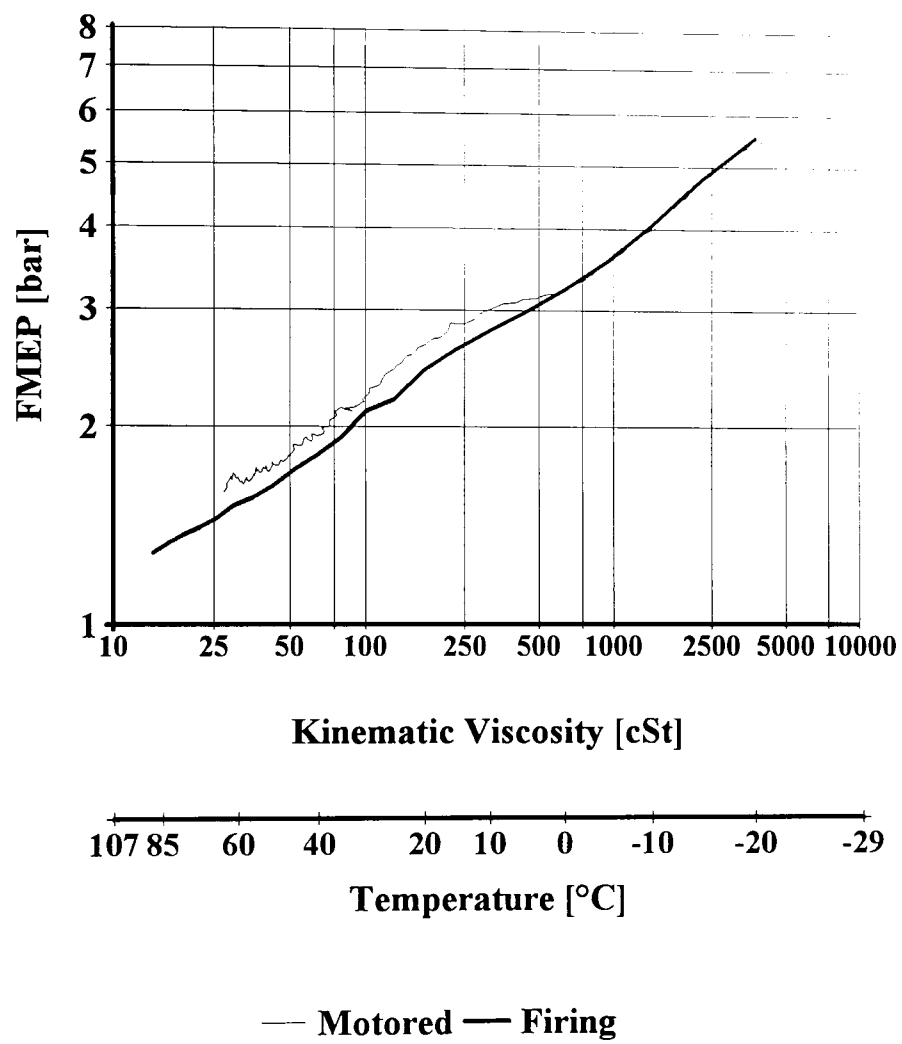


Figure 7.3
FMEP, Firing and Motored
(Ford 1.8L IDI Engine, SAE 10W/30 oil)

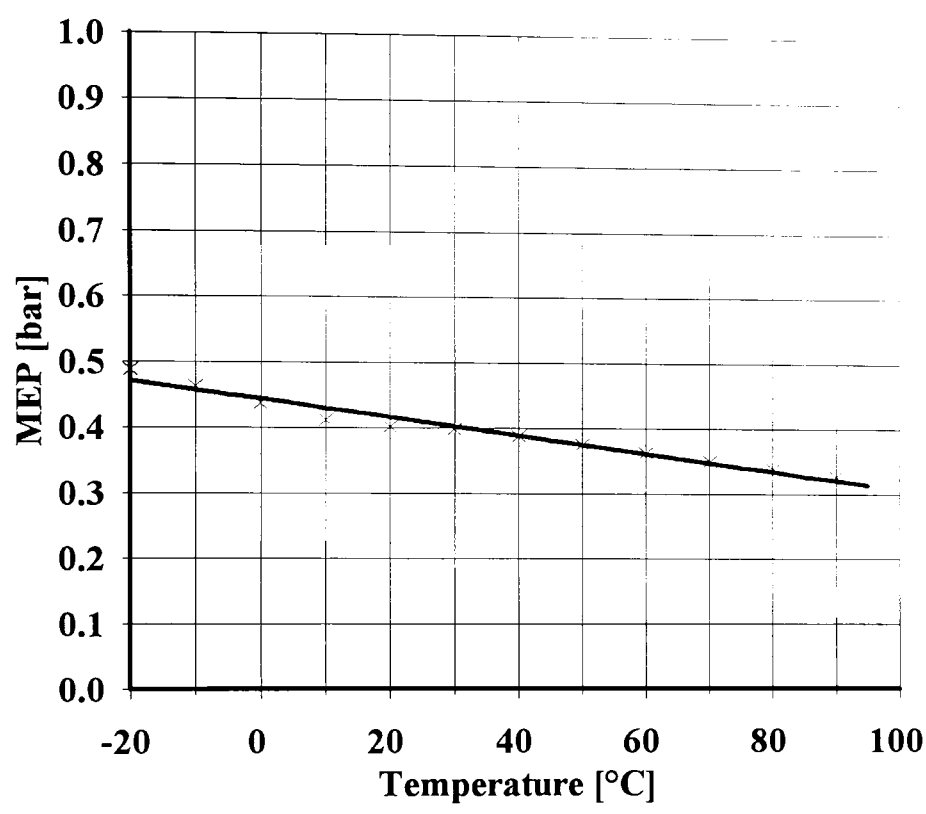


Figure 7.4

Component of FMEP due to gas pressure, 1000 rpm
(Ford 1.8L IDI Engine, SAE 10W/30 oil)

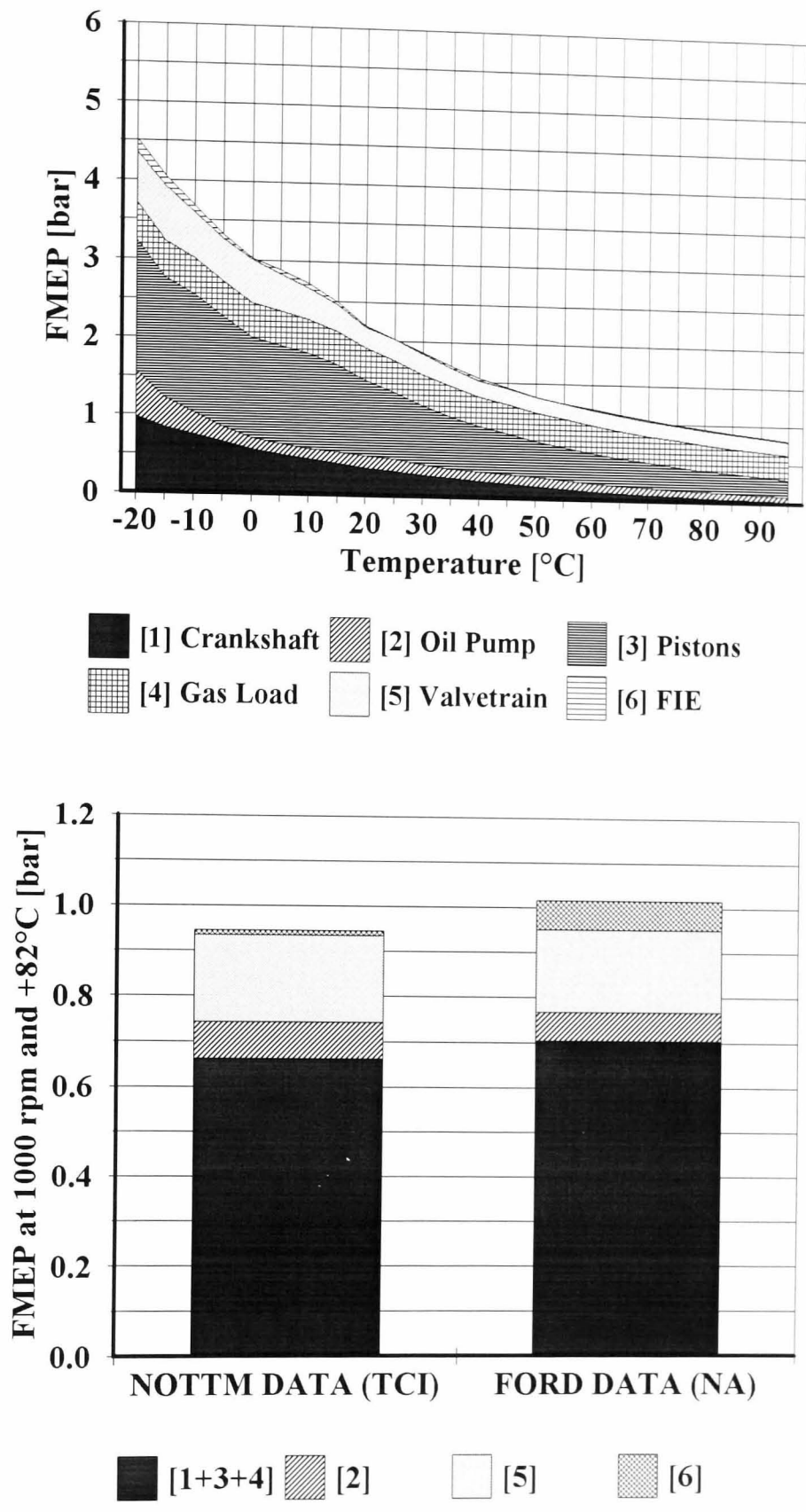
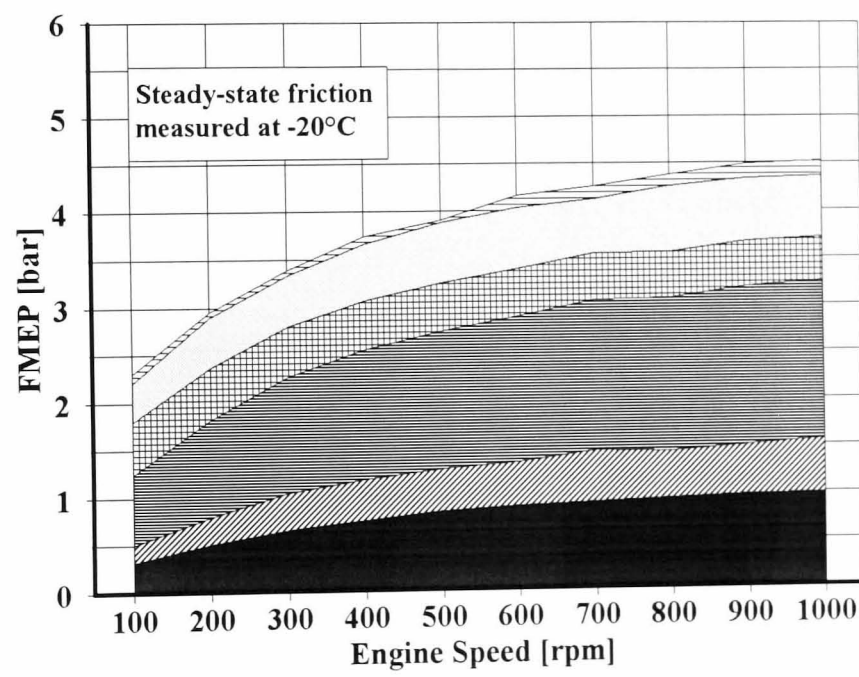
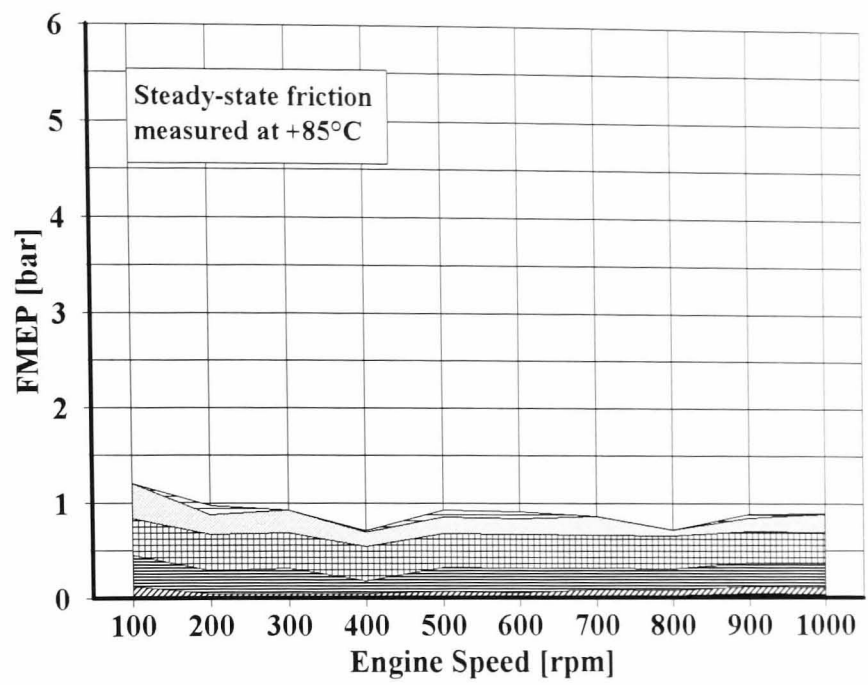


Figure 7.5

Friction breakdown at 1000 rpm

(Ford 1.8L IDI Engine, SAE 10W/30 oil)

NB: Components numbered from bottom







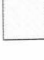
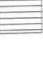
- | | | |
|--|--|---|
|  [1] Crankshaft |  [2] Oil Pump |  [3] Pistons |
|  [4] Gas Load |  [5] Valvetrain |  [6] FIE |

Figure 7.6

Friction breakdown at +85°C and -20°C

(Ford 1.8L IDI Engine, SAE 10W/30 oil)

NB: Components numbered from bottom

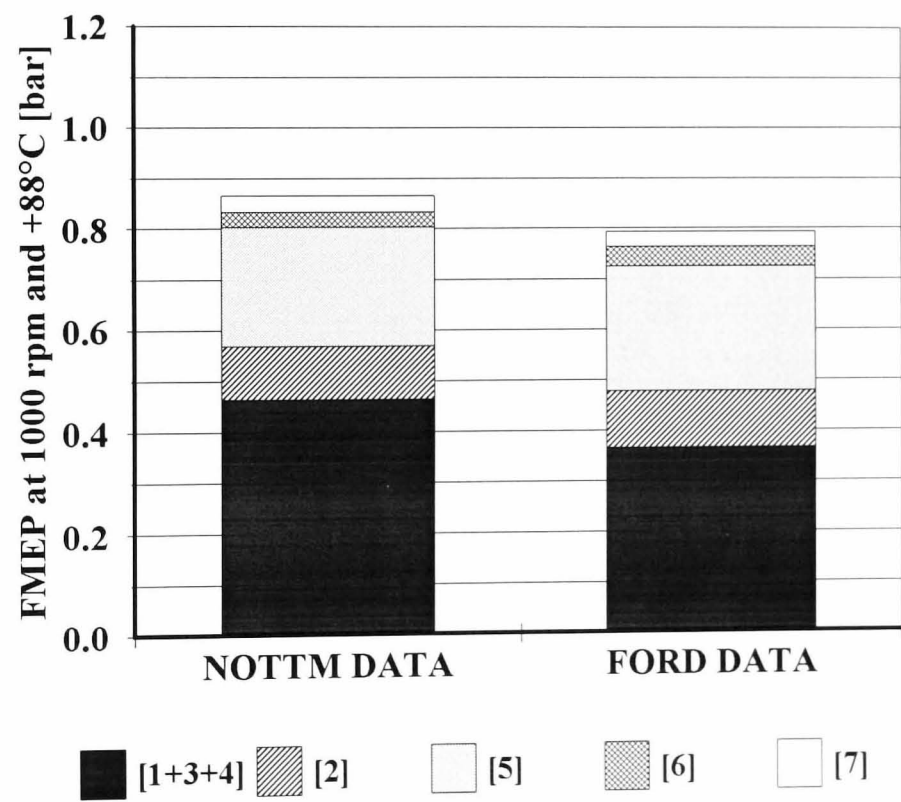
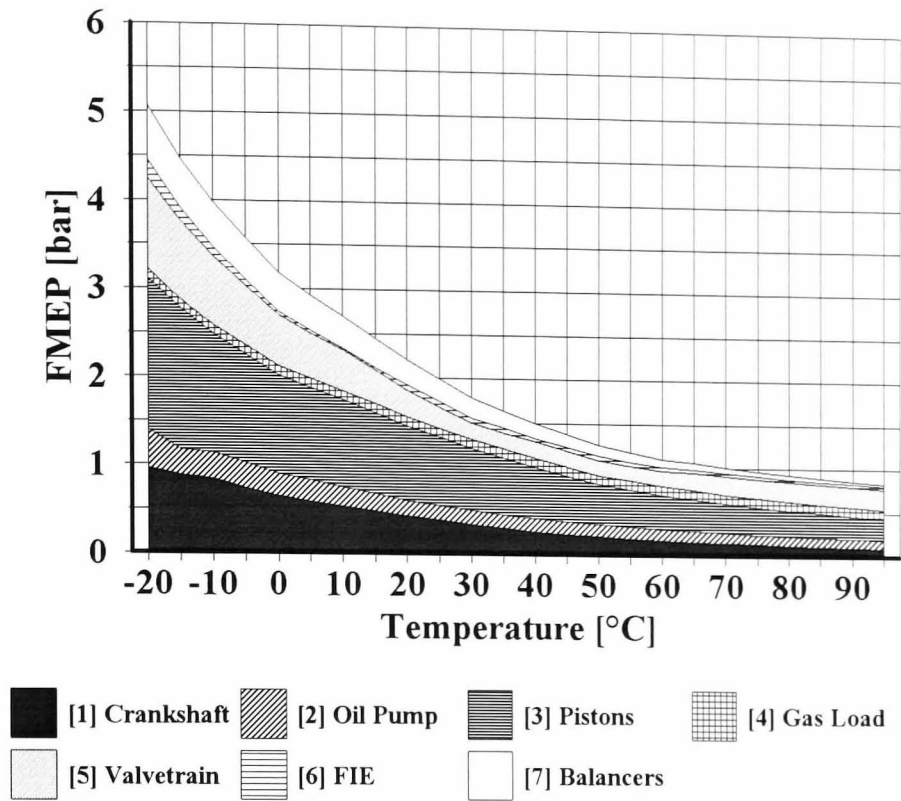


Figure 7.7

Friction breakdown at 1000 rpm

(Ford 2.2L P-type Engine, SAE 10W/30 oil)

NB: Components numbered from bottom

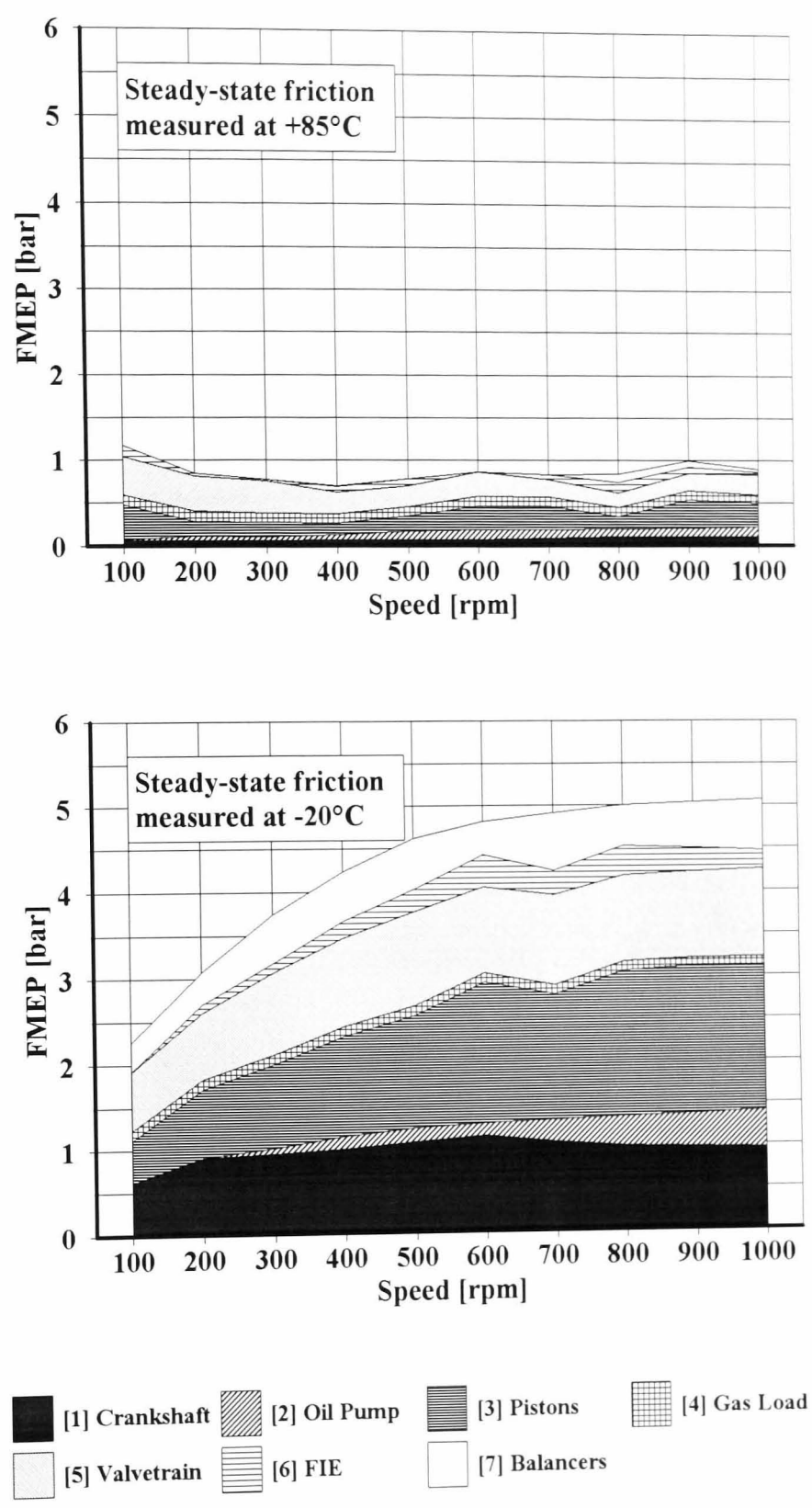


Figure 7.8
Friction breakdown at +85°C and -20°C
(Ford 2.2L P-type Engine, SAE 10W/30 oil)
NB: Components numbered from bottom

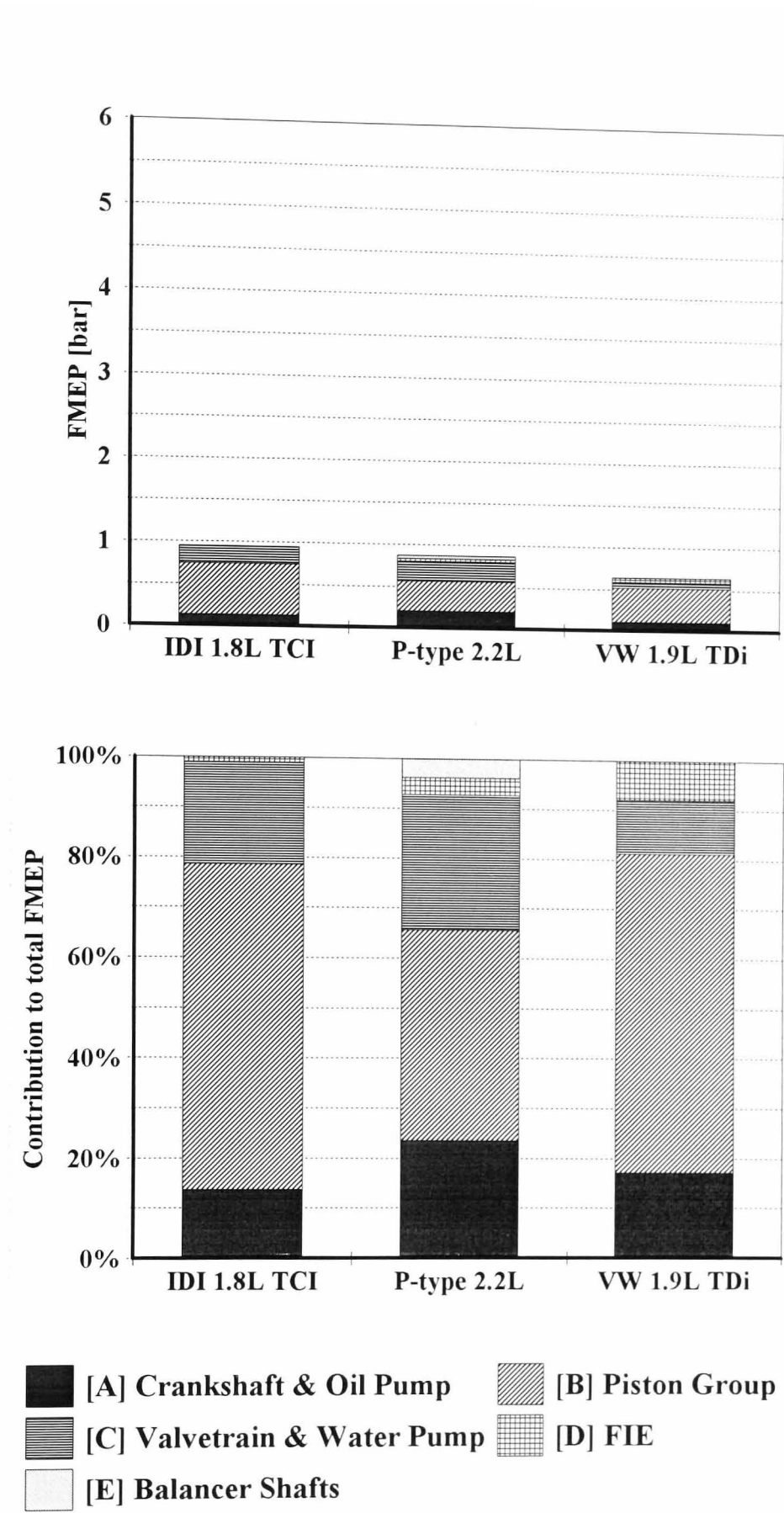


Figure 7.9

FMEP breakdown in three engines, fully warm
(SAE 10W/30 oil, 1000 rpm)
NB: Components labelled from bottom

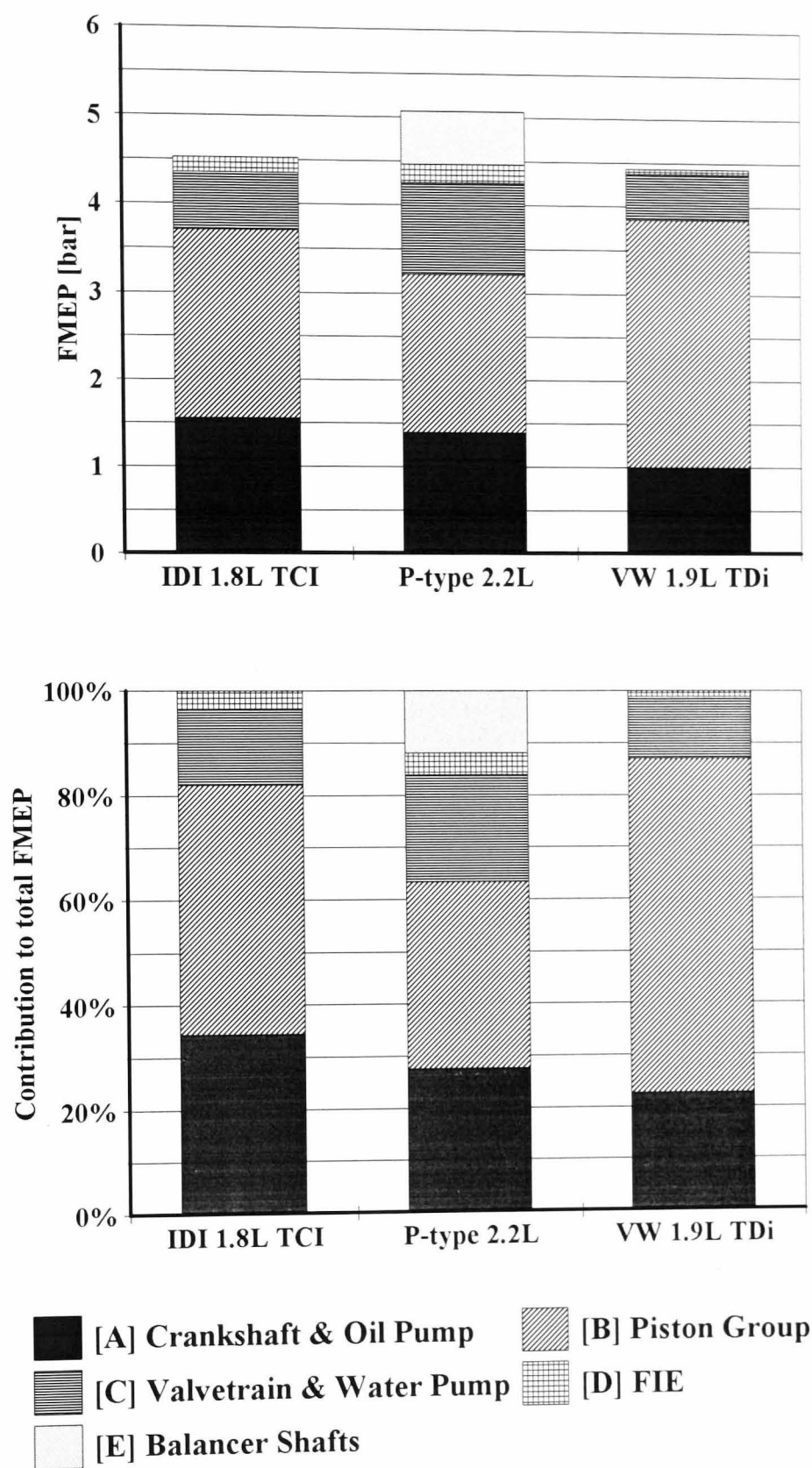


Figure 7.10
 FMEP breakdown in three engines, -20°C
 (SAE 10W/30 oil, 1000 rpm)
 NB: Components labelled from bottom

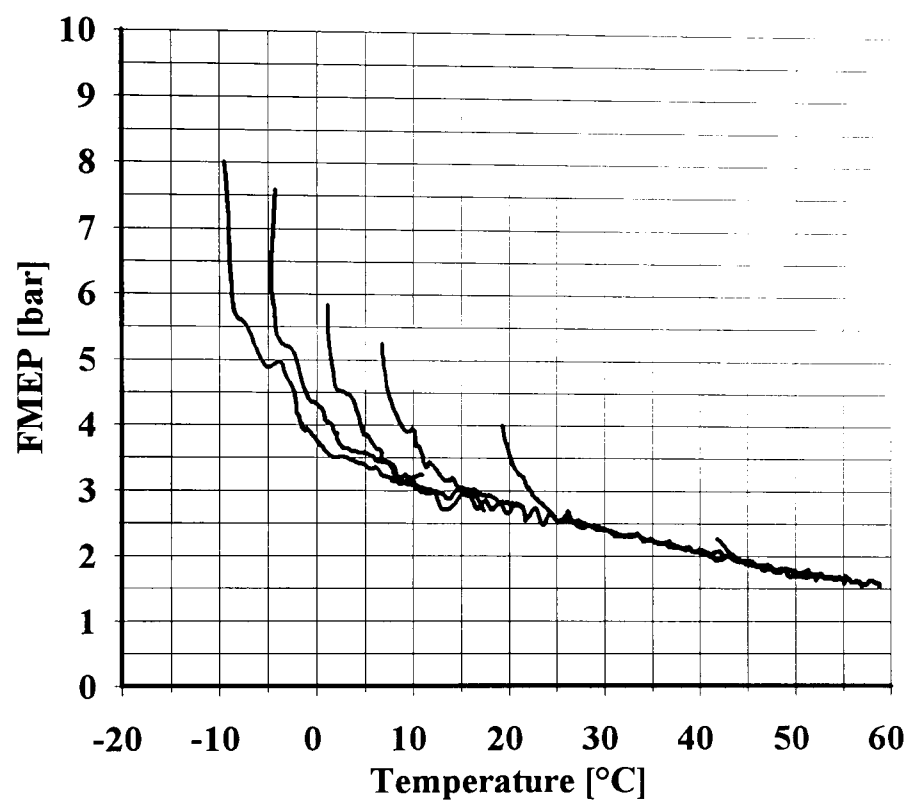


Figure 8.1

Initial Friction Transient, motored at 1000 rpm

(Ford 2.2L P-type Engine, SAE 20W/50 oil)

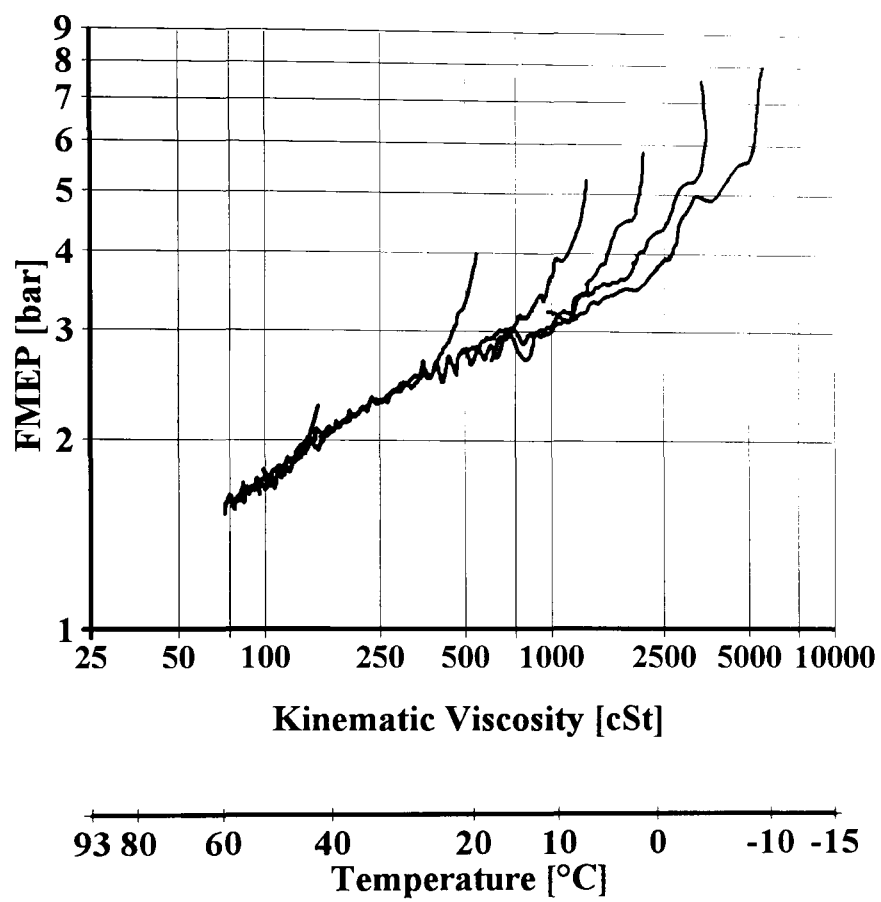


Figure 8.2

Initial Friction Transient, motored at 1000 rpm

(Ford 2.2L P-type Engine, SAE 20W/50 oil)

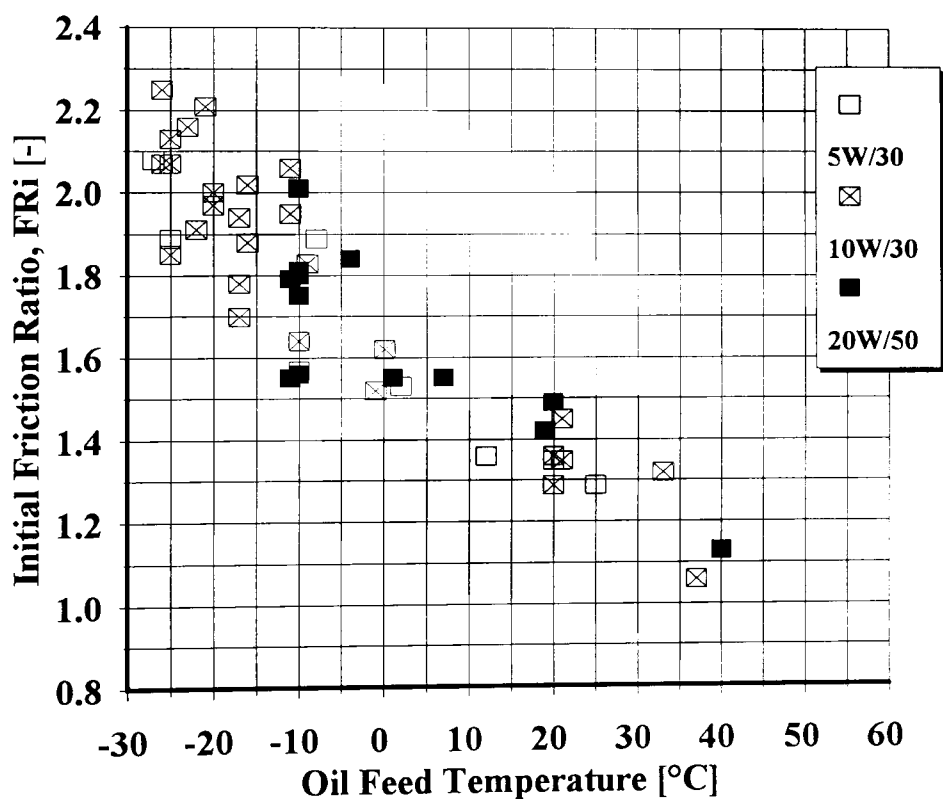
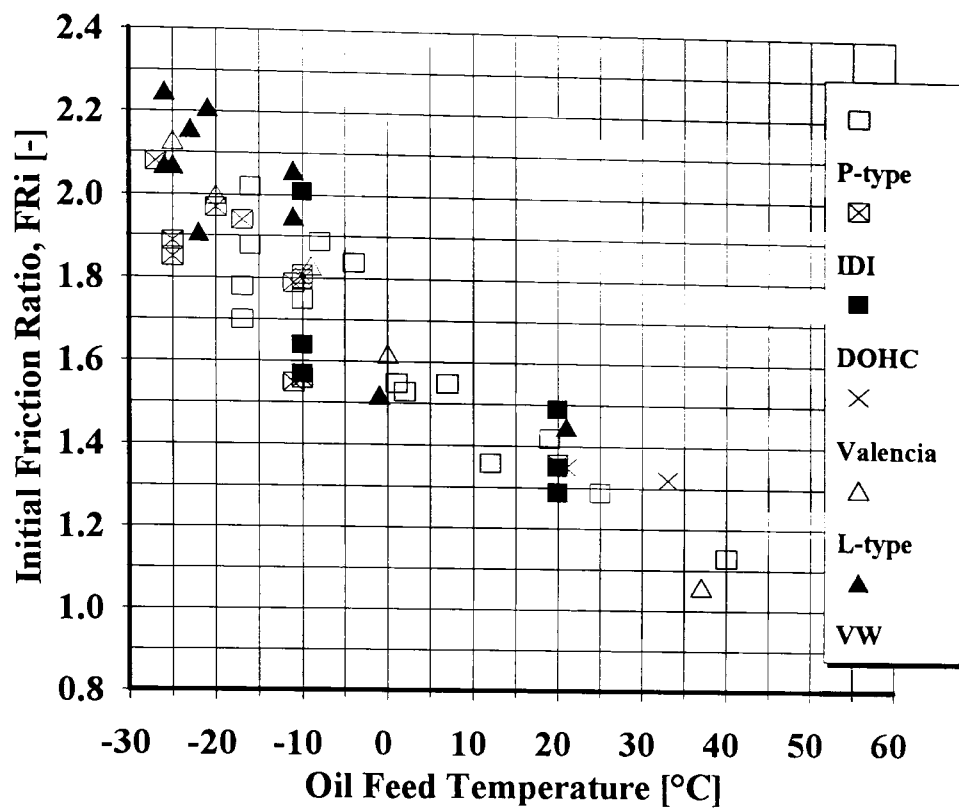


Figure 8.3

Initial Friction Ratio

Showing negligible effect of engine and oil type

(Firing and compressed motoring at 1000 rpm)

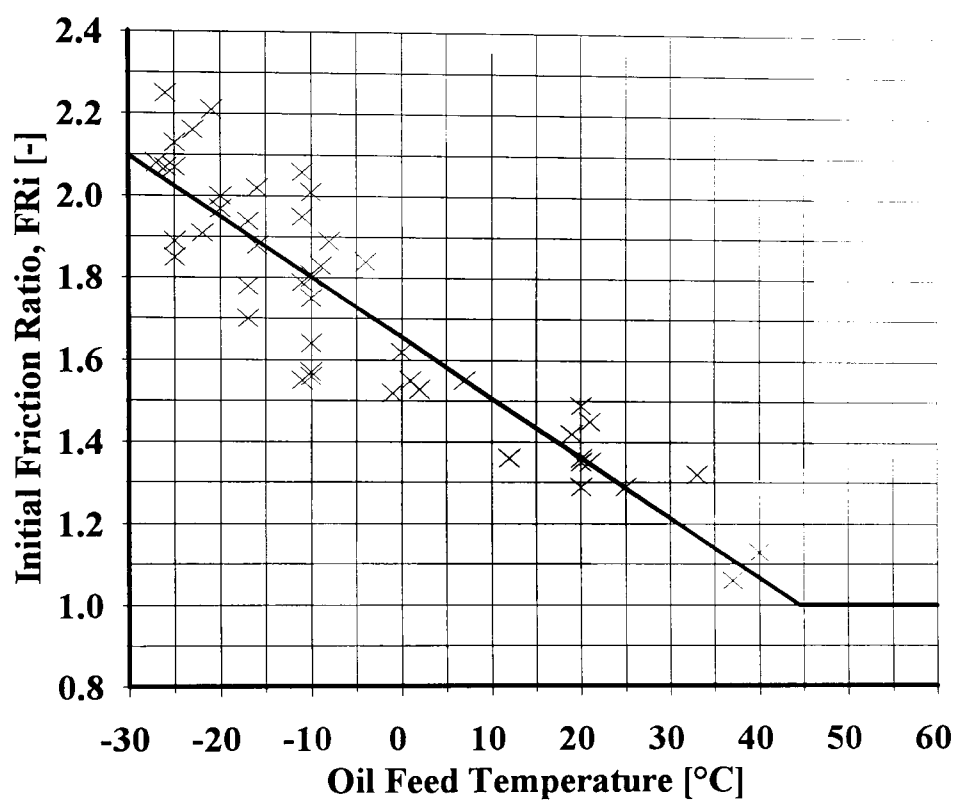


Figure 8.4

Initial Friction Ratio, with Linear Fit

(Firing and compressed motoring at 1000 rpm)

(All engine types, various oil types)

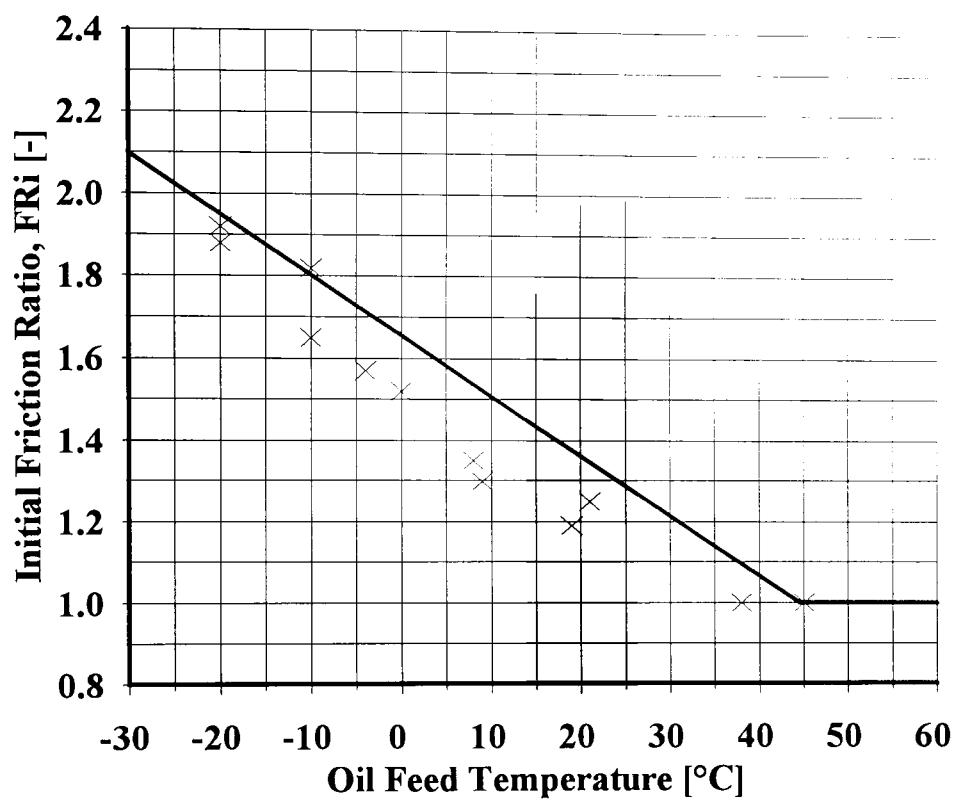


Figure 8.5

Initial Friction Ratio After Decompression

(Solid line shows best fit from compressed data)

(P-type 2.2L, Motoring at 1000 rpm, various oil types)

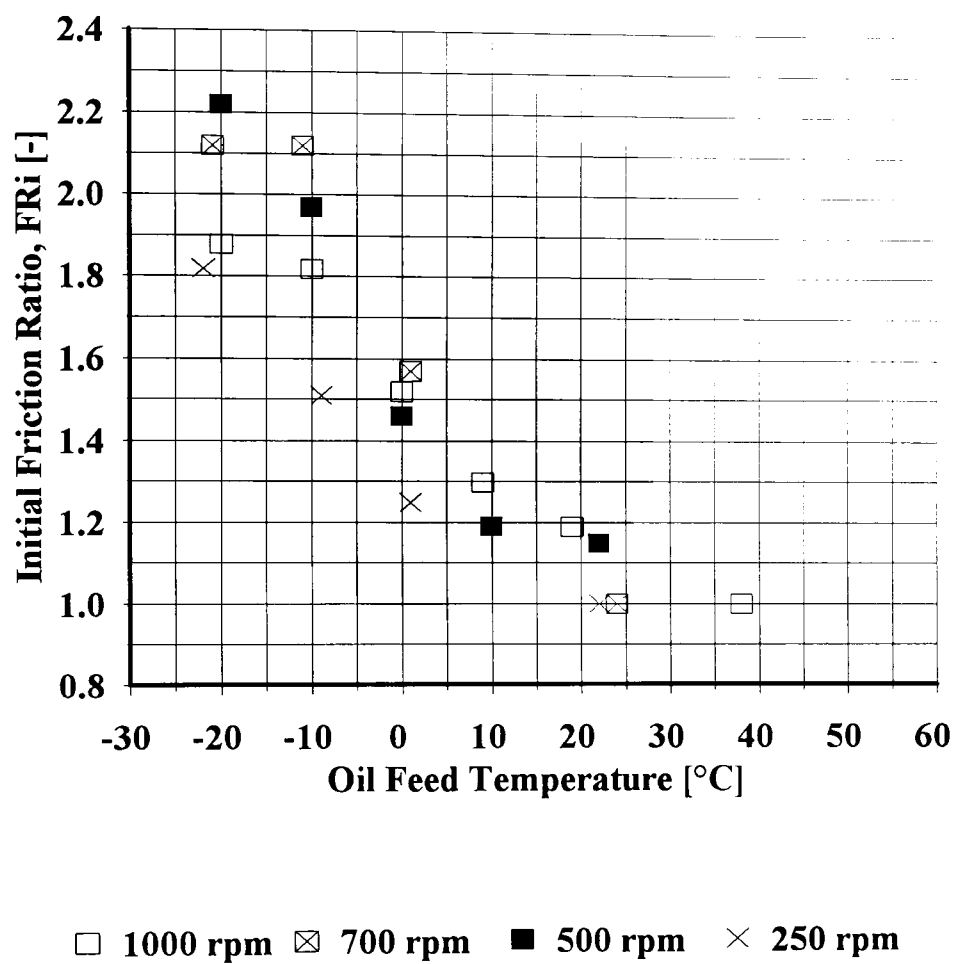


Figure 8.6

Effect of Speed on Initial Friction Ratio

(P-type 2.2L, Decompressed Motoring, SAE 10W/30)

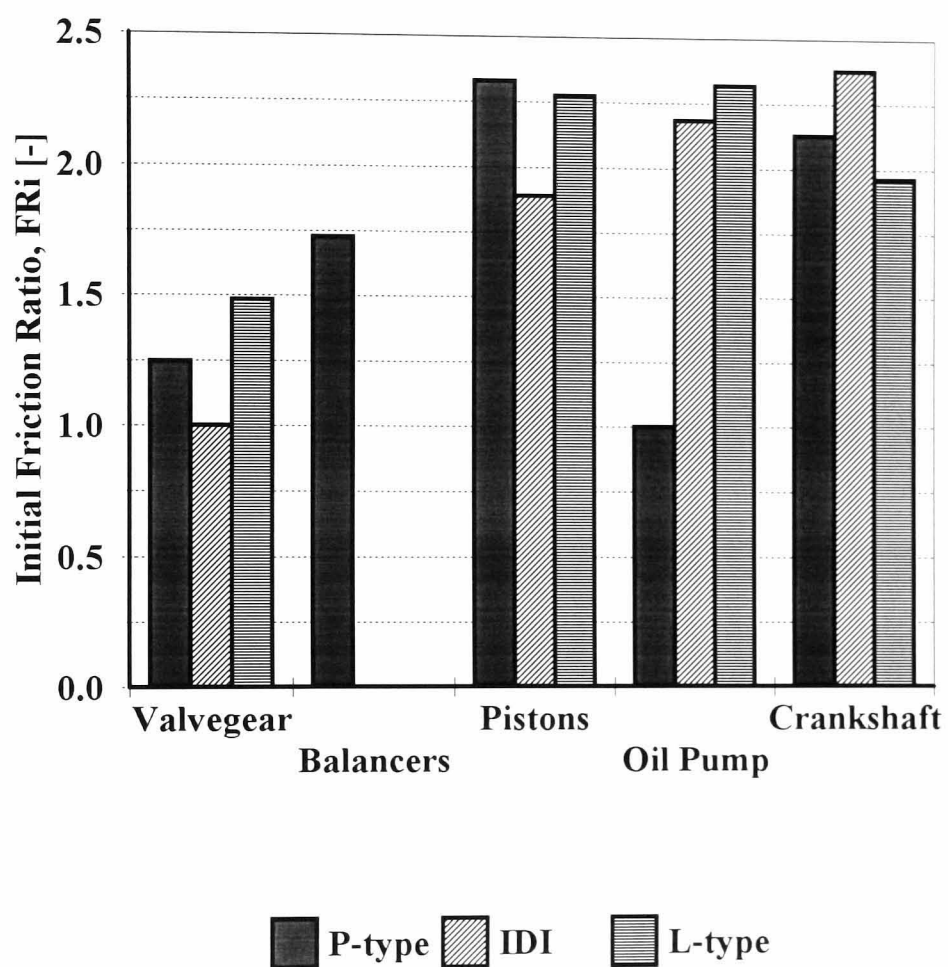


Figure 8.7

Initial Friction Transient Ratio for each component
(Decompressed motoring at 1000 rpm and -20°C)

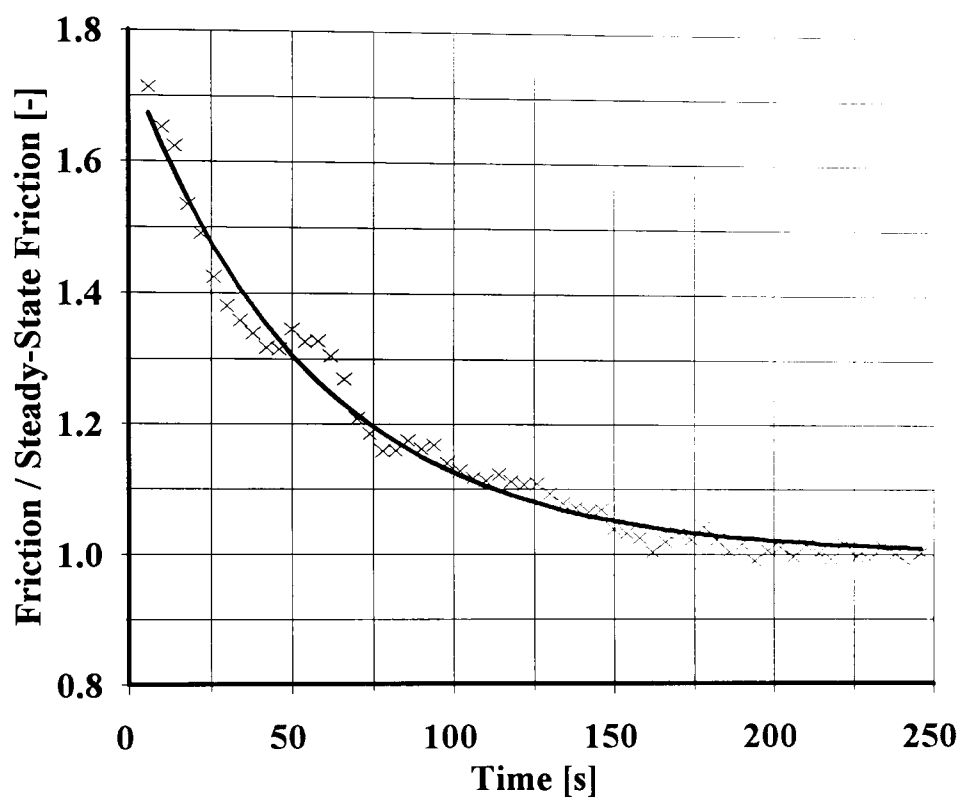


Figure 8.8

Typical Decay of Initial Friction Transient

(Data from compressed P-type engine, motored at 1000 rpm)

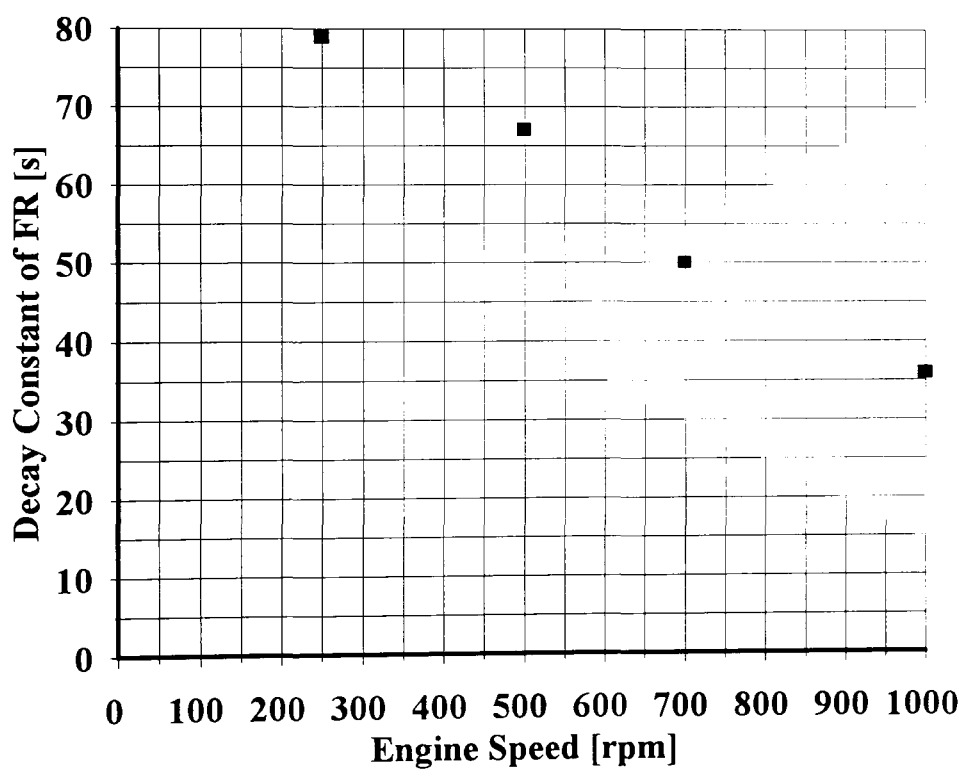
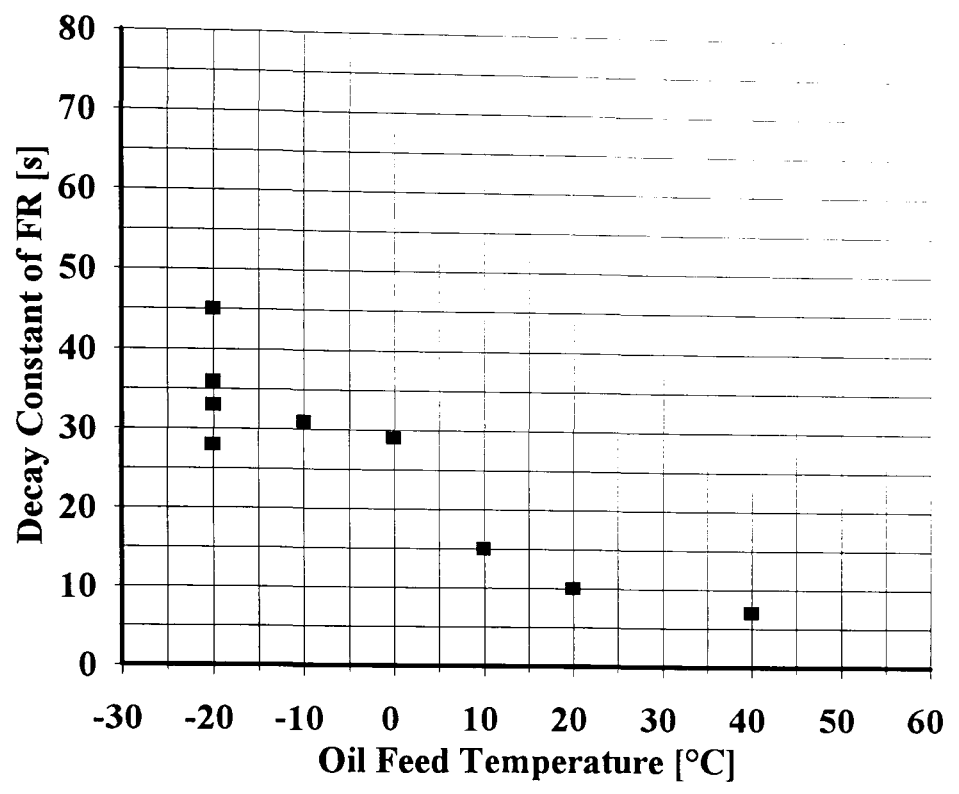


Figure 8.9
 Impact of Operating Conditions on Transient Decay Time
 UPPER GRAPH: 1000 rpm, changing temperature
 LOWER GRAPH: -20°C, changing speed
 (Data from decompressed P-type engine, SAE 10W/30 oil)

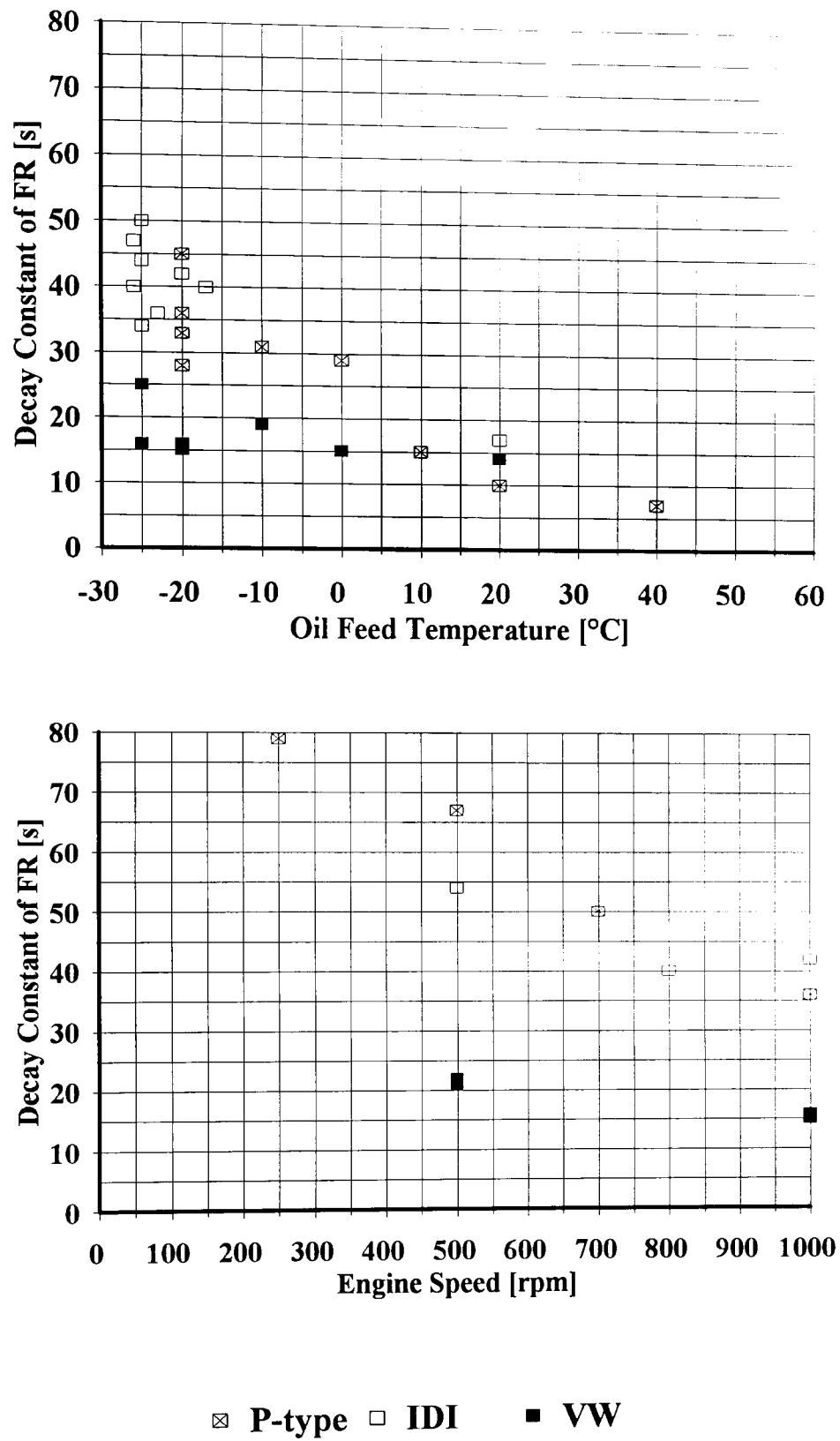


Figure 8.10

Variation of Transient Decay Times Between Engines

UPPER GRAPH: 1000 rpm, changing temperature

LOWER GRAPH: -20°C, changing speed

(All data from decompressed engines, SAE 10W/30 oil)

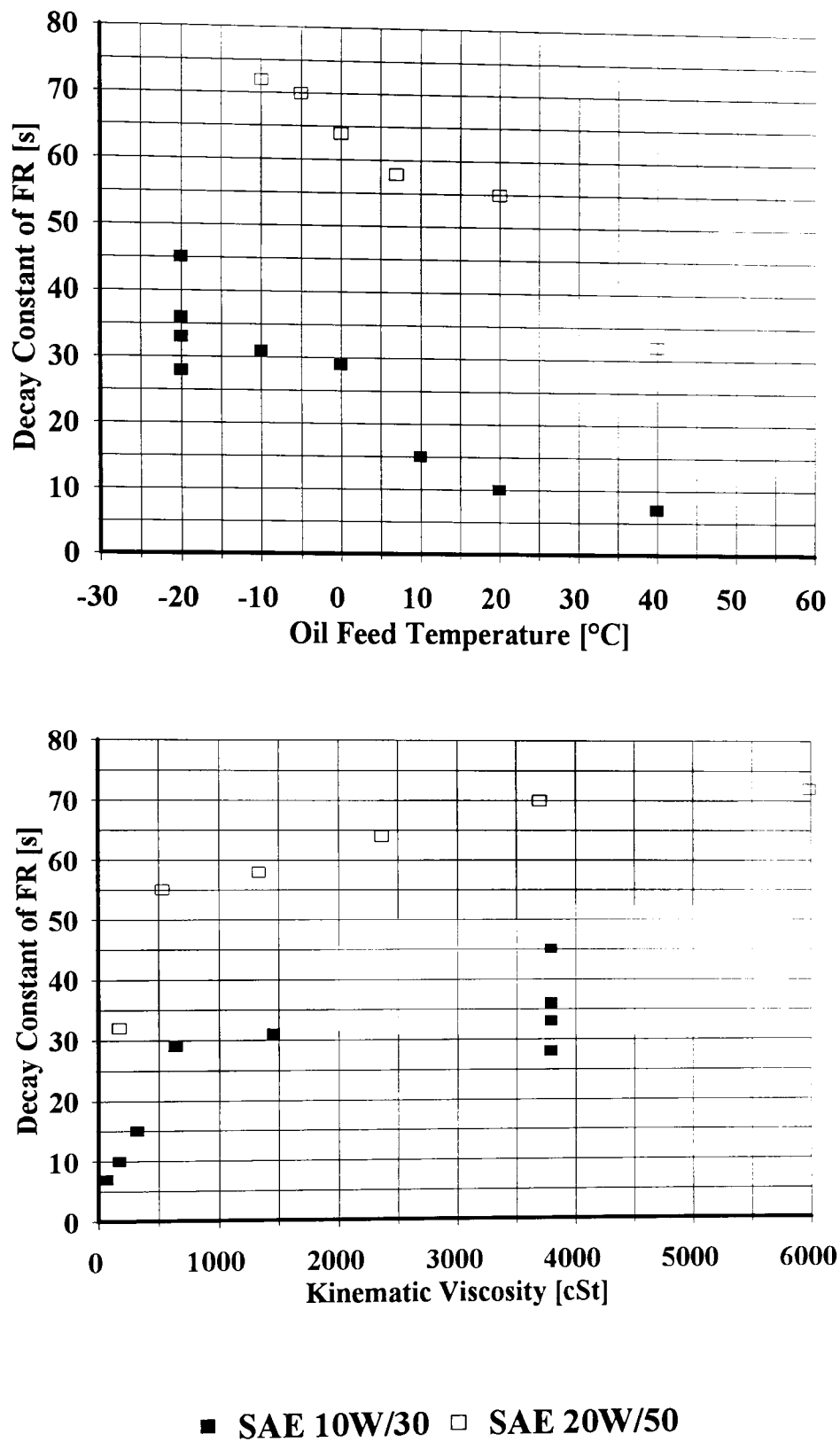


Figure 8.11

Impact of Oil Viscosity Grade on Transient Decay Time

(Data from decompressed P-type engine, motored at 1000 rpm)

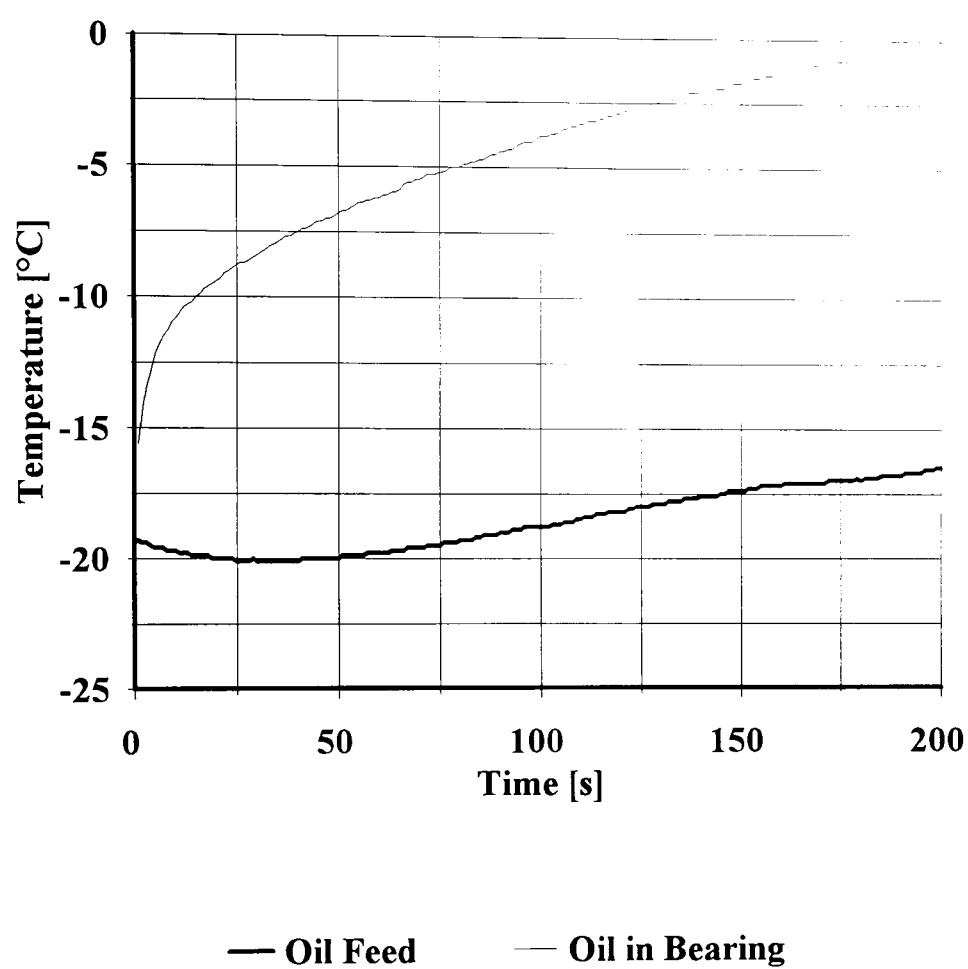


Figure 8.12
Oil Temperature Rise, Feed and Bearing
Motoring at 520 rpm, SAE 10W/30 oil
(Ford 1.8L IDI Crankshaft ONLY)

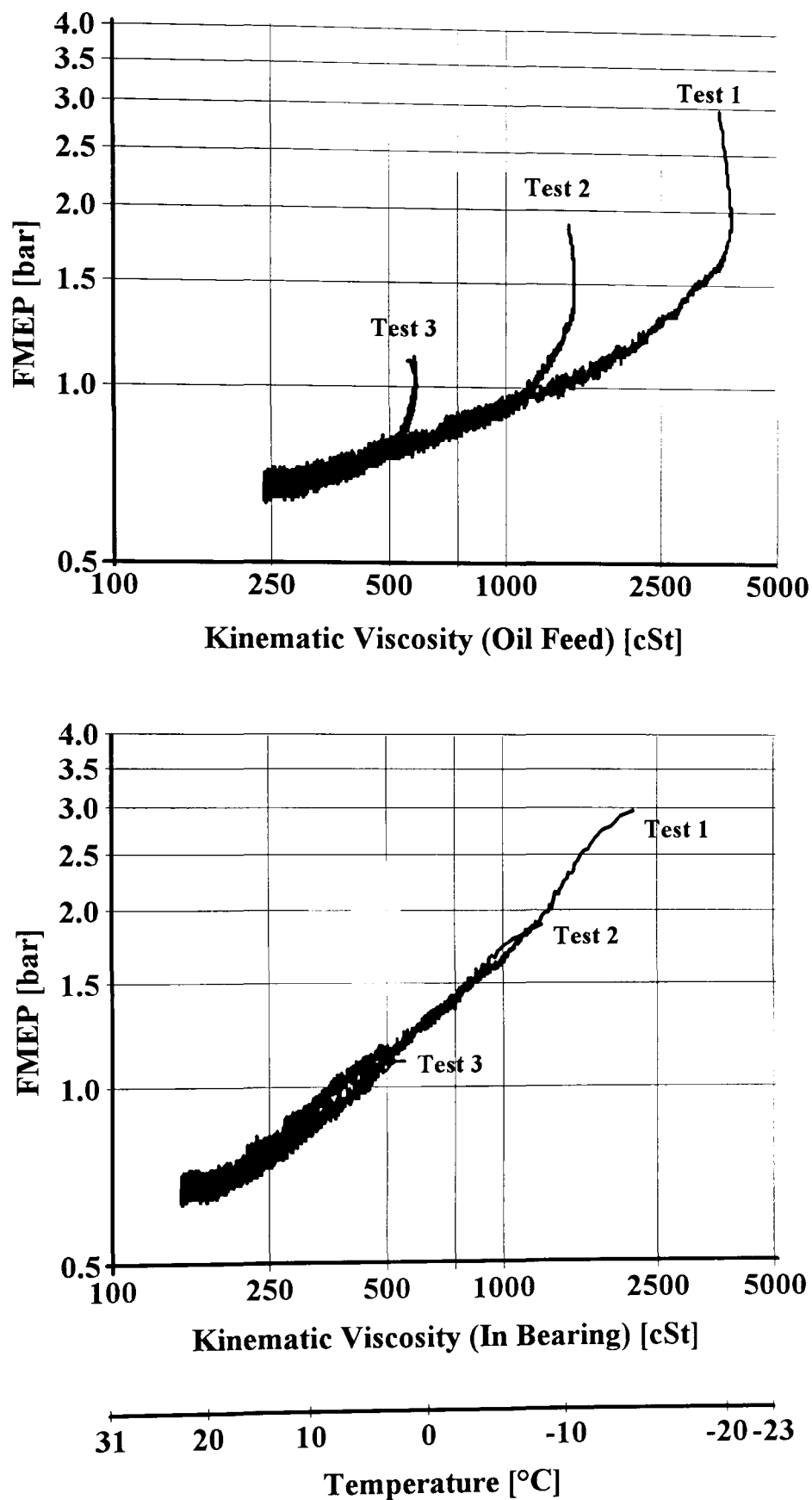


Figure 8.13

Friction Dependence on Oil Viscosity in the Bearing

Motoring at 520 rpm, SAE 10W/30 oil

(Ford 1.8L IDI Crankshaft ONLY)

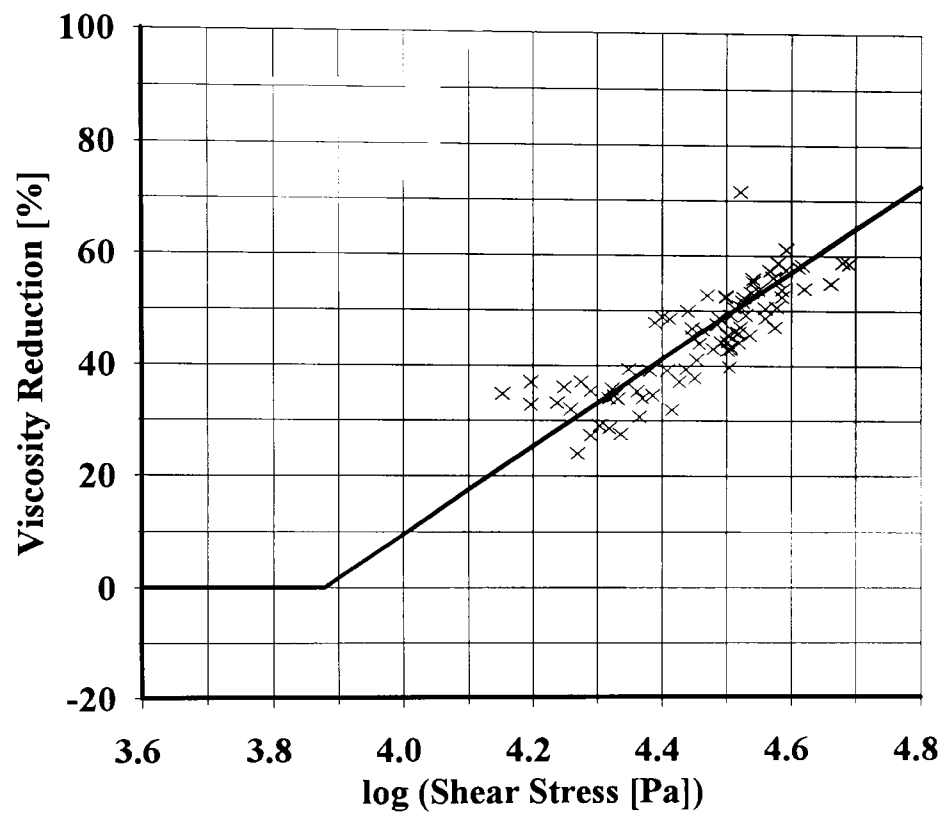


Figure 8.14

Effect of Shear Stress on Viscosity

Speeds 200 to 1000 rpm, Temperatures -20°C to +20°C

SAE 10W/30 oil

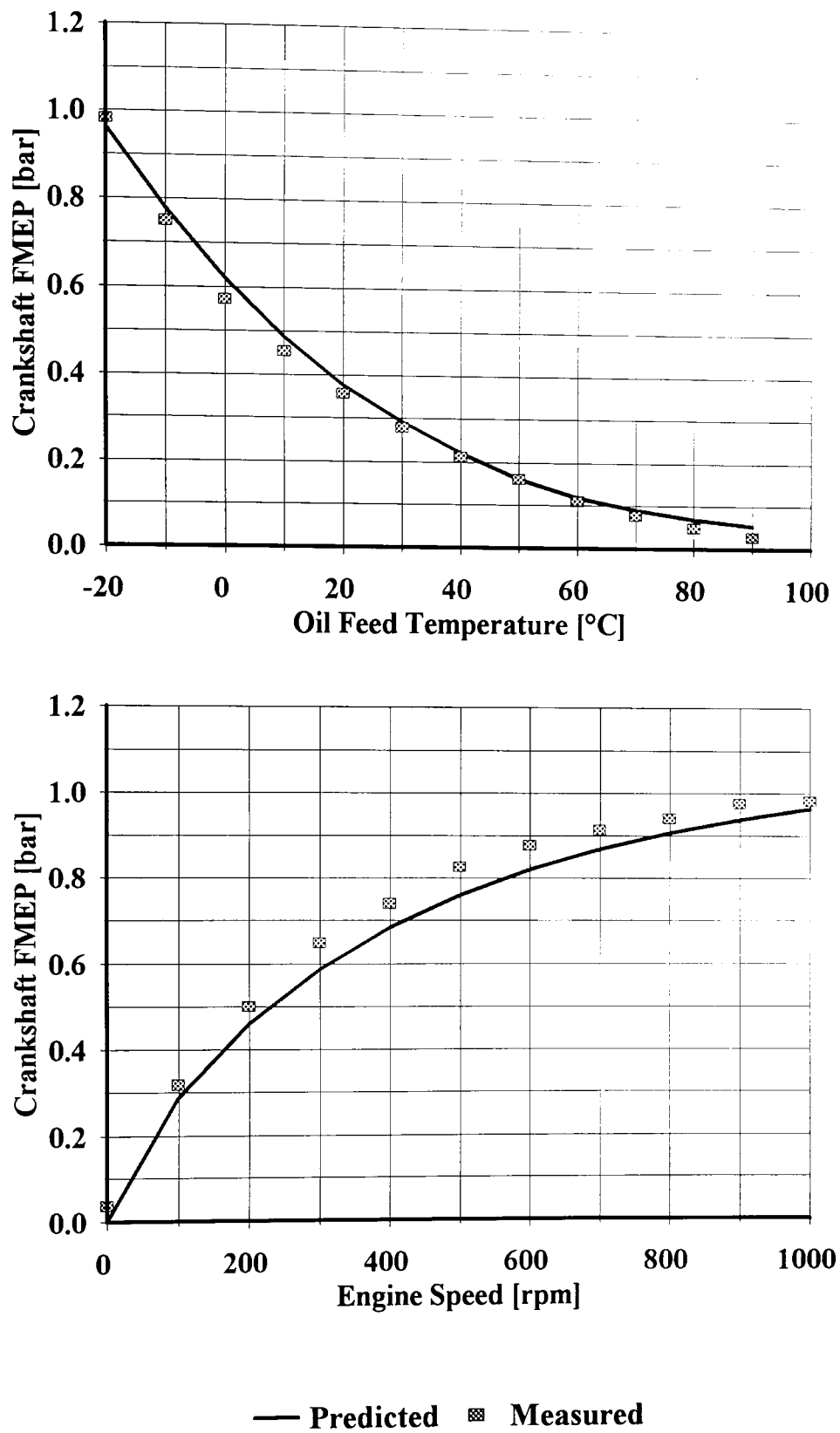


Figure 8.15

Steady-State Crankshaft Model

UPPER GRAPH: 1000 rpm, changing temperature

LOWER GRAPH: -20°C, changing speed

(1.8L IDI crankshaft, SAE 10W/30 oil)

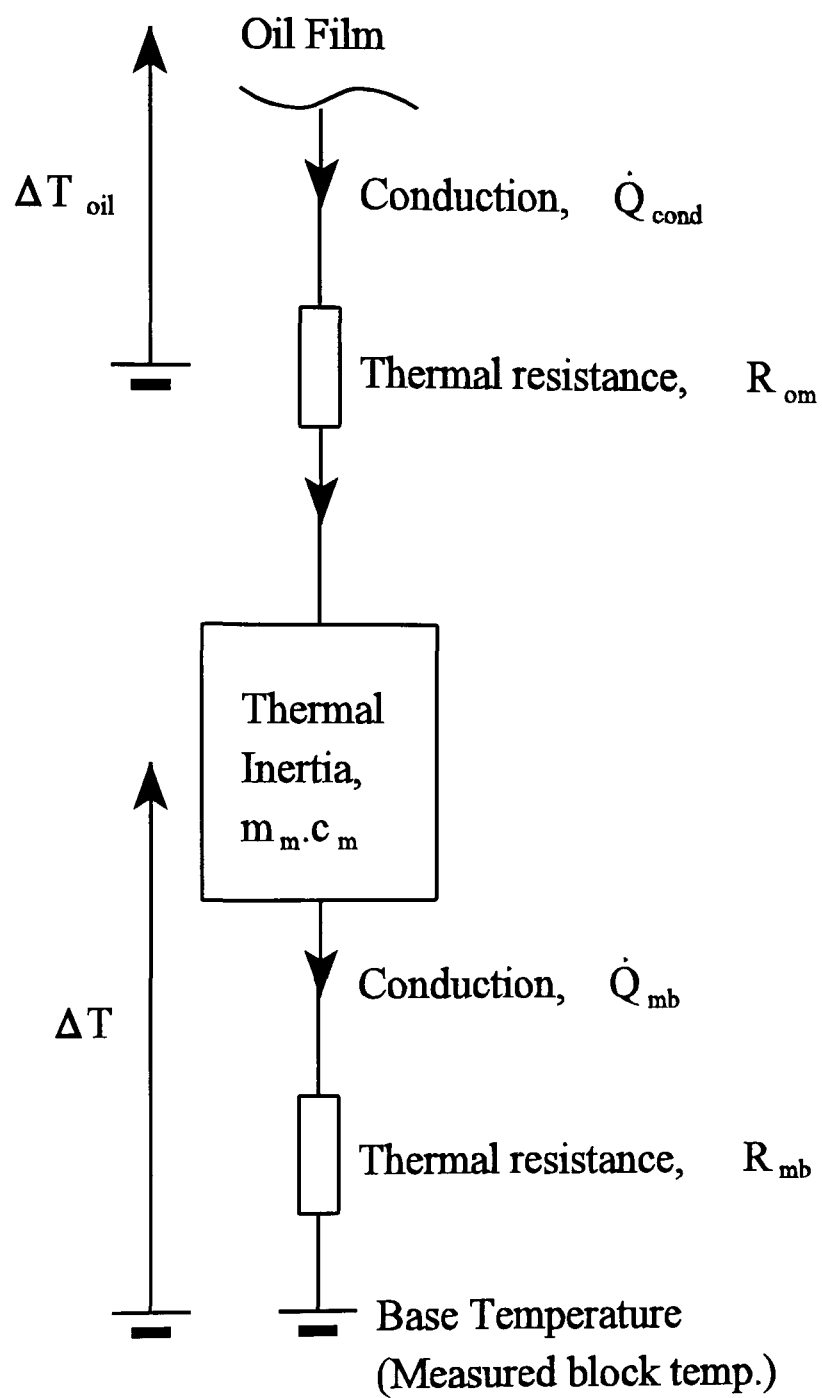


Figure 8.16

Simple thermal model of journal bearing.

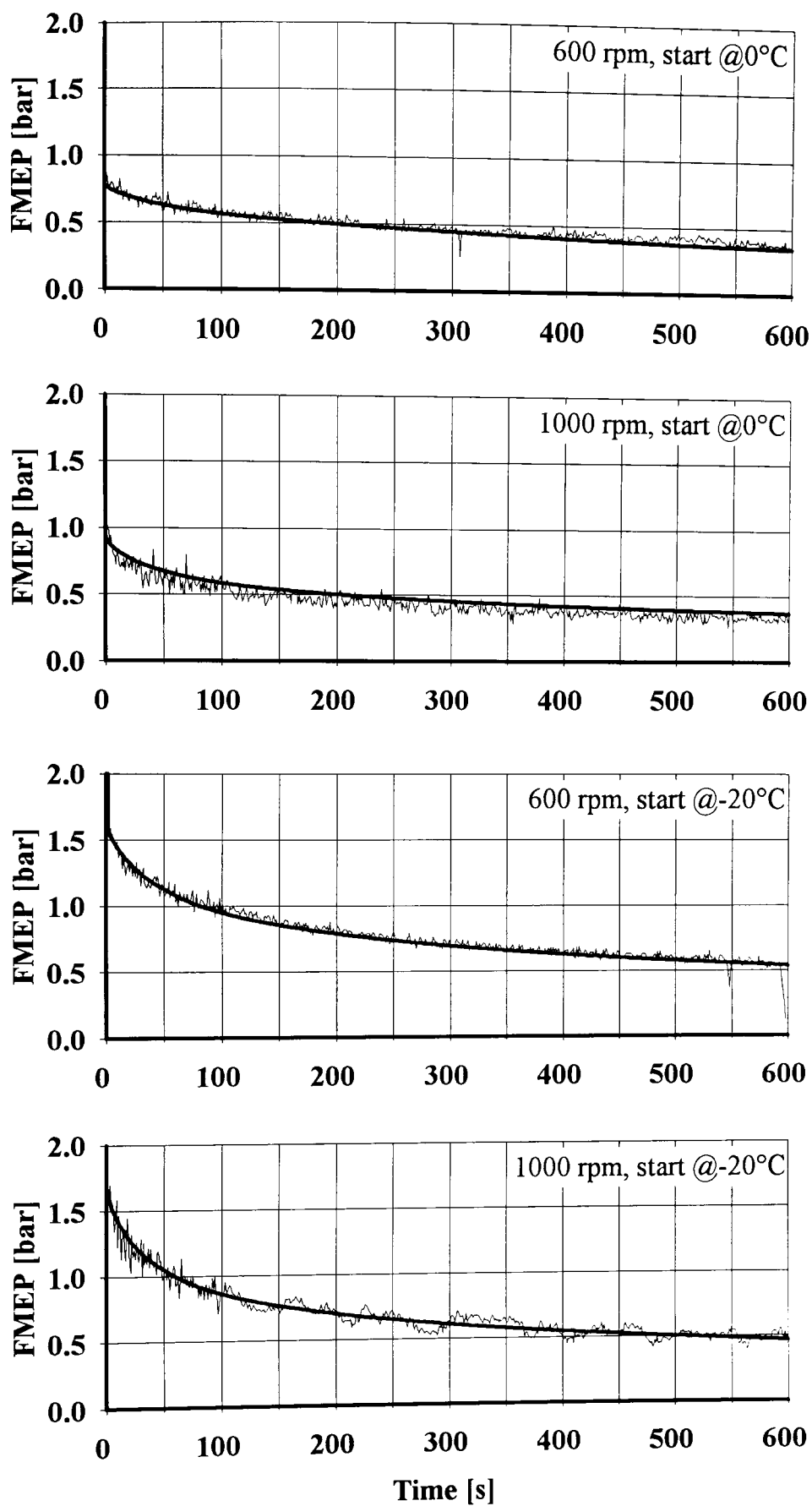


Figure 8.17

Transient Crankshaft Model

Model results compared to measured data

600 rpm and 1000 rpm, 0°C and -20°C

(1.8L IDI crankshaft, SAE 10W/30 oil)